

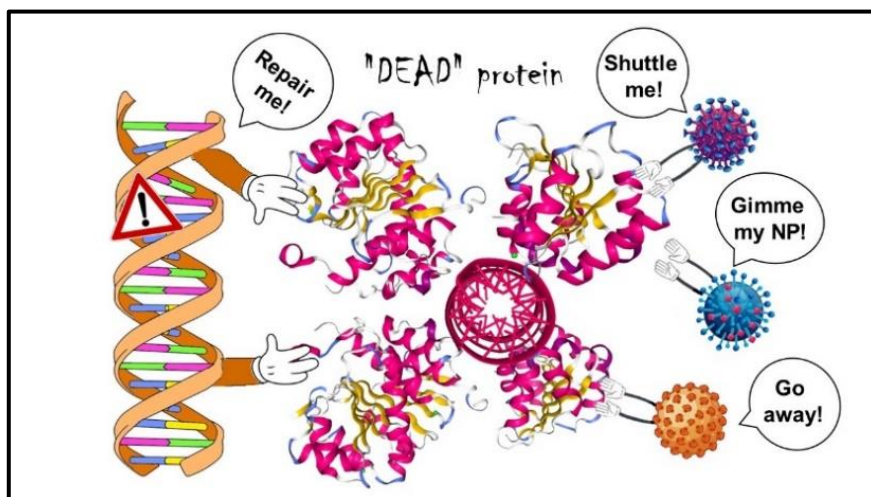


UNIVERSITÀ
DI PAVIA

Dipartimento di Biologia e Biotechnologie "L. Spallanzani"

Consiglio Nazionale delle Ricerche, Istituto di Genetica Molecolare Luigi Luca Cavalli-Sforza

Antiviral potential coupled to genome stability: the multifaceted roles of DDX3X protein



Valentina Riva

Dottorato di Ricerca in
Genetica, Biologia Molecolare e Cellulare
Ciclo XXXII – A.A. 2016-2019



UNIVERSITÀ
DI PAVIA

Dipartimento di Biologia e Biotecnologie “L. Spallanzani”
Consiglio Nazionale delle Ricerche, Istituto di Genetica Molecolare Luigi Luca
Cavalli-Sforza

**Antiviral potential coupled to genome
stability: the multifaceted roles of
DDX3X protein**

Valentina Riva

Supervised by Prof. Giovanni Maga

Dottorato di Ricerca in
Genetica, Biologia Molecolare e Cellulare
Ciclo XXXII – A.A. 2016-2019

Abstract

The human RNA helicase DDX3X is a real multifaceted enzyme. Like all the other DEAD-box proteins of the same family, DDX3X participates into different steps of RNA metabolism. Moreover, DDX3X is one of the actors of cell cycle regulation, innate immunity and apoptosis processes.

Our group started to look at DDX3X as an interesting protein since it has primary roles in viral infections and tumor development too. In the context of viral infections, DDX3X possesses dual roles: it acts as an antiviral or proviral factor regulating viral replication at different levels (regulation of genome duplication and/or gene expression and host innate immunity activation). From these observations, it came the idea to use DDX3X as a possible therapeutic target to inhibit a function essential for the viral replication, but dispensable for the human cell.

In collaboration with the University of Siena (Prof. Maurizio Botta), we developed some inhibitor molecules able to recognize two different DDX3X pockets: the helicase binding pocket and the unique motif of DDX3X. Both two compounds families showed selectivity and no toxicity in cells; even more interesting, our molecules showed considerable broad-spectrum antiviral effects being able to suppress both the replication of WNV and DENV-2 viruses in infected cells.

The development of DDX3X-specific inhibitor molecules in the context of different viral infections is just one of the two projects that I followed during my PhD internship. In parallel, I shifted my attention on the characterization of this enzyme in the context of DNA damage response. Published data have already implicated DDX3X in the resolution of RNA/DNA hybrids and RNA secondary structures, as well as in the degradation of RNAs. Moreover, unpublished data from our lab demonstrated also a possible exoribonuclease activity of DDX3X in addition to the already well-known helicase/ATPase activities. Trying to envision a physiological relevance of this activity, we focused on the possible situations in which RNA/DNA hybrids could be present into the cell. Ribonucleotides (rNMP) are the most abundant type of DNA damage and all the cells have specific enzymes able to remove them avoiding deleterious consequences. This removal activity is essential and it is primarily performed by the ribonucleotide excision repair (RER) pathway. RNaseH2 is believed to be the only enzyme able to incise single rNMPs within a DNA strand activating an error-free RER pathway. Surprisingly, our data demonstrated that DDX3X is able to promote RER initiation, thereby suggesting a possible new role of this enzyme also in genome stability.

Acknowledgements

I want to express my sincere gratitude to my supervisor Giovanni Maga for the opportunity to be part of his laboratory and to follow what for me is” the most beautiful project of the world”.

Nothing would have been possible without my first lab-teacher Anna, that time has transformed into a friend.

My acknowledgements to Doctor Silvio Spadari as well, always optimistic and able to lighten even the heaviest days.

Two special thanks to other two professors not really part of my laboratory, Martina and Simone: without your advices I wouldn't arrive at the end of this manuscript.

During years a lot of people were part of the big “Lab 500”: thanks to everyone, for every single teaching and every single laugh.

A very special thanks to all my students: DDX3 family is something that it will remain into my heart.

Thanks to all my friends, for supporting me in all difficult moments and for being at my side now and over the years.

Thanks to my family without which I wouldn't be what I am.

Thanks to my “Quail”: anyone could understand better than you the complicated world of Biology. Thank to be my complicit, I hope you'll continue to be it for long long time.

Abbreviations

AGS	Aicardi-Goutier syndrome
BAdV-3	Bovine Adenovirus 3
BVDV	Bovine Viral Diarrhea virus
CK1 ϵ	Casein kinase 1 epsilon
CRM1	Chromosomal Maintenance 1 or Exportin 1
DSBs	Double Strand Breaks
DBY	DEAD-box Y RNA helicase 3
DDX1	DEAD-box helicase 1
DDX3X	DEAD-box helicase 3 X-linked
DDX3Y	DEAD-box helicase 3 Y-linked
DENV	Dengue virus
Dicer	Endoribonuclease Dicer
Dox	Doxycycline
ds	Double strand
Dvl1	Segment polarity protein dishevelled homolog DVL-1
Dvl2	Segment polarity protein dishevelled homolog DVL-2
eIF3	Eukaryotic translation initiation factor 3
ENKTL-NT or NKTCL	Extranodal NK/T cell lymphoma, nasal type
Exo1	Exoribonuclease 1
Fen1	Flap Endonuclease 1
HBV	Hepatitis B Virus
HCMV	Human cytomegalovirus
HCV	Hepatitis C Virus
HIF-1 α	Hypoxia-inducible factor 1-alpha
HIV-1	Human Immunodeficiency virus type 1
HPV	Human papilloma virus
HSV-1	Herpes simplex virus type 1
IAV	Human Influenza A virus
IC ₅₀	Half maximal inhibitory concentration
IFN	Interferon
IKK ϵ	Inhibitor of nuclear factor kappa-B kinase subunit epsilon

IRF3	Interferon regulatory factor 3
JEV	Japanese encephalitis virus
JUNV	Junin virus
K7	Protein K7
KRAS	GTPase KRas
LASV	Lassa virus
LCMV	Lymphocytic choriomeningitis virus
MDM2	E3 ubiquitin-protein ligase Mdm2
MITF	Microphthalmia-associated transcription factor
MNV	Murine Norovirus
MOI	Multiplicity Of Infection
NES	Nuclear export signal
NF-kB	Nuclear factor kappa-light-chain-enhancer of activated B cells
NLS	Nuclear localization signal
NP	Nucleoprotein
N ^{pro}	Genome polyprotein
NS1	Non-structural protein 1
NS3	Non-structural protein 3
NS5	Non-structural protein 5
NSC cells	Non-silenced cells
nsP3	Non-structural polyprotein 3
nt	nucleotide
NZ51	Ring-expanded nucleoside analogue
OSCC	Oral squamous cell cancer
PB1-F2	Influenza A proapoptotic protein
PCNA	Proliferating Cell Nuclear Antigen
PFU	Plaque Forming Unit
PLK1	Serine/threonine-protein kinase PLK1
Pols	Polymerases
RER	Ribonucleotide Excision Repair
RIG-I	RIG-I-like receptor 1; Probable ATP-dependent RNA helicase DDX58
RK33	diimidazo[4,5-d:40,50-f]-[1,3]diazepine
RNaseH1/2	Ribonuclease H 1/2
RNaseR	Ribonuclease R
rNMPs	Ribonucleotides triphosphates
RS	Arginine-Serine dipeptide
SF1-6	Superfamilies 1-6
SGs	Stress granules

ShDDX3 cells	DDX3X KD cells
Srs2	ATP-dependent DNA helicase SRS2
ss	Single strand
Tat	Transactivating regulatory protein
TBK1	Serine/threonine-protein kinase TBK1
TLC	Thin-Layer Chromatography
TNM	Tumor Node and Metastasis
Top1	Topoisomerase 1
VACV	Vaccinia virus
VEEV	Venezuelan Equine Encephalitis virus
WNV	West Nile virus

Contents

Abstract	3
Acknowledgements	4
Abbreviations	5
Contents	8
1. Introduction	10
2. Review of the literature	11
2.1 Human DDX3 genes.....	11
2.2 DDX3X protein.....	11
2.3 Cellular localization of DDX3X in normal and tumor cells.....	20
2.4 DDX3X and cell proliferation regulation.....	21
2.5 DDX3X in innate immunity and stress response.....	22
2.6 DDX3X and cancer.....	23
2.7 DDX3X as an anticancer drug target.....	28
2.8 Genomic stability: DDX3X in the response of ribonucleotide incorporation.....	30
2.9 DDX3X and viral infections.....	34
2.10 DDX3X as a target for antiviral therapies.....	42
3. Aims of the research	45
4. Materials and methods	47
4.1 DDX3X AS A PRIME CELLULAR TARGET TO FIGHT OLD AND EMERGING VIRUSES.....	47
4.1.1 Chemistry.....	47
4.1.2 Proteins production and purification.....	47
4.1.3 Helicase assay based on Fluorescence Resonance Energy Transfer (FRET).....	48
4.1.4 ATPase assay.....	49
4.1.5 Kinetic analysis.....	50
4.1.6 Cell extracts and DDX3X quantification.....	51
4.1.7 Antiviral assay: WNV and DENV inhibitory viral plaque reduction assay.....	52
4.1.8 Cytotoxicity assay.....	53
4.1.9 Site directed mutagenesis.....	54
4.2 AN ALTERNATIVE RIBONUCLEOTIDE EXCISION REPAIR BY THE RNA HELICASE/NUCLEASE DDX3X.....	56

4.2.1 Chemicals.....	56
4.2.2 Nucleic acids substrates	56
4.2.3 Proteins production and purification.....	57
4.2.4 2-D electrophoresis (2-DE) and mass spectrometry analysis	57
4.2.5 Nuclease assays.....	59
4.2.6 Non denaturing gel-based helicase assays	59
4.2.7 Ribonucleotide excision repair assays	60
4.2.8 Kinetic analysis	60
4.2.9 Transfection of HEK293T cells for engineered lentivirus preparation: calcium phosphate precipitation	61
4.2.10 Cells Transduction and DDX3X KD induction	63
4.2.11 Cell extracts and Western Blot.....	64
4.2.12 Riboassay	64
5. Results.....	65
5.1 <i>DDX3X AS A PRIME CELLULAR TARGET TO FIGHT OLD AND EMERGING VIRUSES.....</i>	<i>65</i>
5.1.1 DDX3X helicase inhibitors to fight West Nile virus infections .	65
5.1.2 A novel strategy to develop selective DDX3X RNA helicase inhibitors to fight emerging viruses	75
5.2 <i>AN ALTERNATIVE RIBONUCLEOTIDE EXCISION REPAIR BY THE RNA HELICASE/NUCLEASE DDX3X.....</i>	<i>87</i>
6. Discussion.....	104
6.1 <i>DDX3X AS A PRIME CELLULAR TARGET TO FIGHT OLD AND EMERGING VIRUSES.....</i>	<i>104</i>
6.2 <i>AN ALTERNATIVE RIBONUCLEOTIDE EXCISION REPAIR BY THE RNA HELICASE/NUCLEASE DDX3X.....</i>	<i>107</i>
7. Conclusions and perspectives	110
7.1 <i>DDX3X AS A PRIME CELLULAR TARGET TO FIGHT OLD AND EMERGING VIRUSES.....</i>	<i>110</i>
7.2 <i>AN ALTERNATIVE RIBONUCLEOTIDE EXCISION REPAIR BY THE RNA HELICASE/NUCLEASE DDX3X.....</i>	<i>111</i>
References.....	113
List of original manuscripts.....	132

1. Introduction

DDX3X is an ATPase/RNA helicase belonging to the DEAD-box helicase family that is conserved from bacteria to humans (Cordin *et al.*, 2006).

All the RNA and DNA helicases are enzyme able to catalyse the unwinding of a double-strand nucleic acid. RNA helicases are currently divided into six superfamilies (SF1-6), depending on conserved motifs sequence similarities. Most RNA helicases belong to the SF-2 superfamily that includes DEAD-box proteins too (Cordin *et al.*, 2006).

DDX3X appears to be one of the most multifaceted helicases known up to date. It is involved, exactly like other DEAD-box proteins, in almost all the aspects of RNA metabolism and it is one of the actors in regulation of transcription, translation, RNA splicing, RNA transport and RNA degradation processes. Moreover, it has also been suggested to be involved in cell cycle control as well as in the regulation of apoptosis and innate immunity.

DDX3X is also considered a promising target for anticancer and antiviral chemotherapy since it can play a dual role both in cancer (oncogene versus oncosuppressor) and in viral infections (proviral versus antiviral factors) (Riva and Maga, 2019).

2. Review of the literature

2.1 Human DDX3 genes

There are two human DDX3-homologous genes: DDX3X and DDX3Y. The two genes are highly homologous (91.9% identity, 97.7% similarity), despite their expression pattern and functions are completely different (Kim *et al.*, 2001).

The X-homolog is located in the X chromosomal region Xp11.4 and codes for a transcript of 5.3 kb corresponding to a polypeptide of 662 amino acids rich in serines (11.3%) and glycines (11.4%) (Kim *et al.*, 2001).

The Y-homolog is located in the Yq11.21 non-recombining region of the Y-chromosome and it is named DDX3Y or DBY. Specifically, it is expressed only in the male germline and is essential for spermatogenesis since its deletion leads to a significant reduction in germ cells (oligozoospermia) or even to their complete absence (azoospermia) (Lahn and Page, 1997; Foresta, 2000; Ditton *et al.*, 2004).

DDX3X, on the contrary of DBY, is ubiquitously expressed in a wide range of tissues. As a matter of fact, Human Multiple Tissue Northern blots exhibits DDX3X expression in testis, colon, lung, liver, skeletal muscle and kidney (Kim *et al.*, 2001).

In the next paragraphs, it follows a large review of the literature about the DDX3X homologue that is the key player of my studies.

2.2 DDX3X protein

As previously mentioned in the 1. Introduction paragraph, RNA helicases are currently divided into six superfamilies (SF1–6), depending on conserved motifs sequence similarities.

The largest family is SF-2 superfamily that includes DEAD-box proteins, a family of more than 50 related RNA helicases, which can have overlapping compensatory roles in cell metabolism. The name of the DEAD-box helicase family derives from the sequence D-E-A-D (Asp–Glu–Ala–Asp) that is present in the Walker B motif II. This short sequence represents the catalytic core essential for ATP hydrolysis (Tanner and Linder, 2001; Meier-Stephenson *et al.*, 2018).

DEAD-box proteins are characterized by the presence of nine conserved motifs that were shown to be involved in ATPase and helicase activities and in their regulation (Tanner *et al.*, 2003). In DDX3X, all the conserved motifs are present in two RecA-like subdomains (Domain 1 and Domain 2, from N- to C-terminal) connected via a short flexible linker.

In DDX3X, the amino-terminal domain 1 contains the following motifs: the ATP binding Motifs Q, I (Walker A) and II (Walker B) as well as the RNA-binding Motifs Ia, Ib and the Motif III. In domain 2 there are all the motifs able to coordinate the ATPase and unwinding activities, respectively named Motifs IV, V and Motif VI. (*Figure 1*) (Cordin *et al.*, 2006; Garbelli *et al.*, 2011).

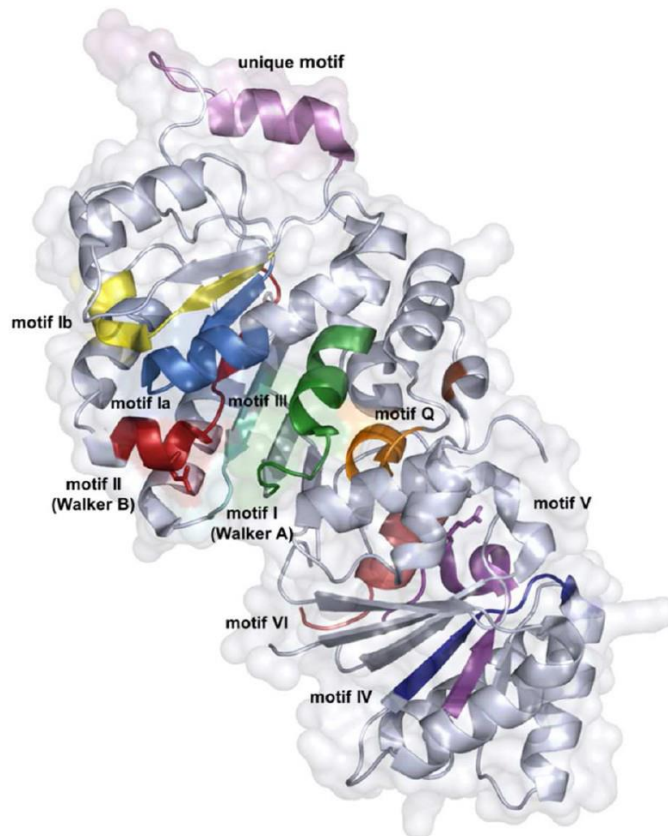


Figure 1: Nine conserved motifs of the DEAD-box family are highlighted with different colours in the 3D cartoon representation of the human DDX3X open conformation in complex with AMP (down): motif Q (orange), motif I (forest green), unique motif (violet), motif Ia (marine), motif Ib (yellow), motif II or DEAD motif (firebrick), motif III (aquamarine), motif IV (deep blue), motif V (purple), and motif VI (salmon) (Fazi et al., 2015).

Domains 1 and 2 have a fold typical to the RecA superfamily, characterized by five β -strands surrounded by five α -helices. Sequences alignment of all different human DExD-box helicases shows a DDX3-specific insertion between Motifs I and Ia both in the X/Y homolog genes. The crystal structure of DDX3X reveals that this inserted sequence of ten residues (250–259, E-A-L-R-A-M-K-E-N-G) forms a helix that positions a positively charged loop in close proximity to the putative RNA ligand. This unique insertion, namely unique motif, is not generally found in other human DExD-box helicases and could be an important determinant in RNA–substrate recognition/activation by DDX3X (*Figure 2*) (Högbom *et al.*, 2007).

	Domain I	Domain Ia
hsDDX1	SKAPDGYIVKSQHSNAQVTQTKFLP-----	NAPKALIVEPSRELAEQ
hsDDX3X	AQTGSGKTA AFLLPIL SQIYSDGPG EALRAMKENG RYGRRK QYPISLVLAPTRELAVQ	
hsDDX3Y	AQTGSGKTA AFLLPIL SQIYTDGPG EALKAVKENG RYGRRK QYPISLVLAPTRELAVQ	
hsDDX4	AQTGSGKTA AFLLPILAHMMHDGITASR---FKEL-----	QEPECIIVAPTRELVNQ
hsDDX5	AQTGSGKTLSYLLPAIVHINHQP-----	FLER--G---DGPICLVLAPTRELAAQ
hsDDX6	AKNGTGKSGAYLIP-----	LLER-LDLKKDNIQAMVIVPTRELALQ
hsDDX10	AKTGSGKTLAFLVPVLE-----	ALYRLQWTS TDGLGVLIISPTRELAYQ
hsDDX17	AQTGSGKTLAYLLPAIVHINHQP-----	YLER--G---DGPICLVLAPTRELAAQ
hsDDX18	AKTGSGKTLAFLIPAVELI-----	VKLRF--MPRNGTGVLIISPTRELAAQ
hsDDX19	SQSGTGKTA AFLVLA MLSQ-----	VEPA-----NKYPQCLCLSPTYELALQ
hsDDX20	AKSGTGKTCVFSTIALDSL-----	VLEN-----LSTQILILAPTR EIAVQ
hsDDX21	ARTGTGKTFSFAIPLIEKL-----	HGELQDRKRGRAPQVVLVAPTRELANQ
hsDDX23	AETGSGKTA AFLIPLLVWITTLPKIDR---	IEESDQG----PYAIILAPTR EIAVQ
hsDDX25	SQSGTGKTA AFLVLA MLSRVN-----	ALELF-----PQCLCLAPTYELALQ
hsDDX27	AATGTGKTA AFLPVLERLIYKPRQAPV-----	TRVLVLPVPTRELGIQ
hsDDX28	AETGSGKTLSYLLPLLQRLGQP-----	SLDSL---PIPAPRGLVLVPSRELAQQ
hsDDX31	SQTGSGKTLAYCIPVVQSLQAMESKIQRSDG-----	PYALVLVPTRELALQ
hsDDX39	AKSGMGKTA AVFVLATLQQIEPVNGQ-----	VTVLVMCHTRELAFQ
hsDDX41	AFTGSGKTLVFTLPVIMFCLEQEKRLPF---	SKREG-----PYGLIICPSRELARQ
hsDDX42	AKTGSGKTA AFLIWPMLIHIMDQK-----	ELEPGD---PIAVIVCPTREL CQQ
hsDDX43	AQTGTGKTLCLYMPGF IHLVLQPSLKGQRNR-----	PGMLVLTPTRELALQ
hsDDX46	AKTGSGKTI AFLPMPFRHIMDQR-----	SLEEGEG---PIAVIMTPTRELALQ
hsDDX47	AETGSGKTGAFALPILNA-----	LLE----TPQRLFALVLTPTRELAFQ
hsDDX48	SQSGTGKTATFSISVLQCLDIQVRE-----	TQALILAPTR EIAVQ
hsDDX49	AKTGSGKTA AFLVLPILQK-----	LSEDPYG---IFCLVLTPTRELAYQ
hsDDX50	ARTGTGKTFSFAIPLIERLQRNQETIKKSRS-----	PKVLVLAPTRELANQ
hsDDX51	APTGSGKTLA FVIPVVQALLSRVVCH-----	IRALVVLPTKELAAQ
hsDDX52	APTGSGKTLA FSIPILMQLKQPANKG-----	FRALISPTRELASQ
hsDDX53	AQTGTGKTLSYLMPGFIHLDSQPI-----	SREQRNG---PGMLVLTPTRELALH
hsDDX54	ARTGSGKTACFLPMPFERLKTHSAQTG-----	ARALISPTRELALQ
hsDDX55	AVTGSGKTLA FVPIPILEILL-----	RRE--EKLKKSQVGAI IITPTRELAIQ
hsDDX56	ARTGSGKTA AYAI PMLQLLLHRKATGPVVEQ-----	AVRGLVLVPTKELARQ
hsDDX58	APTGCGKTFVSLICEHHLKFPQGG-----	KGVVFFANQIPVYEQQKS
hsDDX59	ADTGSGKTA AFLPVIMRALFESKT-----	PSALILTPTRELAIQ
Consensus	GSGKT	LVLxPTRELAXQ

Figure 2: Sequences alignment of 40 different human DExD-box helicases covering the conserved region between motif I and motif Ia (amino acid residues 229-279 in DDX3X) and showing the DDX3X/Y-specific insertion between residues 250 and 259 (red box). Conserved residues are shaded in grey (Garbelli et al., 2011).

On the contrary of such conserved motifs in the protein core, N- and C-terminal DDX3X regions are largely unstructured but contain regions responsible for unique functions. At its C-terminal domain, DDX3X contains an arginine-serine (RS) dipeptide rich segment. RS domains are typical modules of the SR (serine-arginine) proteins family, generally involved in the recruitment of components of the spliceosome complex (Ma and He, 2003).

Within its 22 amino acids N-terminal domain, DDX3X contains a nuclear export signal (NES) that has been confirmed in different cell lines. Then, at least three different and independent nuclear localization signals (NLS) have been recently identified in HeLa cells respectively in DDX3X N-terminal region (aa 1-139), between aa 259–263 and in the C-terminal RecA-like domain (aa 409–572). It follows that the different DDX3X localization could be the reflection of its specific role in various cellular processes and/or in malignant transformations (Brennan *et al.*, 2018).

The C-terminal region is then fundamental for DDX3X oligomerization since DDX3X seems to work as a trimer: a dimer complex is responsible for the RNA unwinding and the third monomer probably promotes the RNA-loading optimizing the unwinding efficiency (Song and Ji, 2019).

In solution, DDX3X exists in two conformational states: open and closed conformation. The transition between the two states depends on the ATP and RNA binding at each catalytic cycle and it was elegantly described by Schütz *et al.* (Figure 3) (Schütz *et al.*, 2010).

The process through which DDX3X passes from one conformation to the other one has been summarized in a model subdivided into three different steps corresponding to three specific acquired conformational state. Specifically, DDX3X could assume the following conformations: open conformation, pre-RNA binding and closed conformation.

DDX3X open conformation (structure solved in the 2I4I crystal) is not able to bind the RNA substrate because the α -helix 8 of the DEAD-motif partially blocks the helicase pocket (Figure 3A). After ATP binding, the

helicase domain 2 rotates by about 180° with respect to domain 1 generating a compact pre-RNA binding conformation (*Figure 3B*) that creates a reduced space for about five nucleotides of the duplex. Next, RNA substrate binds to the DEAD-domain completing the cleft closure and allowing the placement of α -helix 8 out of the RNA binding site (*Figure 3C*). The closed conformation is finally stabilised by a salt-bridge between the conserved arginine of motif V (Arg 503) and the aspartic acid of the DEAD motif (Asp 350). The closure of the ATP-binding site promotes ATP hydrolysis and the subsequent fast release of the RNA substrate. In this way, after the movement of α -helix 8 of the DEAD-motif that occludes the RNA-binding site, the enzyme is able to come back to the open state and free to start another catalytic cycle.

Analysing the model proposed by Schütz *et al.*, it is clear that the transition between open and closed conformation is not compatible with a dsRNA substrate. Probably it is the conformation change itself that is responsible for the local unwinding of the helix. This is true not only for DDX3X; as a matter of fact, DEAD-box proteins are not processive enzymes able to couple opening of the double helix to translocation along the lattice, but classically they are able to open the RNA substrate via a local strand reaction mechanism: one molecule of ATP is necessary to melt few (4-7) base pairs at each catalytic cycle. Thus, unwinding requires ATP binding, while hydrolysis is required for recycling of the enzyme (Schütz *et al.*, 2010).

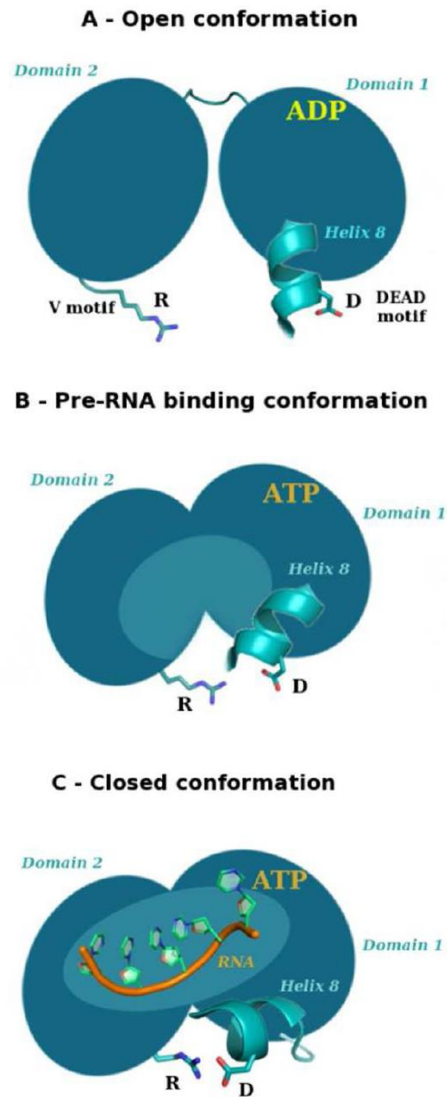


Figure 3: Schematic model proposed by Schütz et al. for the RNA binding site activation.

*The structural mechanism for unblocking the RNA binding site involved a transition between different conformational states at each catalytic cycle depending on ATP and RNA binding. (A) Open conformation: in the free substrate state, subdomains are separated and the RNA binding site is partway covered by α -helix 8 (ended segment of DEAD-motif). The pictured aspartate is the terminal residue of the DEAD sequence, while the arginine highlighted in domain 2 is a conserved residue of motif V. (B) Pre RNA-binding conformation: the ATP binding promotes the closure of the cleft partially unblocking the RNA binding site by rotation of α -helix 8. (C) Closed conformation: RNA binding completes the cleft closure. A salt bridge stabilizes the closed conformation (Schütz *et al.*, 2010).*

Now, this vision has been partially overcome since the recently published work of Song and Ji (Song and Ji, 2019). The mechanism proposed by Schütz *et al.* has to be rearranged since DDX3X has been shown to work in a cooperative way. Two DDX3X molecules function together, one of them binds ATP and also recognizes one RNA strand and the other one mainly binds the second RNA strand of the duplex. Then, two dsRNA-bound DDX3X monomers undergo dramatic conformational changes upon the binding of Mg/ATP and thereby unwind dsRNA (Song and Ji, 2019).

More it is known from *in vitro* experiments about the biochemical behaviour of DDX3X. Specifically, it requires ATP for an efficient dsRNA unwinding, but it can also bind DNA and unwind RNA/DNA duplexes. Similarly, ATP hydrolysis is stimulated by both RNA and DNA (Garbelli *et al.*, 2011; Sharma *et al.*, 2017). On the other hand, DDX3X seems unable to efficiently open DNA/DNA substrates, which has been reported only *in vitro* at high enzyme concentrations. Finally, DDX3X shows a preference for unwinding substrates with single-strand overhangs (Garbelli *et al.*, 2011; Sharma *et al.*, 2017).

2.3 Cellular localization of DDX3X in normal and tumor cells

Initially, DDX3X has been described as a nuclear-cytoplasmic shuttling protein, which binds CRM1 and localizes to the outer side of nuclear membrane pores. Moreover, it has been shown that CRM1 inhibition results in nuclear accumulation of DDX3X (Yedavalli *et al.*, 2004; Schröder *et al.*, 2008). Now we know that through its shuttling, DDX3X is able to release its binding partners from the nucleus to the cytoplasmic side of the nuclear pore facilitated by its enzymatic activity (Yedavalli *et al.*, 2004).

The subcellular localization of DDX3X, however, is still controversial and it seems different in healthy and tumoral cells. Two studies found DDX3X predominantly nuclear in HeLa cell, in the absence of any treatment (Owsianka and Patel, 1999; You *et al.*, 1999). In other studies, DDX3X was found to be a nuclear protein in healthy primary epidermoid cells, but mainly cytoplasmic in squamous cell carcinoma skin cells (Chao *et al.*, 2006).

Recently, nuclear localization of DDX3X has been shown to correlate also with worse patient outcomes in cohorts of breast and colorectal cancers (Heerma Van Voss *et al.*, 2017).

An accumulation of nuclear DDX3X is observed also in early mitosis probably because of its role in centrosome regulation and chromosome segregation. Thus, preliminary speculations suggest that increased nuclear DDX3X expression in tumour samples could be due to the higher number of tumour dividing cells compared to healthy cells (Chen *et al.*, 2017).

In conclusion, it seems that the nuclear-cytoplasmic shuttling of DDX3X is under multiple levels of regulation and could, possibly, be cell type-specific.

2.4 DDX3X and cell proliferation regulation

DDX3X plays specific roles in different cellular proliferation pathways whose deregulation could be associated with tumor transformation (Ariumi, 2014; Bol et al., 2015; Zhao et al., 2016).

One of them is the Wnt/ β -catenin signalling pathway in which β -catenin is the main player. This protein acts as a transcription factor in transducing signals coming from the Wnt signaling pathway to the nucleus and it is also a component of the cadherin complex regulating cell-cell adhesion (Grainger and Willert, 2018). DDX3X acts at the very beginning of the cascade; it is a positive regulator of kinase CK1 ϵ and this interaction leads to increased phosphorylation of the Dvl1 and Dvl2 proteins, which results in increased β -catenin nuclear translocation and transcriptional activation. This DDX3X-role seems independent from its catalytic activity and has to be finely regulated to avoid malignant cell proliferation (Cruciat *et al.*, 2013).

DDX3X is also involved in the regulation of cell-cell adhesion being one of the regulators of the E-cadherin protein expression through the modulation of the levels of its transcription factor Snail (Sun *et al.*, 2011). Specifically, DDX3X appears to increase Snail levels leading to reduced E-cadherin expression. This represents the signal that favours the epithelial-mesenchymal transition causing altered cell mobility. In addition, overexpression of DDX3X also leads to E-cadherin repression, facilitating tumor invasivity (Botlagunta *et al.*, 2011; Bol *et al.*, 2013; Wu *et al.*, 2017).

DDX3X also participates in the regulation of cell cycle progression (Fukumura et al., 2003; Li et al., 2014) and its knockdown resulted in a global delay of the cell cycle (Heerma van Voss *et al.*, 2018). This effect on the cell cycle could be explained by the fact that DDX3X has been shown to positively regulate mRNA translation of cyclin D1, cyclin E1 and the CDK inhibitor p21 (Chang *et al.*, 2006; Chao *et al.*, 2006; Lai *et al.*, 2010).

DDX3X associates also with the DNA damage response protein p53 through a complex network of interactions.

Specifically DDX3X, associating with wild type p53, increases its nuclear accumulation and induces apoptosis in response to DNA damage (Sun *et al.*, 2013). Conversely, in cells expressing mutated p53, DDX3X was shown to inhibit apoptosis. However, the exact molecular mechanisms underlying these differences remain to be elucidated (Sun *et al.*, 2013).

2.5 DDX3X in innate immunity and stress response

Into the cell, one of the most powerful ways to react to pathogens is the activation of innate immunity early responses through the interferon (IFN) production. DDX3X has been shown to stimulate IFN response at different levels. It interacts with the protein kinases TBK1 and IKK ϵ that are both able to phosphorylate DDX3X. These interactions lead to the activation of the transcription factor IRF3 and consequent IFN production (Schröder *et al.*, 2008). In addition, DDX3X directly interacts with IRF3 and is recruited to the IFN promoter itself (Gu *et al.*, 2013). DDX3X also interacts with IPS-1 and TRAF3 proteins that, together with the sensor protein RIG-I, are involved in recognition of viral RNA and activation of the IFN-mediated response (Oshiumi *et al.*, 2010; Gu *et al.*, 2017).

Finally, DDX3X has been shown to stimulate the production of inflammatory cytokines in the NF- κ B axis, however, there are conflicting reports about the effects of DDX3X silencing in the context of NF- κ B regulation (Xiang *et al.*, 2016; Wang *et al.*, 2017).

A very common response of eukaryotic cells to cellular stresses, including viral infections, is to block translation of a subset of mRNA that are sequestered into cytoplasmic RNA-protein complexes called stress granules (SGs). DDX3X is a component of SGs and it seems to be important for SGs formation and translation of stress-specific factors under a variety of pathological conditions (Shih *et al.*, 2012; Pène *et al.*, 2015; Oh *et al.*, 2016).

2.6 DDX3X and cancer

DDX3X overexpression is also associated with large tumor size and high TNM (Tumor, Node and Metastasis) suggesting a possible use of DDX3X as biomarker for cancer prognosis and a target for chemotherapy (Ariumi, 2014; Bol et al., 2015).

A peculiar DDX3X characteristic is that it has contradictory roles in different cancer types acting as either an oncogene or tumor suppressor gene during cancer progression (Zhao *et al.*, 2016). Thinking to its dual role as oncogene or tumor suppressor like a consequence of the different cell lines and different conditions used in different experiments could be a simplification. For sure, it depends on the genetic background present in a certain tumor type too. DDX3X could present mutations leading to its altered function but, due to the multiple pathways in which this protein is involved, loss of DDX3X function can lead to completely different outcomes which are often difficult to be interpreted. This is also evident from the DDX3X silencing experiments leading to a wide range of different and sometimes contradictory phenotypes in different tumor cell lines (Riva and Maga, 2019).

Not only DDX3X is by far involved in a wide range of viral infections, but also its roles in virus-infected patients could be completely different compared to patients without virus infection; it follows that virus infections might be a key factor to explain the altered role of DDX3X in different cancers.

In this paragraph I will summarize all the already characterized cancers types in which a DDX3X involvement has been reported; successively, I will also mention all the strategies already developed to inhibit its functions.

Breast cancer

The oncogenic role of DDX3X in breast cancer is well established. DDX3X was found to be overexpressed in breast cancer patients leading to an uncontrolled growth and proliferation of breast epithelial cells. DDX3X could enhance also cell migration and metastasis both inhibiting E-cadherin expression and via Rac1-mediated signalling pathway (Botlagunta *et al.*, 2008; Bol *et al.*, 2013).

In addition, DDX3X expression in breast cancer was found to be increased by HIF-1 α , a transcriptional factor inducible by hypoxia. As a consequence, E-cadherin expression is reduced, increasing tumor invasivity (Botlagunta *et al.*, 2011).

Since its effects in the context of breast cancer, it has already shown that DDX3X knockdown reduces cell migration but also cell proliferation probably by preventing the G1/S-phase transition of the cell cycle (Ariumi, 2014).

Sarcomas

DDX3X expression is quite high in most sarcomas and its inhibition resulted in decreased survival and tumorigenicity of Ewing sarcoma cells. Proteomic analysis revealed that DDX3X suppression in Ewing sarcoma had an impact on several pathways, including translation, ribosome assembly, cell cycle regulation and DNA damage response, highlighting the complexity of the intracellular functions of DDX3X (Wilky *et al.*, 2016).

Interestingly, DDX3X has been found to be positively regulated by the protein Ezrin, an important regulator of cell motility and a metastasis mediator. Overexpression of Ezrin was shown to increase DDX3X protein levels as well, while its silencing had an opposite effect (Wilky *et al.*, 2016).

It is also known that physical interaction between DDX3X and Ezrin inhibits DDX3X-helicase activity while stimulated ATP hydrolysis.

Since silencing or chemical inhibition of Ezrin has an antimetastatic effect, these results might suggest a link between DDX3X activity and increased osteosarcoma invasivity (Wilky *et al.*, 2016).

Lung cancer

The precise role of DDX3X in lung cancer is still contradictory and it is one of the best examples of the DDX3X-dual role in the cancer context. In some studies, it was reported a DDX3X tumor suppressor behaviour: it causes the induction of p21 expression, the activation of p53 and the repression of its negative regulator MDM2, resulting in increased E-cadherin expression. Indeed, decreased levels of DDX3X via loss of p53 promoted tumor malignancy in lung cancer cells (Wu *et al.*, 2014).

However, in other reports, DDX3X was found to act as an oncogene and its loss of function impaired Wnt signalling pathway and causing disruption of the DDX3- β -catenin axis (Wu *et al.*, 2011, 2014).

This seemingly contradictory role of DDX3X in lung cancer could be connected, at least in some cases, with the combination of both cancer and viral infection. As a matter of fact, it has been shown that human papillomavirus (HPV) E6 protein suppressed DDX3X expression, thus reducing p21 levels. Accordingly, loss of DDX3X was associated with poor survival in early-stage HPV-associated lung cancer (Wu *et al.*, 2011).

Colorectal cancer

It is hypothesized an oncogenic role of DDX3X in colorectal cancer since DDX3X knockdown reduced cell proliferation and caused a G1 arrest (van Voss *et al.*, 2015; Heerma van Voss *et al.*, 2017). It has been shown that DDX3X enhances KRAS oncogene transcription and activates β -catenin signalling through the CK1 ϵ /Dvl1 and HIF-1 α axes, promoting tumor invasion (He *et al.*, 2016; Wu *et al.*, 2017).

However, conflicting results show that DDX3X downregulation leads to Snail upregulation decreasing E-cadherin expression and reducing cell aggregation as well. Consistently, low DDX3X expression in colorectal cancer patients has been correlated with poor prognosis and frequent metastasis (Su *et al.*, 2015).

It derives that the precise DDX3X role in colorectal cancer still needs to be clarified.

Oral squamous cell cancer

DDX3X seems to act as a protective factor especially in non-smoker patients with oral squamous cell cancer (OSCC) (Lee *et al.*, 2014). Vice versa, high DDX3X expression was correlated with poor survival in smokers (van Voss *et al.*, 2015). Again, these differences could be in part explained taking into account the incidence of HPV-positive OSCC both in smokers and in non-smokers patients.

It has also been reported that cigarette smoke carcinogens are able to induce DDX3X expression and, on the other hand, DDX3X was found to enhance oncogene expression in OSCC through interaction with the translational factor eIF3 (Lee *et al.*, 2008; Chen *et al.*, 2018).

Other DDX3X-related cancers

In the last years, an increasing amount of scientific works brought to light DDX3X involvement in many different cancer types, despite the exact molecular mechanisms still need to be clearly elucidated. For example, while initial evidence suggested an oncogenic role of DDX3X overexpression in hepatocellular carcinoma cell lines, other evidence supported its role as an oncosuppressor (Huang *et al.*, 2004; Chang *et al.*, 2006).

Preliminary studies showed an oncogenic role of DDX3X both in glioblastoma multiforme as in gallbladder cancers (Sun *et al.*, 2011; Miao *et al.*, 2013). The DDX3X oncogenic function was also reported in medulloblastoma patients, both in children and in adults. The oncogenic role of DDX3X in medulloblastoma has been proposed to act through the deregulation of the Wnt/ β -catenin axis. More into details, specific DDX3X mutations seem to impair its ATP hydrolysis capacity or helicase activity, suggesting that catalytic function lost was important for the role of DDX3X in promoting medulloblastoma (Chen *et al.*, 2015; Epling *et al.*, 2015; Floor *et al.*, 2016).

In the past few years, thanks to the diffusion of next-generation sequencing techniques, novel DDX3X gene mutations have been identified in extra-nodal NK/T cell lymphoma, nasal type (ENKTL-NT or NKTCL) which haven't been identified before with the traditional Sanger sequencing (Jiang *et al.*, 2015; Dobashi *et al.*, 2016). Also in this case, the mutations abrogate DDX3X helicase activity indicating that the absence of catalytic activity contributes to the pathogenesis and poor prognosis of NKTCL.

Recently, a work by B. Phung and collaborators described for the first time also a DDX3X involvement in melanoma whose progression and aggressiveness are poorly understood up to date (Phung *et al.*, 2019). Specifically, they showed that somatic DDX3X mutations cause a DDX3X depletion associated with impairment in protein synthesis and invasive phenotype. The proliferative signature seems to be caused by the dysregulation of MITF-DDX3X translation network that promotes metastasis (being MITF, in addition to a molecular DDX3X target, also a central transcription factor involved in melanocyte development and a lineage survival oncogene in melanoma) (Phung *et al.*, 2019).

2.7 DDX3X as an anticancer drug target

The previously mentioned contradictory “dual role” of DDX3X in cancer could be complicated to understand since it is necessary to consider the relevant number of different pathways in which this protein is involved and in which way its loss or impaired function could affect them. On the other hand, its so diversified implications in cancer, allow scientists to exploit DDX3X to discover novel promising targets usable in anticancer therapies facilitating the “personalized medicine” to come into clinic.

So far, three DDX3X inhibitors have been tested as potential anticancer agents respectively named RK-33, NZ51 and Ketorolac salt (*Figure 4*).

The most well-known DDX3X inhibitor proposed as a possible candidate for cancer treatment is RK-33 (diimidazo[4,5-d:40,50-f]-[1,3]diazepine). RK-33 makes nine hydrogen bonds contacts with various amino acids of DDX3X (Kondaskar *et al.*, 2011, 2013). Specifically, RK33 binds to the DDX3X ATP-binding cleft and perturbs its helicase activity leading to a series of secondary effects that can vary in different cancer types. It shows an inhibition potency in the low micromolar range in breast, lung, sarcoma and colorectal cancer (Riva and Maga, 2019).

Moreover, BRCA pro/deficient breast cancer cells treated with RK-33 are more sensitive to PARP inhibition with Olaparib and they have an altered expression of proteins involved in mitochondrial translation, cell division and cell cycle progression (Heerma van Voss *et al.*, 2017, 2018).

Also in multiple preclinical lung cancer models, RK-33 molecule was used in combination with radiation representing a possible radio-sensitizer. Unfortunately, *in vivo* results were less impressive (Bol *et al.*, 2015).

RK-33 could be useful also in colorectal cancer treatments since it caused inhibition of Wnt signalling pathway (van Voss *et al.*, 2015).

Another small DDX3X inhibitor which showed some anticancer activity is the ring-expanded nucleoside analogue NZ51, which has been reported to inhibit the ATP dependent helicase activity of DDX3X and was initially developed as an anti-HIV inhibitor (Yedavalli *et al.*, 2008). Later, the same molecule was used also in anti-cancer studies with IC₅₀ values in the low micromolar range (Xie *et al.*, 2015; Riva and Maga, 2019). In breast cancer cell models this molecule decreases motility and cell viability and it was active both under normoxic as in hypoxic conditions with the same potency. Unfortunately, *in vivo* preliminary results in animal models didn't show tumor volume reduction but, hopefully, improvements in drug formulation, dose and delivery could lead to better results (Sun *et al.*, 2011; Xie *et al.*, 2015; Riva and Maga, 2019).

The third DDX3X inhibitor which possesses interesting anticancer activity is Ketorolac salt, ((6)-5-benzoyl-2,3-dihydro-1H-pyrrolizine- 1-carboxylic acid, tris (hydroxymethyl) amino methane salt), a pyrrolizine carboxylic acid derivative. This compound is able to inhibit ATP hydrolysis by directly interacting with DDX3X and forming stable hydrogen bonds with Gly 227, Gly 229, Thr 231 and Ser 228 DDX3X residues (Samal *et al.*, 2015). This compound belongs to the family of non-steroidal anti-inflammatory drugs which are mainly used for the treatment of inflammation and pain and it is already available on the market with the commercial name of Toradol™. Ketorolac salt was shown to suppress early breast cancer relapse in the triple negative subgroup of tumors and it is was used in breast cancer surgery to improve postoperative oncological outcome (<http://clinicaltrials.gov/show/NCT01806259>).

Moreover, this compound inhibits the growth of human oral squamous carcinoma cell models in a dose-dependent manner and reduced tongue lesions in mice models (BALB/c mice) of oral cancer (Riva and Maga, 2019).

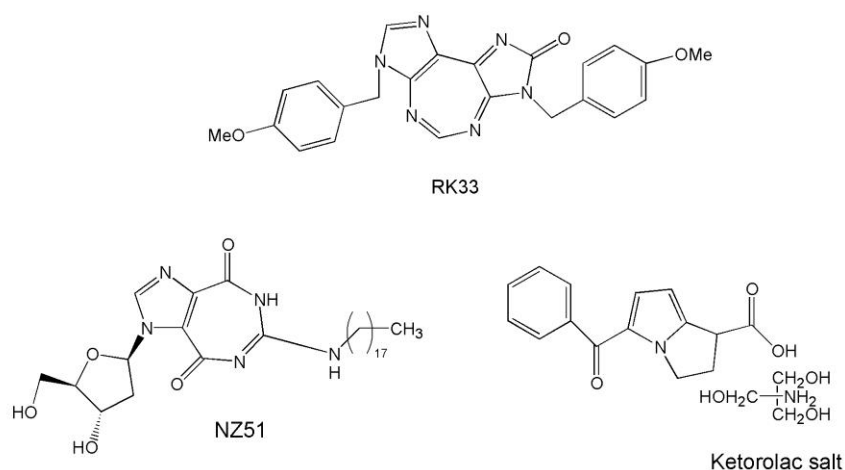


Figure 4: DDX3X inhibitors designed as anticancer agents (Riva and Maga, 2019).

2.8 Genomic stability: DDX3X in the response of ribonucleotide incorporation

It has been recently reported that ribonucleotides (rNMPs) inserted in the genome, both to ensure initiation of replication or inserted erroneously by DNA polymerases (Pols), are not always removed, provoking deleterious consequences (Caldecott, 2014). Specifically, as result of erroneous incorporation by replicative and repair Pols $>10^6$ rNMPs can be present in the mammalian genome, making rNMPs the most abundant type of DNA damage even more than thymidine dimers. The presence of rNMPs makes the sugar-phosphate backbone about 100,000- times more prone to hydrolysis because the presence of the 2'-OH in their ribose ring renders DNA chemically unstable. This may cause DNA breaks, double helix distortion and replication fork arrest; not only, it could affect protein-DNA interactions, nucleosome structure and the activity of DNA-processing enzymes such as topoisomerases and ligases.

Several studies have also linked accumulation of rNMPs in the genome to increased mutagenesis and genetic instability in eukaryotic cells (Caldecott, 2014).

Specific enzymes remove rNMPs from the genome. This removal activity is essential and it is primarily performed by the ribonucleotide excision repair (RER) pathway. In RER, RNaseH2-dependent cleavage at the 5'-side of the rNMP creates a nick which is followed by strand displacement DNA synthesis by Pols δ/ϵ and PCNA, generating a single strand flap terminating with a 5'-rNMP, which is cleaved by either Fen1 or digested by Exo1. Ligase1 seals then the nick between the newly synthesized DNA strand and the parental strand (*Figure 5*). RNaseH2 is believed to be the only enzyme able to incise single rNMPs within a DNA strand activating an error-free RER pathway. Inactivation of RNaseH2 in eukaryotic cells promotes an alternative and highly mutagenic RER pathway, initiated by topoisomerase1 (Topo1)-dependent cleavage of the rNMP (Wallace and Williams, 2014). In *Saccharomyces cerevisiae* in the absence of RNaseH2, Top1 processes the ribonucleotide followed by Srs2-ExoI helicase nuclease pathway which allows an error-free repair mechanism avoiding secondary processing by the highly mutagenic pathway directed by Top1 (Potenski *et al.*, 2014).

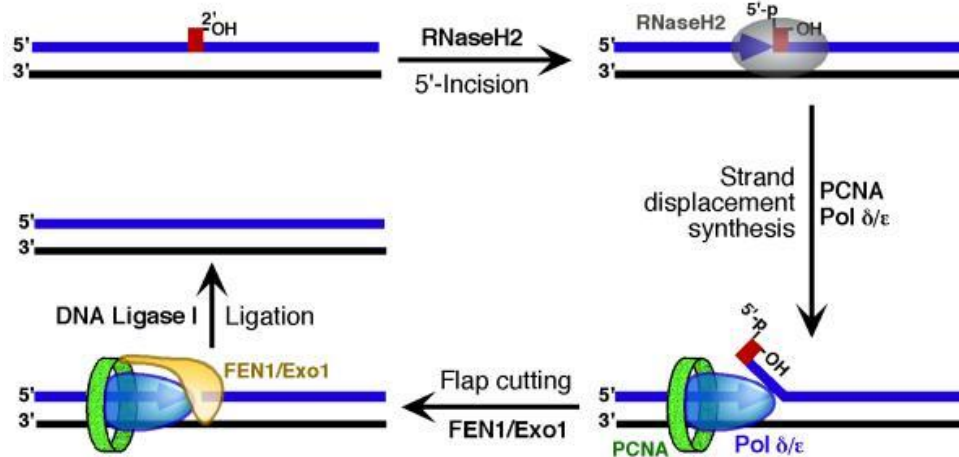


Figure 5: Schematic representation of Ribonucleotide Excision Repair (RER) pathway. RNaseH2 cleaves at the 5'-side of one rNMP (in red) erroneously incorporated into the genome. Pols δ/ϵ and PCNA coordinate strand displacement synthesis generating a single strand flap that is processed by either Fen1 or digested by Exo1. Ligase1 finally seals the nick (Sparks et al., 2012).

It appears clear that the cell must have alternative ways to remove ribonucleotides erroneously inserted into the genome. A hint to that is the fact that in prokaryotes the absence of both RNaseH1 and 2 in mutant strains causes a level of spontaneous mutagenesis that is lower compared to the expected. This means that there are probably some “backup enzymes” into the cell, less effective than RnaseH2, but still able to maintain partial genome integrity (Vaisman and Woodgate, 2015).

In this perspective, published data have implicated DDX3X in the resolution of RNA/DNA hybrids and RNA secondary structures, as well as in the degradation of RNAs (Schröder, 2010). Moreover, unpublished data from our lab demonstrate also a possible exoribonuclease activity of DDX3X in

addition to the already well-known helicase/ATPase activities, similarly to what has been observed with the related DDX1 protein (Li *et al.*, 2008).

Since we know from the literature two well-established examples of RNase/helicase enzymes like Dicer and RNaseR, it is feasible to think at DDX3X as a double-functioning protein as well (Awano *et al.*, 2010; Kidwell *et al.*, 2014).

In eukaryotes, no alternative RNaseH2-like enzymes have been identified up to date, but structural comparison between human DDX3X and RNaseH2 catalytic subunit showed amino acid similarities between the two proteins (successively discussed in Results paragraph 5.2) leading us think to a possible DDX3X involvement in RER pathway.

Taking together all these considerations, one of the aims of my work was to investigate whether DDX3X could be involved in the response to ribonucleotides incorporation functioning as an alternative RNaseH2-type enzyme acting in RER. This will be discussed in detail in the Results section 5.2.

2.9 DDX3X and viral infections

Likewise as it happens in cancer, also in viral infections DDX3X can have a “dual role” acting both as a pro-viral factor as an anti-viral factor (Ariumi, 2014). Thus, while some viruses benefit from DDX3X activity, others inhibit its functions in order to suppress its antiviral effects (Schröder, 2010). Again, this dual role of DDX3X in viral infections is a consequence of its interaction with different viral proteins that are able to modulate its function.

More in general, the different DDX3X-dependent molecular pathways which are important for the infection by different viruses are summarized in *Figure 6*. They can be grouped into three main categories:

- viral genome replication
- regulation of viral gene expression (transcription and translation)
- innate immunity (interferon-mediated response).

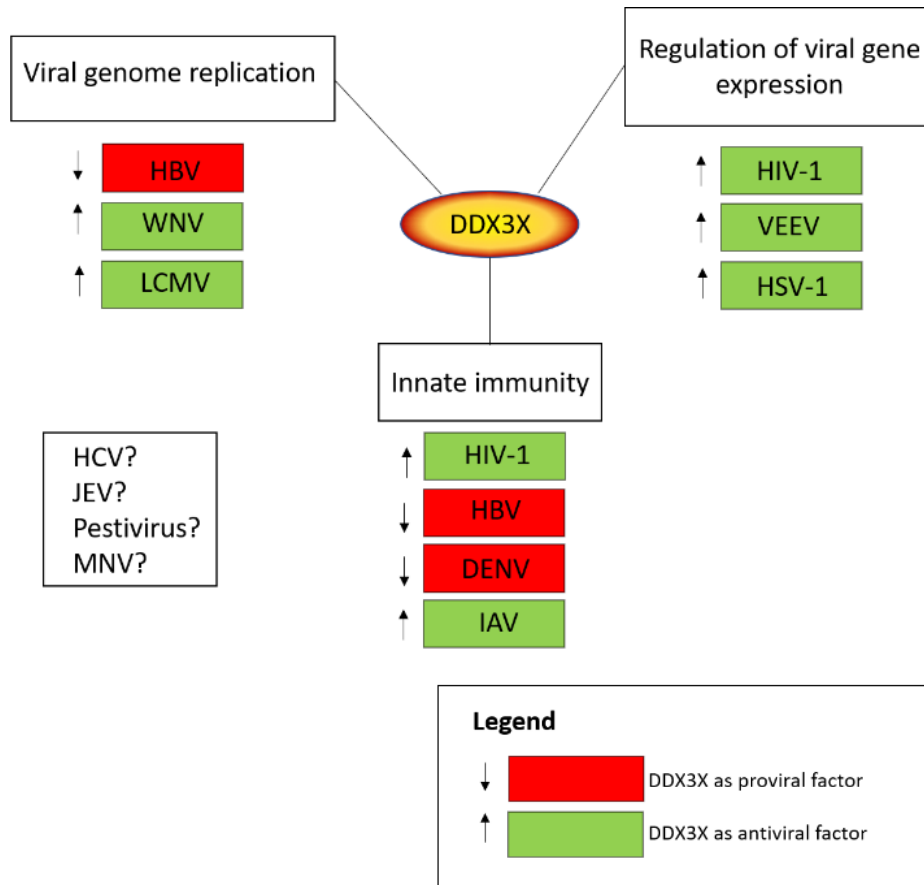


Figure 6: DDX3X can act as proviral (in red) or antiviral (in green) factor depending on the virus and the metabolic pathway involved (Riva and Maga, 2019).

More in general, DDX3X roles in viral replication and gene expression generally require its ATPase/RNA helicase activities, while its functions in innate immunity are mostly independent from of its catalytic activities.

In this paragraph, I will summarize all the viruses in which DDX3X has been shown to have a prominent role in their replication and/or regulation. Successively, I will mention the strategies already developed to inhibit its functions in the context of viral infections.

Human immunodeficiency virus (HIV-1)

The first direct evidence that DDX3X is involved in a case of viral infection came from Yedavalli researches in the context of HIV-1 infection (Yedavalli *et al.*, 2004). Initially it was thought that DDX3X was required to facilitate the Rev-mediated export of unspliced/partially spliced viral mRNAs, interacting with the cellular exportin CRM1 (Mahboobi *et al.*, 2015; Fröhlich *et al.*, 2016). Consistently, knockdown of DDX3X was shown to suppress HIV-1 replication without affecting cell viability (Ishaq *et al.*, 2008; Maga *et al.*, 2011).

However, later studies showed that the DDX3X roles in HIV-1 infection are multiple and not limited to mRNA export. As a matter of fact, DDX3X was shown to be important also for the translation of a subset of cellular mRNAs containing specific secondary structures near their 5' m(7)GTP capping element (Soto-Rifo *et al.*, 2013). Not only, DDX3X interacts also with the viral transcriptional coactivator Tat forming a proteins complex that facilitates a Tat-dependent transcription of viral genes (Lai *et al.*, 2013; Yasuda-Inoue *et al.*, 2013).

DDX3X is also able to act as a “molecular sensor” by binding to HIV-1 RNA in infected cells and activating type I interferon (IFN) response; function that HIV-1 tries to counteract downregulating DDX3X-dependent pathway by activating the cellular kinase PLK1 (Gringhuis *et al.*, 2017).

Hepatitis C virus (HCV)

The DDX3X roles in HCV infections are still contradictory and may be genotype specific.

Initially, it was found that DDX3X C-terminal domain interacts with the HCV core protein both *in vitro* and in cells localizing in cytoplasmic stress granules (P-bodies) suggesting a possible role in modulating viral/cellular RNA turnover (Owsianka and Patel, 1999).

On the other hand, HCV core/DDX3X interaction was found to inhibit the translation of capped cellular mRNAs (Mamiya and Worman, 1999).

The same interaction is also responsible for the DDX3X sequestering, abrogating its ability to stimulate IFN-mediated antiviral response (Oshiumi *et al.*, 2010; Kang *et al.*, 2012).

Human hepatitis B virus (HBV)

DDX3X was found to be incorporated into HBV capsids and, through a physical interaction with the HBV polymerase, is able to inhibit reverse transcription. On the other hand, HBV polymerase was found to sequester DDX3X, competing for its interaction with the TBK/IKK ϵ complex and suppressing IFN response (Wang and Ryu, 2010).

DDX3X has been shown to inhibit HBV replication also in a different mechanism: it was found to repress transcription of HBV genes through direct modulation of the activity of the viral promoter. As a matter of fact, knockdown of DDX3X leads to an increase in HBV transcription, while its overexpression has the opposite effect (Ko *et al.*, 2014).

Thus, DDX3X appears to exert an antiviral effect in HBV infections and this is in agreement with previous findings, demonstrating that DDX3X was downregulated in hepatocellular carcinomas associated to HBV, but not in HCV chronic infections (Chang *et al.*, 2006).

West Nile virus and Dengue virus (WNV, DENV)

DDX3X knockdown significantly suppressed both WNV and DENV infections. Specifically, DDX3X interacts with the viral NS3 protein of WNV at perinuclear foci and with the NS5 viral RNA polymerase of DENV (Khadka *et al.*, 2011; Chahar *et al.*, 2013).

Unfortunately, later studies disagreed and put into discussion the positive role of DDX3X in DENV infections demonstrating that DDX3X knockdown promoted DENV replication, likely through the suppression of the IFN-mediated response (Li *et al.*, 2015). So, the precise role of DDX3X in DENV replication is still controversial.

Human influenza A virus (IAV)

DDX3X was found to interact with the NP and NS1 proteins of human Influenza A virus (IAV). As mentioned above in HCV paragraph, DDX3X is involved in SGs formation. Upon IAV infection, DDX3X was shown to colocalize to SGs together with the viral NP protein. Researches showed that the DDX3X helicase activity was not required for the interaction, but it was essential for viral recruitment at the level of the SGs. Moreover, DDX3X knockdown led to impaired SGs formation and increasing in IAV replication, but only in viruses having a defective viral NS1 protein (Thulasi Raman *et al.*, 2016). So, it has been proposed that DDX3X could be involved in the IAV antiviral response probably mediated through sequestration of NP protein into SGs.

On the other hand, viral NS1 has been shown to inhibit SGs formation. Thus, its interaction with DDX3X might be a mechanism through which IAV counteracts the antiviral effect of DDX3X (Khapersky *et al.*, 2014).

Recently it has been shown that DDX3X interacts also with the multifunctional viral protein PB1-F2. Authors showed that this interaction led to DDX3X degradation constituting a potent INF antagonist and being a

prime pathogenesis determinant for the 1918 influenza strain (Park *et al.*, 2019).

Arenaviruses

Arenaviruses are a large family of RNA viruses unfortunately known because they can cause severe hemorrhagic fevers in humans (such as in the case of Lassa virus (LASV) or Junin virus (JUNV) infections) and neurological diseases (such as in the case of lymphocytic choriomeningitis virus (LCMV)).

L protein of LCMV is an RNA-dependent RNA polymerase protein able to interact with DDX3X. CRISPR-Cas9 knockout of DDX3X, resulted in decreased viral load, suggesting that DDX3X has a proviral function in the context of LCMV infections (Khamina *et al.*, 2017). In another study, DDX3X was found to interact also with the viral NP protein, another essential component of the replication machinery, of all LASV, JUNV and LCMV viruses. Again, silencing of DDX3X causes a reduction in viral proliferation suggesting that DDX3X promotes viral replication; promotion that is dependent on its ATPase and RNA helicase activities (Loureiro *et al.*, 2018).

An additional proviral function of DDX3X was detected in the context of type-I IFN production in LCMV-infected cells. As a matter of fact, DDX3X KD was found to partially restore type-I IFN production in infected cells thus repressing innate immunity. Specifically, it appears that suppression of IFN production by DDX3X was important only at late stage of the infection, while at early time points its proviral function was mainly dependent upon its stimulation of viral RNA synthesis (Loureiro *et al.*, 2018).

Venezuelan equine encephalitis virus (VEEV)

VEEV is a mosquito-borne RNA virus, responsible of frequent zoonotic

infections in humans. DDX3X acts as a proviral factor interacting with the replicative viral protein nsP3. As a matter of fact, DDX3X KD potently inhibits viral replication. The viral nsP3 protein localizes to virus-induced SGs and interacts with several translation factors, leading to the hypothesis that recruitment of DDX3X might facilitate viral mRNAs translation (Amaya *et al.*, 2016).

Japanese encephalitis virus (JEV)

JEV normally causes epidemic viral encephalitis in humans and animals. DDX3X has been found to interact with the viral replicative proteins NS3 and NS5 both *in vitro* and in infected cells. Again, DDX3X KD inhibited viral replication meaning that DDX3X acts as a proviral factor in the context of JEV replication. This is possible because DDX3X upregulated viral mRNA translation, through the binding of 5'- and 3'-UTR regions of the JEV genome (Li *et al.*, 2014).

Pestiviruses

Pestiviruses are a group of RNA viruses belonging to the *Flavivirus* family, that includes the bovine viral diarrhea virus (BVDV) responsible of frequent epidemics in cattle. Jefferson and collaborators demonstrated that the viral protease N^{pro} interacts with DDX3X at cytoplasmatic SGs together with several other cellular proteins. It is known that N^{pro} counteracts IFN response in infected cells, inhibiting the transcriptional factor IRF3, but the exact role of N^{pro} /DDX3X interaction in the viral life cycle has not been understood up to now (Jefferson *et al.*, 2014).

Murine Norovirus (MNV)

MNV is routinely used as a surrogate model for studying the viral life cycle

since Noroviruses are one of the most frequent causes of gastroenteritis and no efficient culture system has been established for the human virus. By immunostaining experiments, DDX3X was identified as host factor interacting with the MNV genome. In addition, knockdown of DDX3X reduced MNV replication (Vashist *et al.*, 2012). However, like in Pestiviruses, the molecular mechanism underlying the proviral function of DDX3X in MNV infection has not been elucidated.

Herpesviruses

Herpesviruses have large DNA-based genomes and represent the perfect example to demonstrate that DDX3X is involved not only in the replication of RNA-based genome, but also of DNA-based genome. As a matter of fact, DDX3X has been found to be incorporated into the virions of herpes simplex virus type 1 (HSV-1) (Loret *et al.*, 2008). Interestingly it has been shown that exist an optimal range of DDX3X protein that could be beneficial for HSV-1 replication. Specifically, an excessive overexpression of DDX3X was detrimental to HSV-1 replication, but HSV-1 replication in a cell line harboring a temperature sensitive mutant of DDX3X was strongly reduced at no permissive temperature.

In the context of HSV-1 infection, DDX3X was required for proper viral particles assembly too. Essential is also the ATPase/helicase activities of DDX3X, but not its ability to stimulate IFN response (Khadvijam *et al.*, 2017).

Another herpesvirus which exploits DDX3X is the human cytomegalovirus (HCMV), but the precise molecular mechanism determining the DDX3X proviral effect has not been determined yet. What we know up to date is that DDX3X associates with HCMV transcripts and is incorporated into mature viral particles. DDX3X protein levels are increased upon HCMV infection and DDX3X KD reduces HCMV replication (Cavignac *et al.*, 2015; Lenarcic *et al.*, 2015).

Vaccinia virus (VACV)

In the case of VACV, DDX3X shows an antiviral behavior. Schroder and collaborators showed that the viral K7 protein of VACV inhibits the cellular IFN response through the sequestration of DDX3X. This interaction specifically impairs the TBK1/IKK ϵ -IRF3 pathway (Schröder *et al.*, 2008). Structural studies mapped the DDX3X domain necessary for this interaction in its N-terminal region (aa 82-88) allowing the interaction with an hydrophobic cleft of K7 protein (Kalverda *et al.*, 2009; Oda *et al.*, 2009).

Adenovirus

Last, but not least, the Bovine Adenovirus 3 (BAdV-3) protein pVIII was found to interact with DDX3X. This interaction led to the inhibition of the host mRNA translation *in vitro* and *in vivo*, by disturbing the DDX3X-dependent recruitment of the eIF3 translation factor to the 5'-cap structure of cellular mRNAs (Ayalew *et al.*, 2016).

2.10 DDX3X as a target for antiviral therapies

As extensively described above, DDX3X appears to play prominent roles in the context of the replication of several RNA and DNA viruses sometimes acting as a proviral factor, sometimes as an antiviral factor. Its positive role in the life cycle of several different viruses, for many of which there are currently no available therapies, it is considered interesting for the development of cellular-based antiviral chemotherapies.

Starting from the original observation that DDX3X can act as a cellular cofactor for HIV-1, a series of ring-expanded nucleoside analogues were identified by a random-screening approach. These molecules were able to inhibit DDX3X RNA helicase activity and to suppress HIV-1 replication (Ariumi, 2014). Simultaneously, our group started a rational drug design

approach to identify specific DDX3X inhibitors. We built a structure-based pharmacophoric model starting from the X-ray crystallographic structure of the human helicase DDX3X in complex with AMP (PDB code: 2I4I). This model was used in a virtual screening approach of commercial databases that allowed the identification of a suitable chemical scaffolds, which, after further optimization, led to the development of rhodanine and triazine derivatives as the first classes of ATP-competitive inhibitors of DDX3X active against HIV-1 replication (named FE inhibitors and show in *Figure 7*) (Maga *et al.*, 2008, 2011).

Unfortunately, the ATP binding site of DDX3X is structurally similar to many other ATP-hydrolysing enzymes, so we moved our attention next to the RNA binding domain, with the aim of improving inhibitor selectivity. We built a second homology model based on the structure of the closed conformation of the DEAD-box helicase eIF4AIII17 due to the absence at that moment of three-dimensional structures of human DDX3X in the catalytically competent complex with the RNA substrate. This approach was useful for a new drug design procedure that finally resulted in the identification of a class of N,N'-diarylurea derivatives (*Compound 6* in the *Figure 7*) able to inhibit both the helicase activity of DDX3X and to suppress viral replication in HIV-1 infected cells (Radi *et al.*, 2012; Brai *et al.*, 2016). Further molecules optimizations led to the discovery of a novel family of RNA-competitive inhibitors of DDX3X helicase activity. The best compound of this series, 16d (1-(4-(4-Methyl-1H-1,2,3-triazol-1-yl)phenyl)-3-*o*-tolylurea) shown in *Figure 7*, was able to suppress the replication of different RNA viruses (HIV-1, HCV, WNV, DENV). Not only, 16d was active also against HIV-1 strains resistant to clinically used antiretroviral drugs, showing virtually no toxicity in cellular and animal models (Brai *et al.*, 2016).

All these results suggested that DDX3X might potentially be exploited as a target for the development of broad-spectrum antiviral agents.

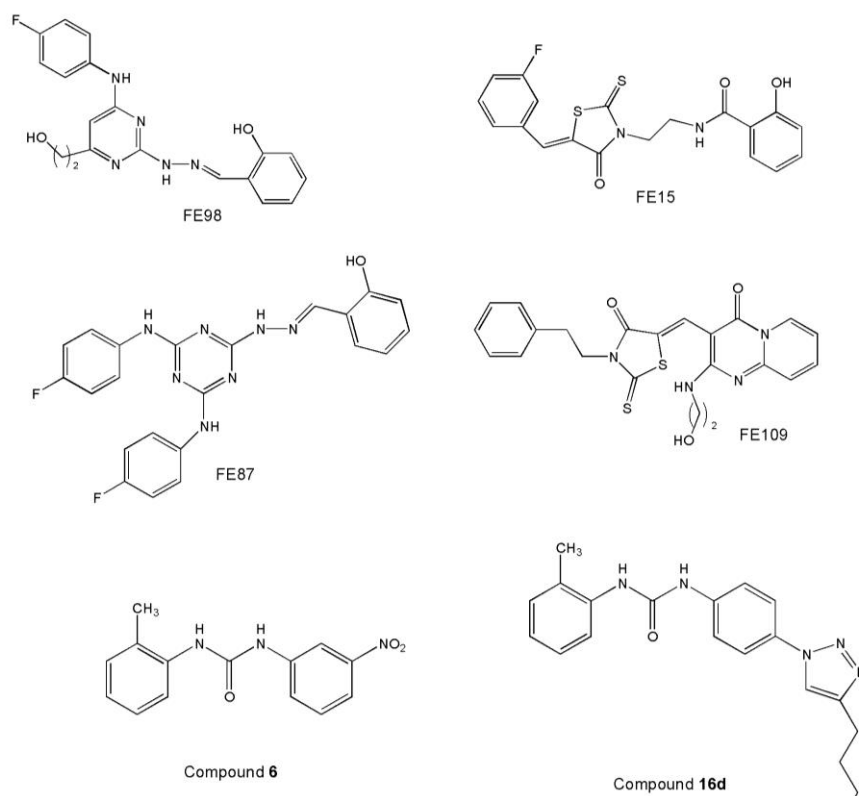


Figure 7: DDX3X inhibitors designed as antiviral agents (Riva and Maga, 2019).

3. Aims of the research

Despite the increasing emergency of new viral epidemics due to the spread of the arthropod vectors and the increased movement of people among different geographical areas, there are not approved drugs against emerging viruses like DENV, WNV, JEV, CHIKV and ZIKV.

My research group has ten-years' experience in the biochemical characterization of the human DEAD-box helicase 3 (DDX3X). We had already demonstrated that DDX3X could represent a promising antiviral target being able to suppress the replication of different RNA viruses (HIV-1, HCV, WNV, DENV). Not only, a previously characterized molecule named *16d* was active against HIV-1 strains resistant to clinically used antiretroviral drugs, showing virtually no toxicity in cellular and animal models (Brai *et al.*, 2016).

One of the aims of my research project was to find new molecules improving the chemical characteristics of the previous ones and their selectivity. This was possible both creating new molecule scaffolds able to recognize the helicase binding pocket of DDX3X, both creating a completely new class of molecules able to recognize a unique motif of DDX3X. This motif is only ten residues long (250–259, E-A-L-R-A-M-K-E-N-G) and is not generally found in other human DExD-box helicases and/or cellular proteins representing a promising druggable target (Garbelli *et al.*, 2011).

In addition to the well-known DDX3X involvements in the replication of different viruses, in the last years emerge that DDX3X is also associated with large tumor size and high TNM (Tumor, Node and Metastasis) suggesting a possible use of DDX3X as biomarker for cancer prognosis and a target for chemotherapy (Ariumi, 2014; Bol *et al.*, 2015). The specific DDX3X role in cancer needs further investigations and it is quite peculiar since DDX3X has contradictory roles in different cancer types acting either as an oncogene or tumor suppressor gene during cancer progression (Zhao *et al.*, 2016).

Chromatin immunoprecipitation analysis also demonstrated a possible DDX3X role in genome stability maintenance: it binds promoter regions regulating the expression of two DNA repair factors, DDB2 and XPA (Chan *et al.*, 2019). Published data have implicated DDX3X in the resolution of RNA/DNA hybrids and RNA secondary structures, as well as in the degradation of RNAs (Schröder, 2010).

Moreover, unpublished data from our lab demonstrated also a possible exoribonuclease activity of DDX3X in addition to the already-known helicase/ATPase activities. From these preliminary observations, we decided to examine in depth the role of DDX3X in genome stability.

Specifically, the second aim of my research project was to verify if DDX3X could possess an RNaseH2-like activity being able to process ribonucleotides erroneously inserted into the genome with the following risks of helix distortion and DNA breaks formation.

I divided my PhD thesis elaborate in two parts that will be maintained from this moment in advance and I entitled them as following:

- DDX3X AS A PRIME CELLULAR TARGET TO FIGHT OLD AND EMERGING VIRUSES
- AN ALTERNATIVE RIBONUCLEOTIDE EXCISION REPAIR BY THE RNA HELICASE/NUCLEASE DDX3X

I deepened both the DDX3X involvement in virus infection as well as in genome stability. In the first case, I contributed to develop new antiviral chemotherapeutics based on a cellular target, DDX3X. Then, I shed light on a possible DDX3X involvement in genome stability as a new RNaseH2-like enzyme never reported in literature up to date.

This double-aim reflects in part the double- (or better, multiple-) roles of DDX3X into the cells, one of the most multifunctional proteins that we know.

4. Materials and methods

4.1 DDX3X AS A PRIME CELLULAR TARGET TO FIGHT OLD AND EMERGING VIRUSES

4.1.1 Chemistry

Compounds were designed and synthesized by our collaborators at the University of Siena (Prof. Maurizio Botta). For all the details about the anti-WNV compounds synthesis see the work of Brai and collaborators (Brai *et al.*, 2019).

All the chemical specifications for UM compounds are not reported in this manuscript since they will be part of a Patent Application currently in progress.

4.1.2 Proteins production and purification

Human recombinant full length DDX3X was cloned in the *E. coli* expression vector pET-30a(+). ShuffleT7 *E. coli* cells were transformed with the plasmid and grown at 37°C up to OD₆₀₀ = 0.7. DDX3X expression was induced with 0.5 mM IPTG at 15°C O/N. Cells were harvested by centrifugation, lysed, and the crude extract centrifuged at 100.000x g for 60 min at 4°C in a Beckman centrifuge before being loaded onto a FPLC Ni-NTA column (GE Healthcare). Column was equilibrated in Buffer A (50 mM Tris-HCl pH 8.0, 250 mM NaCl, 25 mM Imidazole and 20% glycerol). After extensive washing in Buffer A, the column was eluted with a linear gradient in Buffer A from 25 mM to 250 mM Imidazole for 8 column volumes. Proteins in the eluted fractions were visualized on SDS-PAGE and tested for the presence of DDX3X by Western blot with anti-DDX3X A300-475A (BETHYL) polyclonal antibody at 1:4000 dilution in 5% milk. Fractions containing the purest DDX3X protein were pooled and dialyzed in Slide-A-Lyzer® MINI Dialysis Devices 20K MWCO (Thermo Scientific) for 3 hours (25 mM Tris

HCl pH 8.0, 0.5 mM DTT, 100 mM NaCl, Glycerol 20%) in order to remove the salt excess. Finally, proteins were stored at -80°C.

The double mutant protein E256A/R262A and the single mutants E256A and R262A were cloned in the *E. coli* expression vector pET-30a(+) and BL21(DE3) cells were transformed with the plasmids. Proteins induction and purification were the same of the full-length protein. Only the double mutant E256A/R262A was dialysed as the wild-type enzyme, whereas the single mutants E256A and R262A were maintained in elution buffer avoiding further loss of material due to the dialysis procedure.

4.1.3 Helicase assay based on Fluorescence Resonance Energy Transfer (FRET)

The dsRNA substrate for the helicase assay was prepared by hybridizing two ssRNA oligonucleotides with the following sequences:

Fluo-FAM

5' UUUUUUUUUUUUUUUUAGUACCGCCACCCUCAGAACC 3'

Qu-BHQ1

5' GGUUCUGAGGGUGGCGGUACUA 3'

DNA capture

5' TAGTACCGCCACCCTCAGAACC 3'

The sequence portion of the Fluo-FAM that is complementary to Qu-BHQ1 is underlined. Fluo-FAM carries a 6-carboxyfluorescein fluorophore at its 3' end, while Qu-BHQ1 carries a Black Hole quencher group at its 5' end. The DNA capture oligonucleotide is complementary to the Qu-BHQ1 oligonucleotide but bears no modifications.

Helicase assay using the dsRNA substrate was performed in 20 mM Tris HCl (pH 8), 70 mM KCl, 2 mM MgCl₂, 2 mM dithiothreitol, 12 units RNasin (Promega), 2 mM ATP, 50 nM dsRNA and 100 nM capture strand in 20 µl of reaction volume. The unwinding reaction was started by adding 60 pmols of DDX3X recombinant protein and carried out at 37°C for 40 min using a

LightCycler 480 instrument (Roche). The fluorescence intensity was recorded every 30s.

Data of fluorescence signal were analyzed by linear interpolation and the corresponding slope values were used to determine the apparent unwinding rate.

4.1.4 ATPase assay

The ATPase activity was determined, as previously described (Franca *et al.*, 2007; Garbelli *et al.*, 2011), by directly monitoring [γ -³³P] ATP hydrolysis by thin-layer chromatography (TLC).

[γ -³³P] ATP (3000Ci/mmol) and TLC PEI Cellulose F plates were respectively purchased from Hartmann Analytic and Merck.

The reaction was carried out in a final volume of 5 μ l which contained: different amount of DDX3X proteins as specified in the figure legends, 0.1 μ M [γ -³³P] ATP (3000 Ci/mmol) as tracer plus 1 μ M of cold ATP, 5 mM MgCl₂ and nucleic acids as indicated. Samples were incubated for 30 minutes at room temperature and 1.5 μ l of the reaction were dotted onto TLC sheets of polyethyleneimine cellulose. The reaction products were separated by ascending chromatography with 0.5 M KH₂PO₄ (pH 3.4). The intensities of the radioactive bands corresponding to ATP and Pi were quantified by densitometric scanning with PhosphoImager (Typhoon-TRIO, GE Healthcare).

The ATPase activity was also determined using the commercial kit ADP-Glo Kinase Assay (Promega) as previously described in the work of Brai and collaborators (Brai *et al.*, 2016). Reaction was performed in 30 mM Tris HCl pH 8, 9 mM MgCl₂, 0.05 mg/mL BSA, 50 μ M ATP, nucleic acids as indicated and different amount of DDX3X proteins as specified in the figure legends. Reaction was performed following the ADP-Glo Kinase Assay Protocol, and luminescence was measured with MicroBeta TriLux instrument (Perkin-Elmer).

4.1.5 Kinetic analysis

Data (in triplicate) were plotted and analysed by least-squares nonlinear regression, with the computer program GraphPad Prism 6.0. Data were fitted to the following equation:

$$(1) \quad v = V_{\max} / (1 + (K_m / [S]^n))$$

Where v is the apparent reaction velocity at each substrate concentration, V_{\max} is the maximum rate of the reaction, K_m is the Michaelis-Menten constant, S is the variable substrate concentration, n is an exponential term to take into account sigmoidal dose–response curves due to the positive cooperativity of DDX3X binding to RNA (Sharma *et al.*, 2017).

The turnover constant k_{cat} was calculated as $V_{\max} / [\text{enzyme concentration}]$ and the RNA substrate binding efficiency of our enzymes was calculated as the k_{cat}/K_m ratio.

For the inhibition assays, the IC_{50} values have been calculated from dose–response curves. Data (in triplicate) were plotted and analysed by least-squares nonlinear regression, according to the method of Marquardt–Levenberg, with the computer program GraphPad Prism 6.0. Data were fitted to the following equation:

$$(2) \quad E_{\text{obs}} = E_{\max} / (1 + ([I]/IC_{50})^n)$$

where E_{obs} is the observed enzymatic activity in the presence of each inhibitor dose $[I]$; E_{\max} is the maximal enzymatic activity in the absence of the inhibitor; n is an exponential term to take into account sigmoidal dose–response curves.

4.1.6 Cell extracts and DDX3X quantification

10^7 cells (HUH-7/VERO/A549) (Brai *et al.*, 2019) were ruptured with a Dounce homogenizer in Lysis Buffer (50 mM Tris HCl pH 8.0, 0.1% SDS, 350 mM NaCl, 0.25% Triton X-100, protease inhibitor cocktail (Sigma-Aldrich)). The lysate was incubated 30 min on ice, sonicated for 5 min (at 30 s intervals) and centrifuged at $15.000 \times g$ for 10 min at 4°C . The protein concentration in the supernatant (crude extract) was quantified with Bradford assay (Bio-Rad). For DDX3X quantification, increasing concentrations of crude extract (5 μg , 10 μg , 20 μg , 40 μg) were loaded on a SDS-PAGE alongside with known concentrations (50 ng, 100 ng, 150 ng, 200 ng) of recombinant purified DDX3X. Separated proteins were subjected to Western Blot analysis with anti-DDX3X A300-A475 (*BETHYL*) at 1:2000 dilution in 5% milk. The blot was next incubated with 1:5000 HRP-conjugated secondary antibody (Jackson ImmunoResearch) and the bands corresponding to DDX3X were visualized with Enhanced Chemiluminescent Substrate (Westar Nova 2.0, Cyanagen) using a ChemiDoc™ XRS (Bio-Rad) apparatus. The intensity of the bands was measured by densitometry and the values obtained for the purified DDX3X were plotted as a function of the protein concentration and analyzed by linear interpolation to derive a reference curve, whose slope corresponded to the estimated intensity (I) \times ng^{-1} (DDX3X) value. This parameter was used to calculate the $I \times \text{ng}^{-1}$ values for the DDX3X in the cell extract, from the intensities of the DDX3X bands in the corresponding cell extract (CE) samples. The mean $I \times \text{ng}^{-1}$ (CE) value was used to calculate the ng of DDX3X \times μL^{-1} of extract, and then the total ng of DDX3X present in the extract. This value was divided for the total number of cells used (10^7), to derive the ng DDX3X/cell. Based on the known molecular weight of DDX3X, the Avogadro number and assuming a mean cellular volume of 6.55×10^{-11} L, the final molar concentration of DDX3X per cell was calculated. Each experiment was repeated three times, with each blot carrying a reference curve alongside the extract samples, to account for variations in loading/transfer efficiency. The reference $I \times \text{ng}^{-1}$ (DDX3X) value obtained was anyway comparable across the different experiments ($\pm 20\%$ variation).

4.1.7 Antiviral assay: WNV and DENV inhibitory viral plaque reduction assay

This assay was conducted by our collaborators under the supervision of Professor Giannecchini (University of Florence).

The protocol used was as published for WNV (Brai *et al.*, 2019). Huh7 cells, derived from human hepatoma were used for the viral plaque reduction assay. Cells were cultured in Dulbecco's Modified Eagle's Medium (DMEM; SIGMA) supplemented with 10% Fetal Bovine Serum (FBS; SIGMA) and 1% Penicillin/Streptomycin (SIGMA). WNV (strain of lineage 2) or DENV-2 (New Guinea C strain) viral stock, consisting of cell-free supernatants of acutely infected Huh7 cells, were aliquoted and stored at -80°C until used. Titration of the viral stocks as plaque-forming unit (PFU) was carried out in Huh7 cells. WNV was used to infect Huh7 cell line in duplicate and viral plaques were visualized 4 days following infection. Briefly, 6-well plates were seeded with 2.5×10^5 cells in 3 ml of growth medium and maintained overnight at 37°C with 5% CO_2 . The day of infection, medium was removed and Huh7 cells (monolayers at 80–90% confluence) were infected with WNV and DENV-2 viral stocks with a multiplicity of infection (MOI) respectively of 0.1 and 0.005 in a final volume of 0.3 ml. Then, cells were incubated for 1 h at 37°C with 5% CO_2 . Prior to the addition of inhibitory compounds, cells were washed with PBS 1X. Finally, 30 μL dimethylsulfoxide (DMSO) alone (viral positive control) or with 10-fold serial dilutions of DDX3X inhibitory compounds were immediately added in duplicates together with 300 μl of fresh DMEM complete medium (compound final concentrations of 100, 10, 1, 0.1, and 0.01 μM). Ribavirin (1- β -d-Ribofuranosyl-1,2,4-Triazole-3-Carboxamide; SIGMA) diluted in DMSO was used as inhibitory reference control. Then, the overlay medium composed by 0.5% Sea Plaque Agarose (Lonza) diluted in propagation medium was added to each well. After 4 days of incubation at 37°C , the monolayers were fixed with methanol (Carlo Erba Chemicals) and stained with 0.1% crystal violet (Carlo Erba Chemicals) and the viral titers were calculated by Plaque forming unit (PFU) counting. Percent of Plaque reduction activity was calculated by dividing the average PFU of treated samples by the average of DMSO-treated samples (viral positive control). Fifty percent inhibitory concentrations (IC_{50}) were

calculated using the predicted exponential growth function in Microsoft Excel, which uses existing x-y data to estimate the corresponding anti DDX3X compound concentration (x) from a known value (y), which in this case was 50% PFU. Mean IC₅₀ + standard deviations (SD) were calculated using all replicates. All experiments were repeated at least twice. All experimental procedures were conducted under biosafety level 3 containment at University of Florence.

4.1.8 Cytotoxicity assay

This assay was conducted by our collaborators under the supervision of Professor Giannecchini (University of Florence).

2.5×10^4 Huh7 cells were seeded per well in a flat-bottom 96-well culture plates and led overnight at 37°C degrees in 5% CO₂ atmosphere. Then, the medium was removed and cells were washed twice with PBS, treated with 100 µl of DMEM with 10 µl DMSO alone (cell positive control) or with various concentrations of DDX3X inhibitory compounds under study (compound final concentrations of 100, 10, 1, 0.1, and 0.01 µM) and incubated for 3 days at 37°C in a CO₂ atmosphere. After treatment, an MTT (3-(4,5-dimethylthiazol-2-yl)-2,5-diphenyltetrazolium bromide) kit (Roche, Milan, Italy) was used according to the supplier's instructions, and the absorbance of each well was determined using a microplate spectrophotometer at a wavelength of 570 nm. Cytotoxicity was calculated by dividing the average optical density of treated samples by the average of DMSO-treated samples (cell positive control). Results were confirmed measuring cytotoxicity with a second approach: the CellTiter-Glo 2.0 assay (Promega). Cells were seeded at 40,000 cells/well in duplicate in presence of serial dilutions of compounds and incubated for 72 hours. Cell viability was calculated by measuring cellular ATP as a marker of metabolically active cells through a luciferase based chemical reaction and expressed as the concentration that reduce cell viability by 50%.

All the following methods:

- *Virus RNA quantification and Capsid protein detection assay*
- *ADME assay*
- *Parallel Artificial Membrane Permeability Assay (PAMPA and PAMPA-BBB).*
- *Water Solubility Assay*
- *Microsomal Stability Assay.*

were all performed by our collaborators at the University of Siena and Florence (Professors Botta and Giannecchini respectively) and all the protocols used were already published and available. (Brai *et al.*, 2019)

4.1.9 Site directed mutagenesis

The double mutant E256A/R262A was obtained by Biofab Research srl (Rome, Italy) and cloned into a pET30a (Novagen) expression vector. The two single mutants E256A and R262A were obtained by site-directed mutagenesis as described in the work of Liu and collaborators (Liu and Naismith, 2008).

Specifically, the DDX3X double mutant E256A/R262A cDNA cloned into pET30a was used to obtain the single mutants. Couples of primers of 36/42 bp overlapping for the whole length except for a nucleotide, were used that reverts one of the two alanines into the previous wild type amino acid. In order to quickly verify the introduction of the correct mutation a restriction site of SfiI was removed from the gene sequence of single mutants, without introducing any additional amino acid substitution.

The sequences of the primers were as follows (primer-primer overlapping sequences are underlined):

E256A fw 5' tatgggcgccgcaaacaataccaatctccttggtattagca 3'

E256A rv 5' gcggcgccataccttcattggccttcattgcct 3'

R262A fw 5' atgaaggaaaatggaaggtatggggcccgcaaacaa 3'

R262A rv 5' atttccttcattgcctcaaagcctcgctggacc 3'

The mutagenesis was carried out in the following reaction mixture: Pfu buffer 1X (Promega), dNTPs 0.2 mM (Roche Molecular Biochemicals), Primers 1 μ M and 3 U of Pfu (Promega).

The PCR cycles were: 94°C for 2 minutes (to denature the template DNA); 3 amplification cycles at 94°C for 1 minute, 62°C for 1 minute and 68°C for 12 minutes. After that, additional 12 amplification cycles were performed as follow: 94°C for 1 minute, 57°C for 1 minute and 68°C for 12 minutes. The PCR cycles were followed by an extension step at 68°C for 60 minutes.

The PCR products were treated with 10 units of DpnI (Promega) at 37°C for 2 hours and then 10 μ l of each PCR reactions were analysed by agarose gel electrophoresis.

Amplified DNA was transformed into *E. coli* DH5 α competent cells by heat shock following standard protocol. The transformed cells were spread on a LB plate containing 50 μ g/ μ l Kanamycin and incubated at 37°C over night. Colonies from each plate were grown and the plasmid DNA was isolated. To verify the mutations, 400 ng of plasmid DNA was first linearized with 10 units of Hind III (Promega) for 1 hour at 37 °C and then digested with 12 units of Sfi I (Promega) for 5 hours at 50 °C. Positive colonies were sent to Eurofins Genomics (Ebersberg, Germany) for Sanger sequencing to verify correct mutations insertions.

4.2 AN ALTERNATIVE RIBONUCLEOTIDE EXCISION REPAIR BY THE RNA HELICASE/NUCLEASE DDX3X

4.2.1 Chemicals

Unlabelled dNTPs were from Roche Molecular Biochemicals. All other reagents were of analytical grade and were purchased from Merck or Fluka.

4.2.2 Nucleic acids substrates

Oligonucleotides were purchased from Biomers.net GmbH (Ulm, Germany) or Metabion AG (Steinkirchen, Germany). The sequences of the substrates used are (bold letters indicate ribonucleotides):

ss 24mer Substrate 1

3'-GATGCCGAGTGTGATAGAGTGTGA-5'FAM

ds 24/24mer Substrate 2

5'-CTACGGCTCACACTATCTCACACT-3'

3'-GATGCCGAGTGTGATAGAGTGTGA-5'FAM

ds 24/24mer Substrate 3

5'-CTACGGCTCACACTATCTCACACT-3'

3'-GATGCCGAGTGTGATAGAGTGTGA-5'FAM

ds 55/55 mer Substrate 4

5'-

CCAACACACAACACCGTGTGAATTCGGCACTGGCCGTCGTATGCT

CTTGGTTGTA -3'

3'-

GGTTGTGTGTTGTGGCACACTTAGCCGTGAACCGGCAGCATAACG

AGAACCAACAT-5'FAM

4.2.3 Proteins production and purification

Human recombinant full-length DDX3X was purified as already specified in Paragraph 4.1.2. Human recombinant D357A/D350A (DADA) was expressed and purified as described in Garbelli *et al.*, 2011. Human recombinant Pols β (Crespan *et al.*, 2016) and δ (van Loon *et al.*, 2009) were expressed and purified as described. The plasmid pET-hH2ABC and the *E. coli* MIC1066 [rnhA339:cat, recB270(Ts)] strain for the expression of recombinant human trimeric RNaseH2 were kindly provided by Prof. Robert Crouch (NIHCD, Bethesda). RNaseH2 was expressed and purified as described (Chon *et al.*, 2009). Human Fen-1 and Human DNA ligase1 were both purchased from Origene (Rockville, United States).

4.2.4 2-D electrophoresis (2-DE) and mass spectrometry analysis

This part of the work was done by our collaborators in Siena University supervised by Professor Bini. Protein samples were treated with a conventional 2-DE buffer composed of 8 M urea, 4% (w/v) CHAPS, and 1% (w/v) dithioerythritol (DTE) and stored at -20°C until use. The first dimension (IEF, the isoelectrofocusing) was performed on 18 cm long, non-linear pH 3-10 gradient Immobiline-polyacrylamide DryStrip gels (IPG strips; GE Healthcare, Uppsala, Sweden) using the Ettan™ IPGphor system (GE Healthcare). For MS-preparative gels, strips were rehydrated with 60 μ g of protein in 350 μ l of 2-DE buffer and 2% (v/v) IPG-buffer (pH 3-10; GE Healthcare), for 1 h at 0 V and overnight at 30 V, at 16°C. IEF was achieved

at 16 °C as follows: 200 V for 8 h, from 200 V to 3500 V in 2 h, 3500 V for 2 h, from 3500 V to 5000 V in 2 h, 5000 V for 3 h, from 5000 V to 8000 V in 1 h, 8000 V for 1 h, from 8000 V to 10.000 V in 1 h, 10.000 V until a total of 100.000 Vh was reached. The focused strips were equilibrated for 12 min in 6 M urea, 30% (v/v) glycerol, 2% (w/v) SDS, 0.05 M Tris-HCl pH 6.8, 2% (w/v) DTE; and for further 5 min in 6 M urea, 30% (v/v) glycerol, 2% (w/v) SDS, 0.05 M Tris-HCl pH 6.8, 2.5% (w/v) iodoacetamide, and trace of bromophenol blue. The second dimension (SDS-PAGE) was run on house-made 9-16% polyacrylamide linear gradient gels. at 10°C, in Protean II Multi Cell (Bio-Rad Laboratories, Hercules, CA) applying 40 mA/gel constant current. The run was stopped when the bromophenol blue dye reached the end of the gel. Analytical and MS-preparative gels were stained with ammoniacal silver nitrate and with a MS-compatible silver staining, respectively. 2-DE stained gels were scanned using the ImageScanner III (GE Healthcare), and the acquired images were analyzed by ImageMaster 2D Platinum v6.0 software (GE Healthcare).

Protein spots cut from MS-preparative gels, were destained and acetonitrile dehydrated. Spots were rehydrated in trypsin solution (Sigma Aldrich, Italy) and in-gel trypsin digested overnight at 37 °C. 1.25 µl of each tryptic peptide sample was directly spotted onto the MALDI target and air-dried. Then 0.75 µl of matrix solution (a saturated solution of alpha-cyano-4-hydroxycinnamic acid in 50% v/v acetonitrile and 0.5% v/v trifluoroacetic acid) was added to the dried samples and allowed to dry again. Protein identification was carried out by peptide mass fingerprinting (PMF) using an Ultraflex III MALDI-TOF/TOF mass spectrometer (Bruker Daltonics, Billerica, MA, USA). Mass spectra were acquired with the mass spectrometer in reflector positive mode with a laser frequency of 100 Hz and analyzed by Flex Analysis software v.3.0. PMF database searching was carried out in SwissProt database (version 2018_01; 556568 sequences; 199530821 residues) using the on-line available Mascot software (Matrix Science Ltd., London, UK, <http://www.matrixscience.com>). The following database search criteria were set: *Escherichia coli* or *Homo sapiens* as taxonomy, 100 ppm as peptide tolerance, trypsin as the digestion enzyme with one allowed missed cleavage, cysteine carbamidomethylation as fixed modification, and methionine oxidation as variable modification.

For protein identifications the number of matched peptides, the extent of sequence coverage, and the probabilistic score were considered.

4.2.5 Nuclease assays

The nuclease activity of both human RNaseH2 and DDX3X enzymes was monitored on a double stranded (ds) DNA bearing a single ribonucleotide in the strand labelled at the 5'-end with a 6-FAM fluorescent group. A final concentration of 50 nM DNA substrate was used in the experiments. The amounts of RNaseH2 and DDX3X proteins are indicated in the respective figure legends. Reactions were performed in 20 mM Tris-HCl pH 8.8, 10 mM (NH₄)₂SO₄, 10 mM KCl, 2 mM MgSO₄, 0.1% TritonX-100 at 37°C degrees for 60 minutes (unless specified in figure legends). Finally, the reaction mixtures were stopped by addition of standard denaturing gel loading buffer (95% formamide, 10 mM EDTA, xylene cyanol and bromophenol blue), heated at 95°C for 5 min and loaded on 7 M urea 12% polyacrylamide (PA) gel, run at 40 W for 2 hours in TBE buffer. Substrates and products were quantified by laser scanning densitometry (Typhoon-TRIO, GE Healthcare).

4.2.6 Non denaturing gel-based helicase assays

The helicase activity of DDX3X was monitored by measuring the conversion of a double stranded (ds) RNA (labelled at the 5'-end of one strand with a 6-FAM fluorescent group) into single stranded (ss) nucleic acid. A final concentration of 50 nM RNA substrate was used in the experiments, unless otherwise stated. The amounts of DDX3 proteins are indicated in the respective figure legends. Reactions were performed in 20 mM Tris HCl pH 8, 2 mM DTT, 70 mM KCl, and 1 mM ATP, 2 mM MgCl₂ at 37°C degrees for 30 minutes (unless otherwise stated in figure legends) and stopped by adding EDTA 50 mM pH 8. Products were separated through non-denaturing 7% PAGE at 5 W for 3 hours in TBE buffer at 4°C.

Substrates and products were quantified by laser scanning densitometry (Typhoon-TRIO, GE Healthcare).

4.2.7 Ribonucleotide excision repair assays

The ribonucleotide excision repair (RER) assay was reconstituted by reproducing all steps of RER *in vivo*: incision of a single rNMP embedded in a dsDNA by RNaseH2 or DDX3X, was followed by DNA synthesis with Pols δ or β , 5' rNMP-terminated flap removal by hFen1 and ligation by hDNA ligase1 to generate as final product a dsDNA without embedded rNMP. A final concentration of 50 nM DNA substrate was used in the experiments. The amounts of RNaseH2, DDX3X, Pols δ and β , PCNA and dNTPs are indicated in the respective figure legends. Reactions were performed in 20 mM Tris-HCl pH 8.8, 10 mM (NH₄)₂SO₄, 10 mM KCl, 2 mM MgSO₄, 0.1% TritonX-100 at 37°C degrees for 60 minutes (unless specified in the figures). To prove that no more ribonucleotides were present into the fully repaired DNA substrate at the end of the reaction, we inactivated all the enzymes present in the reaction at 75°C for 10 minutes. Then, we left the reaction at room temperature for 10 minutes and we proceeded adding 100 nM of human RNaseH2 for 45 minutes. The dsDNA product without embedded rNMP, will be resistant to the digestion of RNaseH2 enzyme. Finally, the reaction mixtures was stopped by addition of standard denaturing gel loading buffer (95% formamide, 10 mM EDTA, xylene cyanol and bromophenol blue), heated at 95°C degrees for 5 min and loaded on 7 M urea 12% polyacrylamide (PA) gel at 40 W for 2 hours in TBE buffer. Substrates and products were quantified by laser scanning densitometry (Typhoon-TRIO, GE Healthcare).

4.2.8 Kinetic analysis

Time-dependent product accumulation was fitted to the simple exponential equation:

$$\text{Eq. (1): } A(1 - e^{-k_{app} t})$$

where A is the burst constant, k_{app} is the apparent reaction rate and t is time. Dependence of the reaction products from DDX3X concentrations was fitted to the equation:

$$\text{Eq. (2): } E_{obs} = E_{max} / (1 + (K_{1/2}/E_0)^{n_H})$$

where $E_{(obs)}$ is the observed enzymatic activity in the presence of each enzyme dose E_0 ; $E_{(max)}$ is the maximal enzymatic activity; n_H is an exponential term to take into account sigmoidal dose–response curves.

Dose-dependent inhibition of the DDX3X nuclease reaction by ATP was fitted to the equation:

$$\text{Eq. (3): } E_{obs} = E_{max} / (1 + ([ATP]/ID_{50})^{n_H})$$

where $E_{(obs)}$ is the observed enzymatic activity in the presence of each ATP dose ($[ATP]$); $E_{(max)}$ is the maximal enzymatic activity in the absence of the inhibitor; ID_{50} is the ATP concentration inhibiting the enzymatic reaction by 50%; n_H is an exponential term to take into account sigmoidal dose–response curves.

Data were fitted to Eq. (1), (2) and (3) with the program GraphPad Prism 6.0.

4.2.9 Transfection of HEK293T cells for engineered lentivirus preparation: calcium phosphate precipitation

2X HBS:

100 mM Hepes

281 mM NaCl

1.5 mM Na₂HPO₄

Adjust pH to 7.12

1X TE buffer:
10 mM Tris
1 mM EDTA

For lentiviruses preparation, $3 - 3.5 \times 10^6$ HEK293T cells were seeded in 10 cm tissue culture dishes in 10 ml Dulbecco's Modified Eagle's medium (Euroclone, Milan) containing 10% fetal bovin serum (Immunological Sciences, Rome) and 20 $\mu\text{g/ml}$ gentamycin (Euroclone, Milan) and led them grow for 24 hours in a humidified 5% CO_2 atmosphere. After 2 hours before transfection, cell medium was replaced. Then, a transfection mix was prepared adding all the components in the specified order and it was maintained for 10/20 at room temperature:

- 13,2 μg Inducible Dharmacon™ TRIPZ™ Lentiviral shRNA (GE Healthcare) (Lafayette, United States)
- 10 μg pSPAX2 vector (Dharmacon™, Ge Healthcare) (Lafayette, United States)
- 4 μg pMD2 vector (Dharmacon™, Ge Healthcare) (Lafayette, United States)
- 450 μl H_2O /0.1 X TE buffer
- 500 μl 2X HBS
- 50 μl 2,5 M CaCl_2

To enhance transfection efficiency, 100 μM Chloroquine (Sigma, St. Louis United States) was added to the cells followed by the transfection mix (1 ml/10 cm tissue culture dish). Cell medium was changed 14-16 hours after transfection and viruses were collected for the two following days.

All this work was done in Biosafety Level 2 (BSL2) laboratory at Maynooth University (Ireland) under the supervision of Professor M. Schroeder.

4.2.10 Cells Transduction and DDX3X KD induction

One day prior to transduction, 500.000-600.000 U2OS cells were seeded in 2 ml Dulbecco's Modified Eagle's medium (Euroclone, Milan) containing 10% fetal bovin serum (Immunological Sciences, Rome) and 20 µg/ml gentamycin (Euroclone, Milan) in 6 well plates and let them grow in a humidified 5% CO₂ atmosphere. Then, cell medium was replaced with 2 ml of viral particles and 4 µg/ml protamine sulfate (Sigma, St. Louis United States) to enhance the transduction efficiency. After 3-4 hours, new fresh medium containing viral particles was added for each plate and leave O/N. Finally, cells were washed with Phosphate Saline Buffer (Euroclone, Milan) and new fresh medium Dulbecco's Modified Eagle's medium (Euroclone, Milan) containing 10% fetal bovin serum (Immunological Sciences, Rome) and 20µg/ml gentamycin (Euroclone, Milan) was added. Cells were let grow for 24 hours in a humidified 5% CO₂ atmosphere without any additional selection. Then, since cells that have integrated the Inducible Dharmacon™ TRIPZ™ Lentiviral shRNA possess a Puromycin resistance too, a dose-escalation curve of Puromycin (Euroclone, Milan) was used to select resistant cells (specifically, the amount of antibiotic should be enough to kill wild type cells within 5 days).

All this work was done in Biosafety Level 2 (BSL2) laboratory at Maynooth University (Ireland). After at least two weeks of cell culture in in Biosafety Level 2 (BSL2) laboratory, transduced cells could me move in in Biosafety Level 1 (BSL2) laboratory.

Knockdown (KD) of DDX3X in U2OS cells (shDDX3X cells) or KD of the scrambled shRNA (NSC cells) used as control were both induced adding 1 µg/ml Doxycycline (SIGMA) into the cell medium and simultaneously maintaining cells in Puromycin selection (2 µg/ml). Doxycycline was maintained for 48-72 hours and then cells were harvested and KD was checked by Western Blot.

4.2.11 Cell extracts and Western Blot

Cell pellets from U2OS NSC/shDDX3X cell lines were lysed for 30 minutes on ice in 50 mM pH 8 Tris HCl, 0.1% SDS, 350 mM NaCl, 0.25% Triton X-100 in the presence of Protease Inhibitor Cocktail 1X (Sigma). Then, samples were sonicated (at 30s intervals) and centrifugated at 4°C for 10 minutes at 15.000 x g. The soluble portion of the extract was then quantified by Bradford assay (Bio-Rad) and loaded on SDS-Page gels. After gels running, proteins were transferred to a nitrocellulose membrane with a pore size of 0.45 µm (Ge Healthcare) using Trans-Blot® Turbo TM device (Bio-Rad). Finally, the presence of DDX3X protein was revealed by Western blot with anti-DDX3X A300-475A polyclonal antibody (BETHYL) at 1:2000 dilution in 5% milk.

4.2.12 Riboassay

We developed this protocol thanks to the kind help of Doctor Simone Sabbioneda (IGM-CNR, Pavia) and being inspired by previously published work (Meroni *et al.*, 2018).

Genomic DNA was extracted using NucleoSpin® Tissue kit (Macherey-Nagel). Then, 1 µg of genomic DNA was digested with 1 U of *E. coli* RNase H2 (BioLabs, Euroclone) at 37°C 550 rpm for 2.5 hours. Reaction was stopped on ice for 30 minutes and nick translation reaction started trough the addition of 1 U of *E. coli* DNA pol I (Biolabs, Euroclone) and 2 µl of Atto647N-dUTP pH 7.5 NT Labelling Kit (Jena Biosciences, Germany) at 16°C for 1 hour.

Finally, the reaction was stopped by addition of standard gel loading buffer 1X (6X stock: Glycerol 40%, 0.25% xylene cyanol and 0.25% bromophenol blue) and loaded on a 1% agarose gel at 100 V for 2 hours in TBE buffer. Ethidium bromide and Atto647N-dUTP signals were detected by laser scanning densitometry (Thyphoon-TRIO, GE Healthcare) and quantified with ImageQuant TL (Thyphoon-TRIO, GE Healthcare) normalizing Atto647N-dUTP signals with the Ethidium bromide ones. Quantitation of undigested genomic DNAs were subtracted from quantitation of digested genomic DNAs and P values were calculated using the Student's T test.

5. Results

5.1 DDX3X AS A PRIME CELLULAR TARGET TO FIGHT OLD AND EMERGING VIRUSES

5.1.1 DDX3X helicase inhibitors to fight West Nile virus infections

As mentioned in the Introduction paragraph 2.10, we demonstrated for the first time to our knowledge that DDX3X could be a prime target to develop broad-spectrum antiviral compounds. Specifically, compound *16d* was able to suppress the replication of different RNA viruses (HIV-1, HCV, WNV, DENV) and some HIV-1 strains resistant to clinically used antiretroviral drugs. This was possible without showing toxicity in cellular and animal models. However, the primary limitation of the compound *16d* is its poor aqueous solubility that limits its bioavailability in preclinical models (LogS=-7.05) (Brai *et al.*, 2016). Thus, we sought to improve the lead compound through a structure-based rational design approach.

Molecular Modeling

One of the available crystal structures (PDB code: 2I4I) of human DDX3X is co-crystallized with AMP in the absence of nucleic acid and in its open conformation (inactive conformation). It differs from the closed conformation in complex with the RNA which involves some structural modifications to accommodate both RNA and ATP substrate (active conformation).

In order to study the human DDX3X active conformation, our collaborators at the University of Siena (Prof. Maurizio Botta) built a homology model using as template the crystal structure of *Drosophila* Vasa DEAD box helicase (PDB code: 2DB3) which is co-crystallized with AMP and an RNA fragment and shows a 44% sequence homology with DDX3X.

The homology model was built using the software PRIME and allowed us to develop during years some promising DDX3X inhibitors already tested *in vitro* and *in vivo* (Riva and Maga, 2019).

Keep moving forward our researches in order to propose DDX3X as a good cellular target for antiviral therapies, we decided to develop new inhibitors against the DDX3X RNA binding site essential for the helicase activity. Using the previously mentioned model, we found a new inhibitor (*compound 2*) characterized by a sulfonamide moiety. Despite its low passive permeability, *compound 2* was characterized by a very good aqueous solubility and at the same time by a promising anti-enzymatic activity value of 0.36 μM (*Table 1*) (Fazi *et al.*, 2015).

We designed a new series of hybrid compounds by merging the key structural moieties of *16d* and *compound 2* (*Table 1*). These hybrid compounds were able to interact with Arg276 and Arg480 and to take profitable contacts also with Gly325, Pro274 and Arg503 that are predicted to create important interactions with the RNA strand bound to the helicase site of DDX3X.

Table 1: DDX3X anti-enzymatic activity (Brai et al., 2019)

Cmpd.ID ^[a]	Structure	IC ₅₀ ^[b] (μ M)	Cmpd.ID ^[a]	Structure	IC ₅₀ ^[b] (μ M)
16d		0.3	13		0.2
1		0.4	14		0.4
7		4.4	15		>100
8		0.4	16		nd
9		0.4	17		52.2
10		10	18		nd
11		61.2	19		15.5
12		14			

[a] Data represent mean values of the least two experiments.

[b] IC₅₀: 50% inhibiting concentration or needed concentration to inhibit 50% of the enzyme.

[c] na: not active. nd: not determined, compound precipitated from medium.

Inhibition potency and selectivity

Moving forward from the positive predicted interactions of the homology model, we tested all the derivatives compounds in *in vitro* helicase assays. Seven of them have promising inhibitory values higher than of 80% (compounds 8, 9, 10, 14, 15, 19 and 31) (Table 1).

In silico studies also suggested that this family of compounds could act as competitive inhibitors in the helicase binding site. In order to prove our hypothesis, we generated dose-response curves titrating compound 8 in DDX3X FRET-based helicase assays (Material and Methods, paragraph 4.1.3), in the presence of increasing fixed concentrations of the RNA substrate (Figure 8). We saw that the inhibitory potency (ID_{50}) of the compound decreased (higher absolute values) as the RNA concentrations increased consistently with the predicted competitive mechanism of inhibition, with respect to the RNA substrate.

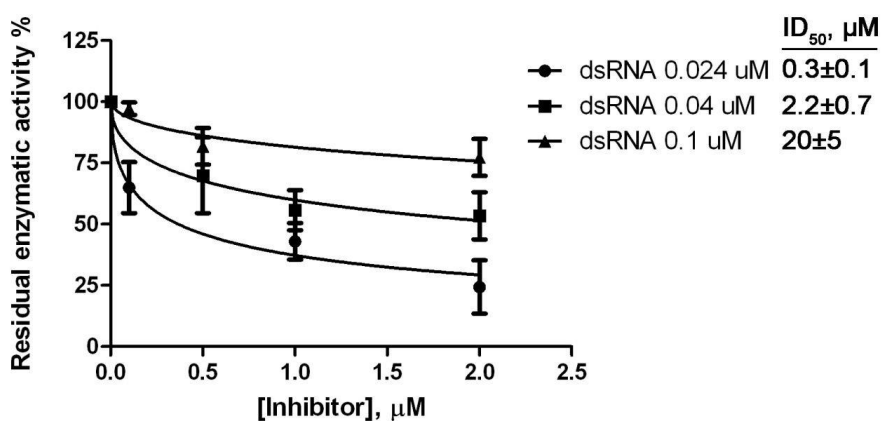


Figure 8: Increasing concentrations of compound 8 were titrated in helicase assays, in the presence of 30 pmols of DDX3X and increasing fixed concentrations of the dsRNA substrate (Brai et al., 2019). Values are the mean of three independent measurements \pm S.D. The residual enzymatic activity values were plotted as a function of the inhibitor concentrations and the corresponding ID_{50} values calculated for each dsRNA concentration are indicated on the right side of the panel.

Finally, in order to prove the selectivity of our compounds, we tested the ability of the *compounds 1, 2, 9 and 14* to inhibit the ATPase activity of DDX3X and the helicase activity of the related DDX1 protein. As shown in *Table 2*, no inhibition was found with any compound concentration proving their capability to recognize specifically the RNA binding pocket of DDX3X.

Table 2: Enzymatic data on selected compounds (Brai et al., 2019)

Compound ID	ATPase DDX3X IC50, μ M	Helicase DDX1 IC50, μ M
<i>16d</i>	>200*	>200*
<i>2</i>	>200*	>200*
<i>9</i>	>200*	>200*
<i>14</i>	>200*	>200*

**The value >200 indicates that less than 20% of inhibition was observed at 200 μ M, the highest concentration tested.*

Cytotoxicity and antiviral assays

Through a quantitative Western Blot approach devised in our laboratory (Material and Methods, paragraph 4.1.6), we checked the presence of our target protein in three different cell lines: Huh-7, VERO and A549 showing that they possess, respectively, 755, 421 and 103 nM intracellular total concentrations of DDX3X protein (*Table 3*).

Table 3: DDX3X cellular expression in Huh-7, A549 and VERO[a] (Brai *et al.*, 2019)

	Huh-7[b]	VERO [c]	A549[d]
DDX3X (nM)	755±170	421±140	103±20

[a] Values represent mean \pm standard deviation (SD) of three independent experiments. For details see Methods [b] Evaluated in Huh7: Hepatocellular carcinoma cells. [c] Evaluated in VERO: African green monkey kidney cells. [d] Evaluated in A549: adenocarcinomic human alveolar basal epithelial cells.

The three cell lines were infected with WNV at a MOI of 0.1 and the antiviral activity of *compound 9* was assayed. As reported in *Table 3* the compound activity seems proportional to DDX3X concentrations.

For the following experiments we selected human Huh-7 cell line characterized by the highest DDX3X concentration. When challenged with our inhibitors, A549 displayed a cytotoxic activity at an inhibitor dose of 21.3 μ M probably due to DDX3X implications in pulmonary cancer already showed by Bol and collaborators (Bol *et al.*, 2015). This result forced us to eliminate A549 in our following experiments in order to avoid interferences due to anticancer related cytotoxic effects.

Subsequently, Huh-7 cells were infected with WNV and all the compounds with the best IC₅₀ values. As reported in *Table 4*, compounds showed interesting antiviral activities, ranging from 2.3 to 65.9 μ M, comparable or even higher than the broad-spectrum antiviral ribavirin, which was used as a reference compound.

Table 4: Antiviral Activities and cytotoxicity of selected compounds against WNV infected Huh-7 cells[a] (Brai et al., 2019)

Compound ID	WNV ^[d]	Huh-7	
	EC ₅₀ ^[b] (μ M)	CC ₅₀ ^[c] (μ M)	SI ^[e]
16d	8.8 \pm 0.2	>200	>22.7
1	120 \pm 5.2	175 \pm 11	1.5
7	2.3 \pm 0.5	>200	>87
8	23.1 \pm 0.4	>200	>8.7
9	65.9 \pm 2.3	>200	>3
11	>200	>200	nd
12	39.9 \pm 1.1	>200	>5
13	55 \pm 1.1	>200	>3.6
14	13 \pm 0.8	>200	>15.4
Ribavirin	95.5 \pm 3.2	>200	>2.1

[a] Data represent mean + standard deviation (SD) of three experiments. [b] EC₅₀: half maximal effective concentration or needed concentration to inhibit 50% viral induced cell death [c] CC₅₀ Cytotoxic concentration 50 or needed concentration to induce 50% death of non-infected cells [d] Huh7: Hepato cellular carcinoma cells. Ribavirin was used as a reference compound. [e] Selectivity index (CC₅₀ / EC₅₀ ratio) is a ratio that measures the window between cytotoxicity and antiviral activity.

In vitro ADME analysis

Aqueous solubility, liver microsomal stability and membrane permeability were tested by our collaborators at the University of Siena (Prof. Maurizio Botta) for compounds 2, 8, 9, 10, 14 and 15. In Table 5 are listed all the values, demonstrating an improved solubility especially for compounds 10, 14 and 15. Also the membrane permeability assays (PAMPA) are encouraging: all

the values are under the limit with the exception of *compound 2* that is also inactive in antiviral assay probably for that reason.

Finally, we proved that in human liver microsomes (HLM) all our compounds showed a high metabolic stability (>95.6%).

Table 5: *In vitro* ADME studies of selected compounds (Brai et al., 2019)

Cpd. ID	AppP ^[a]	Memb. Ret.% ^[b]	LogS ^[c]	HLM Stability
16d	$2.86 \cdot 10^{-6}$	19.1	-7.05	99.0±0.6
1	$<0.1 \cdot 10^{-6}$	22.5	-4.36	98.3±1.1
7	$<0.1 \cdot 10^{-6}$	31.4	-7.5	95.6±0.8
8	$0.21 \cdot 10^{-6}$	30.4	-7.5	99.0±1.2
9	$0.71 \cdot 10^{-6}$	10.1	-4.6	97.1±0.6
13	$0.68 \cdot 10^{-6}$	0	-5.4	98.0±0.9
14	$0.44 \cdot 10^{-6}$	0	-4.7	96.0±0.4

[a] Apparent permeability reported in $cm \cdot s^{-1}$. [b] membrane retention %. [c] Aqueous solubility. [d] Human Liver Microsomes Metabolic Stability

Compound 9 characterization

In order to better evaluate the antiviral activities of our compounds, we selected *compound 9* as representative of the series, to investigate its mechanism of action (Figure 9).

For this reason, our collaborators at the University of Florence (Prof. Giannecchini) performed time of addition studies: WNV infected cells were

treated with the compound at concentration near and under the IC_{50} value. As shown in *Figure 9a*, *compound 9* seems to act in the two first hours of virus life cycle since its addition after 3 hours post-infection did not affect viral replication.

This antiviral activity is not limited to the very early phase, but it appears to be substantial also two hours after infection. This result could be indicative of the fact that *compound 9* main target is in a step of the viral replication subsequent to viral entry.

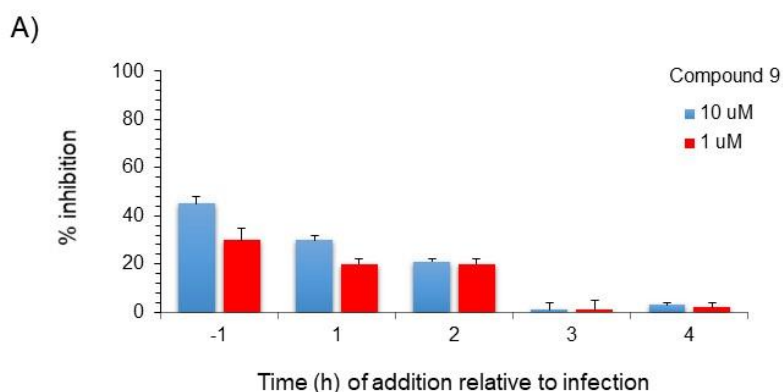
Successively, we evaluated the effect of *compound 9* in the production of both genomic and complementary viral RNA (*Figure 9b*).

Our inhibitor molecule, if added 1-3 hours post infection, is able to interfere with the concentration of genomic RNA in early time of infection (2-12 hours post infection).

We also checked the level of complementary RNA showing that our inhibitor molecule was able to interfere marginally with the concentration of genomic RNA, without significant changes in the quantity of the complementary not infective RNA.

Finally, we evaluated possible effects on the production of WNV nucleocapsid protein (NC). *Figure 9* shows that the addition of our compound 1-hour post infection significantly reduced the concentration of NC, while its addition after 3 hours did not change NC concentrations.

Summing up all these results we hypothesised a possible implication of *compound 9* in the first phases of viral replication, probably during early



protein translation, after the entry process.

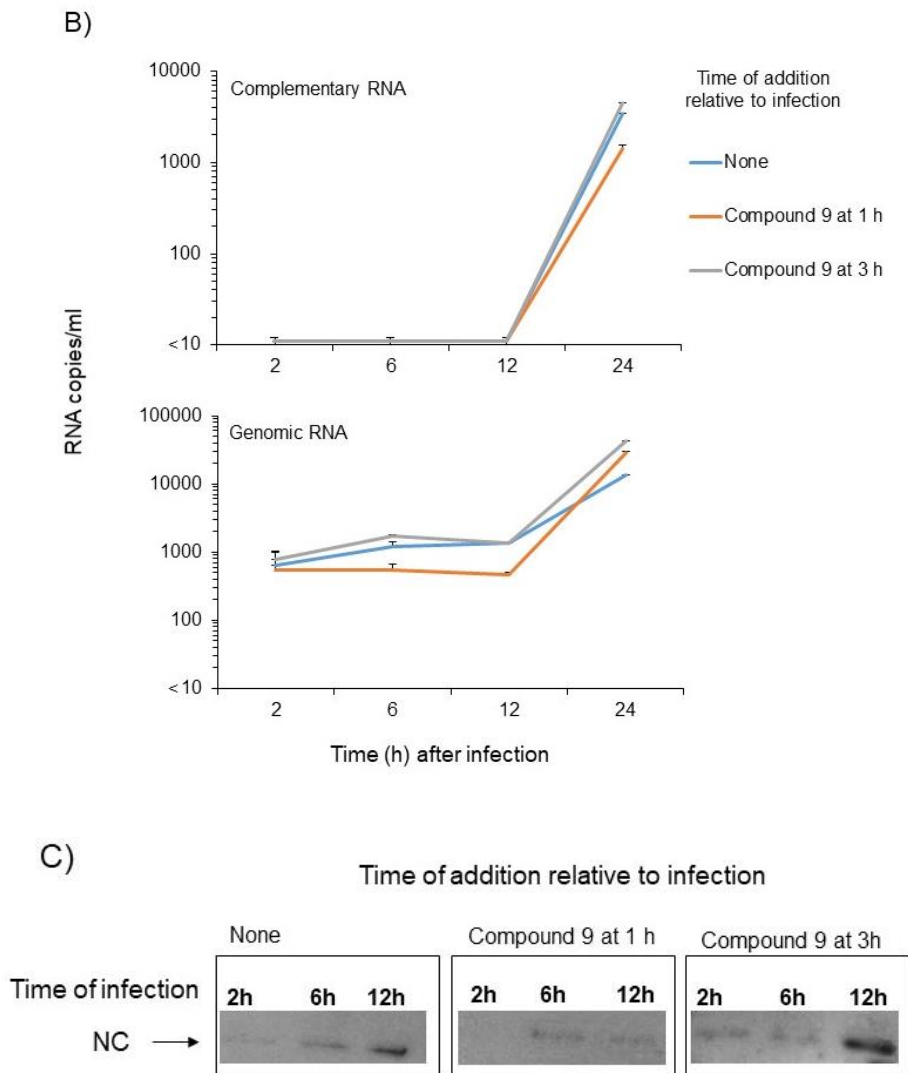


Figure 9: Effect of varying anti-DDX3X compound 9 time of administration on WNV replication (Brai et al., 2019). A) WNV infection of Huh7 cells at

MOI of 0.1 in presence of compound 9 at 1 μ M and 10 μ M added at indicated time (h) relative to the infection and assayed with the viral plaque reduction assay. Data represent means + standard deviation. B) WNV genomic and complementary viral RNA in Huh7 cells assayed after infection in absence or in presence of compound 9 at 1 μ M added at 1 h and 3 h of the infection. Data represent means + standard deviation. C) WNV capsid protein electrophoretic mobility obtained from Huh7 cells after infection in absence or in presence of compound 9 at 1 μ M added at 1 h and 3 h of the infection. None, no compound 9 addition.

5.1.2 A novel strategy to develop selective DDX3X RNA helicase inhibitors to fight emerging viruses

As previously mentioned in Introduction paragraph 2.2, DDX3X protein has been shown to possess a unique insertion (sequence -ALRAMKENGGRYGRRK- aa 250-264) between motif I and motif Ia. Such insertion is not present in other human members of the DEAD-box family and BLAST analysis indicated that no other human protein shares significant homology with the aminoacidic sequence of the unique motif (UM) (Högbom *et al.*, 2007). Based on biochemical studies, UM has been proposed to bind the RNA substrate (Garbelli *et al.*, 2011). Specifically, we have previously shown that the deletion of this short motif affected the RNA helicase activity of DDX3X, by reducing its affinity for the nucleic acid and that blocking this domain with a peptide reduced HIV-1 replication in infected cells (Garbelli *et al.*, 2011). These results suggested that inhibitors targeting the UM could be highly selective for DDX3X, due to the absence of such domain in other human proteins and might retain the ability to suppress viral replication. In light of these preliminary data, we decided to undertake a novel strategy to design highly selective and broad-spectrum antiviral molecules, by targeting this unique DDX3X motif. Since without a crystal structure of the DDX3X-RNA complex it is difficult to precisely determine the precise nature of the contacts between the UM residues and the nucleic acid lattice, we referred to our homology model, described in the previous section.

Molecular modelling

Molecular modelling was performed in collaboration with the group of Prof. Maurizio Botta at the University of Siena. Using PocketPicker, a Pymol plugin able to detect all the possible pockets on a protein surface, we found a potential little pocket lined by the α -helix formed by the DDX3X unique motif (UM) (Figure 10).

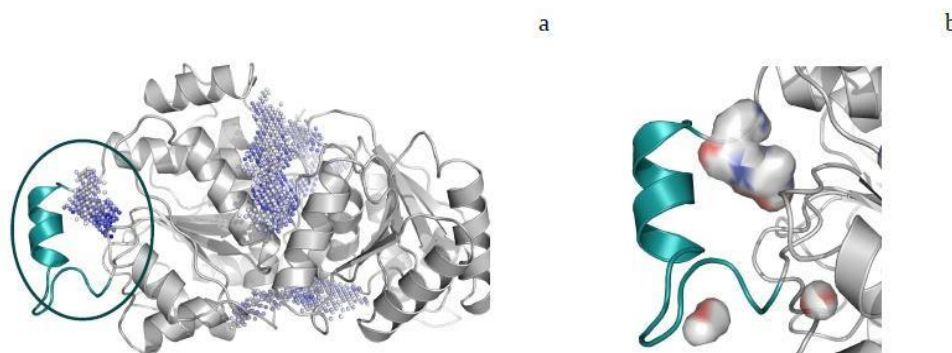


Figure 10: Pockets identified by PockerPicker are represented in dots (a), zoom on the little pocket around the unique motif (UM), in cyan (b).

Since we had no previous information about active molecules able to bind this pocket within the UM, we performed a preliminary screening to search theoretically active scaffolds among two commercial libraries by means of two different docking programs (Asinex Gold and Platinum consisting of 583040 molecules).

From this large number of molecules, we chose the best scoring molecules (74.783, 20% of total) to process in the next step.

Selected molecules were docked within the pocket using the docking program GOLD (CHEMSCORE). Docked molecules were then selected by our chemists' collaborators from the University of Siena on the basis of: i) score values above 23; ii) the number of clusters generated (less than 7), iii) visual inspection. Because of the small and narrow properties of the pocket, a fair number of compounds were docked outside and so they were discarded.

Among the molecules which passed the filter analysis and were docked inside the pocket (about 103), 13 compounds were finally selected as interesting, on the basis of their chemical structures and their polar interactions into the active site. These molecules were then tested for their ability to inhibit DDX3X RNA helicase activity.

Table 6 lists the chosen compounds with their anti-enzymatic activities.

Structures, docking scores and solubility index data were omitted in this Thesis since they are part of a Patent Application still under preparation.

Table 6: Selected compounds targeting DDX3X unique motif.

Compound	Activity (μM)
#1 UM	n.a.
#2 UM	n.a.
#3 UM	n.a.
#4 UM	n.a.
#5 UM	7
#6 UM	n.a.
#7 UM	n.a.
#8 UM	> 200
#9 UM	n.a.
#10 UM	n.a.
#11 UM	0.002
#12 UM	0.007
#13 UM	0.006

*n.a. = not active

*The value >200 indicates that less than 20% of inhibition was observed at 200 μM , the highest concentration tested.

A first group of these molecules (Compounds #4 UM, #8 UM and #10 UM) was selected on the basis of an interesting polar interaction of the terminal amino-group with three amino acids in the pocket (Glu256, Tyr266, Cys317). Another group of compounds (Compounds #1 UM, #2 UM and #7

UM) was selected considering the shape and the residues involved in the hydrophobic interactions that are Arg262, His318 and Pro247.

Compound #5 UM has an interesting shape that fits into the pocket like a 'cap'. Remarkably, #5 UM is the only compound among the selected ones characterized by the presence of a hydroxyl-group able to interact with both Glu256 and Cys317 (Figure 11). In order to confirm the activity of this commercially available compound, #5 UM was re-synthesized and converted into the corresponding acetate salt, compound #1 UM. This simple synthetic modification provided a water-soluble derivative. Furthermore, the R and S enantiomers were synthesized. Compounds were analyzed through biochemical assays described below.

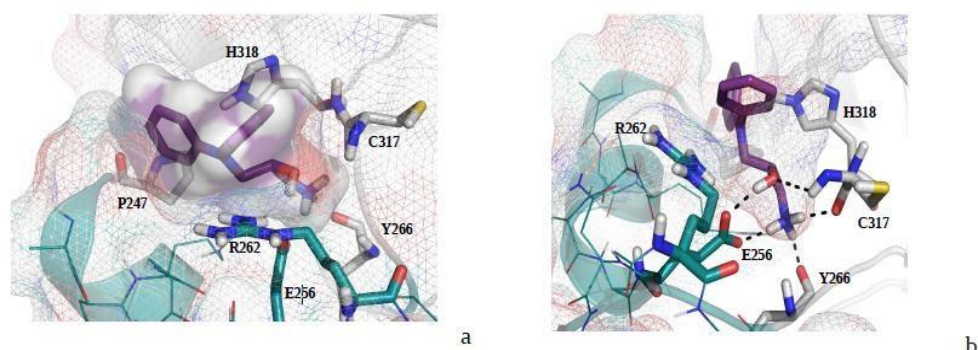


Figure 11: Two different orientation of compound #5 UM docked pose showing (a) its particular shape profile and (b) its specific polar interactions into the UM pocket.

The modelling study identified the aminoacids Glu256, Cys317 and Tyr266 as the most involved in the polar interactions with Compound #5 UM while Arg262, His318 and Pro247 as the residues involved in the hydrophobic interactions. On the basis of the docking analysis, Glu256 and Arg262, respectively located at the N- and C-terminal sides of the UM sequence, seemed to be the major responsible of Compound #5 UM binding and they were further investigated by biochemical analysis, to validate the predicted binding mode of the compound.

Glu 256 is essential for the RNA helicase activity of DDX3X

In order to validate the molecular modelling predictions and to better characterize the role(s) of the aminoacidic residues Glu256 and Arg262 on the enzymatic activity of DDX3X, both residues in DDX3X were changed to Ala by site-directed mutagenesis to generate, respectively, the two single E256A and R262A mutants and the double E256A/R262A mutant. The wild type protein and all the three different mutants were purified as illustrated in detail in Materials and methods, paragraph 4.1.2 (see *Figure 12* and *13*).

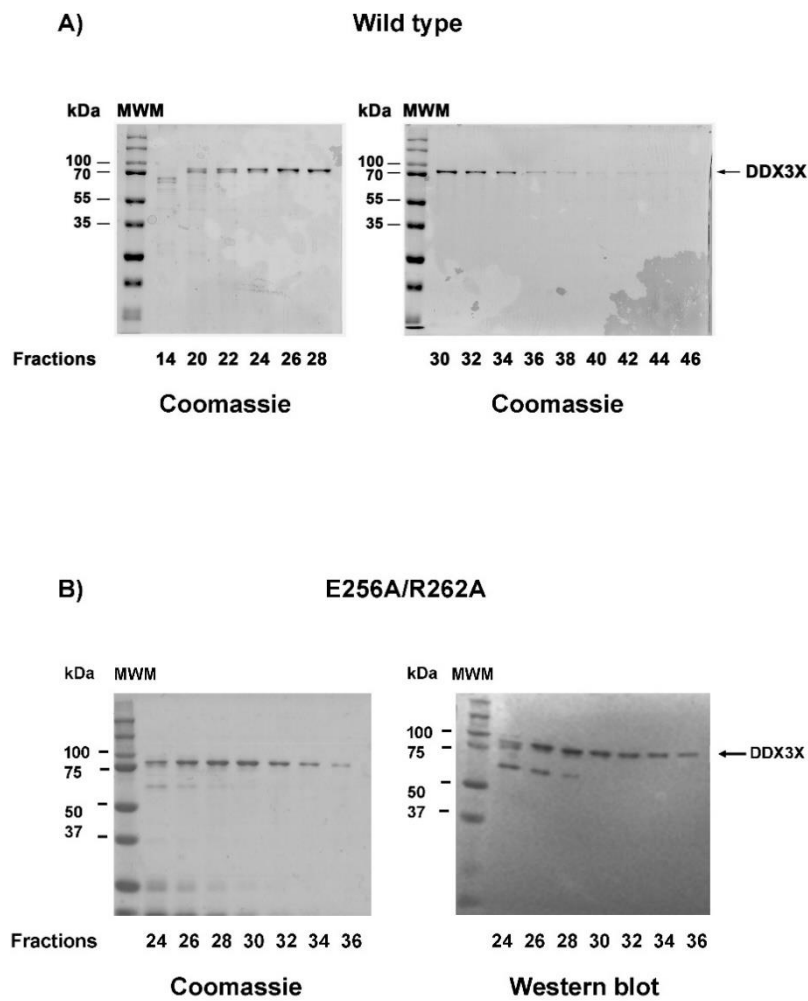


Figure 12: Recombinant DDX3X wild type and double mutant E256A/R262A proteins.

A) Coomassie of the wild type protein

B) Coomassie (on the left) and Western blot (on the right) of the double mutant E256A/R262A protein.

MW stays for molecular weight marker –kDa- (Dual color marker, BIO-RAD); L for Load, FT for Flow Through and W for Wash. Numbers indicate the respective eluted fractions.

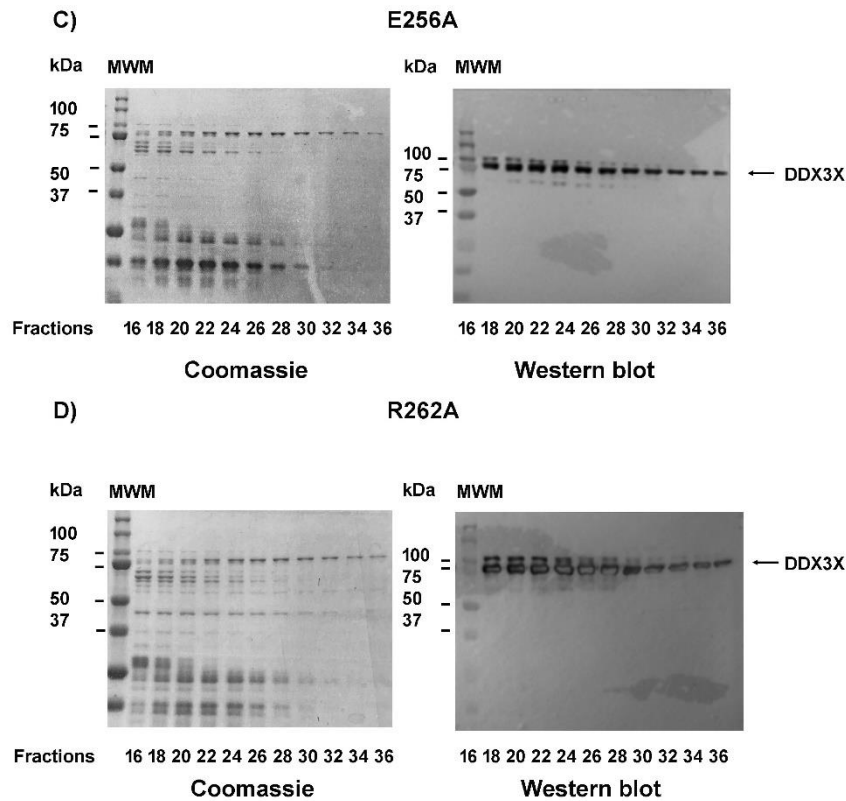


Figure 13: Recombinant DDX3X wild type and single mutant E256A and R262A proteins.

C) Coomassie (on the left) and Western blot (on the right) of the single mutant E256A protein.

D) Coomassie (on the left) and Western blot (on the right) of the single mutant R262A protein.

MW stays for molecular weight marker –kDa- (Dual color marker, BIO-RAD); L for Load, FT for Flow Through and W for Wash. Numbers indicate the respective eluted fractions.

The mutated enzymes were tested for their RNA helicase activity in a FRET-based assay (see Materials and methods, paragraph 4.1.3, for details) and the kinetic parameters for the reaction are reported in *Table 7*.

The E256A substitution had the greatest impact on the enzymatic efficiency, causing a 10.8-fold reduction of the k_{cat}/K_m value for RNA unwinding, with respect to wild type DDX3X. The R262A mutation also reduced the k_{cat}/K_m value by 4.4-fold with respect to the wild type enzyme. Combining the two mutations did not result in an additive effect and the double mutant showed an intermediate phenotype (7.4-fold reduction in the k_{cat}/K_m value with respect to the wild type), suggesting that the effect of the E256A mutation was not changed by the presence of the additional R262A substitution.

Table 7. Kinetic parameters for the RNA helicase activity of DDX3X wild type and the DDX3X(E256A), DDX3X(R262A) and DDX3X(E256A/R262A) mutants.

Enzyme	$K_m(\text{RNA})^a$ (μM)	k_{cat} (FU^b · min⁻¹)	k_{cat}/K_m (μM^{-1}, FU · min⁻¹)	-fold reduction^c
wild type	0.5 ± 0.1	1146 ± 22	2278	1
E256A	0.6 ± 0.2	126 ± 10	210	10.8
R262A	9 ± 2	4794 ± 62	522	4.4
E256A/ R262A	0.6 ± 0.25	148 ± 70	307	7.4

Kinetic parameters K_m and k_{cat} were calculated as described in Material and Methods, values represent the mean of three independent experiments ± S.D.; b. FU, arbitrary fluorescence emission units; c. ratio $k_{cat}/K_m(\text{wt})/k_{cat}/K_m(\text{mut})$.

The single mutants were also compared for their ATPase activities. As shown in *Figure 14*, the E256A mutant showed comparable activity with respect to the wild type enzyme, while the ATPase activity of the R262A mutant was reduced, similar to the double E256A/R262A mutant. In summary, these results indicated that the residue Glu256 is essential for the RNA helicase, but not for the ATPase activity of DDX3X, while Arg262 plays an ancillary role likely coupling ATP hydrolysis to RNA unwinding.

These results are in agreement with previous published data indicating a role of the DDX3X UM in substrate binding and highlight the central role of the residue Glu256 in this motif for RNA interaction (Garbelli *et al.*, 2011).

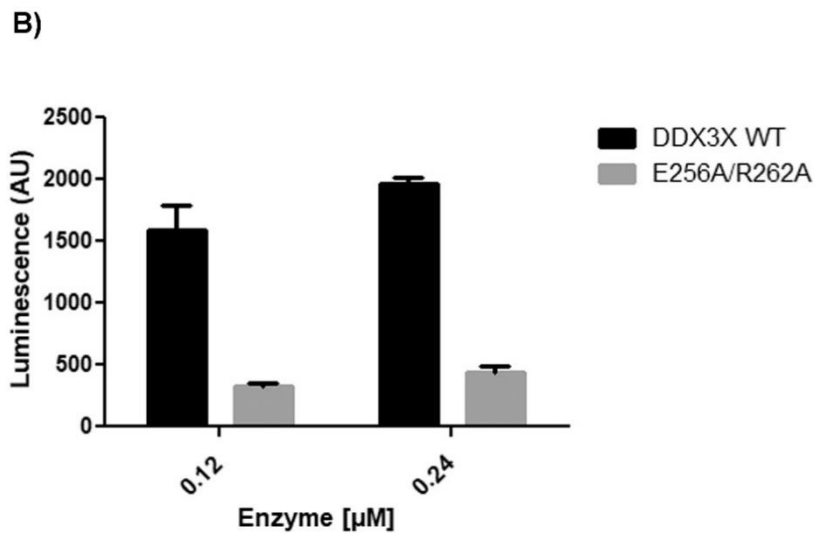
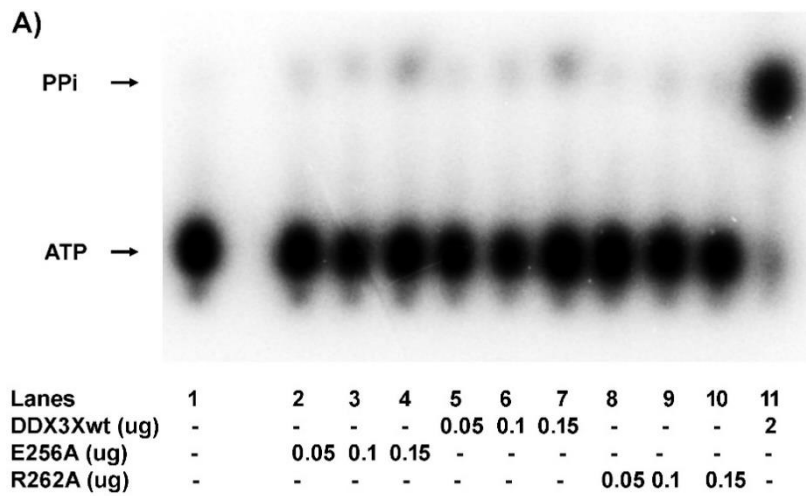


Figure 14: ATPase activity of all the recombinant DDX3X proteins.

- A) *Wild type versus single mutants E256A and R262A ATPase activities. Reactions were performed as described in Material and methods, paragraph 4.1.4. Unreacted substrate (ATP) was separated from the product (phosphate, P_{Pi}) by thin layer chromatography.*
- B) *Wild type versus double mutant E256A/R262A ATPase activities. The ATPase activity was determined using the commercial kit ADP-Glo Kinase Assay (Promega) as described in Material and methods, paragraph 4.1.4.*

Glu 256 is the major determinant for the interaction of the UM compounds with the DDX3X unique motif

Next, selected compounds, designed to selectively bind the DDX3X UM and suggested by *in silico* docking studies to interact with the mutated residues, were tested for their ability to inhibit the RNA helicase activity of DDX3X wild type and mutant proteins. As shown in *Table 8*, the E256A substitution caused a reduction of the inhibitory potencies of the *Compounds #11 UM* and *#13 UM* of 36,500- and 43- fold, respectively. On the other hand, the mutation R262A did not significantly change the inhibitory potencies of the compounds, with respect to the wild type enzyme. Thus, the residue Glu 256 was the major determinant for inhibitor binding.

Table 8. Inhibition of the RNA helicase activity of DDX3X wild type and the DDX3X(E256A) and DDX3X(R262A) mutants.

Compound	wild type ID ₅₀ , μM ^a	E256A ID ₅₀ , μM (-fold resistance) ^b	R262A ID ₅₀ , μM (-fold resistance)
#11 UM	0.002 ± 0.0005	73 ± 10 (36,500)	0.001 ± 0.0003 (0.5)
#13 UM	0.007 ± 0.0001	0.3 ± 0.1 (43)	0.004 ± 0.002 (0.6)

ID₅₀, 50% inhibitory concentration. Values were calculated as described in Material and Methods (paragraph 4.1.5) and represent the mean of three independent experiments ± SD; b. ratio ID₅₀(mut)/ID₅₀(wt).

These results are in good agreement with the molecular modelling and the kinetic analysis (Table 7), which indicated that Glu256 provides essential interactions of DDX3X with its RNA substrate. The binding of the inhibitor to this key residue, likely disrupts those interactions, corroborating the selectivity of the mechanism of action of our compounds.

To further prove the specificity of inhibition of the selected compounds towards DDX3X, inhibition assays were performed also with three RNA helicases: the DEAD-box family member human DDX1, the viral NS3 helicase of hepatitis C virus and the RNA helicase STRS2 from *Arabidopsis thaliana*. As shown in Table 9, all the compounds tested inhibited DDX1 with potencies from two to four orders of magnitude lower than towards DDX3X and were completely inactive against STRS2 and NS3, confirming the high selectivity of inhibition for DDX3X.

Table 9 Inhibition of the RNA helicase activity of human DDX1, Arabidopsis STRS2 and HCV NS3.

Compound	DDX1 ID ₅₀ , μM ^a (-fold selectivity) ^b	STRS2 ID ₅₀ , μM (-fold selectivity)	NS3 ID ₅₀ , μM (-fold resistance)
#11 UM	18±1.202 (9,000)	>100 (> 50,000)	>100 (> 50,000)
#13 UM	58± 4.5 (8285)	>100 (> 10,000)	>100 (> 10,000)

*ID*₅₀, 50% inhibitory concentration. Values were calculated as described in Material and Methods (paragraph 4.1.5) and represent the mean of three independent experiments ± SD; b. ratio *ID*₅₀/*ID*₅₀(wt DDX3X), the *ID*₅₀ (wt DDX3X) values used were those reported in Table X.

Finally, compounds #11, #12 and #13 were tested for their ability to reduce WNV and DENV-2 replication in Huh-7 cells. As reported in Table 10, Compound #11 and its enantiomers possess promising antiviral activities in the micromolar range, major than the broad-spectrum antiviral ribavirin, and no significant toxicity.

Table 10: Antiviral activity and cytotoxicity of selected compounds against DENV-2 and WNV.

Cpd ID	EC ₅₀ ^{b,d} (DENV-2) (μM)	EC ₅₀ ^{b,d} (WNV) (μM)	CC ₅₀ ^{c,d} (μM)	CC ₅₀ ^{c,e} (μM)
#11 UM	8.60	2.3	100	>200
#12 UM	12.6	n.t.	120	n.t.
#13 UM	6.35	n.t.	79	n.t.
Ribavirin	20.0	95.5	100	>200

[a] Data represent mean of three experiments. [b] EC_{50} : half maximal effective concentration or needed concentration to inhibit 50% viral induced cell death [c] CC_{50} Cytotoxic concentration 50 or needed concentration to induce 50% death of non-infected cells [d] evaluated using Cell Titer-Glo® kit [e] evaluated using MTT kit nt= not tested. Ribavirin was used as a reference compound.

5.2 AN ALTERNATIVE RIBONUCLEOTIDE EXCISION REPAIR BY THE RNA HELICASE/NUCLEASE DDX3X

A nuclease activity for DDX3X, or its orthologs in other organisms, was previously unnoticed. As mentioned in the Introduction paragraph 2.8, DDX3X resolves RNA/DNA hybrids and RNA secondary structures and it is involved in the degradation of RNAs (Schröder, 2010).

We hypothesized that DDX3X could resolve structures normally recognized by RNaseH2 into the genome. Initially, to verify our hypothesis, we compared the structure of the two enzymes. Based on our suggestions on the possible similarities between the catalytic site of the two enzymes, a structural model was built by our collaborators at the University of Siena (Prof. Maurizio Botta) between human DDX3X in the open conformation (PDB ID 5e7I) and mouse RNaseH2 (PDB ID 3KIO). Because of the lack of complete crystal structures of human RNase H2, we selected the structure of the murine enzyme since human and mouse RNaseH2 has a percentage of identity of 86.62%. As shown in *Figure 15*, this analysis showed that the two proteins adopted a similar folding in the catalytic core. Two conserved residues (Arg351 and Arg503 in DDX3X and Arg38 and Arg187 in RNase H2) were similarly positioned and deserved further investigations. In particular, Arg38 of the RNaseH2 catalytic motif -DEAGR- corresponded to Arg351 of the DDX3X catalytic motif -DEADR-, both residues taking similar interactions with the RNA substrate in both enzymes (Fazi *et al.*, 2015; Sharma *et al.*, 2017). Specifically, Arg503 was implicated in the salt-bridge that stabilized the closed conformation of the protein, while Arg351 formed hydrogen bonds with RNA. Similarly, in the RNaseH2 structure, Arg38 is involved in RNA binding, as it is Arg351 of DDX3X.

a

```

>ddx3      DFCKYLVLEEADNMLDMGF (Box II) aa 339-357
>rnaseh2a  EPC-VLGVDEAGGPVLGP      aa 27-44

>ddx3      VRHTMFSATFPKEIQMLARDFI-DEYI-FLAVGRV (Box III) aa 375-408
>rnaseh2a  ERERL-FAKMEDTDFVGWALDVLSPNLISTSMGRV aa 75-109

>rnaseh2a  G-VNVTQVFVDTVGMPETYQARL aa 132-153
>ddx3      GKDSLTLVFVETKKGADSLEDFL (Box IV) aa 439-461

>ddx3      AVAARGLDISNVKHVINF-DLPSDIEE-Y (Box V) aa 499-525
>rnaseh2a  AKVARDQAVKKWQFVEKLQDLDTYGSGV aa 182-210

```

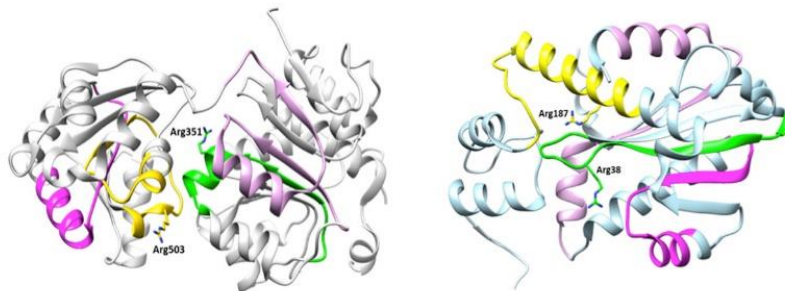
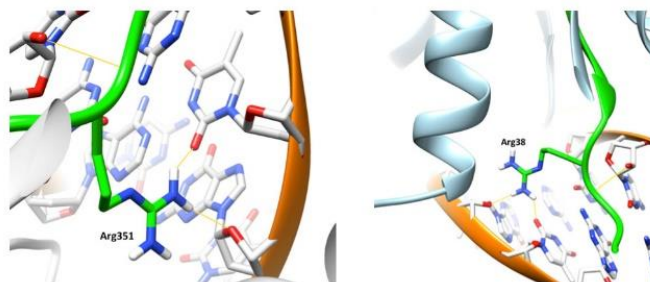
b**c**

Figure 15: Structural comparison between human DDX3X and RNaseH2 catalytic subunit. **a**. Sequence alignment showing amino acid (aa) similarities between selected regions of human RNaseH2 and human DDX3X. Red letters indicate catalytically important residues.

Box numbering refers to the conserved helicase motifs present in DDX3X: DEAD (box II), SAT (Box III), LVF (Box IV) and GLD (Box V). Green shading indicated identical and cyan shading similar aa. The numbers of the aa residues corresponding to each selected region are boxed according to the color coding used in the structures in panel b. **b.** Structure comparison between human DDX3X in the open conformation (PDB ID 5e7I) on the left and mouse RNaseH2 (PDB ID 3KIO) on the right. In green are highlighted the structural elements containing aa 339-357 of DDX3X in comparison with aa 27-44 of mouse RNaseH2. In pink residues 375-408 of DDX3X and residues 75-109 of RNaseH2. In magenta aa 439-461 of DDX3X and aa 133-154 of RNaseH2. In yellow aa 499-525 of hDDX3 and aa 182-210 of mouse RNaseH2. This analysis showed that the two proteins adopted a similar folding in the regions considered. Four conserved residues (Arg351 and Arg503 in DDX3X and Arg38 and Arg187 in RNaseH2) were similarly positioned within these regions. Arg351 and Arg503 are known to play important roles in DDX3X: Arg503 was implicated in the salt-bridge that stabilized the closed conformation of the protein, while Arg351 formed hydrogen bonds with RNA. **c.** Structural details of the region surrounding Arg351 of DDX3X (left) and Arg38 of RNaseH2 (right), showing the hydrogen bond formed by these residues with the RNA substrate. Arg351, placed in the -DEADR- box motif of DDX3X, corresponded to Arg38 of the -DEAGR- catalytic domain of RNaseH2. In the RNaseH2 structure, Arg38 is involved in RNA binding, similarly to Arg351 of DDX3X. (Unpublished data)

Confident of these preliminary *in silico* results, we verified a possible DDX3X RNase-like activity *in vitro*. Interestingly, the purified human DDX3X cut at the 5' side of a single rCMP embedded in a DNA oligonucleotide, either single stranded (ss) or annealed to a complementary DNA strand (Figure 16A). The cutting was absolutely restricted to the rNMP only on the double strand (ds) DNA Substrate 2. Vice versa, the DDX3X double mutant D357A/D350A (DADA) didn't show RNaseH2-like activity being mutated in two essential residues in the DEAD domain, already known as essential for helicase and ATPase activities as well (Garbelli *et al.*, 2011).

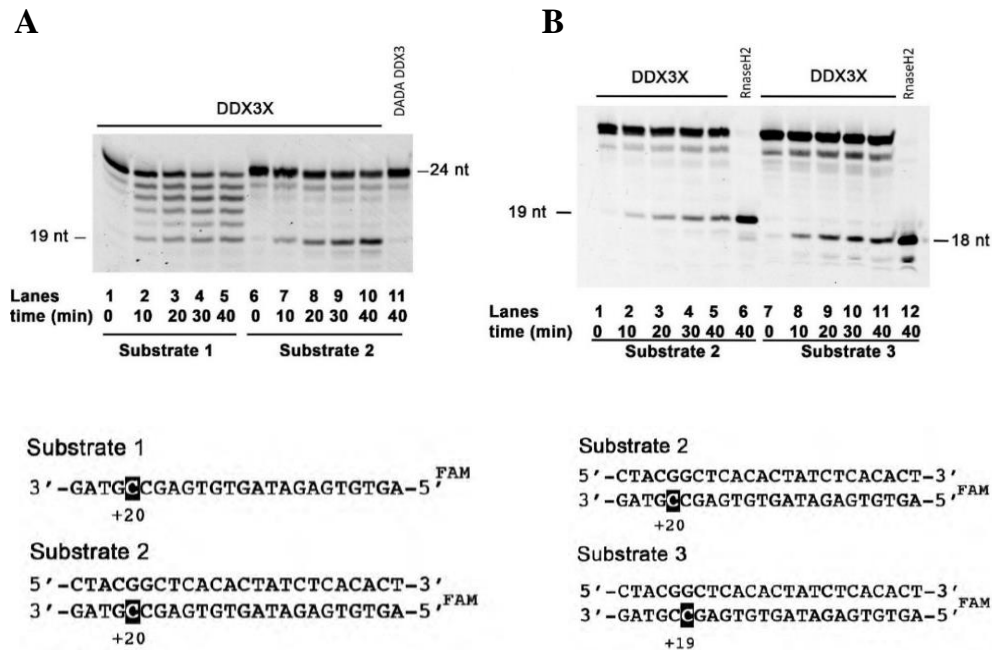


Figure 16: First evidences that DDX3X possesses RNaseH2-like activity.
A: Time course of DDX3X wild type in nuclease assay in the presence of a single stranded DNA oligonucleotide (Substrate 1) bearing a single rNMP in position + 20 (lanes 1-5) or a double stranded DNA oligonucleotide (Substrate 2) bearing a single rNMP in the same position (lanes 6-10). Lane 11 shows that DDX3X DADA mutant (D347A/D350A) in nuclease assay in the presence of the 24/24mer dsDNA bearing a single rCMP at position +20 (Substrate 2) lacks RNase-like activity.
B: Time course of DDX3X wild type in nuclease assay in the presence of the 24/24mer dsDNA bearing a single rCMP at position +20 (Substrate 2) or in position +19 (Substrate 2). DDX3X cutting on substrate 2 (Lanes 2-5) was indistinguishable from that of human RNaseH2 enzyme (Lane 6) as well on substrate 3 (Lanes 7-12).

Moving the rCMP one nucleotide upstream (Figure 16B), also generated the expected products which were undistinguishable from those generated by RNaseH2 confirming that rCMP acted as specific recognition site for

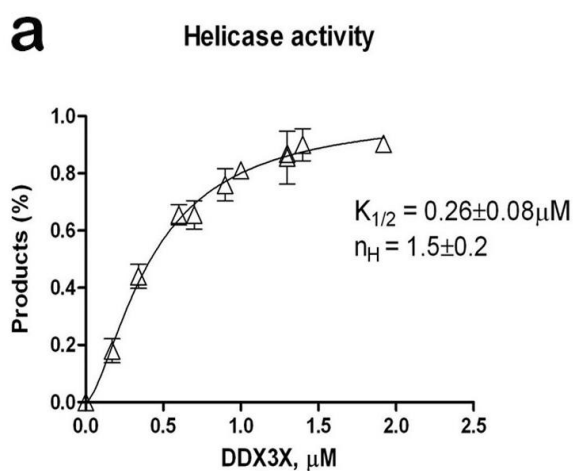
DDX3X. These results indicated that DDX3X possessed a RNaseH2-like activity.

To be sure that our recombinant DDX3X wild type preparation was pure and without *Escherichia coli* contaminations with such activity, we performed a mass spectrometry analysis thanks to our collaborators at the University of Siena supervised by Professor Bini. Mass-spectrometry results showed that none of the few copurifying *E. coli* contaminants possessed RNase activity (*Table 11*). Thus, the observed RNaseH2-like activity resides in the catalytic core of DDX3X and requires its DEAD domain.

Table 11: protein spots from 2D gel of DDX3X identified by MALDI-TOF/TOF MS

Protein description	UniProt ID/name	Mascot search results		
		Score	N. of matched peptides	Sequence coverage (%)
ATP-dependent RNA helicase DDX3X	O00571/DDX3X_HUMAN	354	35/52	48
ATP-dependent RNA helicase DDX3X	O00571/DDX3X_HUMAN	208	18/21	23
ATP-dependent RNA helicase DDX3X	O00571/DDX3X_HUMAN	104	10/14	13
60 kDa chaperonin	Q0T9P8/CH60_EC0L5	118	8/8	17
Elongation factor Tu 1	A7ZSL4/EFTU1_EC024	111	8/12	22
Elongation factor Tu 1	A7ZSL4/EFTU1_EC024	73	5/7	12
Elongation factor Tu 1	A7ZSL4/EFTU1_EC024	116	8/10	19
Elongation factor Tu 1	A7ZSL4/EFTU1_EC024	167	13/21	31
Ferric uptake regulation protein	P0A9B1/FUR_EC057	189	11/15	71
Ferric uptake regulation protein	P0A9B1/FUR_EC057	85	5/5	33
Purine nucleoside phosphoramidase	P0ACE8/HINT_EC057	197	11/15	68

Helicase and RNaseH2-like DDX3X activities are quite different: in helicase assays DDX3X showed a sigmoidal dependence of unwinding with respect to the enzyme concentration ($K_{1/2} = 0.26 \mu\text{M}$, cooperativity index $n_H = 1.5$) (Figure 17a), suggesting protein oligomerization, according to published results (Sharma *et al.*, 2017). In the nuclease reaction no cooperativity was observed ($K_{1/2} = 0.32 \mu\text{M}$, $n_H = 0.7$) suggesting a monomeric interaction with the substrate (Figure 17b). This is not the only difference between the two activities: as a matter of fact our results suggested that DDX3X RNaseH2-like activity it is inhibited by ATP on the contrary of the well-documented DDX3X-helicase activity that is ATP-dependent (Sharma *et al.*, 2017). When ATP was titrated in RNaseH2-like reaction, indeed a strong inhibition was observed by increasing ATP concentrations (Figure 17c).



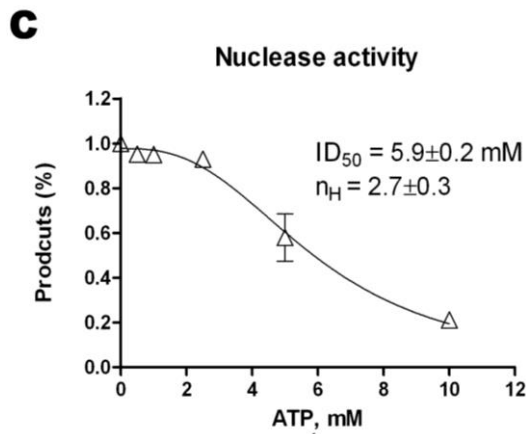
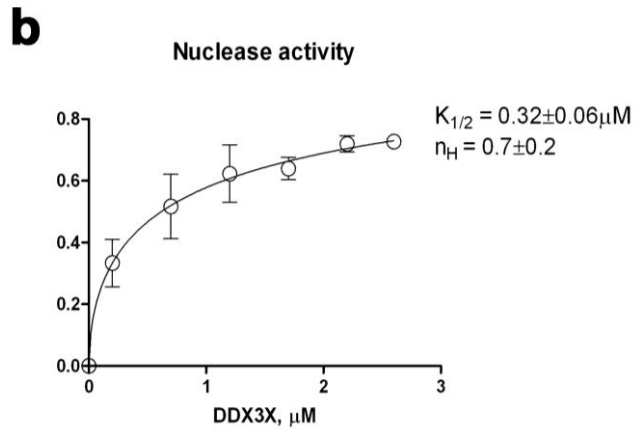


Figure 17: Kinetic analysis of DDX3X in helicase and nuclease reactions.

a Graphical representation of unwinding DDX3X activity in helicase assay in which the protein concentration (μM) is put in correlation with the percentage of processed RNA substrate (Products %).

b Graphical representation of unwinding DDX3X activity in nuclease assay in which the protein concentration (μM) is put in correlation with the percentage of processed DNA substrate embedded with a single rNMP (Products %).

$K_{1/2}$ and n_H indexes are shown.

c Graphical representation of unwinding DDX3X activity in nuclease assay in which the percentage of processed DNA substrate embedded with a single rNMP (Products %) is put in correlation with ATP concentration (ATP, mM) ID_{50} and n_H indexes are shown.

In addition, helicase activity seems not to be essential for RNaseH2-like activity since no unwinding was observed on the dsDNA nuclease Substrate 3, even at high DDX3X concentrations (Figure 18, lanes 1-5). In the absence of ATP, at the DDX3X concentrations which cut Substrate 3 in nuclease assays (Figure 18), digestion of the rCMP on the labelled strand caused the appearance of short products (asterisks in Figure 18, lanes 10-11). Since the gel was run under non-denaturing conditions, rCMP processing possibly destabilized the nicked DNA strand, causing its dissociation during the gel run. Thus, the RNaseH2-like activity of DDX3X did not require its RNA helicase activity.

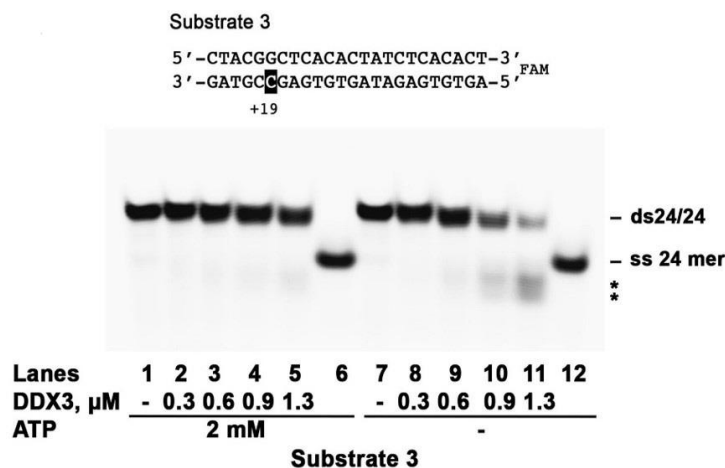


Figure 18: DDX3X titration in helicase assay using a dsDNA substrate bearing a single rNMP in position +19 (Substrate 3). In the presence of 2 mM ATP, no unwinding activity as observed (Lanes 1-5).

In the absence of ATP, there is the appearance of short products (marked with asterisks) that are probably the result of the nicked DNA strand (Lanes 10-11).

Since no other RNaseH2-like enzymes are known so far in human cells, our discovery of RNaseH2-like activity in DDX3X opens the possibility of alternative RER pathway(s), other than the canonical one.

We decided to use our *in vitro* system to reconstitute the entire RER pathway. It is unclear whether other Pols, besides Pols δ/ϵ , might perform the synthesis step of RER in eukaryotes. We incubated RNaseH2, hFen-1 and hDNA ligase1, in combination with the X-family DNA repair enzyme Pols β on a dsDNA substrate bearing a single rCMP at position +40 (Substrate 4, *Figure 19*) and long enough to allow productive binding by hFen-1. RNaseH2 generated the expected 39 nt product (*Figure 19*, lane 2), allowing subsequent incorporation by Pol β in the presence of dNTPs at their intracellular physiological range (50 μ M). Fully ligated 55 nt repair product appeared only in the presence of both hFen-1 and hDNA ligase (*Figure 19*, compare lane 3 with lane 4). This product was resistant to degradation by RNaseH2 added back after the ligation step, indicating that it did not contain rCMP (*Figure 19*, lane 5). When Pol β was replaced with Pol δ , as in the "classic" RER, again a reconstituted 55 nt product resistant to RNaseH2 digestion was observed as expected (*Figure 19*, lane 8).

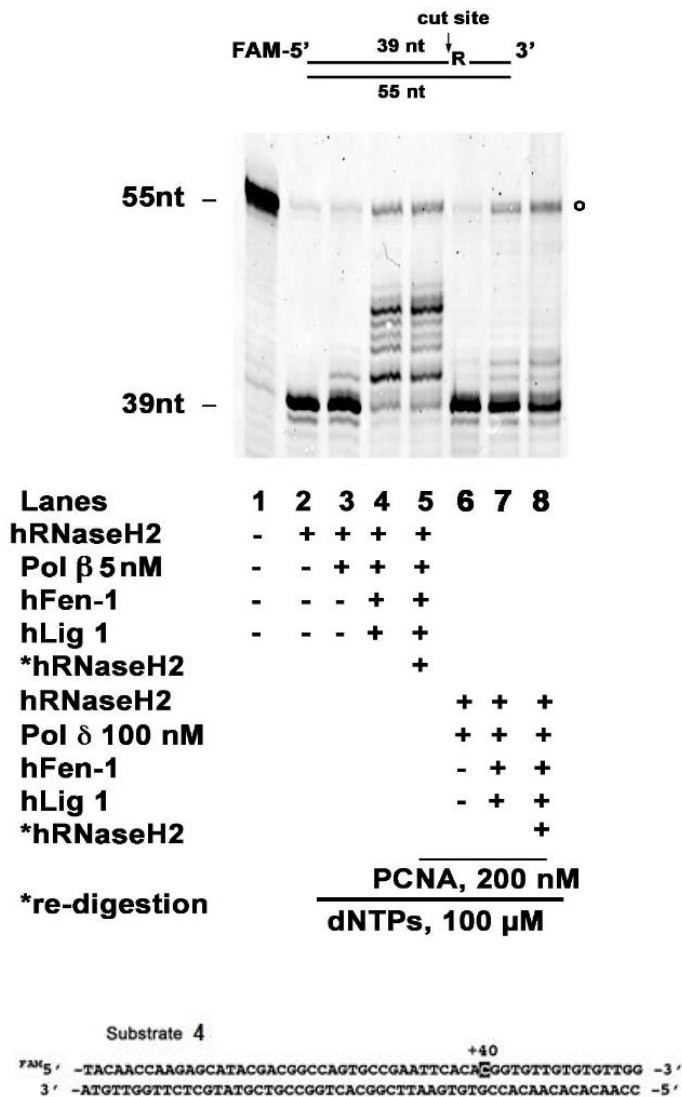


Figure 19: RER reactions in the presence of RNaseH2. The reactions were carried on by both pol β (Lanes 2 – 5) and δ (lanes 6-8) and in the presence of: 100 μM dNTPs, hFen-1 and hDNA ligase (Lanes 4,5,7,8), and 200 nM PCNA (Lanes 5-8). Fresh RNaseH2 was added after the ligation step to the heat inactivated reaction in lanes 5 and 8. Lane 1:

55/55mer substrate alone which sequence is specified under the figure.

Under similar conditions, we repeated the same experiments with DDX3X. Again, fully ligated 55 nt repair product appeared only in the presence of both hFen-1 and hDNA ligase1 (*Figure 20*).

Also, this product was resistant to degradation by RNaseH2 added back after the ligation step (*Figure 20*; Lanes 7 and 11). The DDX3X efficiency is a bit lower if compared with that one of RNaseH2, but we don't know if auxiliary factors or post-translational modifications might also modulate *in vivo* the efficiency of DDX3X. These results led us to three main conclusions:

- i) the human RNA helicase DDX3X has an RNaseH2-like activity
- ii) both RNaseH2- and DDX3X are able to initiate RER in *in vitro* reconstituted systems
- iii) both RNaseH2- and DDX3X- initiated RER reactions can be carried on not only by the canonical Pol δ/ϵ , but also by the repair Pol β , together with hFen-1 and hDNA ligase, leading to fully repaired products. These results suggest a greater flexibility of human cells in responding to the threat posed by rNMPs incorporation.

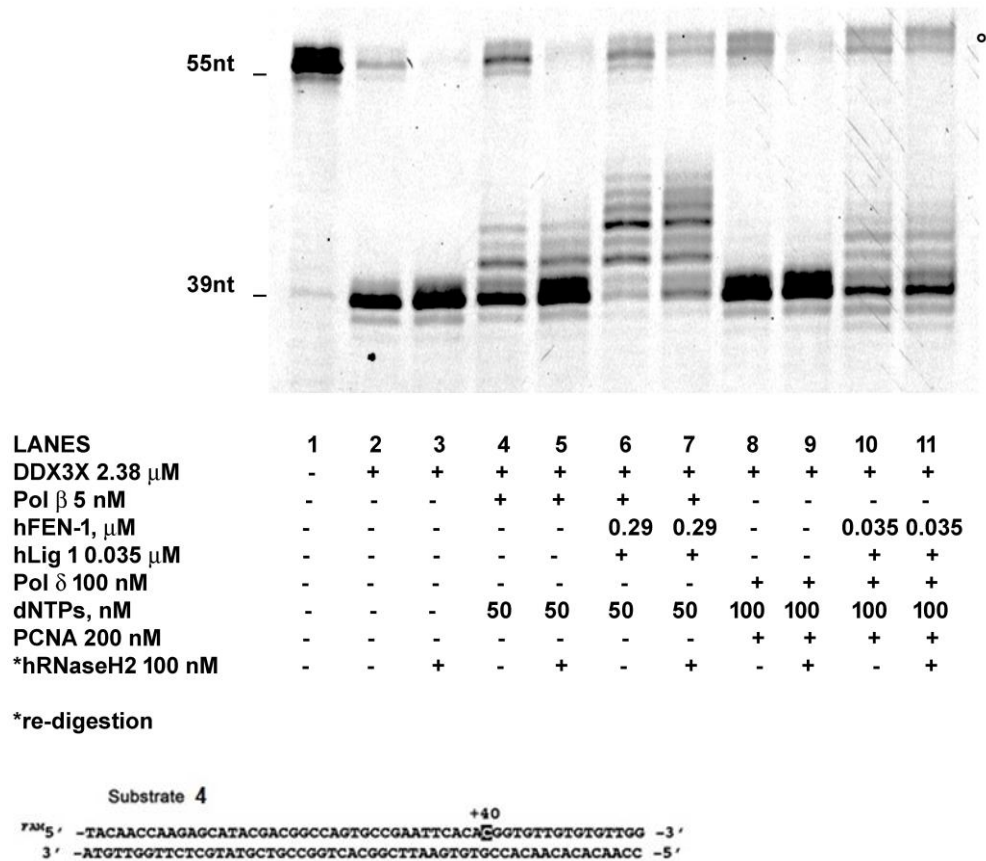


Figure 20: RER reactions in the presence of DDX3X.
 The reactions were carried on by both Pols β (4-7) and δ (Lanes 8-11) and in the presence of: 50/100 μ M dNTPs, hFen-1 and hDNA ligase (Lanes 6-7 and 10-11), and 200 nM PCNA (Lanes 8-11). Fresh RNaseH2 was added after the ligation step to the heat inactivated reaction in lanes 3, 5, 7, 9 and 11. Lane 1: 55/55mer substrate alone which sequence is specified under the figure.

Moving to physiological conditions, we wanted to assess the genome integrity of DDX3X knockdown (KD) cells. If DDX3X acts as an RNaseH2-like enzyme also *in vivo*, what we expected to see in DDX3X KD cells is an

accumulation of ribonucleotides. To this aim, we created DDX3X KD cell lines through lentiviral transduction technology (Material and Methods, paragraph 4.2.9) and we established a riboassay to measure the level of ribonucleotide incorporation into the cell genome (See Material and Methods, paragraph 4.3.12, for details).

To create stable DDX3X KD cell lines we used the Inducible Dharmacon™ TRIPZ™ Lentiviral shRNA (GE Healthcare). Virus particles were produced in HEK 293T cell line through calcium phosphate precipitation; then, the supernatant was used to transduce different tumoral cell lines in which the KD was maintained through puromycin selection and induced by the use of Doxycycline basing on the vector characteristics (*Figure 21*).

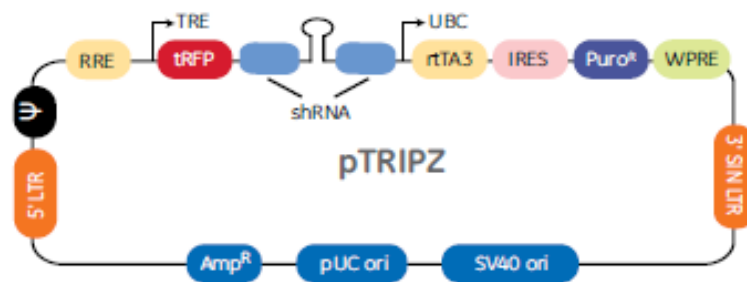


Figure 21: Schematic and features of the pTRIPZ Inducible Dharmacon™ TRIPZ™ Lentiviral shRNA vector (GE Healthcare).

The positive outcome of the KD was first verified by RFP expression (*Figure 22*) and then through Western blot analysis (*Figure 23*). *Figure 22* and *23* show the results obtained with U2OS cell line.

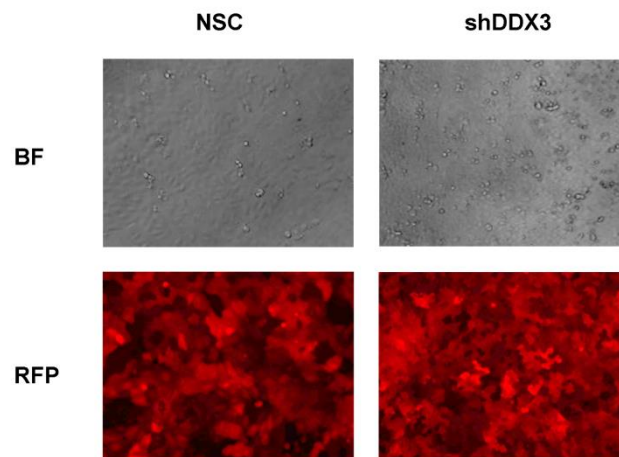


Figure 22: Detection of the correct pTRIPZ vector integration exploiting RFP emission in U2OS cell line.

Left: Bright field (BF) and RFP emission of U2OS non-silenced cells (NSC)

Right: Bright field (BF) and RFP emission of U2OS silenced cells (shDDX3)

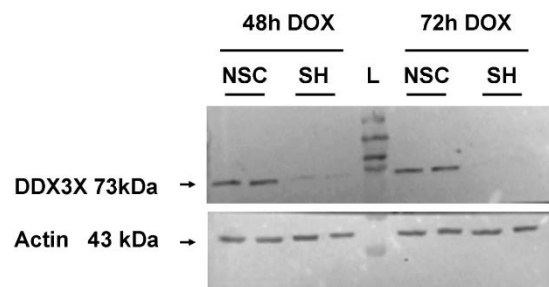


Figure 23: Silencing verification in U2OS cell line after 48- and 72-hours of Doxycycline (Dox) induction.

Western blot result was shown probing for DDX3X and β -actin.

L stays for ladder (Page Ruler™ prestained color ladder). NSC and SH stay for non-silenced cells and silenced cells respectively.

Then, we extracted the genomic DNA from NSC/shDDX3X cells and we performed a riboassay.

As shown in *Figure 24*, the level of ribonucleotides in shDDX3X cells is 3-fold higher than in NSC cell line after both *E. coli* RNaseH2 (*Figure 24 A*, compare the fluorescence increase between NSC untreated and *E. coli* RNaseH2- treated cells and shDDX3 untreated and *E. coli* RNaseH2- treated cells) and human recombinant RNaseH2 (*Figure 24 B*, compare the fluorescence increase between NSC untreated and human RNaseH2- treated cells and shDDX3X untreated and human RNaseH2- treated cells) treatments. This result demonstrated that DDX3X KD U2OS cell line is more prone to accumulate ribonucleotides compared to not silenced cells. This could be visible in different parts of the riboassay experiment. First of all, shDDX3X untreated genomic DNA seems partially nicked compared to the NSC untreated genomic DNA (*Figure 24*, compare NSC/shDDX3X untreated columns) meaning that shDDX3 genome, containing more ribonucleotides, is more prone to be broken. Unfortunately, this difference is not statistical significant (Kruskal Wallis statistical test, data not shown), despite the result seems reproducible among the different experiments. However, after RNaseH2 digestions, ribonucleotides accumulation appeared

more and more visible in shDDX3 cells than in NSC cells confirming our starting hypothesis. Specifically, the increased Atto647 fluorescence signal between untreated NSC and RNaseH2- treated cells is lower compared to the same increasing in shDDX3X cells. This result shows a P value significance lower than 0.05 (Student's T test) for both the treatments: *E. coli* and human RNaseH2 digestion (Figure 24).

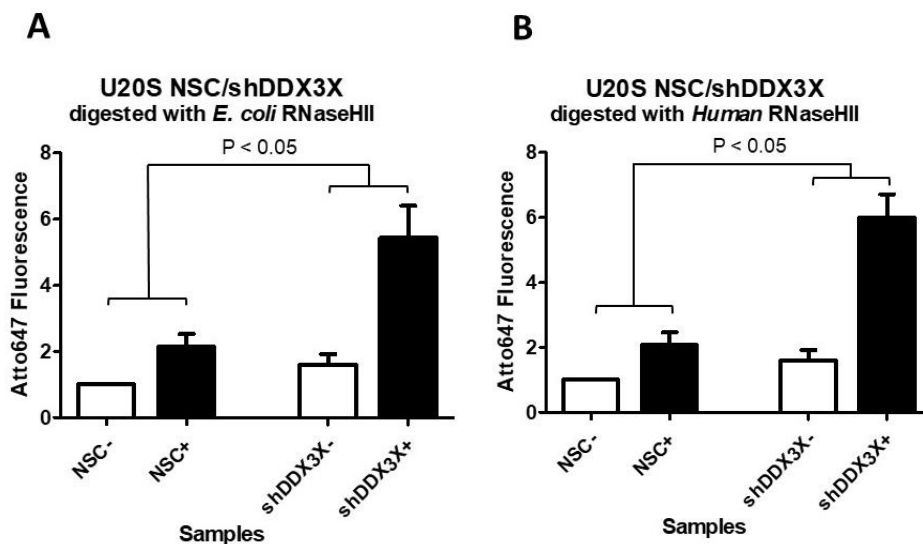


Figure 24: Graphical representation of Riboassay results for *E. coli* RNaseH2 digestion (A) and human RNaseH2 digestion (B). Data represent mean + standard error of the mean (SEM) of at least four independent experiments. Atto647 fluorescence is represented in Y-axis in arbitrary units setting NSC untreated cells signal as 1 fluorescence arbitrary unit. In the X-axis different treatments are indicated: Untreated genomic DNA (-), genomic DNA treated with 1 U of *E. coli* RNaseH2 or with 50 nM of human recombinant RNaseH2 (+).

6. Discussion

6.1 DDX3X AS A PRIME CELLULAR TARGET TO FIGHT OLD AND EMERGING VIRUSES

A limited number of broad-spectrum antivirals targeting different families of viruses (RNA viruses, DNA viruses and retroviruses), have been reported in the scientific literature up to now and only very few targeting cellular proteins (Aman *et al.*, 2009; Furuta *et al.*, 2009; Wolf *et al.*, 2010; Hoffmann *et al.*, 2011). However, none of these compounds have been rationally designed against its target, with the specific aim of achieving optimal selectivity.

The relevance and potential impact of this approach are further enhanced by the fact that, besides being active against different viruses, an antiviral agent targeting a host factor could have the additional advantage of overcoming the problem of drug resistance. In fact, a cell harbouring a mutated version of the target protein, will be more easily infected and thus either killed by the virus or by the host immune system, without gaining a fitness advantage. This, coupled with the low mutation rate of cellular proteins, could result in a very high genetic barrier towards drug resistance.

On the other hand, the main drawback of targeting a cellular protein is the possibility of unwanted side effects, either through the inhibition of the protein itself or by off-targeting of the drug towards other cellular enzymes (Garbelli *et al.*, 2017; Riva and Maga, 2019).

The cellular ATPase/RNA helicase DDX3X is considered an attractive molecular target for chemotherapy, since several studies indicated that inhibiting DDX3X can have a therapeutic efficacy both against cancer and viral infections, without significant toxicity. This is likely due to the fact that DDX3X is part of a family of more than 50 related RNA helicases, which can have overlapping compensatory roles in cell metabolism (Meier-Stephenson *et al.*, 2018).

DDX3X is required for the replication of several viruses, including HIV-1, Hepatitis C virus, JEV, DENV and WNV and in the last years, several molecules were developed by our group against DDX3X, providing proof-of-principle for its exploitation as a valuable new target for broad-spectrum antiviral chemotherapy (Brai *et al.*, 2016; Riva and Maga, 2019). However, the significant similarity both from a sequence and structural point of view, in the ATP- and RNA-binding sites among the members of the DEAD-box family of RNA helicases makes it difficult to achieve absolute selectivity for DDX3X only by conventional drug design, leaving the problem of possible off-targeting effects still open (Meier-Stephenson *et al.*, 2018).

The spread of the arthropod vectors and the frequent movement of people among different geographical areas, increase the risk of sudden outbreaks or even large epidemics caused by mosquito-borne viruses like DENV, WNV, JEV, CHIKV and ZIKV. The number of infected people by the aforementioned viruses is indeed raising. For example, the worldwide incidence of DENV has risen 30-fold in the past 30 years, and more countries are reporting their first outbreaks of the disease (WHO).

Emerging viruses like ZIKV, DENV, CHIKV are transmitted to humans by the *Aedes aegypti* and *Aedes albopictus* mosquitoes. More than half of the world's population live in areas where these mosquito species are present and climatic and human-caused changes can also expand the ecological niche of these animals (Manni *et al.*, 2017).

Classically, strategies to control these arboviral infections aim at reducing the susceptibility to vector infection (reduced competence/transmission) or of the host (antiviral drugs/vaccines). In this latter case, it would be greatly desirable to identify a unique target, whose inhibition could counteract the infection of a wide range of arboviruses. Under this respect, a cellular target, central to the replication of different viruses, will offer the possibility to develop broad-spectrum antivirals and to avoid the drug resistance problem connected with the normal utilization of viral targets (Garbelli *et al.*, 2017). As a consequence, we continuously make an effort to develop new DDX3X-specific molecules acting against these pathogens for which no specific drugs are available up to date.

We identified two completely new families of selective inhibitors of the helicase activity of DDX3X using two different approaches:

- a) On one hand, we created new “hybrid molecules” starting from new chemical scaffolds and already published molecules (Brai *et al.*, 2016) and match them together.
- b) On the other hand, we decided to target a completely unexplored DDX3X domain named “unique motif” that is not shared with other DExD-proteins and has no significant homologies with other cellular proteins.

The first approach allowed us to identify 21 compounds able to specifically target the helicase activity of DDX3X. Accordingly, they were inactive in the ATPase assay and in the helicase assay against the related human DEAD-box helicase DDX1.

Among the 21 compounds that showed promising activities *in vitro*, only 6 of them (*compounds 8, 9, 10, 13, 14 and 15*) possess also antiviral activities in WNV infected cells. Fortunately, all of them didn't show cellular toxicity and some of them (*compounds 10, 14 and 15*) have also a very good aqueous solubility overcoming an important limitation of previously published molecules (Brai *et al.*, 2016; Riva and Maga, 2019).

Noteworthy, in the absence of any approved molecule for the treatment of WNV infections, our study represents a step forward in the antiviral research against this emerging virus.

DDX3X recruitment on WNV replication site is already documented in the literature and our time of addition experiments seem to prove involvement of our compounds in the first phases of WNV replication (Linke *et al.*, 2007). We speculate their possible role in the step of protein translation after the entry process, but this still requires further investigations.

The second approach that we decided to follow allowed us to describe a completely new class of DDX3X inhibitors able to target a short motif (sequence -ALRAMKENGRYGRRK- aa 250-264) for which no molecule was described up to date. This approach could be named a “unique motif for a unique target” since is not shared among other DExD-box proteins, neither with other helicases. Having no information about molecules able to bind this motif, we started from *in silico* analysis. This analysis showed that two DDX3X residues could be important for the contact with UM inhibitors: the Glutamic acid in position 256 and the Arginine in position 262, respectively

located at the N- and C-terminal sides of the UM sequence.

Following *in vitro* mutagenesis and biochemical assays confirmed the predicted binding mode of our molecules. The major determinant for the inhibitor binding is the Glutamic acid in position 256: when we tested our molecules #11 UM and #13 UM against the E256A mutant, we detected a reduction of the compounds inhibitory potencies of 36,500- and 43- fold, respectively. Vice versa, the mutation R262A did not significantly change the inhibitory potencies of the compounds, with respect to the wild type enzyme. Moreover, all the UM molecules are active against the wild type protein in the low micromolar range. Again, to test their selectivity, we tested all the molecules against the related DDX1 protein and other two helicases, NS3 and STRS2, proving the predictive specificity.

Noteworthy, our UM molecules showed also no toxicity in cells and a considerable antiviral effect being able to suppress both the replication of WNV and DENV-2 viruses in infected cells.

6.2 AN ALTERNATIVE RIBONUCLEOTIDE EXCISION REPAIR BY THE RNA HELICASE/NUCLEASE DDX3X

Ribonucleotides erroneously inserted into the genome are the most abundant type of DNA damage, even more than oxidized bases or cyclobutene pyrimidine dimers (Wallace and Williams, 2014). Ribonucleotides misincorporation leads to deleterious consequences: it increases mutation rate and chromosomal abnormality, determines distortion of DNA helix and represents a replication fork barrier. The only enzymes known so far able to remove ribonucleotides into a DNA stretch are RNaseH-type ones. There are two main classes of RNaseH enzymes: RNaseH1 and RnaseH2 that have very different characteristics. The first one is able to remove RNA-DNA hybrids (or R-loops) of at least three-four ribonucleotides. In contrast, RnaseH2 is the only enzyme able to process also single ribonucleotides cleaving on the 5' side of them into a dsDNA context (Potenski and Klein, 2014). In RnaseH2-deficient mammalian cells, there is the activation of alternative and highly mutagenic pathways directed by Top-1 enzyme that

are deleterious for genome stability. Moreover, in humans the inactivation of RNaseH2 causes the Aicardi-Goutier syndrome (AGS), a rare genetic neurological disorder characterized by inflammatory response activation in the absence of exogenous stimuli. However, the exact sequence of molecular events connecting RNaseH2 inactivation and disease development remains to be elucidated (Potenski and Klein, 2014).

Different studies utilized specifically mutated polymerases to increase the level of misincorporated ribonucleotides in the genome. Comparing cells with wild type- and deficient- RNaseH2 enzyme, it appears clear that it is not just the absence of RNaseH2, but also the ribonucleotide processing that cause deleterious consequences. If the level of ribonucleotides exceeds a specific threshold, there is the insurgence of cellular stresses also in the presence of a completely functional RNaseH2.

At the moment there are no direct pieces of evidence that underline a link between RNaseH2 deficiency, genome instability and tumor development and this axis remains a very interesting subject to be studied.

Based on ten years experience in studying DDX3X protein and moved by the increasing conviction that the cell has to possess alternative pathways to control ribonucleotides threshold, we started to look at the two enzymes with a new awareness. We know that DDX3X resolves RNA/DNA hybrids and RNA secondary structures and it is involved in the degradation of RNAs (Schröder, 2010). Moreover, our structural analysis confirms interesting analogies between DDX3X and RNaseH2 catalytic core (see Results, paragraph 5.2, for details).

Using nuclease assays with specific DNA substrates embedded with a single rNTP, we demonstrated that DDX3X possess an RNaseH2-like activity. We were further able to demonstrate that both enzymes are perfectly able to carry on RER reactions *in vitro*. Since RNaseH2 enzyme is the only enzyme known so far able to remove a single ribonucleotide into a DNA sequence, these findings completely broaden the current RER view.

Another interesting result is the fact that not only replicative Pols like Pol δ are able to proceed with strand displacement and synthesis, but also the repair Pol β is able to do the same. Despite these are just preliminary results, they shed light on interesting observations: human cells could be very flexible in responding to rNTPs accumulation.

Moreover, riboassays experiments in control and DDX3X KD cells demonstrated that DDX3X KD cells are more prone to accumulate ribonucleotides in their genome, demonstrating a DDX3X involvement in the context of genome integrity maintenance.

7. Conclusions and perspectives

7.1 DDX3X AS A PRIME CELLULAR TARGET TO FIGHT OLD AND EMERGING VIRUSES

In conclusion our results indicate that DDX3X could be used in the near future as a target for broad-spectrum antiviral drugs endowed with maximal selectivity. The strategy that we decided to follow demonstrated that it is possible to develop a family of small molecules able to couple broad-spectrum antiviral activity with absolute selectivity for their molecular target. Such a seemingly paradoxical goal (broad spectrum activity versus high selectivity for the target), was achieved by exploiting a specific cellular target, the RNA helicase DDX3X, implementing molecular modelling, *in silico* drug design and medicinal chemistry techniques, to develop compounds specifically tailored on such a unique protein. In the case of UM compounds this strategy was also optimized through the targeting against a unique target of a unique protein: as a matter of fact, the DDX3X unique motif is strictly present only in this protein and not shared with others.

Of course, these molecules need further optimization. First of all, we want to test the selectivity of our inhibitors against a broader panel of DDX-family helicase *in vitro*. Then, we want to assess the effect of the same molecules also in cells specifically silenced for DDX3X. We are currently establishing and/or refining both approaches in our laboratory hopefully being able to soon publish all the data presented in this elaborate with new communications.

More important, we need to prove *in vivo* the tolerability and bioavailability of these compounds in order to proceed into the long way of antiviral drugs production. More investigations are useful also to understand the precise mechanism of action of these inhibitors during the virus life cycle. Our preliminary data about the compounds active against WNV demonstrated a possible DDX3X involvement in the very early phases of the infection. This could be useful in the development of prophylactic antiviral drugs before the virus contraction, opening new branches of our research.

7.2 AN ALTERNATIVE RIBONUCLEOTIDE EXCISION REPAIR BY THE RNA HELICASE/NUCLEASE DDX3X

Despite our preliminary results about of a possible DDX3X involvement in RER open new and exciting perspectives, they need further investigations. *In vitro* interactions of DDX3X with other RER components will be tested by pulldowns and co-IPs with both purified proteins and from cell extracts. We are establishing a collaboration with a company (Cogentech, Milan) to perform LC/MS analysis of IP of endogenous DDX3X coupled to the bound proteins. If through this approach we will able to find relevant DDX3X partners, we will proceed with immunofluorescence and PLA experiments.

We had already verified that DDX3X KD caused rNMPs accumulation, but it will be interesting to verify how the expression levels of both Pols, RNaseH2 and DDX3X affect rNMPs accumulation and DNA damage response. Moreover, manipulation of the expression levels of all the above-mentioned proteins could also sensitize tumor cell lines towards DNA damaging agents.

Our preliminary results shed light also on the fact that human cells could be very flexible in responding to rNTPs accumulations since strand displacement/synthesis could be carried on not only by the replicative Pol δ , but also by the reparative Pol β .

During DNA repair in all phases of the cell cycle, Pol β can incorporate rNMPs also opposite damaged bases, thus requiring RER for the removal of the rNMP on one strand and base excision repair (BER) for the removal of the damaged base on the opposite strand (Mentegari *et al.*, 2017). RER and BER can be delayed in the processing of these lesions. Since our experiments also suggest that repair Pols may operate in RER, it also remains to be understood how BER and RER pathways are coordinated in the context of these complex lesions. In *E. coli* has been already demonstrated that both MMR and NER serve as alternative ribonucleotide removal pathways. (Potenski and Klein, 2014) and it is feasible to think about a cross-talking among the eukaryotic DNA damage pathways. The fact that DDX3X could have a role in alternative RER pathways, further increases the complexity of such networks.

Surely more investigations are required in this direction, but we are convinced that our results, even at this preliminary stage, already broaden the current vision on the RER pathways operating in the cells: from one nuclease/one Pol to (at least) two nucleases/different Pols. Also the very closely related BER pathway operates with the contribution of several damage-recognition/incision proteins (the DNA glycosylases) and different Pols, in order to be flexible enough to cope with the many different base alterations occurring in the genome. Our results reveal that RER might have evolved according to the same logic of high flexibility.

References

- Aman, M. J., Kinch, M. S., Warfield, K., Warren, T., Yunus, A., Enterlein, S., Stavale, E., Wang, P., Chang, S. and Tang, Q.** (2009) 'Development of a broad-spectrum antiviral with activity against Ebola virus', *Antiviral Research*, 83(3), pp. 245–251. doi: 10.1016/j.antiviral.2009.06.001.
- Amaya, M., Brooks-Faulconer, T., Lark, T., Keck, F., Bailey, C., Raman, V. and Narayanan, A.** (2016) 'Venezuelan equine encephalitis virus non-structural protein 3 (nsP3) interacts with RNA helicases DDX1 and DDX3 in infected cells', *Antiviral Research*. doi: 10.1016/j.antiviral.2016.04.008.
- Ariumi, Y.** (2014) 'Multiple functions of DDX3 RNA helicase in gene regulation, tumorigenesis, and viral infection', *Frontiers in Genetics*. doi: 10.3389/fgene.2014.00423.
- Awano, N., Rajagopal, V., Arbing, M., Patel, S., Hunt, J., Inouye, M. and Phadtare, S.** (2010) 'Escherichia coli RNase R has dual activities, helicase and RNase', *Journal of Bacteriology*. doi: 10.1128/JB.01368-09.
- Ayalew, L. E., Patel, A. K., Gaba, A., Islam, A. and Tikoo, S. K.** (2016) 'Bovine adenovirus-3 pVIII suppresses cap-dependent mRNA translation possibly by interfering with the recruitment of DDX3 and translation initiation factors to the mRNA cap', *Frontiers in Microbiology*. doi: 10.3389/fmicb.2016.02119.
- Bol, G. M. et al.** (2015) 'DDX3, a potential target for cancer treatment.', *Molecular cancer*. doi: 10.1186/s12943-015-0461-7.
- Bol, G. M. et al.** (2015) 'Targeting DDX3 with a small molecule inhibitor for lung cancer therapy', *EMBO Molecular Medicine*, 7(5), pp. 648–669. doi: 10.15252/emmm.201404368.

- Bol, G. M., Raman, V., van der Groep, P., Vermeulen, J. F., Patel, A. H., van der Wall, E. and van Diest, P. J.** (2013) 'Expression of the RNA Helicase DDX3 and the Hypoxia Response in Breast Cancer', *PLoS ONE*. doi: 10.1371/journal.pone.0063548.
- Botlagunta, M., Krishnamachary, B., Vesuna, F., Winnard, P. T., Bol, G. M., Patel, A. H. and Raman, V.** (2011) 'Expression of DDX3 is directly modulated by hypoxia inducible factor-1 alpha in breast epithelial cells', *PLoS ONE*. doi: 10.1371/journal.pone.0017563.
- Botlagunta, M., Vesuna, F., Mironchik, Y., Raman, A., Lisok, A., Winnard, P., Mukadam, S., Van Diest, P., Chen, J. H., Farabaugh, P., Patel, A. H. and Raman, V.** (2008) 'Oncogenic role of DDX3 in breast cancer biogenesis', *Oncogene*. doi: 10.1038/onc.2008.33.
- Brai, A. et al.** (2016) 'Human DDX3 protein is a valuable target to develop broad spectrum antiviral agents', *Proceedings of the National Academy of Sciences*, 113(19), pp. 5388–5393. doi: 10.1073/pnas.1522987113.
- Brai, A., Martelli, F., Riva, V., Garbelli, A., Fazi, R., Zamperini, C., Pollutri, A., Falsitta, L., Ronzini, S., Maccari, L., Maga, G., Giannecchini, S. and Botta, M.** (2019) 'DDX3X Helicase Inhibitors as a New Strategy To Fight the West Nile Virus Infection', *Journal of Medicinal Chemistry*, 62(5), pp. 2333–2347. doi: 10.1021/acs.jmedchem.8b01403.
- Brennan, R., Haap-Hoff, A., Gu, L., Gautier, V., Long, A. and Schröder, M.** (2018) 'Investigating nucleo-cytoplasmic shuttling of the human DEAD-box helicase DDX3', *European Journal of Cell Biology*, 97(7), pp. 501–511. doi: 10.1016/j.ejcb.2018.08.001.
- Caldecott, K. W.** (2014) 'Ribose - An internal threat to DNA', *Science*. doi: 10.1126/science.1248234.
- Cavignac, Y., Lieber, D., Sampaio, K. L., Madlung, J., Lamkemeyer, T., Jahn, G., Nordheim, A. and Sinzger, C.** (2015) 'The cellular proteins

Grb2 and DDX3 are increased upon human cytomegalovirus infection and act in a proviral fashion', *PLoS ONE*. doi: 10.1371/journal.pone.0131614.

Chahar, H. S., Chen, S. and Manjunath, N. (2013) 'P-body components LSM1, GW182, DDX3, DDX6 and XRN1 are recruited to WNV replication sites and positively regulate viral replication', *Virology*. doi: 10.1016/j.virol.2012.09.041.

Chan, C.-H., Chen, C.-M., Lee, Y.-H. W. and You, L.-R. (2019) 'DNA Damage, Liver Injury, and Tumorigenesis: Consequences of DDX3X Loss', *Molecular Cancer Research*, 17(2), pp. 555–566. doi: 10.1158/1541-7786.MCR-18-0551.

Chang, P. C., Chi, C. W., Chau, G. Y., Li, F. Y., Tsai, Y. H., Wu, J. C. and Wu Lee, Y. H. (2006) 'DDX3, a DEAD box RNA helicase, is deregulated in hepatitis virus-associated hepatocellular carcinoma and is involved in cell growth control', *Oncogene*. doi: 10.1038/sj.onc.1209239.

Chao, C.-H., Chen, C.-M., Cheng, P.-L., Shih, J.-W., Tsou, A.-P. and Wu Lee, Y.-H. (2006) 'DDX3, a DEAD Box RNA Helicase with Tumor Growth-Suppressive Property and Transcriptional Regulation Activity of the p21 waf1/cip1 Promoter, Is a Candidate Tumor Suppressor', *Cancer Research*, 66(13), pp. 6579–6588. doi: 10.1158/0008-5472.CAN-05-2415.

Chen, H. H., Yu, H. I., Cho, W. C. and Tarn, W. Y. (2015) 'DDX3 modulates cell adhesion and motility and cancer cell metastasis via Rac1-mediated signaling pathway', *Oncogene*. doi: 10.1038/onc.2014.190.

Chen, H. H., Yu, H. I., Yang, M. H. and Tarn, W. Y. (2018) 'DDX3 Activates CBC-eIF3-Mediated translation of uORF-containing oncogenic mRNAs to promote metastasis in HNSCC', *Cancer Research*. doi: 10.1158/0008-5472.CAN-18-0282.

Chen, W.-J., Wang, W.-T., Tsai, T.-Y., Li, H.-K. and Lee, Y.-H. W. (2017) 'DDX3 localizes to the centrosome and prevents multipolar mitosis by epigenetically and translationally modulating p53 expression', *Scientific Reports*, 7(1), p. 9411. doi: 10.1038/s41598-017-09779-w.

Chon, H., Vassilev, A., DePamphilis, M. L., Zhao, Y., Zhang, J., Burgers, P. M., Crouch, R. J. and Cerritelli, S. M. (2009) 'Contributions of the two accessory subunits, RNASEH2B and RNASEH2C, to the activity and properties of the human RNase H2 complex', *Nucleic Acids Research*, 37(1), pp. 96–110. doi: 10.1093/nar/gkn913.

Cordin, O., Banroques, J., Tanner, N. K. and Linder, P. (2006) 'The DEAD-box protein family of RNA helicases', *Gene*. doi: 10.1016/j.gene.2005.10.019.

Crespan, E., Furrer, A., Rösinger, M., Bertoletti, F., Mentegari, E., Chiapparini, G., Imhof, R., Ziegler, N., Sturla, S. J., Hübscher, U., van Loon, B. and Maga, G. (2016) 'Impact of ribonucleotide incorporation by DNA polymerases β and λ on oxidative base excision repair', *Nature Communications*, 7(1), p. 10805. doi: 10.1038/ncomms10805.

Cruciat, C. M., Dolde, C., De Groot, R. E. A., Ohkawara, B., Reinhard, C., Korswagen, H. C. and Niehrs, C. (2013) 'RNA helicase DDX3 is a regulatory subunit of casein kinase 1 in Wnt- β -catenin signaling', *Science*. doi: 10.1126/science.1231499.

Ditton, H. J., Zimmer, J., Kamp, C., Rajpert-De Meyts, E. and Vogt, P. H. (2004) 'The AZFa gene DBY (DDX3Y) is widely transcribed but the protein is limited to the male germ cells by translation control', *Human Molecular Genetics*. doi: 10.1093/hmg/ddh240.

Dobashi, A., Tsuyama, N., Asaka, R., Togashi, Y., Ueda, K., Sakata, S., Baba, S., Sakamoto, K., Hatake, K. and Takeuchi, K. (2016) 'Frequent BCOR aberrations in extranodal NK/T-Cell lymphoma, nasal type', *Genes, Chromosomes and Cancer*, 55(5), pp. 460–471. doi: 10.1002/gcc.22348.

- Epling, L. B., Grace, C. R., Lowe, B. R., Partridge, J. F. and Enemark, E. J.** (2015) 'Cancer-associated mutants of RNA helicase DDX3X are defective in RNA-stimulated ATP hydrolysis', *Journal of Molecular Biology*. doi: 10.1016/j.jmb.2015.02.015.
- Fazi, R., Tintori, C., Brai, A., Botta, L., Selvaraj, M., Garbelli, A., Maga, G. and Botta, M.** (2015) 'Homology Model-Based Virtual Screening for the Identification of Human Helicase DDX3 Inhibitors', *Journal of Chemical Information and Modeling*. doi: 10.1021/acs.jcim.5b00419.
- Floor, S. N., Condon, K. J., Sharma, D., Jankowsky, E. and Doudna, J. A.** (2016) 'Autoinhibitory interdomain interactions and subfamily-specific extensions redefine the catalytic core of the human DEAD-box protein DDX3', *Journal of Biological Chemistry*. doi: 10.1074/jbc.M115.700625.
- Foresta, C.** (2000) 'Deletion and expression analysis of AZFa genes on the human Y chromosome revealed a major role for DBY in male infertility', *Human Molecular Genetics*. doi: 10.1093/hmg/9.8.1161.
- Franca, R., Belfiore, A., Spadari, S. and Maga, G.** (2007) 'Human DEAD-box ATPase DDX3 shows a relaxed nucleoside substrate specificity', *Proteins: Structure, Function and Genetics*. doi: 10.1002/prot.21433.
- Fröhlich, A., Rojas-Araya, B., Pereira-Montecinos, C., Dellarossa, A., Toro-Ascuy, D., Prades-Pérez, Y., García-de-Gracia, F., Garcés-Alday, A., Rubilar, P. S., Valiente-Echeverría, F., Ohlmann, T. and Soto-Rifo, R.** (2016) 'DEAD-box RNA helicase DDX3 connects CRM1-dependent nuclear export and translation of the HIV-1 unspliced mRNA through its N-terminal domain', *Biochimica et Biophysica Acta - Gene Regulatory Mechanisms*. doi: 10.1016/j.bbagr.2016.03.009.
- Fukumura, J., Noguchi, E., Sekiguchi, T. and Nishimoto, T.** (2003) 'A temperature-sensitive mutant of the mammalian RNA helicase, DEAD-BOX X isoform, DBX, defective in the transition from G1 to S phase', *Journal of Biochemistry*. doi: 10.1093/jb/mvg126.

Furuta, Y., Takahashi, K., Shiraki, K., Sakamoto, K., Smee, D. F., Barnard, D. L., Gowen, B. B., Julander, J. G. and Morrey, J. D. (2009) 'T-705 (favipiravir) and related compounds: Novel broad-spectrum inhibitors of RNA viral infections', *Antiviral Research*, 82(3), pp. 95–102. doi: 10.1016/j.antiviral.2009.02.198.

Garbelli, A., Beermann, S., Di Cicco, G., Dietrich, U. and Maga, G. (2011) 'A motif unique to the human dead-box protein DDX3 is important for nucleic acid binding, ATP hydrolysis, RNA/DNA unwinding and HIV-1 replication', *PLoS ONE*. doi: 10.1371/journal.pone.0019810.

Garbelli, A., Riva, V., Crespan, E. and Maga, G. (2017) 'How to win the HIV-1 drug resistance hurdle race: running faster or jumping higher?', *The Biochemical journal*, 474(10), pp. 1559–1577. doi: 10.1042/BCJ20160772.

Grainger, S. and Willert, K. (2018) 'Mechanisms of Wnt signaling and control', *Wiley Interdisciplinary Reviews: Systems Biology and Medicine*, 10(5), p. e1422. doi: 10.1002/wsbm.1422.

Gringhuis, S. I., Hertoghs, N., Kaptein, T. M., Zijlstra-Willems, E. M., Sarrami-Foorooshani, R., Sprokholt, J. K., Van Teijlingen, N. H., Kootstra, N. A., Booiman, T., Van Dort, K. A., Ribeiro, C. M. S., Drewniak, A. and Geijtenbeek, T. B. H. (2017) 'HIV-1 blocks the signaling adaptor MAVS to evade antiviral host defense after sensing of abortive HIV-1 RNA by the host helicase DDX3', *Nature Immunology*. doi: 10.1038/ni.3647.

Gu, L., Fullam, A., Brennan, R. and Schroder, M. (2013) 'Human DEAD Box Helicase 3 Couples I B Kinase to Interferon Regulatory Factor 3 Activation', *Molecular and Cellular Biology*. doi: 10.1128/mcb.01603-12.

Gu, L., Fullam, A., McCormack, N., Höhn, Y. and Schröder, M. (2017) 'DDX3 directly regulates TRAF3 ubiquitination and acts as a scaffold to co-ordinate assembly of signalling complexes downstream from MAVS', *Biochemical Journal*. doi: 10.1042/bcj20160956.

He, T.-Y., Wu, D.-W., Lin, P.-L., Wang, L., Huang, C.-C., Chou, M.-C. and Lee, H. (2016) 'DDX3 promotes tumor invasion in colorectal cancer via the CK1 ϵ /Dvl2 axis', *Scientific Reports*, 6(1), p. 21483. doi: 10.1038/srep21483.

Heerma van Voss, M. R., van Diest, P. J. and Raman, V. (2017) 'Targeting RNA helicases in cancer: The translation trap', *Biochimica et Biophysica Acta (BBA) - Reviews on Cancer*, 1868(2), pp. 510–520. doi: 10.1016/j.bbcan.2017.09.006.

Heerma van Voss, M. R., Kammers, K., Vesuna, F., Brilliant, J., Bergman, Y., Tantravedi, S., Wu, X., Cole, R. N., Holland, A., van Diest, P. J. and Raman, V. (2018) 'Global Effects of DDX3 Inhibition on Cell Cycle Regulation Identified by a Combined Phosphoproteomics and Single Cell Tracking Approach', *Translational Oncology*. doi: 10.1016/j.tranon.2018.04.001.

Heerma Van Voss, M. R., Vesuna, F., Bol, G. M., Meeldijk, J., Raman, A., Offerhaus, G. J., Buerger, H., Patel, A. H., Van Der Wall, E., Van Diest, P. J. and Raman, V. (2017) 'Nuclear DDX3 expression predicts poor outcome in colorectal and breast cancer', *OncoTargets and Therapy*. doi: 10.2147/OTT.S140639.

Hoffmann, H.-H., Kunz, A., Simon, V. A., Palese, P. and Shaw, M. L. (2011) 'Broad-spectrum antiviral that interferes with de novo pyrimidine biosynthesis', *Proceedings of the National Academy of Sciences*, 108(14), pp. 5777–5782. doi: 10.1073/pnas.1101143108.

Högbom, M., Collins, R., van den Berg, S., Jenvert, R.-M., Karlberg, T., Kotenyova, T., Flores, A., Hedestam, G. B. K. and Schiavone, L. H. (2007) 'Crystal Structure of Conserved Domains 1 and 2 of the Human DEAD-box Helicase DDX3X in Complex with the Mononucleotide AMP', *Journal of Molecular Biology*, 372(1), pp. 150–159. doi: 10.1016/j.jmb.2007.06.050.

Huang, J. S., Chao, C. C., Su, T. L., Yeh, S. H., Chen, D. S., Chen, C. T., Chen, P. J. and Jou, Y. S. (2004) 'Diverse cellular transformation capability of overexpressed genes in human hepatocellular carcinoma', *Biochemical and Biophysical Research Communications*. doi: 10.1016/j.bbrc.2004.01.151.

Ishaq, M., Hu, J., Wu, X., Fu, Q., Yang, Y., Liu, Q. and Guo, D. (2008) 'Knockdown of cellular RNA helicase DDX3 by short hairpin RNAs suppresses HIV-1 viral replication without inducing apoptosis', *Molecular Biotechnology*. doi: 10.1007/s12033-008-9040-0.

Jefferson, M., Donaszi-Ivanov, A., Pollen, S., Dalmay, T., Saalbach, G. and Powell, P. P. (2014) 'Host Factors That Interact with the Pestivirus N-Terminal Protease, Npro, Are Components of the Ribonucleoprotein Complex', *Journal of Virology*. doi: 10.1128/jvi.00984-14.

Jiang, L. et al. (2015) 'Exome sequencing identifies somatic mutations of DDX3X in natural killer/T-cell lymphoma', *Nature Genetics*, 47(9), pp. 1061–1066. doi: 10.1038/ng.3358.

Kalverda, A. P., Thompson, G. S., Vogel, A., Schröder, M., Bowie, A. G., Khan, A. R. and Homans, S. W. (2009) 'Poxvirus K7 Protein Adopts a Bcl-2 Fold: Biochemical Mapping of Its Interactions with Human DEAD Box RNA Helicase DDX3', *Journal of Molecular Biology*, 385(3), pp. 843–853. doi: 10.1016/j.jmb.2008.09.048.

Kang, J. Il, Kwon, Y. C. and Ahn, B. Y. (2012) 'Modulation of the type I interferon pathways by culture-adaptive hepatitis C virus core mutants', *FEBS Letters*. doi: 10.1016/j.febslet.2012.03.062.

Khadivjam, B., Stegen, C., Hogue-Racine, M.-A., El Bilali, N., Döhner, K., Sodeik, B. and Lippé, R. (2017) 'The ATP-Dependent RNA Helicase DDX3X Modulates Herpes Simplex Virus 1 Gene Expression', *Journal of Virology*. doi: 10.1128/jvi.02411-16.

Khadka, S., Vangeloff, A. D., Zhang, C., Siddavatam, P., Heaton, N. S., Wang, L., Sengupta, R., Sahasrabudhe, S., Randall, G., Gribskov, M., Kuhn, R. J., Perera, R. and LaCount, D. J. (2011) 'A Physical Interaction Network of Dengue Virus and Human Proteins', *Molecular & Cellular Proteomics*. doi: 10.1074/mcp.m111.012187.

Khamina, K. et al. (2017) 'Characterization of host proteins interacting with the lymphocytic choriomeningitis virus L protein', *PLoS Pathogens*. doi: 10.1371/journal.ppat.1006758.

Khapersky, D. A., Emara, M. M., Johnston, B. P., Anderson, P., Hatchette, T. F. and McCormick, C. (2014) 'Influenza A Virus Host Shutoff Disables Antiviral Stress-Induced Translation Arrest', *PLoS Pathogens*. doi: 10.1371/journal.ppat.1004217.

Kidwell, M. A., Chan, J. M. and Doudna, J. A. (2014) 'Evolutionarily conserved roles of the dicer helicase domain in regulating RNA interference processing', *Journal of Biological Chemistry*. doi: 10.1074/jbc.M114.589051.

Kim, Y. S., Lee, S. G., Park, S. H. and Song, K. (2001) 'Gene structure of the human DDX3 and chromosome mapping of its related ...', *Molecules and cells*.

Ko, C., Lee, S., Windisch, M. P. and Ryu, W.-S. (2014) 'DDX3 DEAD-Box RNA Helicase Is a Host Factor That Restricts Hepatitis B Virus Replication at the Transcriptional Level', *Journal of Virology*. doi: 10.1128/jvi.02035-14.

Kondaskar, A., Kondaskar, S., Fishbein, J. C., Carter-Cooper, B. A., Lapidus, R. G., Sadowska, M., Edelman, M. J. and Hosmane, R. S. (2013) 'Structure-based drug design and potent anti-cancer activity of tricyclic 5:7:5-fused diimidazo[4,5-d:4',5'-f][1,3]diazepines', *Bioorganic & Medicinal Chemistry*, 21(3), pp. 618–631. doi: 10.1016/j.bmc.2012.11.050.

Kondaskar, A., Kondaskar, S., Kumar, R., Fishbein, J. C., Muvarak, N., Lapidus, R. G., Sadowska, M., Edelman, M. J., Bol, G. M., Vesuna, F., Raman, V. and Hosmane, R. S. (2011) 'Novel, Broad Spectrum Anticancer Agents Containing the Tricyclic 5:7:5-Fused Diimidazodiazepine Ring System', *ACS Medicinal Chemistry Letters*, 2(3), pp. 252–256. doi: 10.1021/ml100281b.

Lahn, B. T. and Page, D. C. (1997) 'Functional coherence of the human Y chromosome', *Science*. doi: 10.1126/science.278.5338.675.

Lai, M.-C., Chang, W.-C., Shieh, S.-Y. and Tarn, W.-Y. (2010) 'DDX3 Regulates Cell Growth through Translational Control of Cyclin E1', *Molecular and Cellular Biology*. doi: 10.1128/mcb.00560-10.

Lai, M. C., Wang, S. W., Cheng, L., Tarn, W. Y., Tsai, S. J. and Sun, H. S. (2013) 'Human DDX3 Interacts with the HIV-1 Tat Protein to Facilitate Viral mRNA Translation', *PLoS ONE*. doi: 10.1371/journal.pone.0068665.

Lee, C.-H., Lin, S.-H., Yang, S.-F., Yang, S.-M., Chen, M.-K., Lee, H., Ko, J.-L., Chen, C.-J. and Yeh, K.-T. (2014) 'Low/negative expression of DDX3 might predict poor prognosis in non-smoker patients with oral cancer', *Oral Diseases*, 20(1), pp. 76–83. doi: 10.1111/odi.12076.

Lee, C. S., Dias, A. P., Jedrychowski, M., Patel, A. H., Hsu, J. L. and Reed, R. (2008) 'Human DDX3 functions in translation and interacts with the translation initiation factor eIF3', *Nucleic Acids Research*. doi: 10.1093/nar/gkn454.

Lenarcic, E. M., Ziehr, B. J. and Moorman, N. J. (2015) 'An unbiased proteomics approach to identify human cytomegalovirus RNA-associated proteins', *Virology*. doi: 10.1016/j.virol.2015.02.008.

Li, C., Ge, L. ling, Li, P. peng, Wang, Y., Dai, J. juan, Sun, M. xia, Huang, L., Shen, Z. qiang, Hu, X. chun, Ishag, H. and Mao, X. (2014) 'Cellular DDX3 regulates Japanese encephalitis virus replication by interacting with viral un-translated regions', *Virology*. doi:

10.1016/j.virol.2013.11.008.

Li, G., Feng, T., Pan, W., Shi, X. and Dai, J. (2015) 'DEAD-box RNA helicase DDX3X inhibits DENV replication via regulating type one interferon pathway', *Biochemical and Biophysical Research Communications*. doi: 10.1016/j.bbrc.2014.11.080.

Li, L., Monckton, E. A. and Godbout, R. (2008) 'A Role for DEAD Box 1 at DNA Double-Strand Breaks', *Molecular and Cellular Biology*. doi: 10.1128/mcb.01053-08.

Li Q, Zhang P, Zhang C, Wang Y, Wan R, Yang Y, Guo X, Huo R, Lin M, Zhou Z, S. J. (2014) 'DDX3X regulates cell survival and cell cycle during mouse early embryonic development', *Journal of Biomedical Research*. doi: 10.7555/jbr.27.20130047.

Linke, S., Ellerbrok, H., Niedrig, M., Nitsche, A. and Pauli, G. (2007) 'Detection of West Nile virus lineages 1 and 2 by real-time PCR', *Journal of Virological Methods*. doi: 10.1016/j.jviromet.2007.05.021.

Liu, H. and Naismith, J. H. (2008) 'An efficient one-step site-directed deletion, insertion, single and multiple-site plasmid mutagenesis protocol', *BMC Biotechnology*, 8(1), p. 91. doi: 10.1186/1472-6750-8-91.

van Loon, B., Ferrari, E. and Hübscher, U. (2009) 'Isolation of recombinant DNA elongation proteins.', *Methods in molecular biology (Clifton, N.J.)*, 521, pp. 345–59. doi: 10.1007/978-1-60327-815-7_19.

Loret, S., Guay, G. and Lippe, R. (2008) 'Comprehensive Characterization of Extracellular Herpes Simplex Virus Type 1 Virions', *Journal of Virology*. doi: 10.1128/jvi.00904-08.

Loureiro, M. E. et al. (2018) 'DDX3 suppresses type I interferons and favors viral replication during Arenavirus infection', *PLoS Pathogens*. doi: 10.1371/journal.ppat.1007125.

Ma, X. and He, F. (2003) 'Advances in the study of SR protein family.', *Genomics, proteomics & bioinformatics / Beijing Genomics Institute*. doi: 10.1016/S1672-0229(03)01002-7.

Maga, G. et al. (2011) 'Toward the Discovery of Novel Anti-HIV Drugs. Second-Generation Inhibitors of the Cellular ATPase DDX3 with Improved Anti-HIV Activity: Synthesis, Structure-Activity Relationship Analysis, Cytotoxicity Studies, and Target Validation', *ChemMedChem*. doi: 10.1002/cmdc.201100166.

Maga, G., Falchi, F., Garbelli, A., Belfiore, A., Witvrouw, M., Manetti, F. and Botta, M. (2008) 'Pharmacophore Modeling and Molecular Docking Led to the Discovery of Inhibitors of Human Immunodeficiency Virus-1 Replication Targeting the Human Cellular Aspartic Acid–Glutamic Acid–Alanine–Aspartic Acid Box Polypeptide 3', *Journal of Medicinal Chemistry*, 51(21), pp. 6635–6638. doi: 10.1021/jm8008844.

Mahboobi, S. H., Javanpour, A. A. and Mofrad, M. R. K. (2015) 'The interaction of RNA helicase DDX3 with HIV-1 Rev-CRM1-RanGTP complex during the HIV replication cycle', *PLoS ONE*. doi: 10.1371/journal.pone.0112969.

Mamiya, N. and Worman, H. J. (1999) 'Hepatitis C virus core protein binds to a DEAD box RNA helicase', *Journal of Biological Chemistry*. doi: 10.1074/jbc.274.22.15751.

Manni, M., Guglielmino, C. R., Scolari, F., Vega-Rúa, A., Failloux, A. B., Somboon, P., Lisa, A., Savini, G., Bonizzoni, M., Gomulski, L. M., Malacrida, A. R. and Gasperi, G. (2017) 'Genetic evidence for a worldwide chaotic dispersion pattern of the arbovirus vector, *Aedes albopictus*', *PLoS Neglected Tropical Diseases*. doi: 10.1371/journal.pntd.0005332.

Meier-Stephenson, V., Mrozowich, T., Pham, M. and Patel, T. R. (2018) 'DEAD-box helicases: the Yin and Yang roles in viral infections', *Biotechnology and Genetic Engineering Reviews*, 34(1), pp. 3–32. doi:

10.1080/02648725.2018.1467146.

Mentegari, E., Crespan, E., Bavagnoli, L., Kissova, M., Bertoletti, F., Sabbioneda, S., Imhof, R., Sturla, S. J., Nilforoushan, A., Hübscher, U., van Loon, B. and Maga, G. (2017) 'Ribonucleotide incorporation by human DNA polymerase η impacts translesion synthesis and RNase H2 activity.', *Nucleic acids research*, 45(5), pp. 2600–2614. doi: 10.1093/nar/gkw1275.

Meroni, A., Nava, G. M., Sertic, S., Plevani, P., Muzi-Falconi, M. and Lazzaro, F. (2018) 'Measuring the Levels of Ribonucleotides Embedded in Genomic DNA', in, pp. 319–327. doi: 10.1007/978-1-4939-7306-4_22.

Miao, X., Yang, Z.-L., Xiong, L., Zou, Q., Yuan, Y., Li, J., Liang, L., Chen, M. and Chen, S. (2013) 'Nectin-2 and DDX3 are biomarkers for metastasis and poor prognosis of squamous cell/adenosquamous carcinomas and adenocarcinoma of gallbladder.', *International journal of clinical and experimental pathology*, 6(2), pp. 179–90.

Oda, S. ichiro, Schröder, M. and Khan, A. R. (2009) 'Structural Basis for Targeting of Human RNA Helicase DDX3 by Poxvirus Protein K7', *Structure*. doi: 10.1016/j.str.2009.09.005.

Oh, S. et al. (2016) 'Medulloblastoma-associated DDX3 variant selectively alters the translational response to stress', *Oncotarget*. doi: 10.18632/oncotarget.8612.

Oshiumi, H., Ikeda, M., Matsumoto, M., Watanabe, A., Takeuchi, O., Akira, S., Kato, N., Shimotohno, K. and Seya, T. (2010a) 'Hepatitis C virus core protein abrogates the DDX3 function that enhances IPS-1-mediated IFN-beta induction', *PLoS ONE*. doi: 10.1371/journal.pone.0014258.

Oshiumi, H., Sakai, K., Matsumoto, M. and Seya, T. (2010b) 'DEAD/H BOX 3 (DDX3) helicase binds the RIG-I adaptor IPS-1 to up-regulate IFN- β -inducing potential', *European Journal of Immunology*, 40(4), pp. 940–

948. doi: 10.1002/eji.200940203.

Owsianka, A. M. and Patel, A. H. (1999) 'Hepatitis C virus core protein interacts with a human DEAD box protein DDX3', *Virology*. doi: 10.1006/viro.1999.9659.

Park, E. et al. (2019) 'Co-degradation of interferon signaling factor DDX3 by PB1-F2 as a basis for high virulence of 1918 pandemic influenza', *The EMBO Journal*. doi: 10.15252/embj.201899475.

Pène, V., Li, Q., Sodroski, C., Hsu, C.-S. and Liang, T. J. (2015) 'Dynamic Interaction of Stress Granules, DDX3X, and IKK- α Mediates Multiple Functions in Hepatitis C Virus Infection', *Journal of Virology*. doi: 10.1128/jvi.03197-14.

Phung, B. et al. (2019) 'The X-Linked DDX3X RNA Helicase Dictates Translation Reprogramming and Metastasis in Melanoma', *Cell Reports*. doi: 10.1016/j.celrep.2019.05.069.

Potenski, C. J. and Klein, H. L. (2014) 'How the misincorporation of ribonucleotides into genomic DNA can be both harmful and helpful to cells', *Nucleic Acids Research*, 42(16), pp. 10226–10234. doi: 10.1093/nar/gku773.

Potenski, C. J., Niu, H., Sung, P. and Klein, H. L. (2014) 'Avoidance of ribonucleotide-induced mutations by RNase H2 and Srs2-Exo1 mechanisms', *Nature*. doi: 10.1038/nature13292.

Radi, M., Falchi, F., Garbelli, A., Samuele, A., Bernardo, V., Paolucci, S., Baldanti, F., Schenone, S., Manetti, F., Maga, G. and Botta, M. (2012) 'Discovery of the first small molecule inhibitor of human DDX3 specifically designed to target the RNA binding site: Towards the next generation HIV-1 inhibitors', *Bioorganic & Medicinal Chemistry Letters*, 22(5), pp. 2094–2098. doi: 10.1016/j.bmcl.2011.12.135.

- Riva, V. and Maga, G.** (2019) 'From the magic bullet to the magic target: exploiting the diverse roles of DDX3X in viral infections and tumorigenesis', *Future Medicinal Chemistry*, p. fmc-2018-0451. doi: 10.4155/fmc-2018-0451.
- Samal, S. K., Routray, S., Veeramachaneni, G. K., Dash, R. and Botlagunta, M.** (2015) 'Ketorolac salt is a newly discovered DDX3 inhibitor to treat oral cancer', *Scientific Reports*. doi: 10.1038/srep09982.
- Schröder, M.** (2010) 'Human DEAD-box protein 3 has multiple functions in gene regulation and cell cycle control and is a prime target for viral manipulation', *Biochemical Pharmacology*. doi: 10.1016/j.bcp.2009.08.032.
- Schröder, M., Baran, M. and Bowie, A. G.** (2008) 'Viral targeting of DEAD box protein 3 reveals its role in TBK1/IKKε-mediated IRF activation', *EMBO Journal*. doi: 10.1038/emboj.2008.143.
- Schütz, P., Karlberg, T., van den Berg, S., Collins, R., Lehtiö, L., Högbom, M., Holmberg-Schiavone, L., Tempel, W., Park, H. W., Hammarström, M., Moche, M., Thorsell, A. G. and Schüler, H.** (2010) 'Comparative structural analysis of human DEAD-Box RNA helicases', *PLoS ONE*. doi: 10.1371/journal.pone.0012791.
- Sharma, D., Putnam, A. A. and Jankowsky, E.** (2017) 'Biochemical Differences and Similarities between the DEAD-Box Helicase Orthologs DDX3X and Ded1p', *Journal of Molecular Biology*. doi: 10.1016/j.jmb.2017.10.008.
- Shih, J.-W., Wang, W.-T., Tsai, T.-Y., Kuo, C.-Y., Li, H.-K. and Wu Lee, Y.-H.** (2012) 'Critical roles of RNA helicase DDX3 and its interactions with eIF4E/PABP1 in stress granule assembly and stress response', *Biochemical Journal*, 441(1), pp. 119–129. doi: 10.1042/BJ20110739.
- Song, H. and Ji, X.** (2019) 'The mechanism of RNA duplex recognition and unwinding by DEAD-box helicase DDX3X', *Nature Communications*,

10(1), p. 3085. doi: 10.1038/s41467-019-11083-2.

Soto-Rifo, R., Rubilar, P. S. and Ohlmann, T. (2013) 'The DEAD-box helicase DDX3 substitutes for the cap-binding protein eIF4E to promote compartmentalized translation initiation of the HIV-1 genomic RNA', *Nucleic Acids Research*. doi: 10.1093/nar/gkt306.

Sparks, J. L., Chon, H., Cerritelli, S. M., Kunkel, T. A., Johansson, E., Crouch, R. J. and Burgers, P. M. (2012) 'RNase H2-Initiated Ribonucleotide Excision Repair', *Molecular Cell*. doi: 10.1016/j.molcel.2012.06.035.

Su, C.-Y., Lin, T.-C., Lin, Y.-F., Chen, M.-H., Lee, C.-H., Wang, H.-Y., Lee, Y.-C., Liu, Y.-P., Chen, C.-L. and Hsiao, M. (2015) 'DDX3 as a strongest prognosis marker and its downregulation promotes metastasis in colorectal cancer', *Oncotarget*. doi: 10.18632/oncotarget.4329.

Sun, M., Song, L., Zhou, T., Gillespie, G. Y. and Jope, R. S. (2011) 'The role of DDX3 in regulating Snail', *Biochimica et Biophysica Acta - Molecular Cell Research*. doi: 10.1016/j.bbamcr.2011.01.003.

Sun, M., Zhou, T., Jonasch, E. and Jope, R. S. (2013) 'DDX3 regulates DNA damage-induced apoptosis and p53 stabilization', *Biochimica et Biophysica Acta - Molecular Cell Research*. doi: 10.1016/j.bbamcr.2013.02.026.

Tanner, N. K., Cordin, O., Banroques, J., Doère, M. and Linder, P. (2003) 'The Q motif: a newly identified motif in DEAD box helicases may regulate ATP binding and hydrolysis.', *Molecular cell*, 11(1), pp. 127–38.

Tanner, N. K. and Linder, P. (2001) 'DExD/H box RNA helicases: from generic motors to specific dissociation functions.', *Molecular cell*, 8(2), pp. 251–62.

Thulasi Raman, S. N., Liu, G., Pyo, H. M., Cui, Y. C., Xu, F., Ayalew, L. E., Tikoo, S. K. and Zhou, Y. (2016) 'DDX3 Interacts with Influenza A Virus

NS1 and NP Proteins and Exerts Antiviral Function through Regulation of Stress Granule Formation', *Journal of Virology*. doi: 10.1128/jvi.03010-15.

Vaisman, A. and Woodgate, R. (2015) 'Redundancy in ribonucleotide excision repair: Competition, compensation, and cooperation', *DNA Repair*. doi: 10.1016/j.dnarep.2015.02.008.

Vashist, S., Urena, L., Chaudhry, Y. and Goodfellow, I. (2012) 'Identification of RNA-Protein Interaction Networks Involved in the Norovirus Life Cycle', *Journal of Virology*. doi: 10.1128/jvi.00432-12.

van Voss, M. R. H., Vesuna, F., Trumpi, K., Brilliant, J., Berlinicke, C., de Leng, W., Kranenburg, O., Offerhaus, G. J., Bürger, H., van der Wall, E., van Diest, P. J. and Raman, V. (2015) 'Identification of the DEAD box RNA helicase DDX3 as a therapeutic target in colorectal cancer', *Oncotarget*. doi: 10.18632/oncotarget.4873.

Wallace, B. D. and Williams, R. S. (2014) 'Ribonucleotide triggered DNA damage and RNA-DNA damage responses', *RNA Biology*. doi: 10.4161/15476286.2014.992283.

Wang, H. and Ryu, W.-S. (2010) 'Hepatitis B Virus Polymerase Blocks Pattern Recognition Receptor Signaling via Interaction with DDX3: Implications for Immune Evasion', *PLoS Pathogens*. Edited by J. J. Ou, 6(7), p. e1000986. doi: 10.1371/journal.ppat.1000986.

Wang, X., Wang, R., Luo, M., Li, C., Wang, H.-X., Huan, C.-C., Qu, Y.-R., Liao, Y. and Mao, X. (2017) '(DEAD)-box RNA helicase 3 modulates NF- κ B signal pathway by controlling the phosphorylation of PP2A-C subunit', *Oncotarget*, 8(20). doi: 10.18632/oncotarget.16593.

Wilky, B. A., Kim, C., McCarty, G., Montgomery, E. A., Kammers, K., Devine, L. R., Cole, R. N., Raman, V. and Loeb, D. M. (2016) 'RNA helicase DDX3: A novel therapeutic target in Ewing sarcoma', *Oncogene*. doi: 10.1038/onc.2015.336.

- Wolf, M. C. et al.** (2010) 'A broad-spectrum antiviral targeting entry of enveloped viruses', *Proceedings of the National Academy of Sciences*, 107(7), pp. 3157–3162. doi: 10.1073/pnas.0909587107.
- Wu, D.-W., Lin, P.-L., Wang, L., Huang, C.-C. and Lee, H.** (2017) 'The YAP1/SIX2 axis is required for DDX3-mediated tumor aggressiveness and cetuximab resistance in KRAS -wild-type colorectal cancer', *Theranostics*, 7(5), pp. 1114–1132. doi: 10.7150/thno.18175.
- Wu, D.-W., Liu, W.-S., Wang, J., Chen, C.-Y., Cheng, Y.-W. and Lee, H.** (2011) 'Reduced p21WAF1/CIP1 via Alteration of p53-DDX3 Pathway Is Associated with Poor Relapse-Free Survival in Early-Stage Human Papillomavirus-Associated Lung Cancer', *Clinical Cancer Research*, 17(7), pp. 1895–1905. doi: 10.1158/1078-0432.CCR-10-2316.
- Wu, D. W., Lee, M. C., Wang, J., Chen, C. Y., Cheng, Y. W. and Lee, H.** (2014) 'DDX3 loss by p53 inactivation promotes tumor malignancy via the MDM2/Slug/E-cadherin pathway and poor patient outcome in non-small-cell lung cancer', *Oncogene*. doi: 10.1038/onc.2013.107.
- Xiang, N., He, M., Ishaq, M., Gao, Y., Song, F., Guo, L., Ma, L., Sun, G., Liu, D., Guo, D. and Chen, Y.** (2016) 'The DEAD-Box RNA helicase DDX3 interacts with NF- κ B subunit p65 and suppresses p65-mediated transcription', *PLoS ONE*. doi: 10.1371/journal.pone.0164471.
- Xie, M., Vesuna, F., Botlagunta, M., Bol, G. M., Irving, A., Bergman, Y., Hosmane, R. S., Kato, Y., Winnard, P. T. and Raman, V.** (2015) 'NZ51, a ring-expanded nucleoside analog, inhibits motility and viability of breast cancer cells by targeting the RNA helicase DDX3', *Oncotarget*. doi: 10.18632/oncotarget.4898.
- Yasuda-Inoue, M., Kuroki, M. and Ariumi, Y.** (2013) 'DDX3 RNA helicase is required for HIV-1 Tat function', *Biochemical and Biophysical Research Communications*. doi: 10.1016/j.bbrc.2013.10.107.
- Yedavalli, V. S. R. K., Neuveut, C., Chi, Y., Kleiman, L. and Jeang, K.-T.**

(2004) 'Requirement of DDX3 DEAD Box RNA Helicase for HIV-1 Rev-RRE Export Function', *Cell*, 119(3), pp. 381–392. doi: 10.1016/j.cell.2004.09.029.

Yedavalli, V. S. R. K., Zhang, N., Cai, H., Zhang, P., Starost, M. F., Hosmane, R. S. and Jeang, K. T. (2008) 'Ring expanded nucleoside analogues inhibit RNA helicase and intracellular human immunodeficiency virus type 1 replication', *Journal of Medicinal Chemistry*. doi: 10.1021/jm800332m.

You, L. R., Chen, C. M., Yeh, T. S., Tsai, T. Y., Mai, R. T., Lee, Y. H. W. and Lin, C. H. (1999) 'Hepatitis C virus core protein interacts with cellular putative RNA helicase', *Journal of Virology*, 73(4), pp. 2841–2853.

Zhao, L., Mao, Y., Zhou, J., Zhao, Y., Cao, Y. and Chen, X. (2016) 'Multifunctional DDX3: Dual roles in various cancer development and its related signaling pathways', *American Journal of Cancer Research*.

List of original manuscripts

Anna Garbelli, **Valentina Riva**, Emmanuele Crespan, Giovanni Maga; How to win the HIV-1 drug resistance hurdle race: running faster or jumping higher? *Biochemical Journal* 2017, 474(10):1559-1577.

Valentina Riva & Giovanni Maga; From the magic bullet to the magic target: exploiting the diverse roles of DDX3X in viral infections and tumorigenesis. *Future Medicinal Chemistry* 2019, 11(11):1357-1381.

Annalaura Brai, Francesco Martelli, **Valentina Riva**, Anna Garbelli, Roberta Fazi, Claudio Zamperini, Alessandro Pollutri, Lucia Falsitta, Stefania Ronzini, Laura Maccari, Maga Giovanni, Simone Giannecchini, Maurizio Botta; DDX3X Helicase Inhibitors as a New Strategy To Fight the West Nile Virus Infection. *Journal of Medical Chemistry* 2019, 62(5):2333-2347.

Annalaura Brai#, Stefania Ronzini#, **Valentina Riva**#, Lorenzo Botta, Claudio Zamperini, Matteo Borgini, Claudia Trivisani, Anna Garbelli, Carla Pennisi, Francesco Saladini, Maurizio Zazzi, Giovanni Maga*, Maurizio Botta*; Synthesis and antiviral activity of novel 1,3,4-thiadiazole inhibitors of DDX3X. *Molecules* 2019, 24(21).

Review Article

How to win the HIV-1 drug resistance hurdle race: running faster or jumping higher?

Anna Garbelli, Valentina Riva, Emmanuele Crespan and Giovanni Maga

DNA Enzymology & Molecular Virology Unit, Institute of Molecular Genetics — CNR, via Abbiategrosso 207, Pavia 27100, Italy

Correspondence: Giovanni Maga (maga@igm.cnr.it)

Infections by the human immunodeficiency virus type 1 (HIV-1), the causative agent of the acquired immunodeficiency syndrome (AIDS), are still totaling an appalling 36.7 millions worldwide, with 1.1 million AIDS deaths/year and a similar number of yearly new infections. All this, in spite of the discovery of HIV-1 as the AIDS etiological agent more than 30 years ago and the introduction of an effective combinatorial antiretroviral therapy (cART), able to control disease progression, more than 20 years ago. Although very effective, current cART is plagued by the emergence of drug-resistant viral variants and most of the efforts in the development of novel direct-acting antiviral agents (DAAs) against HIV-1 have been devoted toward the fighting of resistance. In this review, rather than providing a detailed listing of all the drugs and the corresponding resistance mutations, we aim, through relevant examples, at presenting to the general reader the conceptual shift in the approaches that are being taken to overcome the viral resistance hurdle. From the classic ‘running faster’ strategy, based on the development of novel DAAs active against the mutant viruses selected by the previous drugs and/or presenting to the virus a high genetic barrier toward the development of resilience, to a ‘jumping higher’ approach, which looks at the cell, rather than the virus, as a source of valuable drug targets, in order to make the cellular environment non-permissive toward the replication of both wild-type and mutated viruses.

Introduction

Since the discovery of HIV-1 as the causative agent of the acquired immunodeficiency syndrome (AIDS) in humans, much effort has been devoted to the development of direct-acting antiviral agents (DAAs), capable of blocking retroviral replication. The first anti-HIV DAA was azidothymidine (AZT, zidovudine), a dideoxythymidine analog whose incorporation leads to termination of proviral DNA synthesis and which was approved for clinical use in 1987. The discovery of AZT established the paradigm for the development of several other DAAs targeting the HIV-1 reverse transcriptase (RT) enzyme, which were all based on the same mechanism and are collectively indicated as nucleoside reverse transcriptase inhibitors (NRTIs). In the almost 30 years following the development of the first NRTIs, over 25 DAAs, belonging to the six different functional classes listed below, have been approved for the antiretroviral therapy (ART) of HIV-1 infections. Moreover, since the mid-1990s, ART became cART (combinatorial antiretroviral therapy), which involves the administration of combinations of three drugs belonging to at least two different functional classes. Clinicians today can choose for cART among: two classes of RT inhibitors [the NRTIs and the non-nucleoside reverse transcriptase inhibitors (NNRTIs)], integrase inhibitors (INIs), protease inhibitors (PIs), and fusion and entry inhibitors [1]. Why do we need so many drugs, also in combination, to treat HIV-1 infections?

In principle, any one of the currently approved drugs can achieve complete virological suppression in the treated patients, when administered alone. Unfortunately, none of these drugs is capable alone of attaining a *sustained* virological response, meaning that within weeks the patients undergoing

Received: 14 December 2016
Revised: 28 February 2017
Accepted: 3 March 2017

Version of Record published:
26 April 2017

monotherapy invariably experience a viral rebound, due to loss of efficacy by the drug. The reason is that drug-resistant HIV-1 variants are readily selected under the pressure of the pharmacological regimen. Thus, the development of novel anti-HIV DAAs over time can be viewed as a race against the ability of HIV-1 to become resistant toward nearly all the developed drugs (Figure 1) [2].

Starting the race: evolution of HIV-1 during cART

Complete suppression of viral replication by a given drug regimen should prevent the accumulation of novel escape variants, allowing clearance of the virus from the infected patient. Unfortunately, current cART does not achieve complete viral suppression. The combined results of several studies measuring the decay of plasma HIV-1 RNA under cART revealed four distinct phases [3,4].

The first one reflects the rapid clearance of an infected cell population with half-lives of 1–2 days, representing the majority of productively infected short-lived immune cells. This is followed by a second, slower phase of decline of CD4⁺ T-cells with half-lives of 2–3 weeks. A third phase is generated by the decline of another subset of cells, probably macrophages or monocytes, with half-lives in the order of several months. However, even after this slow phase, the RNA levels do not fall to zero, but reach a plateau with a decay slope suggesting a theoretical half-life of 60 years or more, indicating the persistence of viral replication from a population of long-lived cells. This probably represents the reservoir of latently infected cells established at early times of infection, before initiating cART. The persistence of such a long-lived population of archived viral genomes is corroborated by studies measuring the decline of integrated HIV-1 proviral DNA, which also reached a plateau in the presence of cART, never falling to zero [5].

The fact that the viral reservoir, responsible for persistent viral replication, is established early during the infection is supported by several observations. In general, multiple studies showed that early initiation of cART can substantially reduce both the number of infected cells and the viral diversity in the patient (reviewed in ref. [6]). An important observation was coming from the analysis of the evolution of HIV-1 in patients initiating treatment after the establishment of a persistent infection. It appeared that cART substantially reduced the genetic variability of HIV-1, resulting in the expression of a stable subset of viral variants even after prolonged therapy [7]. Subsequent investigations also revealed that cells carrying integrated viral variants can undergo a significant clonal expansion under cART. The molecular mechanisms underlying such expansion are not yet clear, but it seems that the integration site of the proviral DNA may play a role [8,9].

Overall, these data led to the general consensus that: (i) viral evolution, and thus the potential generation of viral escape variants, is mainly occurring early in infection, leading to the establishment of an archive of mutated viral genomes in long-lived latently infected cells; (ii) the persistent viremia occurring during cART is mainly due to the viral reactivation from this early reservoir, rather than to ongoing viral replication [6].

Very recent studies, however, challenged this latter point. Ultra-deep sequencing analysis of a limited number of patients on fully suppressive cART revealed the accumulation of novel HIV-1 variants, indicating ongoing viral replication, even if without selection of drug-resistant mutants [10]. These residual rounds of infection have been proposed to occur in a subset of anatomical districts or ‘sanctuaries’, characterized by poor penetration, and hence suboptimal levels, of antiretroviral drugs, most notably lymphoid tissues and microglia [11]. Mathematical models, however, predict that this residual viral replication should not be sufficient to allow significant evolution and would minimally contribute (if at all) to the generation of novel resistant variants [12]. The jury is still out.

Broadly speaking, if viral variants potentially resistant to DAAs can be continuously released by latent reservoirs, an alternative strategy targeting cellular cofactors required for viral replication, rather than viral proteins, may also limit their ability to infect new cells and help eventual clearance of the reservoirs by the immune system.

The importance of being fit: drug-resistant mutations and replicative efficiency

Viral fitness is defined as the efficiency of replication, i.e. the production of an infectious progeny, of a viral strain with respect to another. It is important to understand the relative value of the fitness concept, in the frame of the evolutionary mechanisms of the virus. One viral strain may have an intrinsic high fitness, meaning that its replication leads to the production of a large number of virions, but if the selective pressure of the environment is such as to prevent infection of new cells, such a strain will lose its competition with

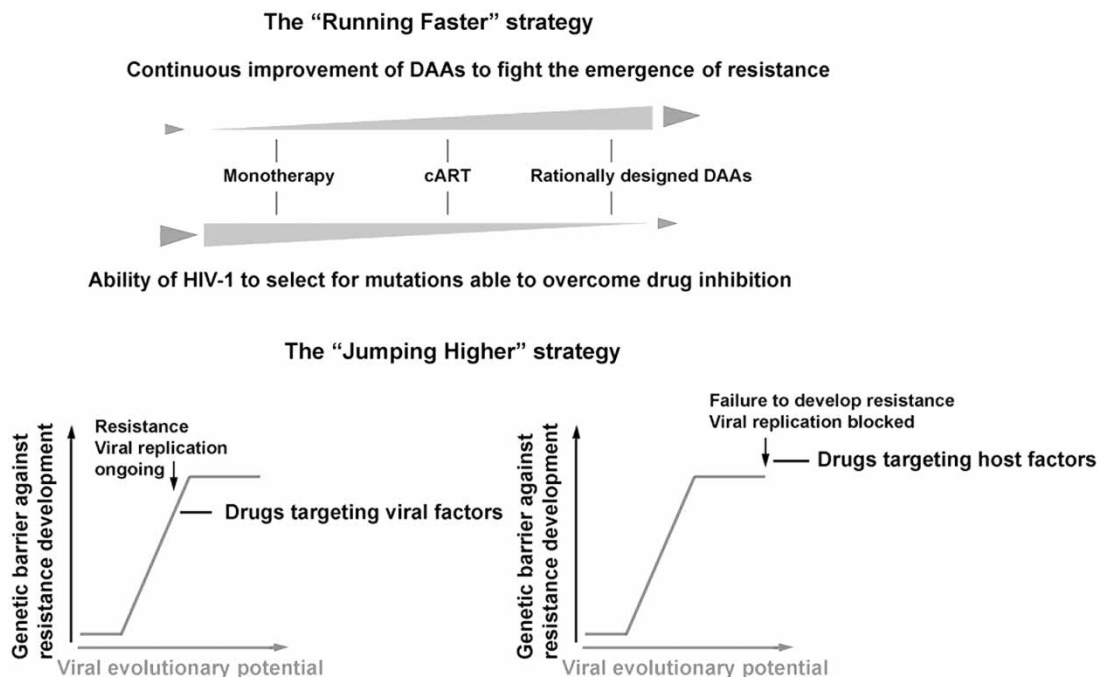


Figure 1. The rationale behind the ‘running faster’ and the ‘jumping higher’ approaches.

For details see text.

another one, whose intrinsic replicative potential may be lower (i.e. less viral particles produced), but is not as sensitive as the former to the same selective pressure. Almost invariably, drug resistance comes with a fitness cost, that is, the mutated strain is less efficient in replication, but it is the only one able to generate a progeny under the pressure of the drug regimen. A typical example is given by the NRTI drug-resistant mutations that are selected in the HIV-1 RT enzyme by cART (Table 1) [13]. There are two major mechanisms, through which mutations in RT can confer resistance to NRTIs: (i) an increased discrimination toward the modified nucleotide base or sugar, with respect to the natural ones, and (ii) an increased rate of removal of the incorporated NRTIs, by PPi- or ATP-dependent phosphorolysis [14]. Several studies have shown that both mechanisms have an impact on the fidelity of proviral DNA synthesis by the HIV-1 RT (reviewed in ref. [15]). In particular, mutations that increase the selectivity of RT generally modify the geometry of the active site, resulting in a lower affinity for the nucleotide analogs. However, these alterations also decrease the potential of HIV-1 RT of generating mismatches, thus increasing the overall fidelity of the reaction. Very common NRTI-resistant mutations such as K65R, L74V, E89G or M184V/I, for example, have been shown by a variety of biochemical and cellular assays to have from 2- to 8-fold increased fidelity, with respect to the wild-type (wt) enzyme (see ref. [15] and references therein). Increased phosphorolysis can also influence incorporation fidelity [16]. However, when the viral strains harboring these mutations have been evaluated in competition assays versus the wt, they all revealed a lower fitness (Table 1) and a high tendency to revert to the wt sequence in the absence of drug pressure [17]. Such a fitness cost for drug resistance is likely due to two major mechanisms: (i) a reduction in the intrinsic mutation rate of HIV-1, which limits the genetic variability of the progeny, thus lowering the probability of generating viral mutants able to escape the selective pressure (either immune- or drug-related), and (ii) a reduced affinity for the natural nucleotides, which may slow down the replicative process, especially in those cell types where the nucleotide pool concentrations are physiologically low, such as macrophages. In this respect, it is highly significant that many NRTI drug-resistant mutants, endowed with higher fidelity, generally have a lower affinity for the nucleotide substrate and a lower processivity than the wt, both of which result in a slower replication rate (see ref. [15] and references therein).

Also, NNRTI-resistant mutations were shown to reduce the viral fitness, but to a lesser extent (Table 1). This may be related to the fact that these amino-acidic substitutions are all located in the NNRTI-binding pocket (NNIBP), which lies outside the catalytic site, so that they do not have a strong impact on the polymerization

Table 1 Common drug-resistant mutations in HIV-1 RT and Pr and their effects on viral fitness¹

Mutation	Drugs most affected ²	Fitness compared with wt virus (%)
HIV-1 reverse transcriptase		
NRTIs		
M41L	D4T, ZDV	80
K65R	ABC, DDI, TDF	55–68
K70R	D4T, ZDV	97
L74V	ABC, DDI	90
Q145M/L	all NRTIs and NNRTIs	1 ³
Q151M	all NRTIs (except TDF, 3TC and FTC)	100
M184V	3TC, FTC	10–57
M184V/K65R	3TC, FTC, ABC, DDI, TDF	30
L210W	all NRTIs (except 3TC, FTC)	21
T215Y	D4T, ZDV	85
NNRTIs		
L100I	NVP, EFV, ETR, RPV	100
K103N	NVP, EFV	100
V106A	NVP, EFV	65–100
Y181C/I	NVP, EFV, ETR	100
Y188C/L	NVP, EFV, RPV	50–100
G190A	NVP, EFV	83
G190S	NVP, EFV	21–50
P225H	EFV	100
P236L	NVP, EFV	35–50
Protease		
M46I/L	ATV, FPV, IDV, LPV, NFV, TPV	79
I54V	All PIs	90
V82A/F/T	All PIs	79–100
I84V	All PIs	90

¹Table compiled according to the Stanford HIV Drug Resistance Database and from refs [13,15,17,47,48] and references therein. The range of fitness values reflects the variations observed in different studies.

²D4T, stavudine; ZDV, zidovudine; ABC, abacavir; DDI, didanosine; TDF, tenofovir disoproxil fumarate; 3TC, lamivudine; FTC, emtricitabine; NVP, nevirapine; EFV, efavirenz; ETR, etravirine; RPV, rilpivirine; ATV, atazanavir; FPV, fosamprenavir; IDV, indinavir; LPV, lopinavir; NFV, nelfinavir; TPV, tipranavir.

³From ref. [21].

activity of RT [18]. Nevertheless, some common NNRTI-resistant mutations, such as V106A, G190S and P236L, have been shown to reduce the replication capacity of the corresponding viral strains [13,17]. The underlying molecular mechanism is probably an impairment in the RNaseH activity, which is also essential for the completion of the reverse transcription [19].

An additional mechanism could be the destabilization of the p66-p51 interaction in the RT heterodimer, especially for mutations at position G190, which lies at the interface between the two subunits [20]. However, the relatively modest impact of NNRTI-resistant mutations on viral fitness is also arguable from the observation that most of these amino-acidic changes tend to persist in the absence of the corresponding selective pressure, i.e. after drug discontinuation.

The fitness cost, however, pays back under the selective pressure of cART. In competition experiments, all resistant strains show superior fitness to the wt in the presence of the corresponding drugs. So, even if viral

strains harboring several mutations, as those selected in patients under cART regimens, have sometimes a severely reduced replication ability, they are still able to sustain a fully productive infectious cycle in the presence of the drug pressure, hence becoming the dominant viral strains. An extreme example is given by the mutations Q145M/L. These substitutions were detected in a cohort of 3595 patients failing cART, at a very low frequency (<0.2%). Viruses carrying these mutations were resistant to virtually all NRTIs and NNRTIs used in therapy. Such high level of resistance, however, came at the cost of a >200-fold reduction in the catalytic efficiency of the mutated RT and a corresponding loss of fitness [21]. This example shows how, even at a high cost, HIV-1 can select viral variants able to sustain replication under the pressure of cART. In some instances, fitness can be rescued by compensatory mutations which are not directly related to the acquisition of resistance, but can counteract the negative impact of the amino-acidic changes leading to drug resistance on the replication efficiency, a phenomenon called ‘pseudo-reversion’. For example, duplications of the proline-rich motif PTAP in the p6 Gag protein region appear to confer an advantage to viral replication in cART-experienced patients, due to increased levels of RT. Similarly, insertion of two amino acids (S-S, S-G or S-A) between positions 69 and 70 of the RT protein improves the fitness of viruses carrying the T215F/Y-resistant mutation, even if by itself the insertion does not confer significant resilience to NRTIs, nor affects the fitness of wt viruses [13].

Running faster than HIV-1: strategies for drug design and combinatorial therapy

Until the recent approval of integrase inhibitors, cART regimens were based on the administration of RT inhibitors (both NRTIs and NNRTIs), in combination with protease inhibitors [1]. The basic concept of combination therapy is to reduce the probability of selecting viral variants resistant to all the drugs in the combination. While the introduction in the 1990s of cART revolutionized the management of HIV-1-infected patients, inverting, for the first time, the mortality trends among AIDS patients and achieving astonishing results in terms of control of the infection and prolongation of life expectancy, still the long-term efficacy of drug treatment has been plagued from the beginning (as it is, at least partly, till now) by the selection of multidrug-resistant viral strains.

Thus, a race took place, where the design of evermore effective drugs tried to outrun the ability of HIV-1 to develop drug resistance (Figure 1). The fight against drug resistance takes place along two main battlefronts: improving drug design and optimizing drug combinations. Both approaches, however, faced several hurdles, which highlighted the need of improving the rationale for drug design. With the introduction into clinical use of the first anti-HIV DDAs, soon came also the realization that they had limitations, both in terms of drug-resistance profiles, toxicity and metabolic activation. This required a more rational approach to drug design, aimed at tackling specific problems. This process of rationalization of drug design now involves all classes of approved anti-HIV DDAs. Here below, we will give some examples taken from those drug classes with which this novel approach was first developed: NRTIs, NNRTIs and PIs.

Rationalization of NRTIs

First-generation NRTIs followed a very simple concept: being modeled upon AZT, they were simple dideoxynucleotides, such as dideoxycytidine or dideoxyinosine. Next, further modifications were introduced to increase intracellular stability, by decreasing the affinity for cellular nucleotidases, and to improve selectivity, by increasing the affinity for HIV-1 RT with respect to cellular DNA polymerases. A first attempt was made in the early 1990s, with the modification of the sugar ring, substituting the deoxyribose with carbocyclic analogs, as in the case of 2',3'-didehydro-2',3'-dideoxythymidine (d4T, stavudine) [22], or with a heterosubstituted L-(β)-ribose enantiomer, as in the case of 2'-deoxy-3'-thiacytidine (epivir, 3TC) [23]. Further structure–activity relationship studies based on the screening of libraries of derivatives of these drugs led to the discovery of the carbocyclic guanosine analog abacavir (ABC) [24] and the 5-fluoro-substituted analog of 3TC, emtricitabine (FTC) [25]. Another common problem of all NRTIs, which are administered as nucleosides prodrugs, was the limited intracellular conversion to their metabolically active triphosphate forms, mainly due to the selectivity of the nucleoside kinases catalyzing the addition of the first phosphate group. This realization led to the approval, in 2001, of the acyclic nucleotide analog 9-(2-phosphonylmethoxypropyl)adenine [26] (Tenofovir, TDF). Bearing a phosphate group, TDF must be subjected only to two phosphorylation events, being more efficiently converted into its active triphosphate form.

The rational approach to the problem of drug resistance, on the other hand, required the combination of high-resolution crystallography and enzyme kinetics studies, in order to understand the molecular mechanisms underlying the resilient phenotype of the corresponding mutated RTs (see ref. [18] and references therein). For example, 3TC and FTC showed sensitivity to the M184V/I substitutions, which, on the other hand, had no effects on the other NRTIs. Crystal structures of the mutated RT in complex with the relevant drugs showed that substitution of a Met with a longer side chain, such as Val or Ile, caused a steric clash specifically with the heterosubstituted sugar in the L -(β)-configuration, which is a unique feature of these analogs. The Q151M mutation, on the other hand, confers resistance to almost all NRTIs, with the exception of 3TC, FTC and TDF. The crystal structures revealed that Q151 normally contacts the 3'-OH ribose of the incoming nucleotide. The 151M mutation increases this interaction, allowing a better discrimination against dideoxynucleotide analogs. The inverted configuration of the sugar ring, in the case of 3TC and FTC, renders these analogs less sensitive to effects of this mutation. TDF, on the other hand, is resilient to the effects of the 151M substitution, due to the substitution of the sugar ring with an acyclic chain, thus escaping entirely the selective barrier imposed by this mutation to the presence of a 2',3'-dideoxyribose moiety.

Crystallography and enzyme kinetics were also instrumental in defining the mechanism of the cluster of thymidine analog resistance-associated mutations or TAMs (M41L, D67N, K70R, L210W, T215F/Y and K219E/Q). Enzymatic assays revealed that this group of mutations increased the rate of ATP-dependent phosphorolytic removal of the last incorporated analog, for example, AZT-monophosphate (AZT-MP). The crystal structure of a mutated RT containing TAMs in complex with the excision product AZT-5'-tetrakisphosphate-5'-adenosine (AZTp4A) showed that these substitutions build up a high-affinity binding site for both ATP and AZTp4A, thus enhancing the efficiency of the reaction (for recent comprehensive reviews on the molecular mechanisms of resistance, see refs [2,18,27]).

The knowledge of the particular mutations selected by a certain type of drug and the underlying molecular mechanisms can be applied to the development of more effective drugs. Here, we will illustrate two examples: (i) the development of NRTIs with a high genetic barrier toward drug resistance that requires the selection of several mutations for RT to become resilient; (ii) the development of nucleotide-competitive inhibitors not based on a nucleoside scaffold.

A novel NRTI, which displays high activity against most drug-resistant viral strains and appears to have a very high genetic barrier toward the selection of resilient RT enzymes, is 4'-ethynyl-2-fluoro-2'-deoxyadenosine (EFdA), currently in Phase II of clinical evaluation. It is one of the most potent NRTIs ever developed, but most importantly, it shows a novel mechanism of action with respect to the other NRTIs. Structurally, EFdA still bears a 3'-OH moiety; nonetheless, it can act as a chain terminator. Kinetic and structural studies have revealed a complex mechanism of RT inhibition by EFdA: (i) it can block the translocation of the enzyme along the template lattice; (ii) it can act as a delayed chain terminator, allowing the incorporation of an additional residue before blocking the enzyme/primer complex in an inactive conformation, which is also resistant to phosphorolytic removal; (iii) it can generate mismatched primer ends, after incorporation, which are elongated at a very slow rate by HIV-1 RT [28]. Three structural features of the molecule are essential to this complex mechanism [29,30]. First, the 4'-ethynyl moiety makes interactions with a conserved hydrophobic pocket in the enzyme's active site, lined by residues Ala114, Tyr155, Phe160 and Met184, which have never been observed before with other NRTIs. In addition, this group introduces a structural rearrangement of the primer, slowing translocation. Second, the 3'-OH group provides a network of interaction facilitating the incorporation of the analog by HIV-1 RT, by stabilizing the α -phosphate at the pre-catalytic step. Third, the C-2 fluoro-substituent provides additional stabilizing interactions for drug binding. Both the 3'-OH and 2-fluoro groups also improve the intracellular metabolism of EFdA, whose pharmacokinetic properties may allow administration even once per week. These multiple mechanisms of inhibition require the selection of several mutations in RT for the enzyme to become resilient, such as the I142V/T165R/M184V triple combination, substantially slowing the development of EFdA resistance. Even more interestingly, the K65R mutant RT, which shows resistance to most NRTIs, including TDF, showed hypersensitivity toward EFdA inhibition, due to a reduced rate of phosphorolytic removal of the incorporated analog [31].

The NRTIs are, by definition, competitive inhibitors with respect to the nucleotide substrate, since they interact with the enzyme's active site in place of normal nucleotides. In 2006, a novel class of DAAs targeting HIV-1 RT by interacting with the active site and competing for binding with the nucleotides has been discovered. Their most remarkable feature was that they were structurally unrelated to nucleosides, being, from a chemical point of view, non-nucleosidic molecules. However, NNRTIs are noncompetitive inhibitors, since they

are binding to a common hydrophobic pocket outside the RT active site. Thus, these novel DAAs, which possess both NNRTI and NRTI characteristics, have been termed nucleotide-competing RT inhibitors (NcRTIs) (reviewed in ref. [32]).

The first compounds that have been identified as belonging to this class are the indolopyridones (INDOPYs). These compounds were active also against HIV-2 and the simian immunodeficiency virus. From a drug-resistant point of view, INDOPYs were active against the most common NNRTI-resistant strains, such as the K103N/Y181C double mutant, as well as against several NRTI-resistant mutants, such as those carrying the TAMs complex, but was sensitive to the double-mutant M184V/Y115F. Similarly to what has been described above for EFdA, the multidrug-resistant K65R mutant was hypersensitive toward INDOPYs. Other INDOPY-resistant mutations, selected in cell culture, were A62V, V118I, Q151M, S68N and G112S. Remarkably, all these substitutions are located within or around the RT active site. Biochemical studies showed that INDOPYs block the enzyme at the post-translocation step, by facilitating the binding of ATP, leading to the formation of a dead-end quaternary complex of the enzyme, nucleic acid, ATP and NcRTI [33].

The other class of NcRTIs is represented by the 4-dimethylamino, 6-vinyl pyrimidines (DAVPs) [34,35]. These compounds were sensitive to the K103N and Y181I mutations, selected by NNRTIs. Biochemical studies showed that DAVPs preferentially bind to the binary complex of RT with the nucleic acid, even though they can interact with the free enzyme. Crystal structures of DAVPs, in complex with HIV-1 RT, revealed that these compounds bind to a novel site located at the interface between the thumb and palm subdomains of the p66 subunit. One interesting feature was that most of the residues interacting with the drug, such as Met230, Gly231, Trp266 and Asp186, belong to a highly conserved region and have been shown to be essential for the catalytic activity, thus arguing for a high genetic barrier toward the development of resistance. However, in spite of their good *in vitro* activity against the purified enzyme and interesting mechanism of action, solubility and stability problems have so far hampered a full evaluation of DAVPs' potency in infected cells.

Novel NRTIs, as those described above, are still being searched for and identified mainly through high-throughput screening approaches. However, the rationalization of the process implies that the identified hits are immediately tested for their ability to inhibit the replication of the most common drug-resistant viral strains, so that only those molecules showing improved activity against the broadest spectrum of mutant viruses are further developed.

Conversely, the development of NNRTIs, whose chemical scaffolds are much less restrained than those of nucleosidic nature, thus enabling ampler freedom of trying different substituents, moved from a purely 'brute force' random screening approach, to a more rational design based on *in silico* techniques. Even the development of PIs has been pursued from the beginning through a rational approach. The strategies applied to the rationalization of these two classes of inhibitors will be discussed below as examples of the rational design approach.

Rationalization of NNRTIs

The availability of over 100 crystal structures of HIV-1 RT, either wt or containing drug-resistant mutations, in complex with approved and investigational NNRTIs, has allowed the identification of the critical interactions taken by the drugs and the enzyme's amino acids in the binding site [18]. This, in turn, has led to the possibility of rationally planning structural modifications in the pharmacophoric scaffolds, in order to design more potent DAAs, able to escape the resilience induced by the mutations and/or having a high genetic barrier against the development of drug resistance. Such an approach goes by the name of computer-aided drug design (CADD) and it is based on many diverse computational methods [36]. The success of rational drug design in the field of anti-HIV DAAs is testified by the several drugs that have met approval for clinical use and which have been developed with this approach, such as the PIs saquinavir (SQV), ritonavir (RTV) and indinavir; the INI raltegravir; the fusion inhibitor enfuvirtide; and the NNRTIs etravirine and rilpivirine.

CADD proceeds through the combination of molecular docking, molecular dynamics (MD) and quantitative structure–activity relationship studies (QSARs). Molecular docking is used for sampling the different poses of a ligand within its active site, based on the available structural data, in order to determine the best reciprocal orientation between the substituents of the ligand and the amino-acidic side chains and water molecules present in the binding site. MD is a powerful technique, enabling the simulation of the atomic-scale movements of macromolecules over a milli- or nanosecond timescale. In this way, it is possible to determine the binding trajectories of a ligand and its subsequent adaptations to the interacting site. QSARs, either based on simulation procedures or on actual inhibition data coming from the screening of libraries of molecules, allow the

correlation of the various physicochemical parameters of a ligand with the strength of its interaction with the binding site. QSARs are thus a very potent tool for the rationalization of the chemical modifications required to achieve an optimal interaction of the drug with its target site. Examples of the application of these techniques have been the development of the NNRTIs etravirine (ETR), rilpivirine (RPV) and doravirine (DOR).

The way to the development of ETR and RPV was paved by the discovery of the imidoyl thiourea (ITU) class of NNRTIs. QSAR-guided modifications in the scaffold of these compounds led to the development of the diaryl triazine (DATA) compounds, characterized by the replacement of the thiourea part of ITU with a triazine ring. This substitution was found to confer high potency of inhibition to the DATA class toward most NNRTI-resistant mutants. Inspection of the crystal structures of HIV-1 RT in complex with DATA revealed a high degree of flexibility between the central triazine ring and the two winged regions (wings I and II) of the molecule. This allowed binding of the DATA compounds in different orientations, thus partially avoiding the negative effects of the drug-resistant mutations. In the attempt of increasing the genetic barrier toward the development of resistance, the wing I region was functionalized through the introduction of a chloroindole moiety, specifically designed to exploit a novel hydrophobic interaction within the NNIBP, with the residue Trp229. This amino acid belongs to the conserved ‘primer grip’ region of HIV-1 RT and its mutation causes the loss of the catalytic activity by the enzyme. The corresponding derivative was shown by structural studies to contact the pocket lined by Trp229, showing excellent activity against NNRTI-resistant mutants. Starting from this DATA scaffold, the triazine ring was next replaced by a pyrimidine ring, generating the diarylpyrimidine (DAPY) class. DAPYs were even more potent than DATAs against NNRTI-resistant mutants. QSAR-guided optimization based on the screening of focused libraries systematically exploring different substituents on the pyrimidine ring and in the wing I region led to the development of ETR, which was approved for clinical use by FDA in 2008 and, later, of RPV, approved in 2011 [37,38].

Structural and MD studies confirmed the ability of RPV of adopting different conformations within the NNIBP, similarly to the other DAPYs. In particular, interaction between the drug and the Lys101 of HIV-1 RT was found to be important for drug binding. Owing to such a peculiar binding mode, RPV selects for a different set of mutations, with respect to the other NNRTIs. The most common substitutions associated with RPV resistance were E138K, K101E and K101P. Overall, 15 different mutations, clustering at the amino-acidic positions 101, 138, 179, 181, 221, 227 and 230, have been associated with a decreased susceptibility to RPV. Biochemical and structural studies revealed that the E138K mutation disrupts a salt bridge between Glu138 and Lys101, affecting the access of RPV within the active site [39,40].

DOR is a novel NNRTI, currently in Phase III of clinical trials. Its development started from an N-alkyl pyridone scaffold, identified through computational analysis and experimentally validated as an effective HIV-1 RT inhibitor [41]. A major shortcoming of this derivative, however, was the poor aqueous solubility. X-ray structural analysis led to the modification of the pyridine nitrogen in the pyrazolopyridine moiety, which yielded an improved solubility. Starting from this scaffold, QSAR studies with focused libraries exploiting different substitutions of the molecule, particularly at the C-4 of the pyridone, allowed the identification of a series of alkylated derivatives with very high potencies of inhibition against NNRTI-resistant viral strains. When the most potent molecules among this class were evaluated for their pharmacokinetics, however, they showed unsatisfactory bioavailability properties. Having identified the $-CF_3$ substitution at position 4 of the pyridone as optimal for the antiviral activity, the further step in optimization was an improvement in the pharmacokinetics. A new series of analogs were synthesized, with the introduction of heterocyclic substituents aimed at reducing either the basicity of the pyridine nitrogen or at increasing the polarity of the compound. QSAR studies were conducted with focused libraries exploiting different heterocycles. This ultimately led to the discovery of the 4-methyl triazolinone derivative DOR, showing nanomolar activity against the K103/Y181C NNRTI-resistant mutants and excellent pharmacokinetic properties in rat and dog [42]. Crystal structures showed that both the C-4 methyl group and the N-NH motif of the triazolinone were essential for drug binding. In particular, the drug makes interaction with the backbone, but not the side chain, of Lys103, thus explaining its insensitivity toward the K103N mutation.

The mechanism leading to DOR resilience have been studied by performing resistant virus selection studies with HIV-1 strains of subtypes A, B and C [43]. The majority of selected resistant mutants showed the V106A substitution. The side chain of Val106 makes interaction with the central ring of DOR, thus its replacement with the shorter side chain of Ala abrogates this contact, giving a moderate resistance (10-fold). A high level of resistance to DOR (>150-fold) was achieved only upon selection of the triple mutant V106A/F227L/V108I.

Interestingly, this mutant was still fully susceptible to the NNRTIs RPV and efavirenz (EFV). Conversely, RPV- and EFV-resistant strains were fully sensitive to DOR.

Nowadays, CADD is widely applied to the rationalization and speeding up of the drug development process, starting from the promising hits obtained by high-throughput enzymatic assays or virtual screening approaches of libraries of synthetic molecules. Obviously, this approach is not limited to NNRTIs. Indeed, historically, one of the first successes of the CADD approach was the development of specific inhibitors of HIV1 protease.

Rationalization of PIs

HIV-1 Protease (Pr) is a homodimeric protein with each monomer constituted by 99 amino acid residues. The homodimer exhibits an aspartyl protease activity that is essential for the maturation of Gag and Gag-Pol polyprotein precursor. The active site of the enzyme is located at the dimer interface, where the two monomers each contribute one of the two catalytic residues (Asp25 and Asp25'). When not bounded to its substrates, Pr exhibits a symmetric shape with the active site partially hidden by two highly flexible flaps. In the bound conformation, the structure results more rigid with the flaps that turn to allow substrate access to the active site. Owing to its fundamental role in the HIV life cycle progression, Pr has been early identified as an interesting target for antiretroviral therapy [44].

The first approved PI, SQV reached the market only 10 years after Pr discovery and, to date, other nine PIs have been approved by the Food and Drug Administration for HIV therapy [45]. All the PIs are peptidomimetic compounds designed to mimic, and thus to compete with, the natural substrates of Pr. Differently from natural peptides, in these analogs the peptide linkage is replaced with a hydroxyethylene scaffold [–CH₂–CH(OH)–] that mimics the peptide transition state within the Pr active site, but which cannot be hydrolyzed by the enzyme. The PI tipranavir (TPV) represents the only exception to this rule, being designed on the basis of a coumarin scaffold [46]. Notably, differently from other anti-HIV drugs, PIs were all developed by a rational design approach based on Pr crystallographic resolution data, aspartyl protease mechanism of action studies and evaluation of inhibition potencies through *in vitro* enzymatic assays.

Even though the first approved PIs were very effective in inhibiting Pr activity, showing potency values in the low nanomolar range, resistant mutants rapidly emerged under the selective pressure of the treatment (Table 1). PI resistance can be achieved in two ways. From one side, mutations can occur at the inhibitor–Pr interface, thus in the active site of the enzyme. Alternatively, mutations can occur within the viral proteins at the level of the Pr recognition sequences [47]. The reason why Pr remains still effective despite accumulation of mutations in its active site and/or in its substrate target sequences is the ability of the enzyme to recognize, not just a specific amino-acidic sequence, but rather a specific shape assumed by the substrates, termed the substrate envelope. This mechanism of action has been hypothesized analyzing high-resolution crystal structures of protease-bound peptides corresponding to cleavage sites in the viral polyprotein [48,49]. This mechanism well explains also the capability of Pr to acquire mutations. In fact, while catalytic residues, as well as other essential amino acids implied in substrate binding, cannot mutate without affecting protease activity, mutations in all the residues which form interactions with the specific PI moiety that protrudes outside the substrate envelope lead to weakened contacts with the drug, thus resulting in resistance. Such a drug-specific resistance mutation pattern had been observed in residues, close to the Pr active site, in specific positions where a specific drug protrudes from the substrate envelope [47]. High-level resistance toward most approved PIs stems principally from different substitutions at the positions Met46, Ile54, Val82 and Ile84.

To avoid the acquiring of resistance, different strategies, two general and a Pr-specific one, can be pursued. A viral enzyme can acquire only hereditary mutations that allow it to maintain its biological activity. Therefore, inhibitors that take contact with essential amino-acidic residues, including the catalytic ones, should minimize the chance to develop resistance mutations. Moreover, it is thought that while the side chain of the residues composing the catalytic site can change in response to the pressure of the therapy, the spatial structure of the peptide backbone is invariant. Thus, Pr could be also unable to develop resistance toward molecules interacting with the peptide backbone atoms of the active site [50,51]. A second strategy consists, as for the new generation of NNRTIs described above, in the design of more flexible compounds. Such molecules, being able to change their spatial conformation, can still interact with their binding site tolerating different mutations [47,52]. Finally, the design of inhibitors that strictly fit within the consensus volume of the substrate envelope represents a promising strategy for the development of new PIs less susceptible to resistance, since mutations affecting such inhibitors will also affect the ability of Pr to process its natural substrates [53].

In such ways, it is possible that the acquisition of one, two or more mutations will not be sufficient to confer a significant level of resistance, preventing the sustained replication of virus and paving the way for a single-drug therapy. Darunavir (DRV), the latest PI approved (in 2006), may be close to achieve such result. Its potency is ~1–2 nM [54] and its administration with RTV is a current first-line antiretroviral regimen. For DRV, even the appearance of a first resistance mutation does not result in a sufficient increase in viral replication efficiency, to allow the evolution of additional mutations. Indeed, substitutions at positions Ile47, Ile54 Leu76 and Val82 confer only moderate resilience toward DRV. In support of this view, derivatives of DRV that extended the molecules without violating the substrate envelope resulted in inhibitors even more effective [55]. However, while therapy failure with DRV is rarely associated with drug-resistant mutations, and DRV monotherapy appears to be acceptable for long-term management of HIV infection [56], the results of two recent clinical studies, PIVOT and PROTEA, showed that protease inhibitor monotherapy is well tolerated in terms of drug resistance, but it is less effective than combination therapy in suppressing HIV viral load [57]. However, first-line treatment of naïve patient with the administration of DRV, for which only minor associated side effects, such as rash, diarrhea, nasopharyngitis and nausea, have been observed, may represent an effective strategy [44].

Rational planning of the drug associations can also lead to better therapeutic regimens. In PI-based cART, for example, an important role is played by pharmacokinetic enhancers (booster), administered in combination with PIs. In particular, RTV, a first-generation PI showing a potency of ~25 nM and approved for the therapy in 1996, was also found to strongly inhibit the cytochrome P450 3A4 (CYP3A4), an enzyme that extensively metabolizes first- and second-generation PIs [58]. RTV, administered at antiretroviral therapeutic doses (i.e. 600 mg twice a day), is poorly tolerated, with side effects such as nausea, diarrhea, taste alterations and hyperlipidemia [59]. Given the remarkable potency of inhibition of RTV toward CYP3A4, the administration of even a subtherapeutic dose is sufficient to achieve a boost of second-generation PIs' concentration in plasma. Moreover, other than inhibiting CYP3A4, RTV is also able to target the cellular transport inhibiting the P-GP efflux channels [60,61]. As a result, this may decrease drug excretion in bile and urine [62]. By inhibiting the CYP3A4 isoenzyme and preventing the metabolism of other protease inhibitors, RTV allows the administration of a lower amount of PIs, thus improving the side effects and toxicity profile of antiretroviral therapy. For the same reason, administration of RTV allows PI regimens that require less frequent dosing, which are easier to follow for the patients.

Jumping higher than HIV-1: overcoming the drug resistance hurdle by exploiting host factors

Recently, the field of antiviral research started to move away from the classic concept that a good antiviral drug must specifically target a viral protein. Since viruses are obligatory intracellular parasites, their replication is heavily dependent on and intimately connected to the whole cell metabolism. Thus, broadening our strategies for antiviral intervention by targeting cellular cofactors that are essential for viral replication, but dispensable for host cell survival, may offer a few additional advantages. First, a drug targeting a host factor could, in principle, inhibit all viruses that are dependent on it and may be of importance in the treatment, for example, of coinfections. Second, the cellular proteins have a very low mutation rate, due to the high fidelity of the cellular DNA replication systems and the limited proliferation of the majority of adult cells in human tissues. In addition, even if the cellular targets were eventually to develop a mutation rendering them resistant to the drug, this would not translate into a selective advantage for the cell itself, since retaining the activity of the cellular proteins will favor viral infection and subsequent cell killing, either by viral cytopathic effects or by the immune system. Thus, such a drug will 'jump higher' than the virus, ideally remaining 'out of reach' of the viral adaptive potential (Figure 1).

There are potential limitations for this approach as well. First, it remains always the possibility that the virus could adapt to the inactivation of a particular cellular pathway, evolving the ability to exploit an alternative one. In the case the mechanism of action of the drug is the inhibition of the interaction between a viral and a cellular protein, the viral protein may select mutations enhancing its affinity for the cellular partner, thus out-competing the drug. As will be discussed below, this has indeed been observed in the case of competitive inhibitors of the viral gp120 binding to the CCR5 cellular co-receptor. A possible solution, however, would be to search for drugs inhibiting a cellular enzymatic activity which is necessary to viral replication, but ideally not requiring a direct physical interaction with any viral protein. For example, enzymes whose activity is

deregulated upon viral infection and modulating metabolic pathways (e.g. cell cycle, intracellular trafficking, transcription/translation and apoptosis) to render the cell more efficient in sustaining viral to replication more efficiently. In this case, a single mutation in a viral gene would not be expected to be sufficient to confer resistance, since a broader genetic reprogramming of the virus should be required, in order for the parasite to exploit another host enzymatic pathway.

Another possible obstacle to the development of such an approach may be the inherent risk of cytotoxicity which goes along with the administration of a drug targeting a cellular component. However, the majority of pharmaceuticals used to treat most illnesses are indeed directed toward cellular enzymes and some of them are extremely toxic, such as the case of anticancer drugs. Again, an approach involving the careful choice of the target and the rational planning of the drug development process may ultimately lead to a compound endowed with a suitable therapeutic window.

Several cellular proteins are thus being exploited as potential targets for anti-HIV chemotherapy (Table 2). The first example of a validated cellular target, and the only one, so far, whose inhibitors have been approved for the clinical use, is the cellular co-receptor CCR5. However, being based on the inhibition of a physical interaction between a viral and a cellular protein, it suffers from the limitation of drug resistance as mentioned above.

Targeting the HIV-1 cellular co-receptor CCR5

The HIV-1 enters target cells by binding its envelope glycoprotein gp120 to the CD4 receptor and at least one of two possible chemokine co-receptors: C-C chemokine receptor type 5 (CCR5; R5) and C-X-C chemokine receptor type 4 (CXCR4; X4). R5-tropic and X4-tropic viral strains use CCR5 and CXCR4, respectively, as co-receptors to enter and infect target cells. R5-tropic viruses predominate during the early stages of infection,

Table 2 Host cell targets for novel generation antiretroviral drugs

Infection step	Cellular target	Viral-interacting protein	Rationale	Mechanism of inhibition
Entry	CCR5	gp120	Blocks CCR5 binding by gp120 with small synthetic molecules	Binding of CCR5 [82]
Viral mRNA nuclear export and translation	DDX3	Rev	Inhibition of DDX3 ATPase activity by small synthetic molecules	DDX3 ATP-binding site inhibition by – ring-expanded nucleoside analogs (REN) [111] – rhodanine derivatives [128] – triazine derivatives [129]
Proviral integration	LEDGF/p75	Integrase (IN)	Avoid LEDGF/p75 interaction with the IN pocket through inhibitor molecules (LEDGFINs)	DDX3 RNA-binding site inhibition by – <i>N,N'</i> -diarylureas [130–132] LEDGF/p75 binding [101–103,105]
Transcription elongation	Cyclin T1/CDK9	Tat	Avoid Cyclin T1/CDK9 recruitment by Tat through inhibitor molecules	Inhibitor molecules against Cyclin T1/CDK9 [106–108]
Reverse transcription	APOBEC3G	Vif	Restore APOBEC3 antiviral activity avoiding Vif–APOBEC3 interaction through inhibitor molecules	Vif–APOBEC3 binding [109,110]

whereas X4 tropic viruses usually emerge during the later stages [63,64]. CCR5 is a seven-transmembrane segment protein involved in the regulation of innate or adaptive immune response, interacting with proinflammatory C–C motif chemokines. CCR5 is expressed on several cell types, including memory/effector T cells, natural killer cells, B cells, monocytes and antigen-presenting cells such as dendritic cells and macrophages (reviewed in ref. [65]).

In 1996, a natural variant of the CCR5 human gene bearing a deletion of 32 base pairs in the open reading frame, named CCR5 Δ 32, was described for the first time. This mutation inserts a premature stop codon resulting in a truncated form of the protein, which is not exposed on the cell surface. In individual homozygotes for this allele, the CCR5 receptor is constitutively absent from the cell surface, providing a natural barrier for viral entry [66,67] and resulting in resistance to HIV-1 infection or very slow progression to AIDS [67,68]. This deleted form of CCR5 is not equally distributed in all populations; in fact, it is present in Caucasian people with a percentage between 10 and 20%, with a prevalence of the homozygous mutation ~1–2%, while in African or Asian populations it is almost not detectable [69,70]. Since CCR5 is involved in the regulation of leukocytes, monocytes and macrophages, it has been noted that deletion of this protein comes with an additional bonus, since its absence has a positive effect on inflammatory states such as atherosclerosis and cardiovascular disease, arthritis and endotoxemia [71–73]. Thus, CCR5 possesses all the essential features to qualify it as an ideal target for antiviral chemotherapy: (i) it is essential for the viral replication cycle and (ii) it is not essential for the host organism (even, in this case, its absence may be beneficial). These observations sparked the interest for the development of novel anti-HIV drugs, blocking the interaction between the virus and this co-receptor.

Development of CCR5 antagonists

Aplaviroc (APL; GW873140) was the first CCR5 antagonist to enter clinical trials. *In vitro*, APL exhibited high-affinity binding to human CCR5 and had subnanomolar activity against a broad panel of laboratory and primary HIV-1 isolates [74]. However, subsequent Phase II trials of APL in antiretroviral therapy were prematurely stopped due to treatment-emergent hepatotoxicity in some subjects treated with APL-containing regimens [75].

Vicriviroc (VCV), a small-molecule CCR5 antagonist, blocks the entry of HIV-1 virus, significantly reducing viral loads [76]. Clinical efficacy and safety have been confirmed in Phase II studies [77,78]. However, in a third Phase II and two Phase III trials, VCV failed to significantly improve the efficacy when added to an optimized background therapy consisting of two or more fully active antiretrovirals [79] and its further development was terminated.

Cenicriviroc (TAK-652, TBR-652), a CCR5 and CCR2 inhibitor, is a novel small-molecule CCR5 antagonist and a potent and selective inhibitor of R5 HIV-1 replication. This compound has completed Phase IIb trials and shown potent antiretroviral activity *in vitro* and *in vivo* [80,81], and appears to be safe in humans.

Maraviroc (MVC; UK-427,857) is a small-molecule, reversible CCR5 antagonist developed by Pfizer [82], currently approved for the treatment of patients infected with R5-tropic HIV-1.

The development of MVC is another example of classic medicinal chemistry coupled to rational drug design. High-throughput screening of proprietary chemical libraries with a specific CCR5-ligand assay allowed Pfizer to identify the imidazopyridine scaffold as a high-affinity interactor. Subsequent QSAR-guided studies were conducted on a library of nearly 1000 analogs, exploring the chemical space of the scaffold, in order to improve binding potency, antiviral activity and pharmacokinetics. MVC emerged as the best compound, endowed with broad antiviral activity against both laboratory and natural strains of HIV-1 and excellent pharmacokinetic and toxicity profiles. It has been approved for clinical use in 2007.

Emergence of MVC-resistant HIV-1 strains can occur by two different mechanisms: (i) selection for minor X4 or R5X4 HIV-1 strains that are not inhibited by CCR5 antagonists [83] (also reviewed in ref. [84]) or (ii) acquisition of the ability of R5 viruses to interact with the MVC-bound conformation of CCR5 [85–87].

Resistance to MVC often occurs when previously undetectable X4-tropic HIV-1 variants are selected under pressure from drug treatment [88]. This phenomenon was investigated and most studies revealed the presence of small populations of non-R5 strains of HIV-1 before maraviroc initiation. Also changes in the gp120 V3 loop contribute to the emergence of resistance to CCR5 antagonists [85,86,89]. Multiple studies have shown that the primary determinants of HIV-1 resistance to CCR5 antagonist lie within the V3 loop of gp120 [85–87,90–94]. In particular, a single Ala insertion between the Gly310 and Pro311 amino-acidic positions of gp120 V3 loop enables HIV-1 subtype B to overcome the inhibition by MVC. Structural modeling and MD

simulations suggested that this insertion alters the flexibility of the V3 loop, increasing its affinity for CCR5 [95]. Also, mutations at position 305 of the V3 loop amino acid sequence can contribute to CCR5 antagonist resistance by clinical HIV-1 subtype C strains [96]. Recently, Borm et al. [97] showed that single V3 loop mutations are necessary but not sufficient for resistance toward MVC inhibition of HIV-1 subtype C. In fact, additional mutations outside of V3 are required to confer the resilient phenotype. Also, resistance to MVC may be due to strain-specific amino acid mutations, as also commonly observed for the CCR5 antagonist-resistant strains generated *in vitro* or selected in patients [85,86,89,97–99].

Cellular HIV-1 cofactors currently under investigation as therapeutic targets

The success obtained by targeting CCR5 has prompted the researchers to investigate other cellular cofactors of HIV-1 replication as potential drug targets. Relevant examples of both positive and negative regulators of HIV-1 infection, currently under study, are provided below.

Lens epithelium-derived growth factor (LEDGF) is a chromatin-associated cellular protein that may promote HIV-1 replication enhancing proviral integration [100]. Specifically, the LEDGF/p75 protein acts as an allosteric stimulator of HIV integrase (IN), making this factor a valuable target for host cell targeting chemotherapy. Different research groups in the last decade pursued the development of specific inhibitors able to block the IN–LEDGF/p75 interaction (p15 LEDGINS): particularly these molecules could block the interaction between IN–LEDGF/p75 inhibiting the HIV IN enzyme itself [101]. However, HIV integrase is also involved in viral particle maturation and, in recent years, alternative IN targets have been found in order to solve the problem of drug resistance. Specifically, some allosteric HIV IN inhibitors (ALLINIs), targeting the LEDGF/p75-binding pocket, not only can disrupt LEDGF/p75–IN binding, but they are also able to enhance IN multimerization. Consequently, the formation of aberrant IN multimers impairs both the catalytic activity of IN and the virus core maturation [102,103]. Currently, some of these new inhibitors are in advanced preclinical drug development [104].

The serine/threonine kinase CDK9 and its associated Cyclin T1, both play an essential role in the HIV-1 replication cycle [100]. The CDK9/T1 complex is essential for HIV-1 transcription elongation, thus potentially qualifying it as a possible antiviral target [105]. Starting from the two known CDK9 inhibitors — Roscovitine and Flavopiridol — that target specific regions of the protein, other molecules are being developed against this cellular factor [106–108].

In addition to classical innate and acquired immune responses, mammals have evolved a set of genes that are capable of suppressing or preventing virus replication at the cellular level. These so-called host ‘restriction factors’ can act as potent inhibitors of HIV-1 replication. The most notable members of this group are the interferon-induced factors APOBEC3G, CD317/tetherin, SAMHD1 and MX2/MxB, and the interferon-independent factor SERINC5. As a response to these restriction factors, HIV-1 has evolved several accessory gene products (Vif, Nef, Vpr, Vpu and Vpx) able to counteract their effects. Thus, the interactions between these cellular and viral factors are being considered as potential sites of chemotherapeutic intervention [100]. So far, drug discovery programs have been reported for the APOBEC family of proteins.

Members of the human APOBEC family of cellular cytidine deaminases, specifically the APOBEC3G and F-proteins, are encapsidated by budding HIV particles. After the encapsidation, they cause the cytidine-to-uridine editing of negative sense reverse transcripts in the newly infected cells; changes that are detrimental for the viral genome. On the other hand, the HIV-1 Vif protein is able to promote polyubiquitylation of APOBEC3 proteins that are subsequently degraded by the proteasome [100]. So, conceptually, restoring the anti-HIV activity of APOBEC3 family members by pharmacological interference with the Vif–APOBEC3 interaction is potentially an attractive therapeutic approach. To reach this goal, several interesting small-molecule inhibitors have been already identified [109,110].

Beyond HIV-1: targeting the host protein DDX3X for the development of broad-spectrum antivirals

DDX3X is a member of the DEAD-box family of helicases, which has been found over the years to play an important role in HIV replication [111], making this protein an attractive target for the development of an alternative anti-HIV1 strategy. In addition, it has been reported that different viruses, besides HIV-1, rely on DDX3X for their replicative cycles: Hepatitis C (HCV) [112–115], Japanese Encephalitis virus [116], Dengue virus (DENV) [117], West Nile virus (WNV, Flaviviridae) [118], Vaccinia virus (Poxviridae) [119–121] and

Norovirus (Caliciviridae) [122]. This raises the intriguing possibility of developing drugs against multiple viral infections, targeting a single host factor [123,124].

DDX3 expression was found to be induced in HIV-1-infected cells by the viral transcriptional activator Tat. Its enzymatic activity, as well as its physical interaction with both Rev and the exportin CRM1, is necessary for the Rev-mediated nuclear export of viral RNAs. Down-regulation of DDX3 expression through antisense or dominant-negative mutant approaches inhibited HIV-1 replication at a post-integration level. DDX3X is not required for the CRM1-dependent export of endogenous transcripts, raising the intriguing possibility that the role of DDX3 might be specific for HIV-1 RNAs [125]. A random screening approach led to the discovery of a series of ring-expanded nucleoside analogs able to inhibit the RNA helicase activity of DDX3X and to suppress HIV-1 replication [126]. At the same time, our group decided to tackle DDX3X through a rational drug design approach. The X-ray crystallographic structure of human helicase DDX3X in complex with AMP [127] has been used to identify the chemical features responsible for AMP–enzyme interactions, which were in turn codified into a structure-based pharmacophoric model. This was used as a three-dimensional query in a virtual screening approach to filter databases of commercially available compounds to identify chemical scaffolds with putative affinity toward the DDX3X ATP-binding site. These compounds were further processed, allowing the retrieval of the most drug-like ones. This led to the discovery of a novel class of ATP-competitive inhibitors of DDX3X active against HIV-1 replication [128, 129]. In search of more selective inhibitors, attention was also turned to the RNA-binding site of DDX3X. It has been also proposed that DDX3X, similarly to other RNA helicases, would adopt a closed RNA-binding conformation once bound to ATP [127]. Since there is no available three-dimensional structure of human DDX3X in the closed conformation, a homology model was built based on the structure of the closed conformation of the DEAD-box helicase eIF4AIII17 [130]. This model was used for structure-based *in silico* drug design, leading to the identification of two compounds able to inhibit both the helicase and ATPase activity of DDX3X and to reduce viral replication in cells infected with HIV-1, with micromolar potencies [130].

A structure-based optimization process was then pursued for the most potent compound. Modeling analysis revealed the presence in the RNA-binding pocket of two pockets that could be exploited in the search of additional interactions. Thus, a small library of derivatives has been designed and screened for QSAR studies, resulting in the identification of a new family of improved DDX3X inhibitors [131,132]. The most active compound 16d showed a broad-spectrum antiviral activity, being able to inhibit the replication of HIV, including strains resistant to all known classes of antiretroviral drugs, but also of HCV, WNV and DENV, with no toxicity in different cell culture systems and promising pharmacokinetics in rat [132]. These results may open the way to the development of broad-spectrum antiviral agents targeting human DDX3X.

Victory without appeal: a cure for HIV-1?

The race against drug resistance is not the only one which is being run in the life-or-death game humans are playing against HIV-1. Alternative strategies are being sought in order to boost the patients' immune system to clear the virus, thus achieving a cure. However, none of these approaches are, so far, mature enough to be translated soon into clinics [133]. For these reasons, development of more potent, long-lasting and less toxic DAAs is our best chance of ensuring lifelong control of HIV-1 replication in the infected patient, allowing a functional cure. To this aim, combining DAAs targeting viral proteins with drugs aiming at cellular factors may result in more effective and less toxic cART regimens, with an extremely high genetic barrier to be overcome by the virus to develop resistance.

The race is still on, but we are gaining.

Abbreviations

ABC, abacavir; AIDS, acquired immunodeficiency syndrome; APL, aplaviroc; ART, antiretroviral therapy; AZT, azidothymidine; AZTp4A, AZT-5'-tetraphosphate-5'-adenosine; CADD, computer-aided drug design; cART, combinatorial antiretroviral therapy; CCR5, C-C chemokine receptor type 5; CXCR4, C-X-C chemokine receptor type 4; CYP3A4, cytochrome P450 3A4; DAAs, direct-acting antiviral agents; DAPY, diarylpyrimidine; DATA, diaryltriazine; DAVPs, 4-dimethylamino, 6-vinyl pyrimidines; DENV, Dengue virus; DOR, doravirine; DRV, darunavir; EFdA, 4'-ethynyl-2'-fluoro-2'-deoxyadenosine; EFV, efavirenz; ETR, etravirine; FTC, emtricitabine; HCV, hepatitis C virus; HIV-1, human immunodeficiency virus type 1; IN, integrase; INIs, integrase inhibitors; ITU, imidoyl thiourea; LEDGF, Lens epithelium-derived growth factor; MD, molecular dynamics; MVC, Maraviroc; NcRTIs, nucleotide-competing RT inhibitors; NNBP, NNRTI-binding pocket; NNRTIs, non-nucleoside reverse

transcriptase inhibitors; NRTIs, nucleoside reverse transcriptase inhibitors; PIs, protease inhibitors; Pr, protease; QSARs, quantitative structure–activity relationships studies; RPV, rilpivirine; RT, reverse transcriptase; TAM, thymidine analogs resistance-associated mutations; TDF, tenofovir; TPV, tipranavir; VCV, vicriviroc; WNV, West Nile virus; wt, wild-type.

Competing Interests

The Authors declare that there are no competing interests associated with the manuscript.

References

- 1 Cihlar, T. and Fordyce, M. (2016) Current status and prospects of HIV treatment. *Curr. Opin. Virol.* **18**, 50–56 doi:10.1016/j.coviro.2016.03.004
- 2 Iyidogan, P. and Anderson, K.S. (2014) Current perspectives on HIV-1 antiretroviral drug resistance. *Viruses* **6**, 4095–4139 doi:10.3390/v6104095
- 3 Perelson, A.S., Essunger, P., Cao, Y., Vesanen, M., Hurley, A., Saksela, K. et al. (1997) Decay characteristics of HIV-1-infected compartments during combination therapy. *Nature* **387**, 188–191 doi:10.1038/387188a0
- 4 Maldarelli, F., Palmer, S., King, M.S., Wiegand, A., Polis, M.A., Mican, J. et al. (2007) ART suppresses plasma HIV-1 RNA to a stable set point predicted by pretherapy viremia. *PLoS Pathog.* **3**, e46 doi:10.1371/journal.ppat.0030046
- 5 Besson, G.J., Lalama, C.M., Bosch, R.J., Gandhi, R.T., Bedison, M.A., Aga, E. et al. (2014) HIV-1 DNA decay dynamics in blood during more than a decade of suppressive antiretroviral therapy. *Clin. Infect. Dis.* **59**, 1312–1321 doi:10.1093/cid/ciu585
- 6 Simonetti, F.R. and Kearney, M.F. (2015) Review: influence of ART on HIV genetics. *Curr. Opin. HIV AIDS* **10**, 49–54 doi:10.1097/COH.0000000000000120
- 7 Kearney, M.F., Spindler, J., Shao, W., Yu, S., Anderson, E.M., O'Shea, A. et al. (2014) Lack of detectable HIV-1 molecular evolution during suppressive antiretroviral therapy. *PLoS Pathog.* **10**, e1004010 doi:10.1371/journal.ppat.1004010
- 8 Maldarelli, F., Wu, X., Su, L., Simonetti, F.R., Shao, W., Hill, S. et al. (2014) Specific HIV integration sites are linked to clonal expansion and persistence of infected cells. *Science* **345**, 179–183 doi:10.1126/science.1254194
- 9 Brodin, J., Zanini, F., Thebo, L., Lanz, C., Bratt, G., Neher, R.A. et al. (2016) Establishment and stability of the latent HIV-1 DNA reservoir. *eLife* **5**, e18889 doi:10.7554/eLife.18889
- 10 Lorenzo-Redondo, R., Fryer, H.R., Bedford, T., Kim, E.-Y., Archer, J., Kosakovsky Pond, S.L. et al. (2016) Persistent HIV-1 replication maintains the tissue reservoir during therapy. *Nature* **530**, 51–56 doi:10.1038/nature16933
- 11 Martinez-Picado, J. and Deeks, S.G. (2016) Persistent HIV-1 replication during antiretroviral therapy. *Curr. Opin. HIV AIDS* **11**, 417–423 doi:10.1097/COH.0000000000000287
- 12 Conway, J.M. and Perelson, A.S. (2016) Residual viremia in treated HIV+ individuals. *PLoS Comput. Biol.* **12**, e1004677 doi:10.1371/journal.pcbi.1004677
- 13 Martinez-Picado, J. and Martinez, M.A. (2008) HIV-1 reverse transcriptase inhibitor resistance mutations and fitness: a view from the clinic and ex vivo. *Virus Res.* **134**, 104–123 doi:10.1016/j.virusres.2007.12.021
- 14 Deval, J., Courcabeck, J., Selmi, B., Boretto, J. and Canard, B. (2004) Structural determinants and molecular mechanisms for the resistance of HIV-1 RT to nucleoside analogues. *Curr. Drug Metab.* **5**, 305–316 doi:10.2174/1389200043335478
- 15 Lloyd, S.B., Kent, S.J. and Winnall, W.R. (2014) The high cost of fidelity. *AIDS Res. Hum. Retroviruses* **30**, 8–16 doi:10.1089/aid.2013.0153
- 16 Sharma, B., Crespan, E., Villani, G. and Maga, G. (2008) The balance between the rates of incorporation and pyrophosphorylytic removal influences the HIV-1 reverse transcriptase bypass of an abasic site with deoxy-, dideoxy-, and ribonucleotides. *Proteins* **71**, 715–727 doi:10.1002/prot.21829
- 17 De Luca, A. (2006) The impact of resistance on viral fitness and its clinical implications. In *Antiretroviral Resistance in Clinical Practice* (Geretti, A.M., ed.), London
- 18 Ren, J. and Stammers, D.K. (2008) Structural basis for drug resistance mechanisms for non-nucleoside inhibitors of HIV reverse transcriptase. *Virus Res.* **134**, 157–170 doi:10.1016/j.virusres.2007.12.018
- 19 Wang, J., Bambara, R.A., Demeter, L.M. and Dykes, C. (2010) Reduced fitness in cell culture of HIV-1 with nonnucleoside reverse transcriptase inhibitor-resistant mutations correlates with relative levels of reverse transcriptase content and RNase H activity in virions. *J. Virol.* **84**, 9377–9389 doi:10.1128/JVI.00618-10
- 20 Huang, W., Gamarnik, A., Limoli, K., Petropoulos, C.J. and Whitcomb, J.M. (2003) Amino acid substitutions at position 190 of human immunodeficiency virus type 1 reverse transcriptase increase susceptibility to delavirdine and impair virus replication. *J. Virol.* **77**, 1512–1523 doi:10.1128/JVI.77.2.1512-1523.2003
- 21 Paolucci, S., Baldanti, F., Maga, G., Cancio, R., Zazzi, M., Zavattoni, M. et al. (2004) Gln145met/Leu changes in human immunodeficiency virus type 1 reverse transcriptase confer resistance to nucleoside and nonnucleoside analogs and impair virus replication. *Antimicrob. Agents Chemother.* **48**, 4611–4617 doi:10.1128/AAC.48.12.4611-4617.2004
- 22 Mansuri, M.M., Starrett, Jr, J.E., Ghazzouli, I., Hitchcock, M.J.M., Sterzycki, R.Z., Brankovan, V. et al. (1989) 1-(2,3-Dideoxy-beta-D-glycero-pent-2-enofuranosyl)thymine. A highly potent and selective anti-HIV agent. *J. Med. Chem.* **32**, 461–466 doi:10.1021/jm00122a029
- 23 Coates, J.A., Cammack, N., Jenkinson, H.J., Jowett, A.J., Jowett, M.I., Pearson, B.A. et al. (1992) (–)-2'-Deoxy-3'-thiacytidine is a potent, highly selective inhibitor of human immunodeficiency virus type 1 and type 2 replication in vitro. *Antimicrob. Agents Chemother.* **36**, 733–739 doi:10.1128/AAC.36.4.733
- 24 Daluge, S.M., Good, S.S., Faletto, M.B., Miller, W.H., St Clair, M.H., Boone, L.R. et al. (1997) 1592U89, a novel carbocyclic nucleoside analog with potent, selective anti-human immunodeficiency virus activity. *Antimicrob. Agents Chemother.* **41**, 1082–1093 PMC:163855
- 25 Gosselin, G., Schinazi, R.F., Sommadossi, J.P., Mathe, C., Bergogne, M.C., Aubertin, A.M. et al. (1994) Anti-human immunodeficiency virus activities of the beta-L enantiomer of 2',3'-dideoxycytidine and its 5-fluoro derivative in vitro. *Antimicrob. Agents Chemother.* **38**, 1292–1297 doi:10.1128/AAC.38.6.1292

- 26 Balzarini, J., Vahlenkamp, T., Egberink, H., Hartmann, K., Witvrouw, M., Pannecouque, C. et al. (1997) Antiretroviral activities of acyclic nucleoside phosphonates [9-(2-phosphonylmethoxyethyl)adenine, 9-(2-phosphonylmethoxyethyl)guanine, (R)-9-(2-phosphonylmethoxypropyl)adenine, and MDL 74,968] in cell cultures and murine sarcoma virus-infected newborn NMRI mice. *Antimicrob. Agents Chemother.* **41**, 611–616 PMID:9056002
- 27 Sluis-Cremer, N., Wainberg, M.A. and Schinazi, R.F. (2015) Resistance to reverse transcriptase inhibitors used in the treatment and prevention of HIV-1 infection. *Future Microbiol.* **10**, 1773–1782 doi:10.2217/fmb.15.106
- 28 Michailidis, E., Huber, A.D., Ryan, E.M., Ong, Y.T., Leslie, M.D., Matzek, K.B. et al. (2014) 4'-Ethinyl-2-fluoro-2'-deoxyadenosine (EFdA) inhibits HIV-1 reverse transcriptase with multiple mechanisms. *J. Biol. Chem.* **289**, 24533–24548 doi:10.1074/jbc.M114.562694
- 29 Kirby, K.A., Singh, K., Michailidis, E., Marchand, B., Kodama, E.N., Ashida, N. et al. (2011) The sugar ring conformation of 4'-ethynyl-2-fluoro-2'-deoxyadenosine and its recognition by the polymerase active site of HIV reverse transcriptase. *Cell. Mol. Biol.* **57**, 40–46 PMID:21366961
- 30 Salie, Z.L., Kirby, K.A., Michailidis, E., Marchand, B., Singh, K., Rohan, L.C. et al. (2016) Structural basis of HIV inhibition by translocation-defective RT inhibitor 4'-ethynyl-2-fluoro-2'-deoxyadenosine (EFdA). *Proc. Natl Acad. Sci. U.S.A.* **113**, 9274–9279 doi:10.1073/pnas.1605223113
- 31 Michailidis, E., Ryan, E.M., Hachiya, A., Kirby, K.A., Marchand, B., Leslie, M.D. et al. (2013) Hypersusceptibility mechanism of Tenofovir-resistant HIV to EFdA. *Retrovirology* **10**, 65 doi:10.1186/1742-4690-10-65
- 32 Maga, G., Radi, M., Gerard, M.-A., Botta, M. and Ennifar, E. (2010) HIV-1 RT inhibitors with a novel mechanism of action: NNRTIs that compete with the nucleotide substrate. *Viruses* **2**, 880–899 doi:10.3390/v2040880
- 33 Ehteshami, M., Nijhuis, M., Bernatchez, J.A., Ablenas, C.J., McCormick, S., de Jong, D. et al. (2013) Formation of a quaternary complex of HIV-1 reverse transcriptase with a nucleotide-competing inhibitor and its ATP enhancer. *J. Biol. Chem.* **288**, 17336–17346 doi:10.1074/jbc.M112.433441
- 34 Maga, G., Radi, M., Zanoli, S., Manetti, F., Cancio, R., Hübscher, U. et al. (2007) Discovery of non-nucleoside inhibitors of HIV-1 reverse transcriptase competing with the nucleotide substrate. *Angew. Chem. Int. Ed.* **46**, 1810–1813 doi:10.1002/anie.200604165
- 35 Freisz, S., Bec, G., Radi, M., Wolff, P., Crespan, E., Angeli, L. et al. (2010) Crystal structure of HIV-1 reverse transcriptase bound to a non-nucleoside inhibitor with a novel mechanism of action. *Angew. Chem. Int. Ed.* **49**, 1805–1808 doi:10.1002/anie.200905651
- 36 Santos, L.H., Ferreira, R.S. and Caffarena, E.R. (2015) Computational drug design strategies applied to the modelling of human immunodeficiency virus-1 reverse transcriptase inhibitors. *Mem. Inst. Oswaldo Cruz* **110**, 847–864 doi:10.1590/0074-02760150239
- 37 Andries, K., Azijn, H., Thielemans, T., Ludovici, D., Kukla, M., Heeres, J. et al. (2004) TMC125, a novel next-generation nonnucleoside reverse transcriptase inhibitor active against nonnucleoside reverse transcriptase inhibitor-resistant human immunodeficiency virus type 1. *Antimicrob. Agents Chemother.* **48**, 4680–4686 doi:10.1128/AAC.48.12.4680-4686.2004
- 38 Janssen, P.A.J., Lewi, P.J., Arnold, E., Daeyaert, F., de Jonge, M., Heeres, J. et al. (2005) In search of a novel anti-HIV drug: multidisciplinary coordination in the discovery of 4-[[4-[[[4-(2-cyanoethenyl)-2,6-dimethylphenyl]amino]-2-pyrimidinyl]amino]benzotrile (R278474, rilpivirine). *J. Med. Chem.* **48**, 1901–1909 doi:10.1021/jm040840e
- 39 Singh, K., Marchand, B., Rai, D.K., Sharma, B., Michailidis, E., Ryan, E.M. et al. (2012) Biochemical mechanism of HIV-1 resistance to rilpivirine. *J. Biol. Chem.* **287**, 38110–38123 doi:10.1074/jbc.M112.398180
- 40 Sharma, M. and Saravolatz, L.D. (2013) Rilpivirine: a new non-nucleoside reverse transcriptase inhibitor. *J. Antimicrob. Chemother.* **68**, 250–256 doi:10.1093/jac/dks404
- 41 Gomez, R., Jolly, S., Williams, T., Tucker, T., Tynebor, R., Vacca, J. et al. (2011) Design and synthesis of pyridone inhibitors of non-nucleoside reverse transcriptase. *Bioorg. Med. Chem. Lett.* **21**, 7344–7350 doi:10.1016/j.bmcl.2011.10.027
- 42 Côté, B., Burch, J.D., Asante-Appiah, E., Bayly, C., Bédard, L., Blouin, M. et al. (2014) Discovery of MK-1439, an orally bioavailable non-nucleoside reverse transcriptase inhibitor potent against a wide range of resistant mutant HIV viruses. *Bioorg. Med. Chem. Lett.* **24**, 917–922 doi:10.1016/j.bmcl.2013.12.070
- 43 Feng, M., Wang, D., Grobler, J.A., Hazuda, D.J., Miller, M.-D. and Lai, M.T. (2015) *In vitro* resistance selection with doravirine (MK-1439), a novel nonnucleoside reverse transcriptase inhibitor with distinct mutation development pathways. *Antimicrob. Agents Chemother.* **59**, 590–598 doi:10.1128/AAC.04201-14
- 44 Lv, Z., Chu, Y. and Wang, Y. (2015) HIV protease inhibitors: a review of molecular selectivity and toxicity. *HIV AIDS* **7**, 95–104 PMC:4396582
- 45 De Clercq, E. (2009) The history of antiretrovirals: key discoveries over the past 25 years. *Rev. Med. Virol.* **19**, 287–299 doi:10.1002/rmv.624
- 46 Pauwels, R. (2006) Aspects of successful drug discovery and development. *Antiviral Res.* **71**, 77–89 doi:10.1016/j.antiviral.2006.05.007
- 47 Kurt Yilmaz, N., Swanstrom, R. and Schiffer, C.A. (2016) Improving viral protease inhibitors to counter drug resistance. *Trends Microbiol.* **24**, 547–557 doi:10.1016/j.tim.2016.03.010
- 48 King, N.M., Prabu-Jeyabalan, M., Nalivaika, E.A. and Schiffer, C.A. (2004) Combating susceptibility to drug resistance: lessons from HIV-1 protease. *Chem. Biol.* **11**, 1333–1338 doi:10.1016/j.chembiol.2004.08.010
- 49 Prabu-Jeyabalan, M., Nalivaika, E. and Schiffer, C.A. (2002) Substrate shape determines specificity of recognition for HIV-1 protease: analysis of crystal structures of six substrate complexes. *Structure* **10**, 369–381 doi:10.1016/S0969-2126(02)00720-7
- 50 Ghosh, A.K., Anderson, D.D., Weber, I.T. and Mitsuya, H. (2012) Enhancing protein backbone binding — a fruitful concept for combating drug-resistant HIV. *Angew. Chem. Int. Ed.* **51**, 1778–1802 doi:10.1002/anie.201102762
- 51 Ghosh, A.K., Chapsal, B.D., Weber, I.T. and Mitsuya, H. (2008) Design of HIV protease inhibitors targeting protein backbone: an effective strategy for combating drug resistance. *Acc. Chem. Res.* **41**, 78–86 doi:10.1021/ar7001232
- 52 Das, K. and Arnold, E. (2013) HIV-1 reverse transcriptase and antiviral drug resistance. Part 1. *Curr. Opin. Virol.* **3**, 111–118 doi:10.1016/j.coviro.2013.03.012
- 53 Nalam, M.N.L., Ali, A., Reddy, G.S.K.K., Cao, H., Anjum, S.G., Altman, M.D. et al. (2013) Substrate envelope-designed potent HIV-1 protease inhibitors to avoid drug resistance. *Chem. Biol.* **20**, 1116–1124 doi:10.1016/j.chembiol.2013.07.014
- 54 Sham, H.L., Kempf, D.J., Molla, A., Marsh, K.C., Kumar, G.N., Chen, C.M. et al. (1998) ABT-378, a highly potent inhibitor of the human immunodeficiency virus protease. *Antimicrob. Agents Chemother.* **42**, 3218–3224 PMID:9835517
- 55 Nalam, M.N.L. and Schiffer, C.A. (2008) New approaches to HIV protease inhibitor drug design II: testing the substrate envelope hypothesis to avoid drug resistance and discover robust inhibitors. *Curr. Opin. HIV AIDS* **3**, 642–646 doi:10.1097/COH.0b013e3283136cee

- 56 Paton, N.I., Stöhr, W., Arenas-Pinto, A., Fisher, M., Williams, I., Johnson, M. et al. (2015) Protease inhibitor monotherapy for long-term management of HIV infection: a randomised, controlled, open-label, non-inferiority trial. *Lancet HIV* **2**, e417–e426 doi:10.1016/S2352-3018(15)00176-9
- 57 Stöhr, W., Dunn, D.T., Arenas-Pinto, A., Orkin, C., Clarke, A., Williams, I. et al. (2016) Factors associated with virological rebound in HIV-infected patients receiving protease inhibitor monotherapy. *AIDS* **30**, 2617–2624 doi:10.1097/QAD.0000000000001206
- 58 Brayer, S.W. and Reddy, K.R. (2015) Ritonavir-boosted protease inhibitor based therapy: a new strategy in chronic hepatitis C therapy. *Expert Rev. Gastroenterol. Hepatol.* **9**, 547–558 doi:10.1586/17474124.2015.1032938
- 59 Moyle, G.J. and Back, D. (2001) Principles and practice of HIV-protease inhibitor pharmacoenhancement. *HIV Med.* **2**, 105–113 doi:10.1046/j.1468-1293.2001.00063.x
- 60 Bruno, R., Cima, S., Maiocchi, L. and Sacchi, P. (2011) Forthcoming challenges in the management of direct-acting antiviral agents (DAAs) for hepatitis C. *Dig. Liver Dis.* **43**, 337–344 doi:10.1016/j.dld.2010.09.007
- 61 Zeldin, R.K. and Petruschke, R.A. (2004) Pharmacological and therapeutic properties of ritonavir-boosted protease inhibitor therapy in HIV-infected patients. *J. Antimicrob. Chemother.* **53**, 4–9 doi:10.1093/jac/dkh029
- 62 Fromm, M.F. (2000) P-glycoprotein: a defense mechanism limiting oral bioavailability and CNS accumulation of drugs. *Int. J. Clin. Pharmacol. Ther.* **38**, 69–74 doi:10.5414/CP38069
- 63 Wilen, C.B., Tilton, J.C. and Doms, R.W. (2012) HIV: Cell binding and entry. *Cold Spring Harb. Perspect. Med.* **2**, a006866 doi:10.1101/cshperspect.a006866
- 64 Naif, H.M. (2013) Pathogenesis of HIV infection. *Infect. Dis. Rep.* **5**(Suppl 1), e6 doi:10.4081/idr.2013.s1.e6
- 65 Allers, K. and Schneider, T. (2015) CCR5Δ32 mutation and HIV infection: basis for curative HIV therapy. *Curr. Opin. Virol.* **14**, 24–29 doi:10.1016/j.coviro.2015.06.007
- 66 Liu, R., Paxton, W.A., Choe, S., Ceradini, D., Martin, S.R., Horuk, R. et al. (1996) Homozygous defect in HIV-1 coreceptor accounts for resistance of some multiply-exposed individuals to HIV-1 infection. *Cell* **86**, 367–377 doi:10.1016/S0092-8674(00)80110-5
- 67 Samson, M., Libert, F., Doranz, B.J., Rucker, J., Liesnard, C., Farber, C.-M. et al. (1996) Resistance to HIV-1 infection in caucasian individuals bearing mutant alleles of the CCR-5 chemokine receptor gene. *Nature* **382**, 722–725 doi:10.1038/382722a0
- 68 Huang, Y., Paxton, W.A., Wolinsky, S.M., Neumann, A.U., Zhang, L., He, T. et al. (1996) The role of a mutant CCR5 allele in HIV-1 transmission and disease progression. *Nat. Med.* **2**, 1240–1243 doi:10.1038/nm1196-1240
- 69 Martinson, J.J., Chapman, N.H., Rees, D.C., Liu, Y.-T. and Clegg, J.B. (1997) Global distribution of the CCR5 gene 32-basepair deletion. *Nat. Genet.* **16**, 100–103 doi:10.1038/ng0597-100
- 70 Novembre, J., Galvani, A.P. and Slatkin, M. (2005) The geographic spread of the CCR5 Δ32 HIV-resistance allele. *PLoS Biol.* **3**, e339 doi:10.1371/journal.pbio.0030339
- 71 Jones, K.L., Smyth, R.P., Pereira, C.F., Cameron, P.U., Lewin, S.R., Jaworowski, A. et al. (2011) Early events of HIV-1 infection: can signaling be the next therapeutic target? *J. Neuroimmune Pharmacol.* **6**, 269–283 doi:10.1007/s11481-011-9268-5
- 72 Zhao, Q., Li, X., Stanton, B., Mao, R., Wang, J., Zhong, L. et al. (2010) HIV/AIDS awareness and knowledge among secondary school students in China. *World Health Popul.* **11**, 38–48 doi:10.12927/whp.2010.21762
- 73 Prahalad, S. (2006) Negative association between the chemokine receptor CCR5-Δ32 polymorphism and rheumatoid arthritis: a meta-analysis. *Genes Immun.* **7**, 264–268 doi:10.1038/sj.gene.6364298
- 74 Lalezari, J., Thompson, M., Kumar, P., Pillero, P., Davey, R., Patterson, K. et al. (2005) Antiviral activity and safety of 873140, a novel CCR5 antagonist, during short-term monotherapy in HIV-infected adults. *AIDS* **19**, 1443–1448 doi:10.1097/01.aids.0000183633.06580.8a
- 75 Nichols, W.G., Steel, H.M., Bonny, T., Adkison, K., Curtis, L., Millard, J. et al. (2008) Hepatotoxicity observed in clinical trials of aplaviroc (GW873140). *Antimicrob. Agents Chemother.* **52**, 858–865 doi:10.1128/AAC.00821-07
- 76 Schürmann, D., Fätkenheuer, G., Reynes, J., Michelet, C., Raffi, F., van Lier, J. et al. (2007) Antiviral activity, pharmacokinetics and safety of vicriviroc, an oral CCR5 antagonist, during 14-day monotherapy in HIV-infected adults. *AIDS* **21**, 1293–1299 doi:10.1097/QAD.0b013e3280f00f9f
- 77 Gulick, R.M., Su, Z., Flexner, C., Hughes, M.D., Skolnik, P.R., Wilkin, T.J. et al. (2007) Phase 2 study of the safety and efficacy of vicriviroc, a CCR5 inhibitor, in HIV-1-infected, treatment-experienced patients: AIDS clinical trials group 5211. *J. Infect. Dis.* **196**, 304–312 doi:10.1086/518797
- 78 Suleiman, J., Zingman, B.S., Diaz, R.S., Madruga, J.V.R., DeJesus, E., Slim, J. et al. (2010) Vicriviroc in combination therapy with an optimized regimen for treatment-experienced subjects: 48-week results of the VICTOR-E1 phase 2 trial. *J. Infect. Dis.* **201**, 590–599 doi:10.1086/650342
- 79 Caseiro, M.M., Nelson, M., Diaz, R.S., Gathe, J., de Andrade Neto, J.L., Slim, J. et al. (2012) Vicriviroc plus optimized background therapy for treatment-experienced subjects with CCR5 HIV-1 infection: final results of two randomized phase III trials. *J. Infect.* **65**, 326–335 doi:10.1016/j.jinf.2012.05.008
- 80 Baba, M., Takashima, K., Miyake, H., Kanzaki, N., Teshima, K., Wang, X. et al. (2005) TAK-652 inhibits CCR5-mediated human immunodeficiency virus type 1 infection in vitro and has favorable pharmacokinetics in humans. *Antimicrob. Agents Chemother.* **49**, 4584–4591 doi:10.1128/AAC.49.11.4584-4591.2005
- 81 Lalezari, J., Gathe, J., Brinson, C., Thompson, M., Cohen, C., DeJesus, E. et al. (2011) Safety, efficacy, and pharmacokinetics of TBR-652, a CCR5/CCR2 antagonist, in HIV-1-infected, treatment-experienced, CCR5 antagonist-naïve subjects. *J. Acquired Immune Defic. Syndr.* **57**, 118–125 doi:10.1097/QAI.0b013e318213c2c0
- 82 Dorr, P., Westby, M., Dobbs, S., Griffin, P., Irvine, B., Macartney, M. et al. (2005) Maraviroc (UK-427,857), a potent, orally bioavailable, and selective small-molecule inhibitor of chemokine receptor CCR5 with broad-spectrum anti-human immunodeficiency virus type 1 activity. *Antimicrob. Agents Chemother.* **49**, 4721–4732 doi:10.1128/AAC.49.11.4721-4732.2005
- 83 Fätkenheuer, G., Nelson, M., Lazzarin, A., Konourina, I., Hoepelman, A.I.M., Lampiris, H. et al. (2008) Subgroup analyses of maraviroc in previously treated R5 HIV-1 infection. *N. Engl. J. Med.* **359**, 1442–1455 doi:10.1056/NEJMoa0803154
- 84 Hütter, G., Bodor, J., Ledger, S., Boyd, M., Millington, M., Tsie, M. et al. (2015) CCR5 targeted cell therapy for HIV and prevention of viral escape. *Viruses* **7**, 4186–4203 doi:10.3390/v7082816
- 85 Westby, M., Smith-Burchnell, C., Mori, J., Lewis, M., Mosley, M., Stockdale, M. et al. (2007) Reduced maximal inhibition in phenotypic susceptibility assays indicates that viral strains resistant to the CCR5 antagonist maraviroc utilize inhibitor-bound receptor for entry. *J. Virol.* **81**, 2359–2371 doi:10.1128/JVI.02006-06

- 86 Roche, M., Salimi, H., Duncan, R., Wilkinson, B.L., Chikere, K., Moore, M.S. et al. (2013) A common mechanism of clinical HIV-1 resistance to the CCR5 antagonist maraviroc despite divergent resistance levels and lack of common gp120 resistance mutations. *Retrovirology* **10**, 43 doi:10.1186/1742-4690-10-43
- 87 Tilton, J.C., Wilen, C.B., Didigu, C.A., Sinha, R., Harrison, J.E., Agrawal-Gamse, C. et al. (2010) A maraviroc-resistant HIV-1 with narrow cross-resistance to other CCR5 antagonists depends on both N-terminal and extracellular loop domains of drug-bound CCR5. *J. Virol.* **84**, 10863–10876 doi:10.1128/JVI.01109-10
- 88 Cooper, D.A., Heera, J., Goodrich, J., Tawadrous, M., Saag, M., Dejesus, E. et al. (2010) Maraviroc versus efavirenz, both in combination with zidovudine-lamivudine, for the treatment of antiretroviral-naïve subjects with CCR5-tropic HIV-1 infection. *J. Infect. Dis.* **201**, 803–813 doi:10.1086/650697
- 89 McNicholas, P.M., Mann, P.A., Wojcik, L., Qiu, P., Lee, E., McCarthy, M. et al. (2011) Mapping and characterization of vicriviroc resistance mutations from HIV-1 isolated from treatment-experienced subjects enrolled in a phase II study (VICTOR-E1). *J. Acquired Immune Defic. Syndr.* **56**, 222–229 doi:10.1097/QAI.0b013e3181ff63ee
- 90 Henrich, T.J., Tsibris, A.M.N., Lewine, N.R.P., Konstantinidis, I., Leopold, K.E., Sagar, M. et al. (2010) Evolution of CCR5 antagonist resistance in an HIV-1 subtype C clinical isolate. *J. Acquired Immune Defic. Syndr.* **55**, 420–427 doi:10.1097/QAI.0b013e3181f25574
- 91 Ogert, R.A., Wojcik, L., Buontempo, C., Ba, L., Buontempo, P., Ralston, R. et al. (2008) Mapping resistance to the CCR5 co-receptor antagonist vicriviroc using heterologous chimeric HIV-1 envelope genes reveals key determinants in the C2-V5 domain of gp120. *Virology* **373**, 387–399 doi:10.1016/j.virol.2007.12.009
- 92 Tsibris, A.M.N., Sagar, M., Gulick, R.M., Su, Z., Hughes, M., Greaves, W. et al. (2008) In vivo emergence of vicriviroc resistance in a human immunodeficiency virus type 1 subtype C-infected subject. *J. Virol.* **82**, 8210–8214 doi:10.1128/JVI.00444-08
- 93 Ogert, R.A., Hou, Y., Ba, L., Wojcik, L., Qiu, P., Murgolo, N. et al. (2010) Clinical resistance to vicriviroc through adaptive V3 loop mutations in HIV-1 subtype D gp120 that alter interactions with the N-terminus and ECL2 of CCR5. *Virology* **400**, 145–155 doi:10.1016/j.virol.2010.01.037
- 94 Pfaff, J.M., Wilen, C.B., Harrison, J.E., Demarest, J.F., Lee, B., Doms, R.W. et al. (2010) HIV-1 resistance to CCR5 antagonists associated with highly efficient use of CCR5 and altered tropism on primary CD4+ T cells. *J. Virol.* **84**, 6505–6514 doi:10.1128/JVI.00374-10
- 95 Garcia-Perez, J., Staropoli, I., Azoulay, S., Heinrich, J.-T., Cascajero, A., Colin, P. et al. (2015) A single-residue change in the HIV-1 V3 loop associated with maraviroc resistance impairs CCR5 binding affinity while increasing replicative capacity. *Retrovirology* **12**, 1 doi:10.1186/s12977-015-0177-1
- 96 Karlsson, I., Antonsson, L., Shi, Y., Oberg, M., Karlsson, A., Albert, J. et al. (2004) Coevolution of RANTES sensitivity and mode of CCR5 receptor use by human immunodeficiency virus type 1 of the R5 phenotype. *J. Virol.* **78**, 11807–11815 doi:10.1128/JVI.78.21.11807-11815.2004
- 97 Borm, K., Jakobsen, M.R., Cashin, K., Flynn, J.K., Ellenberg, P., Ostergaard, L. et al. (2016) Frequency and Env determinants of HIV-1 subtype C strains from antiretroviral therapy-naïve subjects that display incomplete inhibition by maraviroc. *Retrovirology* **13**, 763 doi:10.1186/s12977-016-0309-2
- 98 Anastassopoulou, C.G., Ketas, T.J., Klasse, P.J. and Moore, J.P. (2009) Resistance to CCR5 inhibitors caused by sequence changes in the fusion peptide of HIV-1 gp41. *Proc. Natl Acad. Sci. U.S.A.* **106**, 5318–5323 doi:10.1073/pnas.0811713106
- 99 McNicholas, P., Wei, Y., Whitcomb, J., Greaves, W., Black, T.A., Tremblay, C.L. et al. (2010) Characterization of emergent HIV resistance in treatment-naïve subjects enrolled in a vicriviroc phase 2 trial. *J. Infect. Dis.* **201**, 1470–1480 doi:10.1086/652189
- 100 Dürr, R., Keppler, O., Christ, F., Crespan, E., Garbelli, A., Maga, G. et al. (2014) Targeting Cellular Cofactors in HIV Therapy. *Top. Med. Chem.* **15**, 183–222 doi:10.1007/7355_2014_45
- 101 Christ, F., Voet, A., Marchand, A., Nicolet, S., Desimmie, B.A., Marchand, D.n et al. (2010) Rational design of small-molecule inhibitors of the LEDGF/p75-integrase interaction and HIV replication. *Nat. Chem. Biol.* **6**, 442–448 doi:10.1038/nchembio.370
- 102 Deng, N., Hoyte, A., Mansour, Y.E., Mohamed, M.S., Fuchs, J.R., Engelman, A.N. et al. (2016) Allosteric HIV-1 integrase inhibitors promote aberrant protein multimerization by directly mediating inter-subunit interactions: structural and thermodynamic modeling studies. *Protein Sci.* **25**, 1911–1917 doi:10.1002/pro.2997
- 103 Sharma, A., Slaughter, A., Jena, N., Feng, L., Kessl, J.J., Fadel, H.J. et al. (2014) A new class of multimerization selective inhibitors of HIV-1 integrase. *PLoS Pathog.* **10**, e1004171 doi:10.1371/journal.ppat.1004171
- 104 Weydert, C., De Rijck, J., Christ, F. and Debyser, Z. (2016) Targeting virus-host interactions of HIV replication. *Curr. Top. Med. Chem.* **16**, 1167–1190 doi:10.2174/1568026615666150901115106
- 105 Marshall, R.M. and Grana, X. (2006) Mechanisms controlling CDK9 activity. *Front. Biosci.* **11**, 2598–2613 doi:10.2741/1994
- 106 Van Duyne, R., Guendel, I., Jaworski, E., Sampey, G., Klase, Z., Chen, H. et al. (2013) Effect of mimetic CDK9 inhibitors on HIV-1-activated transcription. *J. Mol. Biol.* **425**, 812–829 doi:10.1016/j.jmb.2012.12.005
- 107 Ali, A., Ghosh, A., Nathans, R.S., Sharova, N., O'Brien, S., Cao, H. et al. (2009) Identification of flavopiridol analogues that selectively inhibit positive transcription elongation factor (P-TEFb) and block HIV-1 replication. *ChemBioChem* **10**, 2072–2080 doi:10.1002/cbic.200900303
- 108 Nemeth, G., Varga, Z., Greff, Z., Bencze, G., Sipos, A., Szantai-Kis, C. et al. (2011) Novel, selective CDK9 inhibitors for the treatment of HIV infection. *Curr. Med. Chem.* **18**, 342–358 doi:10.2174/092986711794839188
- 109 Nathans, R., Cao, H., Sharova, N., Ali, A., Sharkey, M., Stranska, R. et al. (2008) Small-molecule inhibition of HIV-1 Vif. *Nat. Biotechnol.* **26**, 1187–1192 doi:10.1038/nbt.1496
- 110 Cadima-Couto, I. and Goncalves, J. (2010) Towards inhibition of Vif-APOBEC3G interaction: which protein to target? *Adv. Virol.* **2010**, 1–10 doi:10.1155/2010/649315
- 111 Yedavalli, V.S.R.K., Neuveut, C., Chi, Y.-H., Kleiman, L. and Jeang, K.-T. (2004) Requirement of DDX3 DEAD box RNA helicase for HIV-1 Rev-RRE export function. *Cell* **119**, 381–392 doi:10.1016/j.cell.2004.09.029
- 112 Owsianka, A.M. and Patel, A.H. (1999) Hepatitis C virus core protein interacts with a human DEAD box protein DDX3. *Virology* **257**, 330–340 doi:10.1006/viro.1999.9659
- 113 Mamiya, N. and Worman, H.J. (1999) Hepatitis C virus core protein binds to a DEAD box RNA helicase. *J. Biol. Chem.* **274**, 15751–15756 doi:10.1074/jbc.274.22.15751
- 114 You, L.R., Chen, C.M., Yeh, T.S., Tsai, T.Y., Mai, R.T., Lin, C.H. et al. (1999) Hepatitis C virus core protein interacts with cellular putative RNA helicase. *J. Virol.* **73**, 2841–2853 PMID:10074132

- 115 Ariumi, Y., Kuroki, M., Abe, K.-i., Dansako, H., Ikeda, M., Wakita, T. et al. (2007) DDX3 DEAD-box RNA helicase is required for hepatitis C virus RNA replication. *J. Virol.* **81**, 13922–13926 doi:10.1128/JVI.01517-07
- 116 Li, C., Ge, L.-L., Li, P.-p., Wang, Y., Dai, J.-j., Sun, M.-x. et al. (2014) Cellular DDX3 regulates Japanese encephalitis virus replication by interacting with viral un-translated regions. *Virology* **449**, 70–81 doi:10.1016/j.virol.2013.11.008
- 117 Noble, C.G., Chen, Y.-L., Dong, H., Gu, F., Lim, S.P., Schul, W. et al. (2010) Strategies for development of Dengue virus inhibitors. *Antivir. Res.* **85**, 450–462 doi:10.1016/j.antiviral.2009.12.011
- 118 Chahar, H.S., Chen, S. and Manjunath, N. (2013) P-body components LSM1, GW182, DDX3, DDX6 and XRN1 are recruited to WNV replication sites and positively regulate viral replication. *Virology* **436**, 1–7 doi:10.1016/j.virol.2012.09.041
- 119 Ma, X. and He, F. (2003) Advances in the study of SR protein family. *Genomics Proteomics Bioinformatics* **1**, 2–8 doi:10.1016/S1672-0229(03)01002-7
- 120 Kalverda, A.P., Thompson, G.S., Vogel, A., Schröder, M., Bowie, A.G., Khan, A.R. et al. (2009) Poxvirus K7 protein adopts a Bcl-2 fold: biochemical mapping of its interactions with human DEAD box RNA helicase DDX3. *J. Mol. Biol.* **385**, 843–853 doi:10.1016/j.jmb.2008.09.048
- 121 Benfield, C.T.O., Ren, H., Lucas, S.J., Bahsoun, B. and Smith, G.L. (2013) Vaccinia virus protein K7 is a virulence factor that alters the acute immune response to infection. *J. Gen. Virol.* **94**(Pt 7), 1647–1657 doi:10.1099/vir.0.052670-0
- 122 Vashist, S., Urena, L., Chaudhry, Y. and Goodfellow, I. (2012) Identification of RNA-protein interaction networks involved in the Norovirus life cycle. *J. Virol.* **86**, 11977–11990 doi:10.1128/JVI.00432-12
- 123 Garbelli, A., Radi, M., Falchi, F., Beermann, S., Zanolli, S., Manetti, F. et al. (2011) Targeting the human DEAD-box polypeptide 3 (DDX3) RNA helicase as a novel strategy to inhibit viral replication. *Curr. Med. Chem.* **18**, 3015–3027 doi:10.2174/092986711796391688
- 124 Schröder, M. (2011) Viruses and the human DEAD-box helicase DDX3: inhibition or exploitation? *Biochem. Soc. Trans.* **39**, 679–683 doi:10.1042/BST0390679
- 125 Fang, J., Kubota, S., Yang, B., Zhou, N., Zhang, H., Godbout, R. et al. (2004) A DEAD box protein facilitates HIV-1 replication as a cellular co-factor of Rev. *Virology* **330**, 471–480 doi:10.1016/j.virol.2004.09.039
- 126 Yedavalli, V.S.R.K., Zhang, N., Cai, H., Zhang, P., Starost, M.F., Hosmane, R.S. et al. (2008) Ring expanded nucleoside analogues inhibit RNA helicase and intracellular human immunodeficiency virus type 1 replication. *J. Med. Chem.* **51**, 5043–5051 doi:10.1021/jm800332m
- 127 Högbom, M., Collins, R., van den Berg, S., Jenvert, R.-M., Karlberg, T., Kotenyova, T. et al. (2007) Crystal structure of conserved domains 1 and 2 of the human DEAD-box helicase DDX3X in complex with the mononucleotide AMP. *J. Mol. Biol.* **372**, 150–159 doi:10.1016/j.jmb.2007.06.050
- 128 Maga, G., Falchi, F., Garbelli, A., Belfiore, A., Witvrouw, M., Manetti, F. et al. (2008) Pharmacophore modeling and molecular docking led to the discovery of inhibitors of human immunodeficiency virus-1 replication targeting the human cellular aspartic acid–glutamic acid–alanine–aspartic acid box polypeptide 3. *J. Med. Chem.* **51**, 6635–6638 doi:10.1021/jm8008844
- 129 Maga, G., Falchi, F., Radi, M., Botta, L., Casaluca, G., Bernardini, M. et al. (2011) Toward the discovery of novel anti-HIV drugs. Second-generation inhibitors of the cellular ATPase DDX3 with improved anti-HIV activity: synthesis, structure-activity relationship analysis, cytotoxicity studies, and target validation. *ChemMedChem* **6**, 1371–1389 doi:10.1002/cmdc.201100166
- 130 Radi, M., Falchi, F., Garbelli, A., Samuele, A., Bernardo, V., Paolucci, S. et al. (2012) Discovery of the first small molecule inhibitor of human DDX3 specifically designed to target the RNA binding site: towards the next generation HIV-1 inhibitors. *Bioorg. Med. Chem. Lett.* **22**, 2094–2098 doi:10.1016/j.bmcl.2011.12.135
- 131 Fazi, R., Tintori, C., Brai, A., Botta, L., Selvaraj, M., Garbelli, A. et al. (2015) Homology model-based virtual screening for the identification of human helicase DDX3 inhibitors. *J. Chem. Inf. Model.* **55**, 2443–2454 doi:10.1021/acs.jcim.5b00419
- 132 Brai, A., Fazi, R., Tintori, C., Zamperini, C., Bugli, F., Sanguinetti, M. et al. (2016) Human DDX3 protein is a valuable target to develop broad spectrum antiviral agents. *Proc. Natl Acad. Sci. U.S.A.* **113**, 5388–5393 doi:10.1073/pnas.1522987113
- 133 Cillo, A.R. and Mellors, J.W. (2016) Which therapeutic strategy will achieve a cure for HIV-1? *Curr. Opin. Virol.* **18**, 14–19 doi:10.1016/j.coviro.2016.02.001

For reprint orders, please contact: reprints@future-science.com

From the magic bullet to the magic target: exploiting the diverse roles of DDX3X in viral infections and tumorigenesis

Valentina Riva¹ & Giovanni Maga^{*,1}

¹Department of DNA Enzymology & Molecular Virology, Institute of Molecular Genetics IGM-CNR, via Abbiategrosso 207, I-27100 Pavia, Italy

*Author for correspondence: Tel.: +39 0382546354; Fax: +39 0382422286; giovanni.maga@igm.cnr.it

DDX3X is an ATPase/RNA helicase of the DEAD-box family and one of the most multifaceted helicases known up to date, acting in RNA metabolism, cell cycle control, apoptosis, stress response and innate immunity. Depending on the virus or the viral cycle stage, DDX3X can act either in a proviral fashion or as an antiviral factor. Similarly, in different cancer types, it can act either as an oncogene or a tumor-suppressor gene. Accumulating evidence indicated that DDX3X can be considered a promising target for anticancer and antiviral chemotherapy, but also that its exploitation requires a deeper understanding of the molecular mechanisms underlying its dual role in cancer and viral infections. In this review, we will summarize the known roles of DDX3X in different tumor types and viral infections, and the different inhibitors available, illustrating the possible advantages and potential caveats of their use as anticancer and antiviral drugs.

First draft submitted: 7 September 2018; Accepted for publication: 11 February 2019; Published online: 28 February 2019

Keywords: anticancer chemotherapy • antiviral therapy • cancer • DEAD-box proteins • DNA viruses • oncogene • RNA helicases • RNA viruses • tumor suppressor gene

DDX3X, like other DEAD-box proteins, is involved in almost all aspects of RNA metabolism [1,2]. DDX3X is a nucleocytoplasmic shuttling protein [3] and it is one of the actors in regulation of transcription, translation, RNA splicing, RNA transport and RNA degradation processes. Roles for DDX3X have been also found in regulation of cell cycle and apoptosis [4]. DDX3X appears to be one of the most multifaceted helicases known up to date with various roles in innate immunity, viral infection and cancer [5–7]. The multiplicity of roles played by DDX3X is also reflected by the complex network of its interactions with several cellular and viral proteins (Table 1). Based on its involvement in both cell proliferation and viral infections, DDX3X in recent years has been proposed as a valuable target for anticancer and antiviral therapies and several small-molecule inhibitors have been developed and used to provide proof-of-principle for the exploitation of DDX3X as a chemotherapeutic target. However, DDX3X can have a seemingly contradictory ‘dual role’ in different contexts, acting as both an oncogene and a tumor suppressor, or as a pro- or anti-viral factor. Thus, in order to exploit this protein as a novel promising target, usable in anticancer or antiviral therapy, it is important to gain additional insights into DDX3X cellular roles.

In this review, we will summarize the known roles of DDX3X in different tumor types and viral infections, also illustrating the strategies already developed to inhibit its functions.

A brief overview of the structural & enzymatic features of DDX3X

The human *DDX3X* gene is located on the region Xp11.4 of the X chromosome. It encodes a 5.3 kb transcript, translated into a polypeptide of 662 amino acids, which is rich in Serines and Glycines [38,39]. There is also a *DDX3X* homolog in the nonrecombining region of the Y-chromosome (Yq11.21) but this *DDX3Y* gene, also named *DBY*, is expressed only in the male germ line [40]. DDX3X protein is an RNA helicase belonging to the DEAD-box helicase family that is conserved from bacteria to humans [41,42]. RNA helicases are currently divided in six superfamilies (SF1–6), depending on conserved motifs sequence similarities. Most RNA helicases belong to the SF-2 superfamily

Table 1. Known cellular and viral interactors of DDX3X.

Cellular protein	UNIPROT ID	Function	Ref.
PABP1	P11940	mRNA expression/stress response	[8]
TAP	Q9UBU9	mRNA export	[9]
CRM1	O14980	mRNA export	[10,11]
Ago-2	Q9UKV8	miRNA/RNAi	[12]
ALKBH5	Q6P6C2	RNA demethylation	[12]
eIF3	Q14152	Translation initiation	[13]
eIF4E/G	P06730/Q04637	Translation initiation	[8,14]
DDX5	P17844	Cell cycle regulation	[15]
CBP/p300	Q09472	Acetylase/transcription	[16]
p53	P04637	DNA damage response	[17]
CK1 ϵ	Q5R2U3	Protein kinase- β -catenin signaling	
CIKS	O43734	Inflammation	
IPS-1	Q7Z434	IFN response	[18]
IKK ϵ	Q14164	Protein kinase – IFN/innate immunity	[19]
TBK1	Q9UHD2	Protein kinase – IFN/innate immunity	[19]
TRAF3	Q13114	Innate immunity	[20]
NF-kB p65	Q04206	Inflammation/innate immunity	[21]
PPA2C	Q9H2U2	Protein dephosphorylation – inflammation	[22]
IRF3	Q14653	IFN response	[19]
Ezrin	P15311	Inhibits DDX3X helicase	[23]
HNF4	P41235	Lipid metabolism	[16]
Viral protein			
HIV-1 Rev	P04618	mRNA export/promotes viral replication	[24]
HIV-1 Tat	P04608	Promotes viral mRNA translation	[25,26]
HBV pol	Q52XL7_HBV	Inhibits innate immunity/promotes viral replication	[27]
HCV core	Q81486.9HEPC	(?) [†] replication	[28]
WNV NS3	A0A0U2JF09_WNV	Promotes viral replication	[29]
DENV capsid	C4PK10.9FLAV	Inhibits DDX3X antiviral action	[30]
DENV NS5B	P29990	Replication	[31]
IAV NS1/NP	P03496 (NS1_I34A1)/ P03466 (NCAP_I34A1)	Inhibits DDX3X antiviral action	[32]
LCMV L-protein (RNApol)	P14240 (L.LYCVA)	Promotes viral replication	[33]
JEV NS3/5	Q9YNB5.9FLAV/B1P6E5.9FLAV	Promotes viral replication	[34]
VEEV nsP3	Q9WJC7 (PRO_0000232113)	Promotes viral replication	[34]
LCMV NP	P09992 (NCAL.LYCVA)	Inhibits innate immunity/promotes viral replication	[34]
BAdV-3 pVIII	Q03556 (CAP8_ADEB3)	Suppresses host translation	[35]
Pestivirus N(pro)	Q7T9N2.BVDV	(?) [†] stress response/ innate immunity/ translation	[36]
VACV K7	P68466 (K7.VACCW)	Inhibits innate immunity	[37]

[†](?), Hypothesized function.
 BAdV-3: Bovine adenovirus 3; BVDV: Bovine viral diarrhoea virus; DENV: Dengue virus; HBV: Hepatitis B virus; HCV: Hepatitis C virus; HIV-1: Human immunodeficiency virus type 1; IAV: Influenza A virus; JEV: Japanese encephalitis virus; LCMV: Lymphocytic choriomeningitis virus; VACV: Vaccinia virus; VEEV: Venezuelan equine encephalitis virus; WNV: West Nile virus.

that includes DEAD-box proteins [43]. The name of the helicase family derives from the Walker B motif II D-E-A-D (Asp–Glu–Ala–Asp), which contains the catalytic residues essential for ATP hydrolysis. In DDX3X, all the 12 conserved motifs are present in two RecA-like subdomains (Domain 1 and Domain 2, from N- to C-terminal) connected via a short flexible linker. DEAD-box helicases, including DDX3X, contain also additional specific motifs. The Q-motif establishes specific contacts with the adenine base of ATP, while two additional motifs, Ib (also termed GG-motif) and Iv_a (or Q_{xx}R-motif) are involved in specific contacts with the RNA substrate [44]. In DDX3X, an additional unique ATP-interacting domain (ABL, aa 135-168) is involved in RNA stimulation of ATP hydrolysis [45]. In all DEAD-box helicases characterized to date, the ATPase and RNA helicase motifs involved in RNA substrate binding and hydrolysis are distributed in both domains [44]. Structural and biochemical studies

on different members of the DEAD-box helicase family suggested that ATP hydrolysis and RNA unwinding both require the transition of the protein from an 'open' to a 'closed' conformation, whereby the two domains facing each other come in contact, effectively forming the RNA-binding cleft and bringing motifs I and Q located on Domain 1, close to motif VI on Domain 2, thus creating a catalytically competent ATPase active site [46,47]. ATP, however, can be bound also in the open conformation, by the 'open' ATPase site on Domain 1 [48]. A unified model for the RNA unwinding activity of DEAD-box helicases has been proposed [44,48]. Contrary to processive RNA helicases, which couple opening of the double helix to translocation along the lattice, the unwinding reaction by DEAD-box proteins proceeds via a local strand separation mechanism, which uses one molecule of ATP to melt few (4–7) base pairs for each catalytic cycle. This process can be divided into discrete steps. The enzyme in its open conformation can interact with ATP through its Domain 1 and with the RNA duplex via Domain 2. This complex then undergoes a transition to the closed conformation, with formation of the RNA-binding cleft, which can accommodate about five nucleotides of the duplex [49]. The closed form is stabilized by a salt bridge between an Arg in motif V and an Asp in the DEAD-box [44]. Since the transition between the open and closed states proceeds through an intermediate which is incompatible with double strand (ds) RNA binding, it is likely that this conformational change is responsible for the local unwinding of the duplex. Closure of the ATP-binding site also promotes ATP hydrolysis, which results in fast release of the RNA substrate, due to the movement of α -helix 8 of the DEAD-motif that occludes the RNA-binding site, bringing the enzyme back to the open state. Thus, unwinding requires ATP binding, while hydrolysis is required for recycling of the enzyme [44]. Biochemical studies support the requirement of ATP for efficient dsRNA unwinding by DDX3X. DDX3X can also bind DNA and unwind RNA/DNA duplexes. Similarly, ATP hydrolysis is stimulated by both RNA and DNA [50–52]. DDX3X appears unable to efficiently open DNA/DNA substrates [52], even if unwinding of dsDNA has been reported *in vitro* at high enzyme concentrations [51]. Finally, DDX3X shows a preference for unwinding substrates with single strand overhangs [51,52]. No RNA sequence specificity has been reported for DDX3X (or other DEAD-box helicases) unwinding, which is consistent with the fact that these proteins mainly interact with the sugar-phosphate backbone of the nucleic acid [44].

DDX3X & cancer

DDX3X overexpression is associated with large tumor size and metastasis, suggesting a possible use of DDX3X as a biomarker for cancer prognosis and a target for chemotherapy [4,7]. But DDX3X, based on literature data, has also dual roles and can be an oncogene or a tumor suppressor in different cancer types, promoting or repressing cancer progression (Figure 1A & Table 2) [53]. As discussed in the next sections, its dual role as oncogene or tumor suppressor is not just the reflection of the different cell lines and different conditions used in different experiments, but it depends also on the genetic background present in a certain tumor type. DDX3X could also accumulate mutations leading to altered functions, but due to the multiple pathways in which this protein is involved, loss of DDX3X function can lead to complex molecular patterns that are often difficult to be interpreted. This is also evident from the wide range of different and sometimes contradictory phenotypes observed as a consequence of *DDX3X* gene silencing in different tumor cell lines (Table 3). Another point to underline is that DDX3X roles in virus-infected patients could be completely different compared with patients without virus infection; it follows that virus infections might influence the role of DDX3X in different cancers.

DDX3X & the regulation of cell proliferation

DDX3X has been shown to participate in different pathways (Figure 1A), whose deregulation is often associated to tumor transformation and invasivity [4,7,53]. This is also reflected by the several cellular interactors of DDX3X identified to date and listed in Table 1. One important pathway where DDX3X has a positive role, is the Wnt/ β -catenin signaling cascade. The β -catenin protein acts as a transcription factor in transducing signals coming from the Wnt signaling pathway to the nucleus, but it is also a component of the cadherin complex regulating cell–cell adhesion [87]. Alterations of β -catenin expression and localization are associated with several cancers. DDX3X has been shown to act as a positive regulator of the kinase CK1 ϵ , thus increasing phosphorylation of the Dvl1 and Dvl2 proteins, which results in increased β -catenin nuclear translocation and transcriptional activation. The catalytic activity of DDX3X seems not to be required for the stimulation of CK1 ϵ [76]. DDX3X is also involved in the regulation of E-cadherin through the modulation of the levels of its transcription factor Snail [70]. DDX3X appears to increase Snail levels leading to reduced E-cadherin expression, thus favoring epithelial–mesenchymal transition and tumor invasivity. In addition, overexpression of DDX3X by the hypoxia induced transcription factor HIF1 α

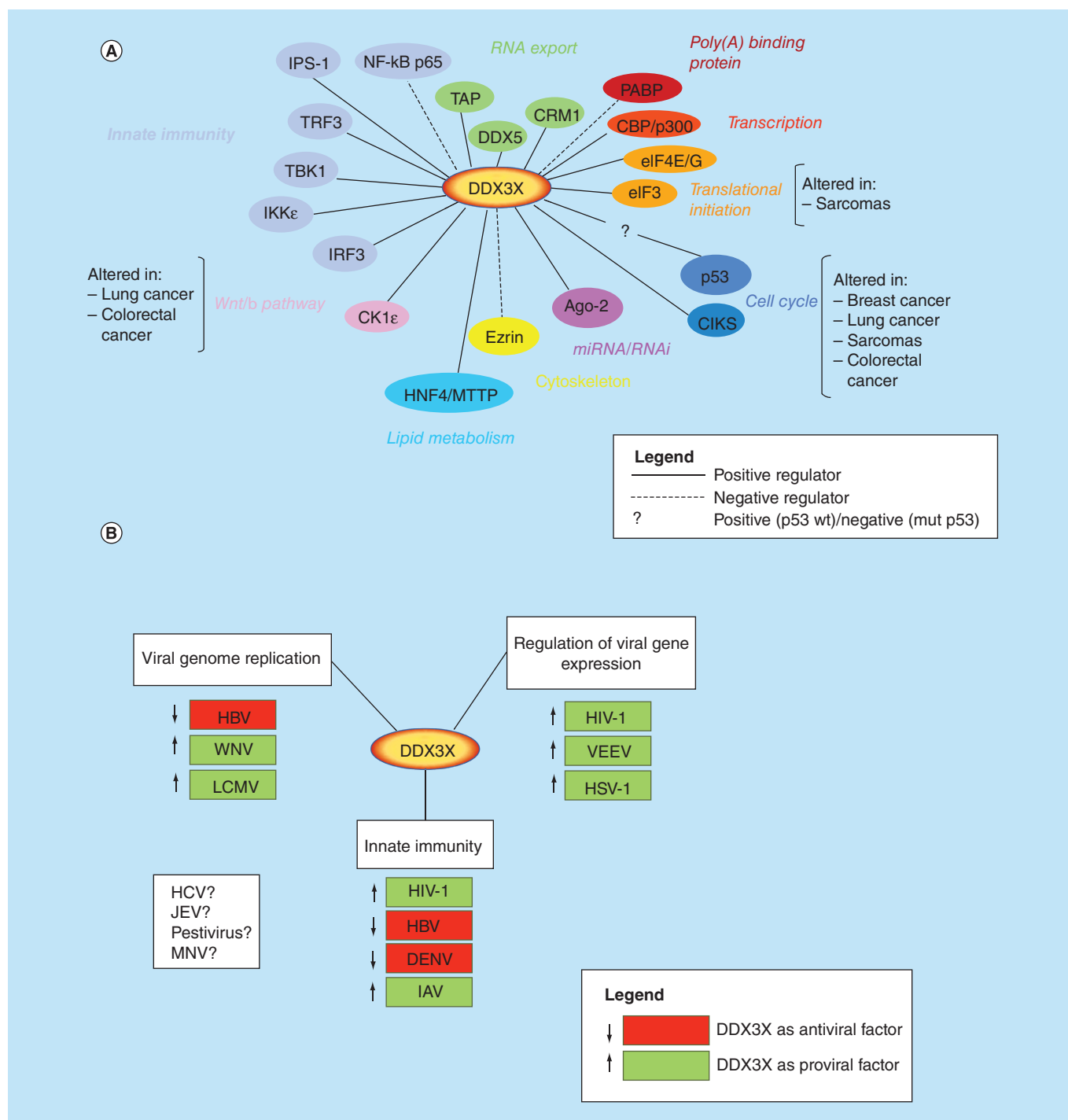


Figure 1. DDX3X has dual roles in tumor proliferation and viral infections. (A) DDX3X involvement in various metabolic pathways is modulated through interaction with multiple partners and often deregulated in different tumors. **(B)** DDX3X can act as a proviral or antiviral factor, depending on the virus and the metabolic pathway involved. For details see text.

also leads to E-cadherin repression, facilitating tumor invasivity [54,55,62]. However, as discussed below, DDX3X appears to be able to both positively and negatively regulate E-cadherin levels depending on the tumor type.

DDX3X also participates in the regulation of cell cycle progression [88,89]. Knockdown of DDX3X resulted in a global delay in cell cycle progression [90]. DDX3X has been shown to positively regulate the transcription of the CDK inhibitor p21 [91] and the mRNA translation of cyclin E1 [78], while DDX3X downregulation led to increased

Table 2. Dual role of DDX3X as an oncogene or oncosuppressor in various cancer types.

Cancer type	DDX3X role(s)	Possible pathways and mechanisms	Connected virus infection	Ref.
Breast cancer	Oncogene	HIF-1/ E-cadherin/ Rac1-mediated signaling pathway	None	[54–56]
Lung cancer	Oncogene/TSG	Oncogene: Wnt/ β -catenin axis TSG: MDM2/ E-cadherin; p53/p21 pathways	Papillomavirus-associated lung cancer: reduced p21 (WAF1/CIP1) via alteration of p53-DDX3X pathway is associated with poor survival in early-stage HPV-associated lung cancer	[57–59]
Ewing sarcoma	Oncogene	DDX3X inhibition resulted in decreased survival and tumorigenicity of Ewing sarcoma cells	None	[60,61]
Colorectal cancer	Oncogene/TSG	Oncogene: Wnt/CK1 ϵ /Div1/ β -catenin; KRAS/HIF-1 α TSG: DDX3X downregulation causes Snail upregulation with decreased E-cadherin expression and reduced cell aggregation	None	[62–66]
OSCC	Oncogene/TSG	Oncogene: DDX3X promotes OSCC progression TSG: DDX3X seems to act both as a protective factor and survival predictor, particularly in non-smoker patients	DDX3X role possibly influenced by HPV positive or negative status of the tumor	[67,68]
HCC	TSG	DDX3X downregulates cyclinD1 and upregulates p21 impeding cell cycle progression	DDX3X expression possibly different in HBV versus HCV-related HCC	[69]
GBM	Oncogene	DDX3X impedes apoptotic processes through Snail pathway	None	[70]
Gallbladder carcinoma	Oncogene	High DDX3X levels connected with poor prognosis	None	[71]
Medulloblastoma	Oncogene	DDX3X loss of function mutations commonly found in patients	None	[72]
Extranodal NK/T-cell lymphoma	TSG	DDX3X loss results in suppression of cell proliferation	None	[73,74]

GBM: Glioblastoma multiforme; HBV: Hepatitis B virus; HCC: Hepatocellular carcinoma; HCV: Hepatitis C virus; HPV: Human papillomavirus; NK: Natural Killer cells; OSCC: Oral squamous cell carcinoma; TSG: Tumor suppressor gene.

cyclin D1 levels, suggesting a negative role of DDX3X in regulating cyclin D1 expression [69], which might explain these cell cycle effects. A complex network of interactions also links DDX3X to the DNA damage response protein p53. DDX3X has been shown to associate with wt p53, increasing its nuclear accumulation and inducing apoptosis in response to DNA damage [17]. Also, p53 inactivation was shown to reduce DDX3X levels [57]. Conversely, in cells expressing mutated p53, DDX3X was shown to inhibit apoptosis, however, the exact molecular mechanisms underlying these differences remain to be elucidated [17]. The complex network of interactions and the several functions of DDX3X in regulating cell proliferation are reflected in the different roles that this protein plays in tumor proliferation, as discussed below.

Breast cancer

Breast cancer is the most common metastatic cancer in females and the second most deadly cancer in women, after lung cancer. Often, women affected by breast cancer present germline mutations in *BRCA1* and *BRCA2* genes, which impair DNA double-strand break (DSB) repair by homologous recombination [92]. Among *BRCA*-related cancers those that are estrogen receptor, progesterone receptor and HER2/neu negative (triple negative; TN) are among the most difficult to treat [93]. Currently, some available therapies exploit PARP inhibitors, like Olaparib, that suppress the base excision repair pathway and are promising agents against *BRCA1* and 2 breast cancers. However, TN breast cancers still lack effective therapies and patients have unfavorable prognosis due to the aggressive behavior of this cancer subtype [94]. Another problem is the development of primary resistance to chemotherapy that consequentially leads to the continuous need of new drugs/alternative therapies for *BRCA1* and 2 patients and the urgency of suitable TN targets discovery. DDX3X seems to be a good candidate since its oncogenic role in breast cancer is well established [55,56]. DDX3X was found overexpressed in breast cancer patients and DDX3X expression promoted growth, proliferation and neoplastic transformation of breast epithelial cells. DDX3X could enhance cell migration and metastasis inhibiting E-cadherin expression or via the Rac1-mediated

Table 3. Phenotypes observed upon *DDX3X* gene silencing in different cellular systems.

System	Silencing	Phenotype	Ref.
HEK293T	siRNA	Reduced TBK1/IKKε-dependent IFN-β expression	[37]
HEK293T	siRNA	20–30% reduced proliferation	[12]
HEK293T	siRNA	Reduced CK1ε activation <i>in vivo</i>	[75]
HEK293T	siRNA	Reduced pDvl1 [‡] , nuclear β-catenin accumulation, reduction of CK1ε activity	[76]
HeLa	siRNA	No effects on proliferation	[77]
HeLa	siRNA	Strong reduction of proliferation, reduced protein expression	[13]
HeLa	shRNA	40–50% reduction of cell proliferation (cell count)	[78]
HeLa; HEK293T	shRNA	G1/S delay; reduced CycE1 translation	[78]
HeLa	shRNA	Reduced DDX5 nuclear accumulation	[15]
HeLa	siRNA	No effect on global translation	[14]
HeLa	shRNA	Reduced SGs formation, 80% reduced viability, increased apoptosis after osmotic stress	[8]
HeLa	siRNA	Reduced IL6/8 and TNF-α upon poly(I-C) stimulation	[22]
HEK293T	shRNA	No effects on cell proliferation and cell cycle	[79]
HEK293T, A549	siRNA	Reduced p(S172)IKKε and p(S396)IRF3 [§]	[19]
HEK293T, HepG2	siRNA	Reduced phosphorylation of P65 (NF-kB), IκBα, IKKβ, reduced p65 nuclear accumulation	[22]
HEK293T, HepG2	sh/siRNA	Increased p65NF-kB transcriptional activity, increased IL6/8 production	[21]
Huh-7	siRNA	No effects on proliferation, 30–60% decreased translation	[80]
MCF-7	shRNA	Reduced apoptosis (caspase-7 activation/PARP cleavage) after Camptothecin (Topo1 inhibitor), reduced p53 induction, reduced p21 expression	[17]
MDA-MB-231, MCF-7	shRNA	Increased E-cadherin, decreased Snail, increased cell adhesion, 20–50% reduced cell proliferation, reduced cell migration	[70]
MDA-MB-231	shRNA	Increased apoptosis after Camptothecin treatment, decreased survival	[17]
HCT116, U2OS	siRNA	G2/M delay, increased γH2AX, pChk1, pCDC2, multipolar mitosis, cell death; decreased pATM and p(S15)p53; increased DNMT1, 3A, 3B expression	[81]
DLD-1, HCT116	shRNA	Increased cell migration, invasivity, no effect on proliferation	[66]
HepG2	Stable KD	Increased Nanog, Oct4, cMyc, Sox2 expression; increased tumor spheres formation; increased resistance to DNA damage	[82]
Hep3B	siRNA	Reduced ATF4 expression (protein not mRNA)	[83]
NSC34(SOD) [†]	siRNA	Reduced CK1ε expression (mRNA and protein) 40% reduced proliferation (MTS)	[84]
CCM2, HCT116	shRNA	Reduced expression of β-catenin, cycD1, cMyc, pDvl2 [‡] ; reduced invasivity	[65]
U87MG	siRNA	No effect on cell viability (at >90% KD)	[85]
Xenopus embryos	AS-morpholino oligonucleotides	Defects in development due to Wnt inhibition	[76]
KO tg mice	Floxed allele	Embryonic/perinatal lethality in heterozygous mice	[86]
Trophoblasts from KO mice	Floxed allele	Reduced Dlx3 expression	[86]
KO mice embryos (E9.5)	Floxed allele	Increased apoptosis; increased DNA damage markers (γH2AX, pP53, p21), decreased Polo-like kinase 1, CDC25B	[86]
C3H10T1/2 (mouse mesenchymal cells)	siRNA	50% reduced proliferation (MTS), G1/S and G2/M delay, γH2AX accumulation	[86]

[†]NSC34(SOD): mouse motor neuron cells expressing a SOD1 mutation linked to ALS.
[‡]pDvl2: phospho-Disevelled (Dvl)2.
[§](S172)IKK: IKK phosphorylated at S172; p(S396)IRF3: IFN-responsive factor 3 phosphorylated at S396.
ALS: amyotrophic lateral sclerosis; MTS: measured by tetrazolium salt colorimetric viability assay; SG: Stress granule.

signaling pathway. According to these data, *DDX3X* knockdown or chemical inhibition reduces cell migration but also delays cell cycle progression [63,95–97]. *DDX3X* expression in breast cancer was found to be increased by HIF-1α, a transcriptional factor inducible by hypoxia, a condition shared by different types of solid tumors such as breast cancer. As a consequence, E-cadherin expression is reduced, increasing tumor invasivity [54,56].

Lung cancer

Lung cancer is the most common cancer worldwide, whose death toll is higher than those of prostate, colon and breast cancers combined [98]. Long-term survival of lung cancer patients is best achieved through surgery, but not all patients are operable, which leaves chemo- and radio-therapy as the only alternative for the majority of those affected by lung cancer [99]. Stereotactic body radiation therapy or stereotactic ablative radiation therapy are possible alternatives that in early stages demonstrated to reduce tumor burden and allowed control in more than 90% of the cases, but are often associated with increased toxicity [100]. Thus, finding novel targets and drugs for the treatment of this cancer is a major priority.

The precise role of DDX3X in lung cancer is still contradictory: in some studies it was reported to act as a tumor suppressor gene by inducing p21 expression, both activating p53 and repressing its negative regulator MDM2, resulting also in increased E-cadherin expression. Indeed, decreased levels of DDX3X via loss of p53 promoted tumor malignancy in lung cancer cells [57,58]. However, in other reports, DDX3X was found to be an oncogene and its overexpression correlated with lower survival of lung cancer patients. Accordingly, DDX3X inhibition resulted in growth arrest due to impairment of the Wnt/ β -catenin pathway [59]. This dual role of DDX3X could be also connected with the combination, in some cases, of both cancer and viral infection. For example, it has been shown that human papillomavirus (HPV) E6 protein suppressed DDX3X expression in a p53-dependent manner, thus reducing p21 levels. Accordingly, loss of DDX3X was associated with poor survival in early-stage HPV-associated lung cancer [58].

Sarcomas

Sarcomas are frequent human cancers with poor survival rates in metastatic patients (life expectancy of approximately 12–18 months). Thus, new target candidates are urgently needed in addition to surgery or radiation. Elevated DDX3X expression is common in most sarcomas and silencing *DDX3X* expression reduced survival and tumorigenicity of Ewing sarcoma cells. Proteomic analysis revealed that DDX3X suppression in Ewing sarcoma had an impact on several pathways, including translation, ribosome assembly, cell cycle regulation and DNA damage response, highlighting the complexity of the intracellular functions of DDX3X [60,61]. In addition, DDX3X has been found to be positively regulated by the protein Ezrin, an important regulator of cell motility and a mediator of metastasis. High Ezrin expression in osteosarcomas correlated with poor survival. Overexpression of Ezrin in osteosarcoma cells was shown to increase DDX3X protein levels, while its silencing had an opposite effect. The physical interaction of DDX3X with Ezrin inhibited its helicase activity but stimulated ATP hydrolysis. Since silencing or chemical inhibition of Ezrin had an antimetastatic effect, these results might suggest a link between DDX3X activity and increased osteosarcoma invasivity [23].

Colorectal cancer

Colorectal cancer is the third cause of cancer-related deaths in the USA and new targeted therapies are urgently needed.

A common genetic alteration of colorectal cancers is the loss of p53 function and the activation of the oncogenic KRAS-RAF signal transduction pathway. Another common feature is the hyperactivation of the Wnt/ β -catenin pathway, which is found in over 90% of cases. Among the most frequent alterations (>70% of cases), are inactivating mutations in the *APC* gene. Inactivating mutations in the β -catenin gene *CTNNB1* are also present, but at lower frequency (5–10%) [101].

Suppression of *DDX3X* expression resulted in reduced proliferation and G1 arrest in colorectal cancer cell lines [64], suggesting an oncogenic role of DDX3X in colorectal cancer [63]. It has been shown that DDX3X enhances *KRAS* oncogene transcription and activates β -catenin signaling through the CK1 ϵ /Dvl1 and HIF-1 α axes, promoting tumor invasion [62,65].

However, conflicting results regarding the role of DDX3X were reported also for colorectal cancer. In fact, DDX3X downregulation caused upregulation of Snail and decreased E-cadherin expression, with consequent reduced cell aggregation, suggesting an oncosuppressive role for DDX3X. Consistently, low *DDX3X* expression in colorectal cancer patients has been correlated with poor prognosis and frequent metastasis [66].

Oral squamous cell cancer

Oral cancer ranks among the ten most common cancers worldwide. Often diagnosed at a late stage, due to absence of specific biomarkers for the disease, it is generally characterized by poor prognosis. In addition, therapeutic

alternatives are few and expensive [102]. While oral cancer shows a general global trend of a slight decrease, the incidence of tongue cancer incidence is, on the other hand, increasing. Thus possible novel therapies are strongly needed.

DDX3X seems to act both as a protective factor and survival predictor, particularly in nonsmoker patients with oral squamous cell cancer (OSCC) [68]. However, high *DDX3X* expression was correlated with poor survival in smokers [67]. These differences could be explained, in part, in the different incidence of HPV-positive OSCC in smoker versus nonsmoker patients, as well as in the ability of cigarette smoke carcinogens in inducing *DDX3X* expression. Moreover, *DDX3X* was found to enhance oncogene expression in OSCC through interaction with the translational factor eIF3 [13,103].

Hepatocellular carcinoma

While initial evidence suggested an oncogenic role of *DDX3X* overexpression in hepatocellular carcinoma (HCC) cell lines [104], another study showed that *DDX3X* knockdown upregulated cyclinD1 and downregulated p21 promoting cell cycle progression, suggesting its role as an oncosuppressor, [69]. These findings were also supported by the observation that *DDX3X* expression was reduced in HCC specimens and that *DDX3X* upregulated p21 expression independently from p53, by transactivating its promoter in an ATPase-dependent and helicase-independent manner [91]. In addition, the natural antitumor agent Rottlerin apparently inhibited HCC proliferation by upregulating *DDX3X*, which in turn increased p21 and decreased cyclinD1 levels, leading to cell cycle arrest [105]. An oncosuppressor role for *DDX3X* is also supported by the observation that *DDX3X* can increase the expression of a set of tumor-suppressive miRNAs in the HCC cell line HepG2, through the inhibition of the methylation of their promoters by the DNA methyltransferase DNMT3A. Accordingly, knockdown of *DDX3X* induced stemness in HepG2 cells and low levels of *DDX3X* expression correlated with poor prognosis in HCC patients [82]. However, an oncogenic role of *DDX3X* in the context of HCC has been recently proposed again, based on the observation that loss of this protein in hepatocyte-specific *DDX3X* knockout mice, promoted liver tumorigenesis in female animals. Molecular analysis showed that loss of *DDX3X* led to accumulation of DNA damage and replicative stress in cells. These effects were ascribed to the role of *DDX3X* in positively regulating the expression of essential DNA repair proteins in wild-type cells [106]. Thus, *DDX3X* apparently can play a dual role in HCC, both as an oncogene or a tumor suppressor.

Medulloblastoma

DDX3X is one the genes most frequently mutated in medulloblastoma, an aggressive cerebellar tumor in both children and adults. Tumors harboring *DDX3X* mutations have been consistently found to be altered in translation response to stress, with increased frequency of cytoplasmic stress granules (SGs) formation and impairment of translation [72,107]. In addition, specific mutations linked to pediatric medulloblastoma, such as G320V and G325E, were shown to impact ATP hydrolysis [45], while other common mutations, such as R276K/Y and R534H, were found to abolish the RNA helicase activity [108], suggesting that loss of catalytic function was important for the role of *DDX3X* in promoting medulloblastoma. The oncogenic role of *DDX3X* in medulloblastoma has been proposed to act through the stimulation of the Wnt/ β -catenin axis. In particular, *DDX3X* was found to positively regulate the expression of the protein Rac1, a member of the Rho family of GTPases, at the translation level. Activation of Rac1 prevents β -catenin degradation, allowing its nuclear translocation. Thus, *DDX3X* promotes the expression of β -catenin target genes both by activating CK1 ϵ and increasing the Rac1 levels [109].

Extranodal NK/T-cell lymphoma

Recently, thanks to the diffusion of next-generation sequencing techniques, novel gene mutations have been identified in extranodal NK/T-cell lymphoma, nasal type, that have not been identified before with the traditional Sanger sequencing. This lymphoma is a rare but aggressive subtype of non-Hodgkin lymphoma that most commonly affects the upper aerodigestive tract and sometimes involves the extranasal one. One of the three most mutated genes in this tumor type is *DDX3X* with a percentage of mutation of about 13.6% [73,74]. *DDX3X* mutations normally cause truncated proteins or variant in the RNA-binding site or close to the ATP site, but all abrogate the helicase activity of the protein. These findings indicate that aberrations in this gene result in loss of RNA-unwinding function, thus contributing to the pathogenesis and poor prognosis of NK/T-cell lymphoma.

Other cancers

An oncogenic role of DDX3X has been reported also in other cancers. Overexpression of *DDX3X* and the cell adhesion molecule Nectin-2 correlated with tumor progression and poor prognosis in pancreatic ductal adenocarcinoma [110] and gallbladder cancers [71]. Similarly, high expression of *DDX3X* and Snail was found in glioblastoma multiforme samples [70]. However, the exact role of DDX3X in these cancers await further elucidation.

DDX3X as an anticancer drug target

So far, three DDX3X inhibitors have been tested as potential anticancer agents.

The DDX3X inhibitor RK-33 (diimidazo[4,5-d:40,50-f]-[1,3] diazepine; Figure 2) was proposed as a possible candidate for cancer treatment. RK-33 makes nine hydrogen bond contacts with various amino acids of DDX3X [111,112]. RK-33 specifically binds the DDX3X ATP-binding cleft and can perturb its helicase activity. This results in increased apoptosis, suppression of the Wnt-signaling pathway and reduction of nonhomologous end-joining repair [59]. This might suggest a role of DDX3X in activating nonhomologous end-joining, which is another major DNA DSBs repair mechanism. Giving the DSB repair deficiency by homologous recombination of *BRCA1*-mutated breast cancers, it could be that these cells could develop DDX3X dependency. However, up to date *BRCA*-deficient breast cancers cell lines seem not to be more dependent on DDX3X, than *BRCA*-proficient cancer cells. Indeed, in preliminary studies, breast cancer cells could be sensitized to PARP inhibition with Olaparib by RK-33 treatments, mainly in *BRCA1*-proficient cell lines, but also in *BRCA1*-deficient cancers [96]. To gain further insights into the mechanism of action of RK-33, a proteomic analysis was performed in the breast cancer cell line MDA-MB-435 either untreated or treated with RK-33. The analysis showed altered expression of proteins involved in mitochondrial translation, cell division and cell cycle progression after RK-33 treatment [90]. Indeed, targeting mitochondrial translation by DDX3X inhibition has been shown to radiosensitize breast cancer cells [97]. Phosphopeptide analysis indicated a decreased activity of CDK1. Cell cycle analysis showed a global delay in all phases and an increased rate of endoreduplication. While not all these effects could be easily rationalized in terms of DDX3X known functions, these results indicated that abrogation of DDX3X activity can have a huge impact on the proteomic landscape, again pointing to a complex network of interactions involving this protein.

RK-33 was also tested against a broad panel of cancer cell lines, showing potency of inhibition in the low micromolar range against most of them, including breast, lung, sarcoma and colorectal cancers (Table 4).

Also for lung cancer, DDX3X can be exploited as a therapeutic target for tumor-selective radiation sensitization. This might allow the reduction of radiation doses, with a gain in efficacy [59]. When treatment with RK-33 inhibitor was combined with radiation, synergistic cell death were observed both *in vitro* and in different *ex vivo* models of lung cancer. Unfortunately, *in vivo* results in animals were not so successful, possibly due to not enough frequent administration of RK-33 to animals in combination with radiation treatments.

The small-molecule inhibitor RK-33 could be useful also in colorectal cancer treatments, since it caused inhibition of Wnt signaling [64]. RK-33 inhibited growth and promoted apoptosis of 3D cultures of colorectal cancer cell lines derived from patients, with IC_{50} values in the low micromolar range. The highest RK-33 efficacy was achieved in tumors with wild-type *APC*- and mutated β -catenin *CTNNB1* gene, with no direct connection between DDX3X protein levels and sensitivity to RK-33 inhibitor.

It is important to underline also the possibility to exploit DDX3X in anticancer therapy in a synergic and combined manner, based on the well-known cellular pathways in which this protein is involved: DDX3X is required in translation, ribosome metabolism and cell cycle regulation including the G1/S transition and facilitation of DNA damage repair. One possibility is to use already available molecules like proteasome inhibitors in combination with RK-33 as a radiosensitizer. This because RK-33 decreases production of several proteasome proteins and could potentiate the effects of other drugs targeting the proteasome pathway [60].

The ring-expanded nucleoside analog NZ51 (Figure 2) inhibited the ATP-dependent helicase activity of DDX3X and was initially developed as an anti-HIV inhibitor (see also the next section), but also showed some anticancer activity [115]. Later, the same molecule was shown to be able to suppress motility and viability of MCF-7 and MDA-MB-231 breast cancer cells with IC_{50} values in the low micromolar range (Table 4) [114]. These effects were consistent with decreased proliferation rates and reduced clonogenicity observed upon silencing of *DDX3X* gene expression in the same cell lines (Table 3 & [70]). Interestingly, this molecule was active both under normoxic and hypoxic conditions with the same potency. Unfortunately, *in vivo* preliminary results in animal models did not show tumor volume reduction, but hopefully improvements in drug formulation, dose and delivery could lead to better *in vivo* activity [114].

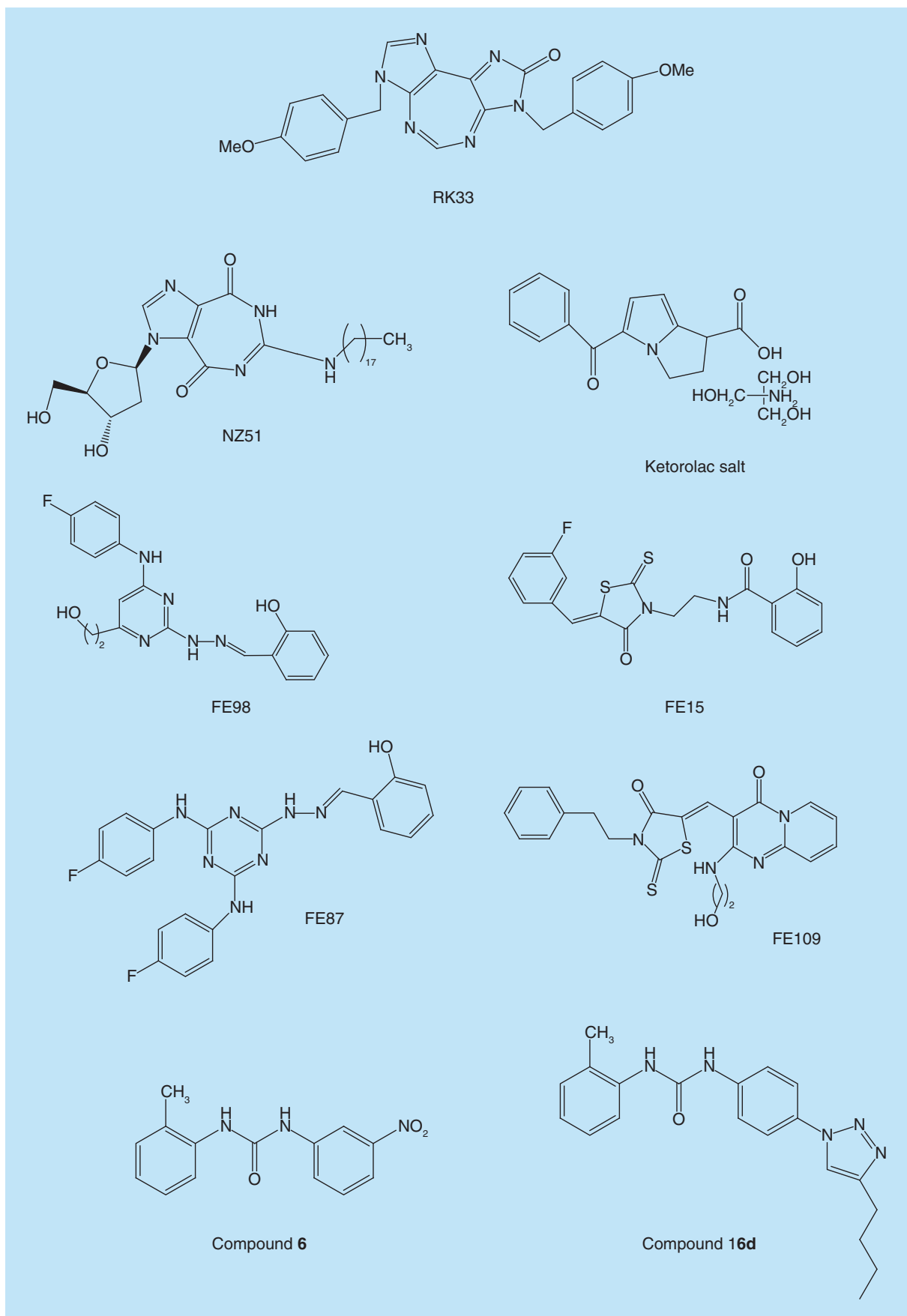


Figure 2. Small-molecule inhibitors of DDX3X. Structures of the DDX3X inhibitors discussed in this Review. For details see text.

Table 4. Antiproliferative activity of DDX3X inhibitors on different tumor cell lines.

Compound	Cell line /tumor	CC50	Ref.
RK-33	PC3 (prostate)	2.5 μ M	[59]
	A549 (lung)	1 μ M	
	DU145 (prostate)	1 μ M	
	OVCAR-8 (ovarian)	0.75 μ M	
	ADR-RES (ovarian)	5 μ M	
	MCF7 (breast) [†]	0.3 μ M	
	MDA-MB-468 (breast) [†]	0.4 μ M	
	T47D (breast)	5.5 μ M	
	HCT116 (colon) [†]	0.4 μ M	
	HT29 (colon) [†]	0.75 μ M	
RK-33	MCF7 (breast) [†]	3 μ M	[96]
	MDA-MB-468 (breast) [†]	3 μ M	
	SUM149PT (breast)	2.9 μ M	
	HCC1937 (breast)	6.6 μ M	
	MDA-MB-435 (breast)	5 μ M	
RK-33	HCT116 (colon) [†]	3 μ M	[64]
	HT29 (colon) [†]	3 μ M	
RK-33	U2OS (osteosarcoma)	3.8 μ M	[61]
	Saos-2 (osteosarcoma)	2.9 μ M	
	BJ (normal fibroblasts)	2.2 μ M	
	293T (human embryonic kidney)	4 μ M	
	3T3 (normal fibroblasts)	57.7 μ M	
	PBMC (white blood cells)	6.6 μ M	
RK-33	MCF10A (normal breast)	7.4 μ M	[97]
	MCF7 (breast), [†] MDA-MB-468 [†] /435/231 (breast)	2.8–4.5 μ M	
Ketorolac	H357 (oral)	2.6 μ M	[113]
NZ51	MCF7 (breast)	2 μ M	[114]
	MDA-MB-468 (breast)	2 μ M	
	MDA-MB-231 (breast)	10 μ M	

[†] Different results on the same cell line in separate studies for the RK-33 compound.

Another DDX3X inhibitor that proved to possess interesting anticancer activity is the pyrrolizine carboxylic acid derivative Ketorolac salt (Figure 2), ((6)-5-benzoyl-2,3-dihydro-1H-pyrrolizine-1-carboxylic acid, tris(hydroxymethyl) amino methane salt), which is structurally related to indomethacin. This bioactive compound is able to inhibit the DDX3X ATPase activity through hydrogen bond interactions with Gly 227, Gly 229, Thr 231 and Ser 228 DDX3X residues [113]. This compound is already available with the commercial name of ToradolTM, a nonsteroidal anti-inflammatory drug that is used for the control of inflammation and pain. Ketorolac salt was effective in reducing early relapse in TN breast cancer tumors. It is also used to improve postoperative outcome after breast cancer surgery (<http://clinicaltrials.gov/show/NCT01806259>). Ketorolac salt was found to effectively inhibit the growth of H357, a human OSCC cell line, in a dose-dependent manner where it downregulated *DDX3X* expression and upregulated the expression levels of E-cadherin. Moreover, Ketorolac salt reduced tongue lesions in animal models (BALB/c mice) of oral cancer. These data suggest that Ketorolac can be considered as possible drug candidate to treat DDX3X-associated oral cancer.

DDX3X & viral infections

Human DDX3X is often hijacked by a number of viruses, in order to promote their own replication [1,4–6,116]. Figure 1B illustrates the different DDX3X-dependent molecular pathways, which are important for the infection by different viruses. They can broadly be grouped into three main categories: viral genome replication; regulation of viral gene expression (transcription and translation); innate immunity (interferon [IFN]-mediated response). DDX3X roles in viral replication and gene expression generally require its ATPase/RNA helicase activities, while its

functions in innate immunity are mostly independent from its catalytic activities. Depending on the virus involved and/or on the cellular context and viral life cycle stage, DDX3X can act either in a proviral fashion or can have an antiviral role [117]. Thus, viruses have evolved mechanisms to benefit, on one side, from the activity of DDX3X, but also, on the other side, to inhibit its functions in order to suppress its antiviral effects. This dual role of DDX3X in viral infections is also reflected by the nature and consequences of its interaction with different viral proteins (Table 1) that are able to modulate DDX3X functions.

DDX3X in innate immunity & stress response

Among the most important innate immunity early responses to pathogens, there is the IFN production. DDX3X has been shown to stimulate IFN response at different levels. It interacts with and is phosphorylated by the protein kinases TBK1 and IKK ϵ , and such interaction was shown to be essential for the activation of the transcription factor IRF3 and IFN production [37]. In addition, DDX3X directly interacts with IRF3 and promotes its phosphorylation by IKK ϵ [19] and it is recruited to the IFN promoter itself [118]. DDX3X also interacts with the protein IPS-1 [18] and TRAF3 [20] which, together with the sensor protein RIG-I, is involved in recognition of viral RNA and activation of the IFN-mediated response. Finally, DDX3X has been shown to stimulate the production of inflammatory cytokines in the NF- κ B axis, through modulation of the IKK β /PPA2C complex activity [22] and also to directly stimulate type I IFN production and NF- κ B response through the activation of the IKK α /NF- κ B-induced kinase NIK pathway [119]. However, conflicting reports about the effects of *DDX3X* silencing in the context of NF- κ B regulation still need to be reconciled (Table 3) [21,22]. It is noteworthy to mention that the catalytic activities of DDX3X seem not to be essential in these pathways. In response to different cellular stresses, including viral infections, eukaryotic cells often block translation of a subset of mRNAs, which are sequestered in cytoplasmic RNA-protein complexes called SGs. DDX3X is a component of SGs and seems to be important for SGs formation and translation of stress-specific factors under a variety of pathological conditions [8,72,120], including anticancer chemotherapy [83]. DEAD-box proteins, including DDX3X, are also important in the formation of virus-induced SGs, which play an important role in innate immunity, for example sequestering viral mRNAs or acting as platforms for viral RNA-sensing receptors, such as those of the RIG-I family, which trigger IFN-mediated antiviral response [32,121–124] (for recent reviews see also [125,126]). The different modulatory activities of DDX3X in innate immunity and stress response are important for its roles in the context of viral infections, as will be discussed below.

HIV type 1

The first direct evidence that DDX3X is involved in HIV type 1 (HIV-1) replication came from the seminal study of Yedavalli *et al.* [10], who showed that DDX3X was required to facilitate the Rev-mediated export of unspliced or partially spliced viral mRNAs, interacting with the cellular exportin CRM1 [11,127]. Consistently, knockdown of *DDX3X* was shown to suppress HIV-1 replication without affecting cell viability [77,79]. However, the functions of DDX3X in HIV-1 replication are not limited to mRNA export. Later research suggested that this protein is also involved in viral mRNA translation [128]. Indeed, DDX3X was shown to be important for the translation of a subset of cellular mRNAs containing secondary structures (stem loops) near their 5'-m(7)GTP capping element, similar to those found near the 5'-m(7)GTP cap of HIV-1 RNA [14], and can specifically promote translation of the HIV-1-unspliced genomic mRNA, binding to its specific 5'-cap structure [129]. An additional role of DDX3X in modulating the expression of *HIV-1* genes was also uncovered, by demonstrating that this cellular protein interacts with the viral transcriptional coactivator Tat. DDX3X forms a complex with Tat at the specific HIV-1 Tat-recognition region present at the 5' of HIV-1 mRNAs and facilitates Tat-dependent translation of viral genes [25,26]. As mentioned above, DDX3X is involved in stimulating innate immunity [116]. A recent study showed that DDX3X functions as a molecular sensor by binding to HIV-1 RNA in infected cells and activating type I IFN response. However, HIV-1 is able to induce downregulation of this DDX3X-dependent pathway by activating the cellular kinase PLK1 [130]. Thus, DDX3X appears an important cellular cofactor in modulating *HIV-1* gene expression in infected cells and, conversely, HIV-1 have evolved strategies to both exploit DDX3X as a proviral factor and repressing its antiviral functions.

Human hepatitis B virus

Although endowed with a DNA genome, hepatitis B virus (HBV) replicates through a RNA intermediate, thanks to its reverse transcriptase polymerase. In one study, DDX3X was found to be incorporated into HBV capsids and to inhibit reverse transcription, through a physical interaction with the HBV polymerase. Its ATPase, but not

helicase, activity was required for such an inhibitory effect [27]. HBV polymerase has been found to inhibit the IFN-induction counteracting the activation of the transcription factor IRF by the TBK1/IKK ϵ kinase complex. As mentioned before, DDX3X is an essential component of the TBK1/IKK ϵ pathway. HBV polymerase was found to sequester DDX3X, competing for its interaction with the TBK/IKK ϵ complex and suppressing IFN response. This inhibitory activity of HBV polymerase could be rescued by overexpressing DDX3X [131,132]. DDX3X has been shown to restrict HBV replication also independently from its interaction with the viral polymerase. In one study, DDX3X was found to repress transcription of HBV genes through direct modulation of the activity of the viral promoter. Knockdown of *DDX3X* led to an increase in HBV transcription, while its overexpression had the effect of reducing it [133]. Thus, DDX3X appears to exert an antiviral effect against HBV infections. These results are in agreement with previous findings, demonstrating that *DDX3X* was downregulated in HCCs associated to HBV, but not to hepatitis C virus (HCV) chronic infections [69]. As discussed in the previous section about the role(s) of DDX3X in tumor transformation, downregulation of DDX3X in HBV-related HCCs also induced cell proliferation. Thus, suppression of DDX3X can initially favor HBV proliferation and, once a chronic infection is established, can promote further tumor transformation of infected cells.

Hepatitis C virus

DDX3X was found to interact with the HCV core protein both *in vitro* and in cells through its C-terminal domain and to localize in cytoplasmic SGs, suggesting a role in modulating viral or cellular RNA turnover [28,134,135]. HCV core was found to inhibit the translation of capped cellular mRNAs, likely through its interaction with DDX3X [28]. Later, it was shown that siRNA-mediated knockdown of *DDX3X* represses HCV replication in HuH-7 cells [136]. However, a DDX3X mutant unable to bind HCV core did not affect HCV genotype 2a replication in cells, suggesting that such an interaction was dispensable for the DDX3X proviral effect [137]. Conversely, HCV core-derived peptides were able to suppress HCV genotype 1b replication and this effect was counteracted by overexpression of *DDX3X*, suggesting that the role(s) of DDX3X-core interaction in HCV replication may be genotype specific [138]. It has been also shown that HCV core protein is required to sequester DDX3X, abrogating its ability to stimulate IFN-mediated antiviral response [139,140]. DDX3X is able to recognize the 3'-UTR of the HCV genome and this interaction activates a signaling cascade mediated by the kinase IKK α , which promotes lipid droplets formation required for viral particles assembly [141]. Upon binding to the HCV 3'-UTR and IKK α , DDX3X relocates to SGs. These DDX3X granules are then recruited, together with the HCV core and nonstructural proteins, to lipid droplets, which function as virus replication and viral particle assembly factories [120]. Thus, several studies indicate that the proviral function of DDX3X in the context of HCV infections involves a complex network of molecular interactions (for a recent review, see also [142]).

West Nile virus & Dengue virus

Several RNA viruses are transmitted to humans through insect vectors such as *Culex* and *Aedes* spp. mosquitoes. Among these, Dengue virus (DENV) and West Nile virus (WNV) seem to hijack DDX3X for their replication. A study showed that upon WNV infections, cytoplasmic P-bodies are disrupted and their cellular components are recruited to sites of viral replication. Among these factors, DDX3X was found to colocalize with the viral NS3 protein at perinuclear *foci*. Silencing of *DDX3X* potently suppressed WNV replication, suggesting a positive role of the DDX3X protein in the life cycle of WNV virus [29].

A proteomic study aimed at characterizing cellular cofactors for DENV replication, found an interaction between DDX3X and the NS5 viral RNA polymerase. In this study, knockdown of *DDX3X* significantly reduced DENV replication in infected cells [31]. The positive role of DDX3X in DENV infections, however, has been later challenged by subsequent work. One study demonstrated that *DDX3X* knockdown promoted DENV replication, likely through the suppression of the IFN-mediated response [143]. A later work identified an interaction between DDX3X and the viral capsid protein, through the respective N-ter domains. The authors showed that endogenous DDX3X was downregulated in DENV-infected cells and that knockdown of *DDX3X* by siRNA, promoted viral replication. However, contrary to the study mentioned above, the authors failed to detect a decrease in IFN-mediated response upon *DDX3X* knockdown, suggesting that the antiviral effects of DDX3X depended on its interaction with the DENV capsid protein [30]. Thus, the precise role of DDX3X in DENV replication is still controversial.

Human influenza A virus

DDX3X was found to interact with the NP and NS1 proteins of human Influenza A virus (IAV) [32]. Cells respond to viral infections also sequestering viral proteins and RNAs in cytoplasmic SGs. DDX3X is an important factor involved in the formation of SGs and it was shown to colocalize to SGs upon IAV infection, together with the viral NP protein. The helicase activity of DDX3X was not required for the interaction, but it was essential for recruitment of DDX3X at SGs. Knockdown of *DDX3X* led to impaired SGs formation and increase in IAV replication, but only in viruses bearing a defective viral NS1 protein [32]. This suggested that DDX3X could be involved in the antiviral response toward IAV, likely mediated through sequestration of NP protein, essential for the replication of the viral genome, into SGs. Viral NS1 has been shown to inhibit SGs formation [121]. Thus, its interaction with DDX3X might be a mechanism through which IAV counteracts the antiviral effect of DDX3X.

Arenaviruses

Arenaviruses are a large family of RNA viruses, including agents causing severe hemorrhagic fevers in humans, such as Lassa virus or Junin virus and neurological diseases such as in the case of lymphocytic choriomeningitis virus (LCMV). LCMV genome is replicated by the viral RNA-dependent RNA polymerase protein L. A proteomic approach revealed DDX3X as an interactor of the viral L protein. CRISPR-Cas9 knockout of the *DDX3X* gene resulted in decreased viral load, suggesting that DDX3X has a proviral function in the context of LCMV infections [33]. In another study [34], DDX3X was found to interact with the viral NP protein, another essential component of the replication machinery, of Lassa virus, Junin virus and LCMV. DDX3X promoted replication of all these three viruses, as revealed by a reduction in viral proliferation by *DDX3X* gene silencing. This stimulation required both its ATPase and RNA helicase activities. Arenaviruses have the ability to potently inhibit IFN response in infected cells. *DDX3X* knockdown was found to partially restore type 1 IFN production in cells infected with LCMV, suggesting an additional proviral function of DDX3X in repressing innate immunity. However, it appears that suppression of IFN production by DDX3X was important only at a late stage of the infection, while at early time points its proviral function was mainly dependent upon its stimulation of viral RNA synthesis [34].

Japanese encephalitis virus

Japanese encephalitis virus (JEV) is a common cause of epidemic viral encephalitis in humans and animals. In one study, DDX3X has been found to interact, both *in vitro* and in infected cells, with the viral replicative proteins NS3 and NS5. Knockdown of *DDX3X* inhibited viral replication. Using a JEV replicon system, the authors demonstrated that DDX3X upregulated viral mRNA translation, through binding to the 5'- and 3'-UTR regions of the JEV genome [144]. Thus, DDX3X appears to act as a proviral factor in the context of JEV infections.

Venezuelan equine encephalitis virus

Venezuelan equine encephalitis virus (VEEV) is a mosquito-borne RNA virus, responsible of frequent zoonotic infections in humans. DDX3X has been found to interact with the replicative viral protein nsP3 and its knockdown potently inhibited viral replication. The authors showed that the viral nsP3 localized to virus-induced SGs and interacted with several translation factors, leading to the hypothesis that recruitment of DDX3X might facilitate viral mRNAs translation [85].

Pestiviruses

Pestiviruses are a group of RNA viruses belonging to the Flavivirus family, that includes the bovine viral diarrhea virus responsible of frequent epidemics in cattle. The viral protease N^{Pto} is known to counteract the IFN response in infected cells, inhibiting the transcriptional factor IRF3. Proteomic analysis identified DDX3X as an interactor of N^{Pto} and observed its colocalization with the viral protein at cytoplasmic SGs, along with several other cellular proteins. However, the exact role of this interaction in the viral life cycle has not been established [36].

Murine norovirus

Infection by noroviruses is one of the most frequent causes of gastroenteritis. Since no efficient culture system has been established for the human virus, murine norovirus (MNV) is being used as a surrogate model for studying the viral life cycle. A proteomic study identified DDX3X as host factor interacting with the MNV genome. Binding of DDX3X to the dsRNA viral genome was further confirmed by immunostaining in infected cells. In addition,

knockdown of *DDX3X* reduced MNV replication [145]. However, the molecular mechanism underlying the proviral function of *DDX3X* in MNV infection has not been elucidated.

The ability to manipulate *DDX3X* functions in infected cells seems also not to be restricted to RNA viruses.

Herpesviruses

Herpesviruses are endowed with a large DNA genome. *DDX3X* has been found to be incorporated into the virions of herpes simplex virus type 1 (HSV-1) [146]. In a subsequent study, it was shown that the levels of *DDX3X* positively correlated with *HSV-1* gene expression and replication levels. HSV-1 replication in a cell line harboring a temperature-sensitive mutant of *DDX3X* was strongly reduced at non-permissive temperature. Also an excessive overexpression of *DDX3X* was detrimental to HSV-1 replication, suggesting the existence of an optimal range of *DDX3X* protein, which could be beneficial to HSV-1 replication. *DDX3X* was found to positively modulate *HSV-1* gene expression, independently from its ability to stimulate IFN response, and was required for proper viral particles assembly. The ATPase/helicase activity of *DDX3X* was required for its proviral functions [147].

Another herpesvirus that exploits *DDX3X* is human cytomegalovirus (HCMV). *DDX3X* has been found to associate with HCMV transcripts [148] and to be incorporated into mature viral particles [149]. The protein levels of *DDX3X* were increased upon HCMV infection and siRNA-mediated knockdown of endogenous *DDX3X* expression reduced HCMV replication [149]. However, the precise molecular mechanism for this proviral effect has not been determined.

Vaccinia virus

The K7 protein of Vaccinia virus (VACV) was shown to inhibit the cellular IFN response through the sequestration of *DDX3X*, thus hampering the TBK1/IKKε-IRF3 pathway [37]. Structural studies mapped the interaction to an hydrophobic cleft of K7, which was bound by a short domain located at the N-terminal of *DDX3X* (aa 82-88) [150,151]. Thus, VACV counteracts the antiviral effects of *DDX3X* by masking a domain critical for the activation of the TBK1/IKKε complex.

Adenovirus

The Bovine Adenovirus 3 protein pVIII was found to interact with *DDX3X* and to inhibit host mRNA translation *in vitro* and *in vivo*, by disturbing the *DDX3X*-dependent recruitment of the eIF3 translation factor to the 5'-cap structure of cellular mRNAs [35].

DDX3X as a target for antiviral therapies

As outlined above, *DDX3X* appears to play a positive role in the life cycle of several different viruses, for many of which there are currently no available therapies. For this reason, *DDX3X* is being regarded as a promising target for antiviral chemotherapy.

Prompted by the original observation that *DDX3X* can act as a cellular cofactor for HIV-1, a series of ring-expanded nucleoside analogs with an imidazo[4,5-*e*] [1-3] diazepine ring system were identified by a random-screening approach, of which the derivative NZ51 (Figure 2) was able to inhibit *DDX3X* RNA helicase activity and to suppress HIV-1 replication [115,152]. Some derivatives of this series, based on the same scaffold, also showed promising dual activity against both HIV and HCV proliferation [153].

In the same years, a rational drug design approach was used to identify specific inhibitors of *DDX3X*. Based on the crystal structure of human *DDX3X* in complex with AMP [154], a pharmacophoric model was built, incorporating the essential chemical features responsible for ATP substrate-enzyme interaction. This model was used in a virtual screening approach of commercial databases that allowed the identification of a suitable chemical scaffold, which led to the development of the compound FE15 (Figure 2), as the first ATP-competitive inhibitor of *DDX3X* active against HIV-1 replication [155]. Analysis of the binding mode of the inhibitor in the ATPase pocket of *DDX3X* showed that the molecule formed hydrogen bonds with Gly229, Lys230, Gln225 and Ser228 of *DDX3X*, and hydrophobic interactions with Ala232 and Tyr200. Taking into account this information, a combination of *in silico* high throughput docking analysis and structure-activity studies, led to the development of the novel pyrimidine, rhodanine and triazine derivatives, FE98, FE109 and FE87, respectively (Figure 2), endowed with better anti-HIV activity and selectivity than FE15 [77].

Since the ATP binding site of *DDX3X* is structurally similar to many other ATP-hydrolyzing enzymes, the attention focused next to the RNA-binding domain, with the aim of improving inhibitor selectivity. In the absence

of three dimensional structures of human DDX3X in the pre-RNA-binding closed conformation, an homology model based on the structure of the analogous conformation of the DEAD-box helicase eIF4AIII was used for rational drug design. A high-throughput docking approach was applied, for the search of specific ligands for the RNA-binding site of DDX3X, identified by a 10Å grid centred on the Thr323 residue of the enzyme. This approach resulted in the identification of a class of *N,N'*-diarylurea derivatives able to inhibit both the helicase activity of DDX3X and to suppress viral replication in HIV-1-infected cells [156]. Further optimization was obtained by building a refined model of DDX3X in complex with its RNA substrate, using the known structure of the related DEAD-box helicase Vasa bound to RNA. This model allowed a more precise definition of the residues involved in the interaction with the nucleic acid, leading to the identification of the hit compound **6** (Figure 2) endowed with low micromolar activity against the DDX3X helicase activity. This inhibitor made contacts with Arg276, Arg480, Pro274 in a mode similar to the modeled RNA strand. Additional hydrophobic interactions were made with Phe357, Val500, Arg503 and Val500 [157]. Further inspection of the homology model suggested the possibility of the introduction of substituents, able to exploit additional interactions within the RNA-binding pocket. This led to the discovery of a novel family of RNA-competitive inhibitors of DDX3X helicase activity. The best compound of this series, **16d** (1-(4-(4-methyl-1H-1,2,3-triazol-1-yl)phenyl)-3-*o*-tolylurea) (Figure 2), maintained the key interactions of the parent derivatives, taking additional contacts with Arg326 and Gly302. The inhibitor **16d** showed potent anti-helicase activity and was able to suppress the replication of different RNA viruses (HIV-1, HCV, WNV, DENV), including HIV-1 strains resistant to clinically used antiretroviral drugs, showing virtually no toxicity in cellular and animal models [158]. These results suggested that DDX3X might potentially be exploited as a target for the development of broad-spectrum antiviral agents.

Recently, an analog-sensitive inhibition approach has been tried for DDX3X. An expanded active site mutant of DDX3X was rationally designed, based on the crystal structure, by mutating the conserved Phe182 in a hydrophobic pocket near the ATP-binding site, into Ala. This F182A mutant was used to screen different libraries of synthetic compounds, leading to the identification of pyrazolopyrimidine and anilinoquinazolines scaffolds as promising starting points for the development of novel inhibitors [159].

Conclusion

The data reviewed above, support the notion of DDX3X as a sort of 'molecular hub', providing connection among different cellular pathways. As shown in Figure 1, the ability of DDX3X to directly regulate gene expression at the transcription and translation levels is important in the context of both cell proliferation and viral replication. On the other hand, perturbation of DDX3X role(s) in the Snail/E-cadherin and Wnt/ β -catenin axes seems to be relevant only in the context of tumorigenesis. Conversely, alteration of the function(s) of DDX3X in the IFN-mediated response is critical for viral infections. The different modulation of DDX3X activity in these various pathways determines whether this protein acts in a positive (i.e., as an oncogene or proviral factor) or in a negative (i.e., as a tumor suppressor or antiviral determinant) fashion. Often, DDX3X can have both positive and negative roles in the context of the same tumor or infection by the same virus. One of the characteristic features of DDX3X is its ability to perform different functions depending on its subcellular localization. DDX3X shuttles from the nucleus to the cytoplasm, thanks to its N-terminal nuclear export signal and to three nuclear localization signal sequences, which can independently mediate its nuclear import [3]. DDX3X is mainly cytoplasmic throughout the cell cycle, with an increase in nuclear accumulation in early mitosis. DNA damage, cytokine stimulation or viral infection were found to cause small changes in the subcellular localization of DDX3X [3]. On the other hand, altered localization of DDX3X has been reported in different tumors. For example, in squamous cell carcinoma of the skin and in OSCC, DDX3X was found to be predominantly cytoplasmic [33,59]. Also, in breast and colon cancer, increased nuclear localization of DDX3X was found to correlate with poor prognosis and higher invasivity [43]. As discussed above, in the cytoplasm, DDX3X participates in the Wnt/ β -catenin pathway, assembly of SGs, innate immunity response, as well as in translation of specific subsets of mRNAs. On the other hand, in the nucleus, DDX3X can regulate the expression of a number of genes, interacting with their promoters or with transcriptional factors. Thus, shifting the balance in the cytoplasmic versus nuclear fraction of DDX3X can significantly alter the equilibrium among these different pathways. Another factor that can influence the role of DDX3X in the context of tumorigenesis is the presence of specific mutations. DDX3X has been found to harbor mutations in leukemia, squamous cell carcinoma and medulloblastoma samples (reviewed in [160]). Mapping of these mutations on DDX3X structure revealed that many of the cancer-associated aminoacidic substitutions involve residues important for the catalytic functions of

DDX3X. As discussed above, some of the physiological functions of DDX3X do not require its catalytic activity, but only its physical interaction with other proteins. Thus, the presence of a catalytically impaired DDX3X fraction can suppress certain pathways, while favoring other ones. Whether DDX3X will predominantly act as an oncogene or a tumor suppressor, ultimately depends on several factors, such as its expression levels, the presence of mutations and the tumor genetic background. Similar considerations might be proposed for the dual role that DDX3X can play in the context of certain viral infections. Depending on the specific virus and/or the particular stage of the virus life cycle, DDX3X can be a proviral or an antiviral factor. For example, as discussed above, in the context of HIV-1 infection, DDX3X is co-opted by the virus to enhance the expression of the viral genes but, at the same time, HIV-1 have evolved mechanisms to repress its role in viral RNA sensing by the innate immunity pathway [161]. This multifaceted roles of DDX3X make it, on one side, an attractive target for anticancer and antiviral chemotherapy, but also, on the other side, render its practical exploitation a complex matter. Future lines of research must be devoted to improve our understanding of the DDX3X molecular mechanisms, as outlined in the next section.

Future perspective

From the magic bullet to the magic target

In spite of the complexity of the network of molecular interactions involving DDX3X, the different studies summarized above have provided a solid proof-of-principle for its exploitation as a chemotherapeutic target for the treatment of a number of pathological conditions, such as different cancer types and different viral infections. The idea of choosing a cellular protein as a target for viral infections is not new, but has been generally regarded as a difficult and potentially dangerous approach, due to the risk of side effects in uninfected cells, as a consequence of altering the functions of a cellular pathway. However, the ever-increasing capability of mapping the whole interactome among viral and cellular proteins, along with the possibility of assessing in cellular and even animal models, the consequences of inhibiting the expression of any given gene in the genome both on cell survival and in the context of viral infections is opening up the possibility of identifying suitable targets. In parallel, our increasing understanding of the differences in the genetic background of healthy versus cancer cells, or even among different cancer types, has paved the way to the molecular-targeted anticancer therapies, exploiting cancer-specific protein alterations in the expression or functions of the target proteins.

DDX3X, thus, is an example of what could be considered a shift in the paradigm of drug development, which could be summarized as 'from the magic bullet to the magic target'. First enunciated by Paul Ehrlich in 1909 along with its discovery of the antisyphilis drug Salvarsan, the 'magic bullet' concept historically defined a molecule able to hit a pathologically relevant molecular target (being it a microbe or a cancer cell), without harming the body. This concept has further developed in the last 100 years, into a drug capable of acting simultaneously on different targets, such as broad-spectrum anticancer tyrosine kinase inhibitors, yet retaining selectivity for the diseased cells [162]. On the other hand, a 'magic target' is a protein which could be exploited for the treatment of both viral infections and cancer, provided that it fulfills two main features: it is essential for the replication of several viruses, but not for the viability of uninfected cells and its expression and/or functions are specifically deregulated, acting in an oncogenic fashion in different types of cancer.

DDX3X is normally expressed in all tissues at relatively high levels, which might suggest an housekeeping function of this protein. Indeed, targeted disruption of the *DDX3X* gene in mice led to early post-implantation lethality, indicating its essential role in mouse embryo development [86]. However, silencing *DDX3X* gene expression in cultured cells did not always result in suppression of cell proliferation, but has been shown to have different outcomes, depending on the particular cell line and on the level of suppression achieved (Table 3). On the other hand, as discussed above, some chemical inhibitors of DDX3X enzymatic activity were able to achieve suppression of viral replication in infected cultured cells, with minimal toxicities for the control uninfected cells. Also, administration of the **16d** helicase DDX3X inhibitor in animals failed to show systemic toxicity at therapeutically effective doses [158]. Similarly, administration of the DDX3X RK-33 inhibitor to nude mice in xenograft models of lung cancer [59], prostate cancer [163] or medulloblastoma [164] showed regression of the tumor up to 6-week administration, without affecting viability of the mice. Based on our current knowledge of DDX3X cellular functions, it is possible to hypothesize two major factors that can modulate the cellular response to DDX3X inhibition: the level of redundancy in DDX3X functions and the specific mechanism of action of the inhibitors. Overall, human cells possess 40 members of the DEAD-box family of RNA helicases and 15 members of the related DHX-family. In the cell, there are other DDX proteins whose functions may, at least in part, overlap with DDX3X. For example, DDX1, DDX21, DHX36, DHX9 and DDX60 also operate in the innate immune pathway, along with DDX3X,

in sensing viral nucleic acids (reviewed in [165]). Similarly, DDX2, DDX6 and DHX36 associate, together with DDX3X, to SGs in response to similar cellular stresses (reviewed in [165]). In general, several DDX-family RNA helicases are involved in the same pathways as DDX3X, from transcription to mRNA processing and translation (reviewed in [166]). Since most of these proteins share significant similarities in their catalytic properties, this suggests the possibility of a significant level of redundancy among their functions. On the other hand, a particular tumor or a virus can become dependent on a specific pathway and/or a specific interaction with a certain DEAD-box helicase, for example DDX3X. As a consequence, partial inhibition of DDX3X may not be excessively detrimental for a normal cell, due to the possibility that other DEAD-box proteins compensate for its loss, while it may become deadly for a cancer cells or a virus. Another point to be taken into consideration, is the fact that, as discussed in the previous sections, not all the functions of DDX3X, being them physiological, proviral or oncogenic, depend on its catalytic activities. Many, in fact, are mediated by direct protein–protein interactions. Others depend on the ATPase, but not on the helicase activity. Thus, by carefully selecting chemical compounds able to target a specific function, either a catalytic activity or a protein–protein interaction, it is also possible to imagine of achieving the desired selectivity against the diseased cells, leaving unaffected the normal ones. Gene disruption or silencing experiments lead to complete or almost complete loss of the protein, thus do not allow to carefully distinguish among these different effects, as chemical inhibition can do.

Of course, at this point we cannot rule out the risk of long-term toxicity problems following sustained suppression of DDX3X. This needs to be more carefully explored in preclinical models. However, a therapeutic efficacy of DDX3X inhibitors might not necessarily require long-term administration. Data from medulloblastoma and prostate cancer animal models suggest that DDX3X inhibition can potentiate the effects of radiation therapy [163,164], thus it could be used for a limited period of the time immediately preceding and following the irradiation of the patient. In the case of viral infections, DDX3X inhibitors can be administered for a defined time during the peak phase of viremia, to help the immune system in clearing the infection, or as part of combination therapies, to potentiate the effects of the other drugs.

In summary, DDX3X can be regarded as a potential ‘magic target,’ to be exploited for the development of broad-spectrum antivirals or anticancer drugs, but also as a cancer- or virus-specific target, or even for the simultaneous treatment of viral chronic infections and associated cancers. Further development of this approach, however, requires the need of a precise knowledge of the role(s) of DDX3X in specific tumors or viral infections, as a starting point for designing personalized therapies based on the modulation of its diverse activities.

Executive summary

- DDX3X plays key roles in cell proliferation, innate immunity and viral infections.
- In cancer, DDX3X can act either as an oncogene or as a tumor suppressor.
- In viral infections, DDX3X can have either an antiviral role or act as a proviral factor.
- The molecular mechanisms underlying the dual function of DDX3X in cancer and viral infections are still not completely understood.
- DDX3X is a validated target for both anticancer and antiviral chemotherapy.
- Still very few inhibitors of DDX3X have been developed and none of them has reached the clinical stage for the treatment of either cancer or viral infections.
- The multifaceted roles of DDX3X in various cancers and viral infections can open the possibility to exploit this protein as a target for broad-spectrum antitumor and/or antiviral therapies.

Financial & competing interests disclosure

Work in the authors' laboratory has been supported by the Italian Association for Cancer Research AIRC Grant IG 2017-20762 to G Maga. The authors have no other relevant affiliations or financial involvement with any organization or entity with a financial interest in or financial conflict with the subject matter or materials discussed in the manuscript apart from those disclosed.

No writing assistance was utilized in the production of this manuscript.

References

Papers of special note have been highlighted as: ● of interest; ●● of considerable interest

1. Schroder M. Human DEAD-box protein 3 has multiple functions in gene regulation and cell cycle control and is a prime target for viral manipulation. *Biochem. Pharmacol.* 79, 297–306 (2010).
2. Soto-Rifo R, Ohlmann T. The role of the DEAD-box RNA helicase DDX3 in mRNA metabolism. *Wiley Interdiscip. Rev. RNA.* 4, 369–385 (2013).
3. Brennan R, Haap-Hoff A, Gu L *et al.* Investigating nucleo-cytoplasmic shuttling of the human DEAD-box helicase DDX3. *Eur. J. Cell Biol.* 97 (7), 501–511 (2018).
4. Ariumi Y. Multiple functions of DDX3 RNA helicase in gene regulation, tumorigenesis, and viral infection. *Front. Genet.* 5, 423 (2014).
5. Garbelli A, Radi M, Falchi F *et al.* Targeting the human DEAD-box polypeptide 3 (DDX3) RNA helicase as a novel strategy to inhibit viral replication. *Curr. Med. Chem.* 18, 3015–3027 (2011).
6. Fullam A, Schroder M. DExD/H-box RNA helicases as mediators of anti-viral innate immunity and essential host factors for viral replication. *BBA Gene Regul. Mech.* 1829, 854–865 (2013).
7. Bol GM, Xie M, Raman V. DDX3, a potential target for cancer treatment. *Mol. Cancer* 14, 188 (2015).
8. Shih JW, Wang WT, Tsai TY *et al.* Critical roles of RNA helicase DDX3 and its interactions with eIF4E/PABP1 in stress granule assembly and stress response. *Biochem. J.* 441, 119–129 (2012).
9. Lai MC, Lee YHW, Tarn WY. The DEAD-box RNA helicase DDX3 associates with export messenger ribonucleoproteins as well as tip-associated protein and participates in translational control. *Mol. Biol. Cell.* 19, 3847–3858 (2008).
10. Yedavalli VSRK, Neuveut C, Chi Y-H, Kleiman L, Jeang K-T. Requirement of DDX3 DEAD box RNA helicase for HIV-1 Rev-RRE export function. *Cell* 119, 381–392 (2004).
- **The first evidence that DDX3X was a proviral factor.**
11. Mahboobi SH, Javanpour AA, Mofrad MRK. The interaction of RNA helicase DDX3 with HIV-1 rev-CRM1-RanGTP complex during the HIV replication cycle. *PLoS ONE* 10, e0112969 (2015).
12. Shah A, Rashid F, Awan HM *et al.* The DEAD-box RNA helicase DDX3 interacts with m(6)A RNA demethylase ALKBH5. *Stem Cells Int.* 2017, 8596135 (2017).
13. Lee CS, Dias AP, Jedrychowski M *et al.* Human DDX3 functions in translation and interacts with the translation initiation factor eIF3. *Nucleic Acids Res.* 36, 4708–4718 (2008).
14. Soto-Rifo R, Rubilar PS, Limousin T *et al.* DEAD-box protein DDX3 associates with eIF4F to promote translation of selected mRNAs. *EMBO J.* 31, 3745–3756 (2012).
15. Choi YJ, Lee SG. The DEAD-box RNA helicase DDX3 interacts with DDX5, co-localizes with it in the cytoplasm during the G2/M phase of the cycle, and affects its shuttling during mRNP export. *J. Cell Biochem.* 113, 985–996 (2012).
16. Tsai TY, Wang WT, Li HK *et al.* RNA helicase DDX3 maintains lipid homeostasis through upregulation of the microsomal triglyceride transfer protein by interacting with HNF4 and SHP. *Sci. Rep. UK* 7, 41452 (2017).
17. Sun MN, Zhou T, Jonasch E, Jope RS. DDX3 regulates DNA damage-induced apoptosis and p53 stabilization. *BBA-Mol. Cell Res.* 1833, 1489–1497 (2013).
18. Oshiumi H, Sakai K, Matsumoto M, Seya T. DEAD/H BOX 3 (DDX3) helicase binds the RIG-I adaptor IPS-1 to up-regulate IFN-beta-inducing potential. *Eur. J. Immunol.* 40, 940–948 (2010).
19. Gu LL, Fullam A, Brennan R, Schroder M. Human DEAD box helicase 3 couples I kappa B kinase epsilon to interferon regulatory factor 3 activation. *Mol. Cell Biol.* 33, 2004–2015 (2013).
20. Gu LL, Fullam A, McCormack N, Hohn Y, Schroder M. DDX3 directly regulates TRAF3 ubiquitination and acts as a scaffold to co-ordinate assembly of signalling complexes downstream from MAVS. *Biochem. J.* 474, 571–587 (2017).
21. Xiang N, He M, Ishaq M *et al.* The DEAD-box RNA helicase DDX3 interacts with NF-kappa B subunit p65 and suppresses p65-mediated transcription. *PLoS ONE* 11, e0164471 (2016).
22. Wang X, Wang R, Luo M *et al.* (DEAD)-box RNA helicase 3 modulates NF-kappa B signal pathway by controlling the phosphorylation of PP2A-C subunit. *Oncotarget.* 8, 33197–33213 (2017).
23. Celik H, Sajwan KP, Selvanathan SP *et al.* Ezrin binds to DEAD-box RNA helicase DDX3 and regulates its function and protein level. *Mol. Cell Biol.* 35, 3145–3162 (2015).
24. Yasuda-Inoue M, Kuroki M, Ariumi Y. Distinct DDX DEAD-box RNA helicases cooperate to modulate the HIV-1 Rev function. *Biochem. Biophys. Res. Commun.* 434, 803–808 (2013).
25. Lai M-C, Wang S-W, Cheng L *et al.* Human DDX3 interacts with the HIV-1 Tat protein to facilitate viral mRNA translation. *PLoS ONE* 8, e68665 (2013).
26. Yasuda-Inoue M, Kuroki M, Ariumi Y. DDX3 RNA helicase is required for HIV-1 Tat function. *Biochem. Biophys. Res. Commun.* 441, 607–611 (2013).

27. Wang H, Kim S, Ryu W-S. DDX3 DEAD-Box RNA helicase inhibits hepatitis B virus reverse transcription by incorporation into nucleocapsids. *J. Virol.* 83, 5815–5824 (2009).
28. Mamiya N, Worman HJ. Hepatitis C virus core protein binds to a DEAD box RNA helicase. *J. Biol. Chem.* 274, 15751–15756 (1999).
29. Chahar HS, Chen SP, Manjunath N. P-body components LSM1, GW182, DDX3, DDX6 and XRN1 are recruited to WNV replication sites and positively regulate viral replication. *Virology* 436, 1–7 (2013).
30. Kumar R, Singh N, Abdin MZ, Patel AH, Medigeshi GR. Dengue virus capsid interacts with DDX3X-A potential mechanism for suppression of antiviral functions in dengue infection. *Front. Cell Infect. Mi.* 7, 542 (2018).
31. Khadka S, Vangeloff AD, Zhang CY *et al.* A physical interaction network of dengue virus and human proteins. *Mol. Cell Proteomics* 10, M111.012187 (2011).
32. Raman SNT, Liu GQ, Pyo HM *et al.* DDX3 interacts with influenza A virus NS1 and NP proteins and exerts antiviral function through regulation of stress granule formation. *J. Virol.* 90, 3661–3675 (2016).
33. Khamina K, Lercher A, Caldera M *et al.* Characterization of host proteins interacting with the lymphocytic choriomeningitis virus L protein. *PLoS Pathog.* 13, e1006758 (2017).
34. Loureiro M, Zorzetto-Fernandes AL, Radoshitzky S *et al.* DDX3 suppresses type I interferons and favors viral replication during arenavirus infection. *PLoS Pathog.* 14, e1007125 (2018).
35. Ayalew LE, Patel AK, Gaba A, Islam A, Tikoo SK. Bovine adenovirus-3 pVIII suppresses Cap-dependent mRNA translation possibly by interfering with the recruitment of DDX3 and translation initiation factors to the mRNA cap. *Front. Microbiol.* 7, 2119 (2016).
36. Jefferson M, Donaszi-Ivanov A, Pollen S *et al.* Host factors that interact with the pestivirus N-terminal protease, N-pro, Are components of the ribonucleoprotein complex. *J. Virol.* 88, 10340–10353 (2014).
37. Schroder M, Baran M, Bowie AG. Viral targeting of DEAD box protein 3 reveals its role in TBK1/IKK epsilon-mediated IRF activation. *EMBO J.* 27, 2147–2157 (2008).
- **The first evidence that DDX3X is involved in innate immunity.**
38. Park SH, Lee SG, Kim Y, Song K. Assignment of a human putative RNA helicase gene, DDX3, to human X chromosome bands p11.3 -> p11.23. *Cytogenet. Cell Genet.* 81, 178–179 (1998).
39. Kim YS, Lee SG, Park SH, Song K. Gene structure of the human DDX3 and chromosome mapping of its related sequences. *Mol. Cells* 12, 209–214 (2001).
40. Ditton HJ, Zimmer J, Rajpert-De Meyts E, Vogt PH. The AZFa gene DBY (DDX3Y) is widely transcribed but the protein is limited to the male germ cells by translation control. *Hum. Mol. Genet.* 13, 2333–2341 (2004).
41. Cordin O, Banroques J, Tanner NK, Linder P. The DEAD-box protein family of RNA helicases. *Gene* 367, 17–37 (2006).
42. Linder P. Dead-box proteins: a family affair - active and passive players in RNP-remodeling. *Nucleic Acids Res.* 34, 4168–4180 (2006).
43. Tanner NK, Linder P. DExD/H box RNA helicases: from generic motors to specific dissociation functions. *Mol. Cell.* 8, 251–262 (2001).
44. Schutz P, Karlberg T, van den Berg S *et al.* Comparative structural analysis of human DEAD-box RNA helicases. *PLoS ONE* 5, pii:e12791 (2010).
45. Epling LB, Grace CR, Lowe BR, Partridge JF, Enemark EJ. Cancer-associated mutants of RNA helicase DDX3X are defective in RNA-stimulated ATP hydrolysis. *J. Mol. Biol.* 427, 1779–1796 (2015).
46. Hilbert M, Karow AR, Klostermeier D. The mechanism of ATP-dependent RNA unwinding by DEAD box proteins. *Biol. Chem.* 390, 1237–1250 (2009).
47. Linder P, Jankowsky E. From unwinding to clamping - the DEAD box RNA helicase family. *Nat. Rev. Mol. Cell. Bio.* 12, 505–516 (2011).
48. Mallam AL, Del Campo M, Gilman B, Sidote DJ, Lambowitz AM. Structural basis for RNA-duplex recognition and unwinding by the DEAD-box helicase Mss116p. *Nature* 490, 121–+ (2012).
49. Sengoku T, Nureki O, Nakamura A, Satoru KI, Yokoyama S. Structural basis for RNA unwinding by the DEAD-box protein Drosophila vasa. *Cell* 125, 287–300 (2006).
50. Franca R, Belfiore A, Spadari S, Maga G. Human DEAD-box ATPase DDX3 shows a relaxed nucleoside substrate specificity. *Proteins* 67, 1128–1137 (2007).
51. Garbelli A, Beermann S, Di Cicco G, Dietrich U, Maga G. A motif unique to the human dead-box protein DDX3 is important for nucleic acid binding, ATP hydrolysis, RNA/DNA unwinding and HIV-1 replication. *PLoS ONE* 6, e19810 (2011).
52. Sharma D, Putnam AA, Jankowsky E. Biochemical differences and similarities between the DEAD-box helicase orthologs DDX3X and Ded1p. *J. Mol. Biol.* 429, 3730–3742 (2017).
53. Zhao LQ, Mao YT, Zhou JH *et al.* Multifunctional DDX3: dual roles in various cancer development and its related signaling pathways. *Am. J. Cancer Res.* 6, 387–402 (2016).

54. Botlagunta M, Krishnamachary B, Vesuna F *et al.* Expression of DDX3 is directly modulated by hypoxia inducible factor-1 alpha in breast epithelial cells. *PLoS ONE* 6, e17563 (2011).
55. Bol GM, Raman V, van der Groep P *et al.* Expression of the RNA helicase DDX3 and the hypoxia response in breast cancer. *PLoS ONE* 8, e63548 (2013).
56. Botlagunta M, Vesuna F, Mironchik Y *et al.* Oncogenic role of DDX3 in breast cancer biogenesis. *Oncogene* 27, 3912–3922 (2008).
57. Wu DW, Lee MC, Wang J *et al.* DDX3 loss by p53 inactivation promotes tumor malignancy via the MDM2/Slug/E-cadherin pathway and poor patient outcome in non-small-cell lung cancer. *Oncogene* 33, 1515–1526 (2014).
58. Wu DW, Liu WS, Wang J *et al.* Reduced p21(WAF1/CIP1) via alteration of p53-DDX3 pathway is associated with poor relapse-free survival in early-stage human papillomavirus-associated lung cancer. *Clin. Cancer Res.* 17, 1895–1905 (2011).
59. Bol GM, Vesuna F, Xie M *et al.* Targeting DDX3 with a small molecule inhibitor for lung cancer therapy. *EMBO Mol. Med.* 7, 648–669 (2015).
60. Loeb DM, Wilky BA, Kim C *et al.* RNA helicase DDX3 is a novel therapeutic target for Ewing sarcoma. *J. Clin. Oncol.* 33, 10026 (2015).
61. Wilky BA, Kim C, McCarty G *et al.* RNA helicase DDX3: a novel therapeutic target in Ewing sarcoma. *Oncogene* 35, 2574–2583 (2016).
62. Wu DW, Lin PL, Wang L, Huang CC, Lee H. The YAP1/SIX2 axis is required for DDX3-mediated tumor aggressiveness and cetuximab resistance in KRAS-wild-type colorectal cancer. *Theranostics* 7, 1114–1132 (2017).
63. van Voss MRH, Vesuna F, Bol GM *et al.* Nuclear DDX3 expression predicts poor outcome in colorectal and breast cancer. *Oncotargets Ther.* 10, 3501–3513 (2017).
64. van Voss MRH, Vesuna F, Trumpi K *et al.* Identification of the DEAD box RNA helicase DDX3 as a therapeutic target in colorectal cancer. *Oncotarget* 6, 28312–28326 (2015).
65. He TY, Wu DW, Lin PL *et al.* DDX3 promotes tumor invasion in colorectal cancer via the CK1 epsilon/Dvl2 axis. *Sci. Rep. UK* 6, 21483 (2016).
66. Su CY, Lin TC, Lin YF *et al.* DDX3 as a strongest prognosis marker and its downregulation promotes metastasis in colorectal cancer. *Oncotarget* 6, 18602–18612 (2015).
67. van Voss MRH, van Kempen PMW, Noorlag R *et al.* DDX3 has divergent roles in head and neck squamous cell carcinomas in smoking versus non-smoking patients. *Oral Dis.* 21, 270–271 (2015).
68. Lee CH, Lin SH, Yang SF *et al.* Low/negative expression of DDX3 might predict poor prognosis in non-smoker patients with oral cancer. *Oral Dis.* 20, 76–83 (2014).
69. Chang PC, Chi CW, Chau GY *et al.* DDX3, a DEAD box RNA helicase, is deregulated in hepatitis virus-associated hepatocellular carcinoma and is involved in cell growth control. *Oncogene* 25, 1991–2003 (2006).
- **The first evidence that DDX3X is involved in cell growth.**
70. Sun MN, Song L, Zhou T, Gillespie GY, Joep RS. The role of DDX3 in regulating Snail. *BBA Mol. Cell. Res.* 1813, 438–447 (2011).
71. Miao XY, Yang ZL, Xiong L *et al.* Nectin-2 and DDX3 are biomarkers for metastasis and poor prognosis of squamous cell/adenosquamous carcinomas and adenocarcinoma of gallbladder. *Int. J. Clin. Exp. Pathol.* 6, 179–190 (2013).
72. Oh S, Flynn RA, Floor SN *et al.* Medulloblastoma-associated DDX3 variant selectively alters the translational response to stress. *Oncotarget.* 7, 28169–28182 (2016).
73. Jiang L, Gu ZH, Yan ZX *et al.* Exome sequencing identifies somatic mutations of DDX3X in natural killer/T-cell lymphoma. *Nat. Genet.* 47, 1061–1066 (2015).
74. Dobashi A, Tsuyama N, Asaka R *et al.* Frequent BCOR aberrations in extranodal NK/T-Cell lymphoma, nasal type. *Gene Chromosome Canc.* 55, 460–471 (2016).
75. Dolde C, Bischof J, Gruter S *et al.* A CK1 FRET biosensor reveals that DDX3X is an essential activator of CK1 epsilon. *J. Cell Sci.* 131, pii:jcs207316 (2018).
76. Cruciat CM, Dolde C, de Groot REA *et al.* RNA helicase DDX3 is a regulatory subunit of casein kinase 1 in Wnt-beta-catenin signaling. *Science* 339, 1436–1441 (2013).
77. Maga G, Falchi F, Radi M *et al.* Toward the discovery of novel anti-HIV drugs. Second-generation inhibitors of the cellular ATPase DDX3 with improved anti-HIV activity: synthesis, structure-activity relationship analysis, cytotoxicity studies, and target validation. *Chemmedchem.* 6, 1371–1389 (2011).
78. Lai MC, Chang WC, Shieh SY, Tarn WY. DDX3 regulates cell growth through translational control of cyclin E1. *Mol. Cell. Biol.* 30, 5444–5453 (2010).
79. Ishaq M, Hu JJ, Wu XY *et al.* Knockdown of cellular RNA helicase DDX3 by short hairpin RNAs suppresses HIV-1 viral replication without inducing apoptosis. *Mol. Biotechnol.* 39, 231–238 (2008).
80. Geissler R, Golbik RP, Behrens SE. The DEAD-box helicase DDX3 supports the assembly of functional 80S ribosomes. *Nucleic Acids Res.* 40, 4998–5011 (2012).

81. Chen WJ, Wang WT, Tsai TY, Li HK, Lee YHW. DDX3 localizes to the centrosome and prevents multipolar mitosis by epigenetically and translationally modulating p53 expression. *Sci. Rep. UK* 7, 9411 (2017).
82. Li HK, Mai RT, Huang HD *et al.* DDX3 represses stemness by epigenetically modulating tumor-suppressive miRNAs in hepatocellular carcinoma. *Sci. Rep. UK* 6, 28637 (2016).
83. Adjibade P, St-Sauveur VG, Bergeman J *et al.* DDX3 regulates endoplasmic reticulum stress-induced ATF4 expression. *Sci. Rep. UK* 7, 13832 (2017).
84. Chen YC, Wang Q, Wang QZ *et al.* DDX3 binding with CK1 epsilon was closely related to motor neuron degeneration of ALS by affecting neurite outgrowth. *Am. J. Transl. Res.* 9, 4627–4639 (2017).
85. Amaya M, Brooks-Faulconer T, Lark T *et al.* Venezuelan equine encephalitis virus non- structural protein 3 (nsP3) interacts with RNA helicases DDX1 and DDX3 in infected cells. *Antivir. Res.* 131, 49–60 (2016).
86. Chen CY, Chan CH, Chen CM *et al.* Targeted inactivation of murine Ddx3x: essential roles of Ddx3x in placentation and embryogenesis. *Hum. Mol. Genet.* 25, 2905–2922 (2016).
87. Grainger S, Willert K. Mechanisms of Wnt signaling and control. *Wires Syst. Biol. Med.* 10, e1422 (2018).
88. Fukumura J, Noguchi E, Sekiguchi T, Nishimoto T. A temperature-sensitive mutant of the mammalian RNA helicase, DEAD-BOX X isoform, DBX, defective in the transition from G1 to S phase. *J. Biochem.* 134, 71–82 (2003).
89. Li Q, Zhang P, Zhang C *et al.* DDX3X regulates cell survival and cell cycle during mouse early embryonic development. *J. Biomed. Res.* 28, 282–291 (2014).
90. van Voss MRH, Kammers K, Vesuna F *et al.* Global effects of DDX3 inhibition on cell cycle regulation identified by a combined phosphoproteomics and single cell tracking approach. *Transl. Oncol.* 11, 755–763 (2018).
91. Chao CH, Chen CM, Cheng PL *et al.* DDX3, a DEAD box RNA helicase with tumor growth-suppressive property and transcriptional regulation activity of the p21(waf1/cip1) promoter, is a candidate tumor suppressor. *Cancer Res.* 66, 6579–6588 (2006).
92. Moynahan ME, Chiu JW, Koller BH, Jasin M. Brca1 controls homology-directed DNA repair. *Mol. Cell.* 4, 511–518 (1999).
93. Lakhani SR, van de Vijver MJ, Jacquemier J *et al.* The pathology of familial breast cancer: Predictive value of immunohistochemical markers estrogen receptor, progesterone receptor, HER-2, and p53 in patients with mutations in BRCA1 and BRCA2. *J. Clin. Oncol.* 20, 2310–2318 (2002).
94. Bianchini G, Balko JM, Mayer IA, Sanders ME, Gianni L. Triple-negative breast cancer: challenges and opportunities of a heterogeneous disease. *Nat. Rev. Clin. Oncol.* 13, 674–690 (2016).
95. van Voss MRH, Schrijver WAME, ter Hoeve ND *et al.* The prognostic effect of DDX3 upregulation in distant breast cancer metastases. *Clin. Exp. Metastas.* 34, 85–92 (2017).
96. van Voss MRH, Brilliant JD, Vesuna F *et al.* Combination treatment using DDX3 and PARP inhibitors induces synthetic lethality in BRCA1-proficient breast cancer. *Med. Oncol.* 34, 33 (2017).
97. van Voss MRH, Vesuna F, Bol GM *et al.* Targeting mitochondrial translation by inhibiting DDX3: a novel radiosensitization strategy for cancer treatment. *Oncogene* 37, 63–74 (2018).
98. Siegel R, Naishadham D, Jemal A. Cancer statistics, 2013. *Cancer J. Clin.* 63, 11–30 (2013).
99. Manser R, Wright G, Hart D, Byrnes G, Campbell DA. Surgery for early stage non-small cell lung cancer. *Cochrane Database Syst. Rev.* (1), CD004699 (2005).
100. Timmerman R, Paulus R, Galvin J *et al.* Stereotactic body radiation therapy for inoperable early stage lung cancer. *J. Am. Med. Assoc.* 303, 1070–1076 (2010).
101. Muzny DM, Bainbridge MN, Chang K *et al.* Comprehensive molecular characterization of human colon and rectal cancer. *Nature* 487, 330–337 (2012).
102. Rivera C. Essentials of oral cancer. *Int. J. Clin. Exp. Pathol.* 8, 11884–11894 (2015).
103. Chen H-H, Yu H-I, Yang M-H, Tarn W-Y. DDX3 activates CBC-eIF3-mediated translation of uORF-containing oncogenic mRNAs to promote metastasis in HNSCC. *Cancer Res.* 78, 4512–4523 (2018).
104. Huang JS, Chao CC, Su TL *et al.* Diverse cellular transformation capability of overexpressed genes in human hepatocellular carcinoma. *Biochem. Biophys. Res. Commun.* 315, 950–958 (2004).
105. Wang Z, Shen GH, Xie JM, Li B, Gao QG. Rottlerin upregulates DDX3 expression in hepatocellular carcinoma. *Biochem. Biophys. Res. Commun.* 495, 1503–1509 (2018).
106. Chan CH, Chen CM, Lee YW, You LR. Damage, DNA, liver injury, and tumorigenesis: consequences of DDX3X loss. *Mol. Cancer Res.* 47 (2), 555–566 (2019).
107. Valentin-Vega YA, Wang YD, Parker M *et al.* Cancer-associated DDX3X mutations drive stress granule assembly and impair global translation. *Sci. Rep. UK* 6, 25996 (2016).
108. Floor SN, Condon KJ, Sharma D, Jankowsky E, Doudna JA. Autoinhibitory interdomain interactions and subfamily-specific extensions redefine the catalytic core of the human DEAD-box protein DDX3. *J. Biol. Chem.* 291, 2412–2421 (2016).

109. Chen HH, Yu HI, Cho WC, Tarn WY. DDX3 modulates cell adhesion and motility and cancer cell metastasis via Rac1-mediated signaling pathway. *Oncogene* 34, 2790–2800 (2015).
110. Liang S, Yang ZL, Li DQ *et al.* The clinical and pathological significance of nectin-2 and DDX3 expression in pancreatic ductal adenocarcinomas. *Dis. Markers* 2015 , 379568 (2015).
111. Kondaskar A, Kondaskar S, Fishbein JC *et al.* Structure-based drug design and potent anti-cancer activity of tricyclic 5:7:5-fused diimidazo[4,5-d:4'5'-f][1,3]diazepines. *Bioorgan. Med. Chem.* 21, 618–631 (2013).
112. Kondaskar A, Kondaskar S, Kumar R *et al.* Novel, broad spectrum anti-cancer agents containing the tricyclic 5:7:5-fused diimidazodiazepine ring system. *ACS Med. Chem. Lett.* 2, 252–256 (2010).
113. Samal SK, Routray S, Veeramachaneni GK, Dash R, Botlagunta M. Ketorolac salt is a newly discovered DDX3 inhibitor to treat oral cancer. *Sci. Rep. UK* 5, 9982 (2015).
114. Xie M, Vesuna F, Botlagunta M *et al.* NZ51, a ring-expanded nucleoside analog, inhibits motility and viability of breast cancer cells by targeting the RNA helicase DDX3. *Oncotarget* 6, 29901–29913 (2015).
115. Yedavalli VSRK, Zhang N, Cai HY *et al.* Ring expanded nucleoside analogues inhibit RNA helicase and intracellular human immunodeficiency virus type 1 replication. *J. Med. Chem.* 51, 5043–5051 (2008).
116. Valiente-Echeverria F, Hermoso MA, Soto-Rifo R. RNA helicase DDX3: at the crossroad of viral replication and antiviral immunity. *Rev. Med. Virol.* 25, 286–299 (2015).
117. Schroder M. Viruses and the human DEAD-box helicase DDX3: inhibition or exploitation? *Biochem. Soc. T.* 39, 679–683 (2011).
118. Soulat D, Burckstummer T, Westermayer S *et al.* The DEAD-box helicase DDX3X is a critical component of the TANK-binding kinase 1-dependent innate immune response. *EMBO J.* 27, 2135–2146 (2008).
119. Fullam A, Gu LL, Hohn Y, Schroder M. DDX3 directly facilitates IKK alpha activation and regulates downstream signalling pathways. *Biochem. J.* 475, 3595–3607 (2018).
120. Pesne V, Li QS, Sodroski C, Hsu CS, Liang TJ. Dynamic interaction of stress granules, DDX3X, and IKK-alpha mediates multiple functions in hepatitis C virus infection. *J. Virol.* 89, 5462–5477 (2015).
121. Khapersky DA, Emara MM, Johnston BP *et al.* Influenza A virus host shutoff disables antiviral stress-induced translation arrest. *PLoS Pathog.* 10, e1004217 (2014).
122. Yoo JS, Takahasi K, Ng CS *et al.* DHX36 enhances RIG-I signaling by facilitating PKR-mediated antiviral stress granule formation. *PLoS Pathog.* 10, e1004012 (2014).
123. Oh SW, Onomoto K, Wakimoto M *et al.* Leader-containing uncapped viral transcript activates RIG-I in antiviral stress granules. *PLoS Pathog.* 12, e1005563 (2016).
124. Nunez RD, Budt M, Saenger S *et al.* The RNA helicase DDX6 associates with RIG-I to augment induction of antiviral signaling. *Int. J. Mol. Sci.* 19, pii:E1877 (2018).
125. Yoneyama M, Jogi M, Onomoto K. Regulation of antiviral innate immune signaling by stress-induced RNA granules. *J. Biochem.* 159, 279–286 (2016).
126. McCormick C, Khapersky DA. Translation inhibition and stress granules in the antiviral immune response. *Nat. Rev. Immunol.* 17, 647–660 (2017).
127. Frohlich A, Rojas-Araya B, Pereira-Montecinos C *et al.* DEAD-box RNA helicase DDX3 connects CRM1-dependent nuclear export and translation of the HIV-1 unspliced mRNA through its N-terminal domain. *Biochim. Biophys. Acta* 1859, 719–730 (2016).
128. Liu J, Henao-Mejia J, Liu H, Zhao Y, He JJ. Translational regulation of HIV-1 replication by HIV-1 rev cellular cofactors Sam68, eIF5A, hRIP, and DDX3. *J. Neuroimmune Pharmacol.* 6, 308–321 (2011).
129. Soto-Rifo R, Rubilar PS, Ohlmann T. The DEAD-box helicase DDX3 substitutes for the cap-binding protein eIF4E to promote compartmentalized translation initiation of the HIV-1 genomic RNA. *Nucleic Acids Res.* 41, 6286–6299 (2013).
130. Gringhuis SI, Hertoghs N, Kaptein TM *et al.* HIV-1 blocks the signaling adaptor MAVS to evade antiviral host defense after sensing of abortive HIV-1 RNA by the host helicase DDX3. *Nat. Immunol.* 18, 225–235 (2017).
131. Wang H, Ryu W-S. Hepatitis B virus polymerase blocks pattern recognition receptor signaling via interaction with DDX3: implications for immune evasion. *PLoS Pathog.* 6, e1000986 (2010).
132. Yu S, Chen J, Wu M *et al.* Hepatitis B virus polymerase inhibits RIG-I- and Toll-like receptor 3-mediated beta interferon induction in human hepatocytes through interference with interferon regulatory factor 3 activation and dampening of the interaction between TBK1/IKKepsilon and DDX3. *J. Gen. Virol.* 91, 2080–2090 (2010).
133. Ko C, Lee S, Windisch MP, Ryu W-S. DDX3 DEAD-box RNA helicase is a host factor that restricts hepatitis B virus replication at the transcriptional level. *J. Virol.* 88, 13689–13698 (2014).
134. Owsianka AM, Patel AH. Hepatitis C virus core protein interacts with a human DEAD box protein DDX3. *Virology* 257, 330–340 (1999).
135. You LR, Chen CM, Yeh TS *et al.* Hepatitis C virus core protein interacts with cellular putative RNA helicase. *J. Virol.* 73, 2841–2853 (1999).

136. Ariumi Y, Kuroki M, Abe KI *et al.* DDX3 DEAD-box RNA helicase is required for hepatitis C virus RNA replication. *J. Virol.* 81, 13922–13926 (2007).
137. Angus AGN, Dalrymple D, Boulant S *et al.* Requirement of cellular DDX3 for hepatitis C virus replication is unrelated to its interaction with the viral core protein. *J. Gen. Virol.* 91, 122–132 (2010).
138. Sun CM, Pager CT, Luo GX, Sarnow P, Cate JHD. Hepatitis C virus core-derived peptides inhibit genotype 1b viral genome replication via interaction with DDX3X. *PLoS ONE* 5, pii:e12826 (2010).
139. Oshiumi H, Ikeda M, Matsumoto M *et al.* Hepatitis C virus core protein abrogates the DDX3 function that enhances IPS-1-mediated IFN-beta induction. *PLoS ONE* 5, e14258 (2010).
140. Kang JI, Kwon YC, Ahn BY. Modulation of the type I interferon pathways by culture-adaptive hepatitis C virus core mutants. *Febs. Lett.* 586, 1272–1278 (2012).
141. Li QS, Pene V, Krishnamurthy S, Cha H, Liang TJ. Hepatitis C virus infection activates an innate pathway involving IKK-alpha in lipogenesis and viral assembly. *Nat. Med.* 19, 722–729 (2013).
142. Upadya MH, Aweya JJ, Tan YJ. Understanding the interaction of hepatitis C virus with host DEAD-box RNA helicases. *World J. Gastroentero.* 20, 2913–2926 (2014).
143. Li GH, Feng TT, Pan W, Shi XH, Dai JF. DEAD-box RNA helicase DDX3X inhibits DENV replication via regulating type one interferon pathway. *Biochem. Biophys. Res. Commun.* 456, 327–332 (2015).
144. Li C, Ge LL, Li PP *et al.* Cellular DDX3 regulates Japanese encephalitis virus replication by interacting with viral un-translated regions. *Virology* 449, 70–81 (2014).
145. Vashist S, Urena L, Chaudhry Y, Goodfellow I. Identification of RNA-protein interaction networks involved in the norovirus life cycle. *J. Virol.* 86, 11977–11990 (2012).
146. Loret S, Guay G, Lippe R. Comprehensive characterization of extracellular herpes simplex virus type 1 virions. *J. Virol.* 82, 8605–8618 (2008).
147. Khadivjam B, Stegen C, Hogue-Racine MA *et al.* The ATP-dependent RNA helicase DDX3X modulates herpes simplex virus 1 gene expression. *J. Virol.* 91, pii:e02411–e02416 (2017).
148. Lenarcic EM, Ziehr BJ, Moorman NJ. An unbiased proteomics approach to identify human cytomegalovirus RNA-associated proteins. *Virology* 481, 13–23 (2015).
149. Cavignac Y, Lieber D, Sampaio KL *et al.* The cellular proteins Grb2 and DDX3 are increased upon human cytomegalovirus infection and act in a proviral fashion. *PLoS ONE* 10, e0131614 (2015).
150. Kalverda AP, Thompson GS, Vogel A *et al.* Poxvirus K7 protein adopts a Bcl-2 fold: biochemical mapping of its interactions with human DEAD box RNA helicase DDX3. *J. Mol. Biol.* 385, 843–853 (2009).
151. Oda S, Schroder M, Khan AR. Structural basis for targeting of human RNA helicase DDX3 by poxvirus protein K7. *Structure* 17, 1528–1537 (2009).
152. Yedavalli V, Zhang N, Cai H, Jeang KT, Hosmane R. Ring-expanded nucleosides (RENs) exhibit potent ATP-dependent helicase activity of RNA helicase DDX3 with little or no toxicity in *ex vivo* cell culture or *in vivo* in mice. *Antivir. Res.* 78, A68–A68 (2008).
- **Initial discovery of inhibitors of DDX3X with anti-HIV activity.**
153. Zhang N, Zhang P, Baier A, Cova L, Hosmane RS. Dual inhibition of HCV and HIV by ring-expanded nucleosides containing the 5:7-fused imidazo[4,5-e][1,3] diazepine ring system. *In vitro* results and implications. *Bioorg. Med. Chem. Lett.* 24, 1154–1157 (2014).
154. Hogbom M, Collins R, van den Berg S *et al.* Crystal structure of conserved domains 1 and 2 of the human DEAD-box helicase DDX3X in complex with the mononucleotide AMP. *J. Mol. Biol.* 372, 150–159 (2007).
- **The first crystal structure of DDX3X.**
155. Maga G, Falchi F, Garbelli A *et al.* Pharmacophore modeling and molecular docking led to the discovery of inhibitors of human immunodeficiency virus-1 replication targeting the human cellular aspartic acid-glutamic acid-alanine-aspartic acid box polypeptide 3. *J. Med. Chem.* 51, 6635–6638 (2008).
- **Initial discovery of ATP-competitive inhibitors of DDX3X with anti-HIV activity.**
156. Radi M, Falchi F, Garbelli A *et al.* Discovery of the first small molecule inhibitor of human DDX3 specifically designed to target the RNA binding site: Towards the next generation HIV-1 inhibitors. *Bioorg. Med. Chem. Lett.* 22, 2094–2098 (2012).
- **The first RNA-competitive inhibitor of DDX3X helicase.**
157. Fazi R, Tintori C, Brai A *et al.* Homology model-based virtual screening for the identification of human helicase DDX3 inhibitors. *J. Chem. Inf. Model.* 55, 2443–2454 (2015).
158. Brai A, Fazi R, Tintori C *et al.* Human DDX3 protein is a valuable target to develop broad spectrum antiviral agents. *Proc. Natl Acad. Sci. USA* 113, 5388–5393 (2016).
- **First broad-spectrum antiviral compound-targeting DDX3X.**
159. Floor SN, Barkovich KJ, Condon KJ, Shokat KM, Doudna JA. Analog sensitive chemical inhibition of the DEAD-box protein DDX3. *Protein Sci.* 25, 638–649 (2016).

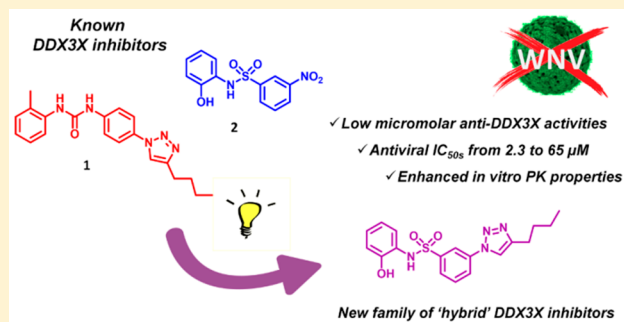
160. Sharma D, Jankowsky E. The Ded1/DDX3 subfamily of DEAD-box RNA helicases. *Crit. Rev. Biochem. Mol.* 49, 343–360 (2014).
161. Stunnenberg M, Geijtenbeek TBH, Gringhuis SI. DDX3 in HIV-1 infection and sensing: a paradox. *Cytokine Growth F R* 40, 32–39 (2018).
162. Garcia-Sanchez J, Garcia E, Merino ML. 100 years of Dr. Ehrlich's magic bullet (1909-2009). *Enferm. Infecc. Micro. Cl.* 28, 521–533 (2010).
163. Xie M, Vesuna F, Tantravedi S *et al.* RK-33 radiosensitizes prostate cancer cells by blocking the RNA helicase DDX3. *Cancer Res.* 76, 6340–6350 (2016).
164. Tantravedi S, Vesuna F, Winnard PT Jr *et al.* Targeting DDX3 in medulloblastoma using the small molecule inhibitor RK-33. *Transl. Oncol.* 12, 96–105 (2018).
165. Shih JW, Lee YHW. Human DExD/H RNA helicases: emerging roles in stress survival regulation. *Clin. Chim. Acta* 436, 45–58 (2014).
166. Bourgeois CF, Mortreux F, Auboeuf D. The multiple functions of RNA helicases as drivers and regulators of gene expression. *Nat. Rev. Mol. Cell Bio.* 17, 426–438 (2016).

DDX3X Helicase Inhibitors as a New Strategy To Fight the West Nile Virus Infection

Annalaura Brai,^{†,‡,§} Francesco Martelli,[§] Valentina Riva,^{||} Anna Garbelli,^{||} Roberta Fazi,[†] Claudio Zamperini,^{†,‡} Alessandro Pollutri,[†] Lucia Falsitta,[†] Stefania Ronzini,[†] Laura Maccari,[‡] Giovanni Maga,^{||,§} Simone Giannecchini,[§] and Maurizio Botta^{*,†,‡,§,||,⊥}[†]Dipartimento Biotecnologie, Chimica e Farmacia, Università degli Studi di Siena, Via A. De Gasperi 2, I-53100 Siena, Italy[‡]Lead Discovery Siena S.r.l., Castelnuovo Berardenga, I-53019 Siena, Italy[§]Department of Experimental and Clinical Medicine, University of Florence, I-50134 Florence, Italy^{||}Istituto di Genetica Molecolare, IGM-CNR, Via Abbiategrosso 207, I-27100 Pavia, Italy[⊥]Biotechnology College of Science and Technology, Temple University, BioLife Science Building, Suite 333, 1900 North 12th Street, Philadelphia, Pennsylvania 19122, United States

Supporting Information

ABSTRACT: Increased frequency of arbovirus outbreaks in the last 10 years represents an important emergence for global health. Climate warming, extensive urbanization of tropical regions, and human migration flows facilitate the expansion of anthropophilic mosquitos and the emerging or re-emerging of new viral infections. Only recently the human adenosinetriphosphatase/RNA helicase X-linked DEAD-box polypeptide 3 (DDX3X) emerged as a novel therapeutic target in the fight against infectious diseases. Herein, starting from our previous studies, a new family of DDX3X inhibitors was designed, synthesized, validated on the target enzyme, and evaluated against the West Nile virus (WNV) infection. Time of addition experiments after virus infection indicated that the compounds exerted their antiviral activities after the entry process, likely at the protein translation step of WNV replication. Finally, the most interesting compounds were then analyzed for their in vitro pharmacokinetic parameters, revealing favorable absorption, distribution, metabolism, and excretion values. The good safety profile together with a good activity against WNV for which no treatments are currently available, make this new class of molecules a good starting point for further in vivo studies.



INTRODUCTION

West Nile virus (WNV) is a neurotropic arbovirus member of *Flaviviridae* family.¹ Since its introduction in Europe and America the number of novel infections is increasing, counting during 2017, 204 novel reported cases in Europe² and 2002 in America.³ The number is impressive considering that about 80% of WNV infections is usually asymptomatic and only the remaining 20% may cause meningitis, encephalitis, or rarely death in 1%.⁴ In addition, probably due to climate warming, the number of novel human cases sharply increased in EU member states during the current year, reaching 710 infections and 63 deaths as of 30 August.¹ The rapid diffusion of WNV is dependent on its zoonotic life cycle, which involves migratory birds, *Culex* and *Aedes* mosquitos, and mammals including horses and humans. In this context, inadequate vector control, globalization, and human travel networks are only a few factors that are contributing to this and other arboviruses spreading. Despite continuous efforts being made to identify new drugs (Figure 1) or vaccines, no specific therapy or prophylaxis is actually available on the market and the treatment remains

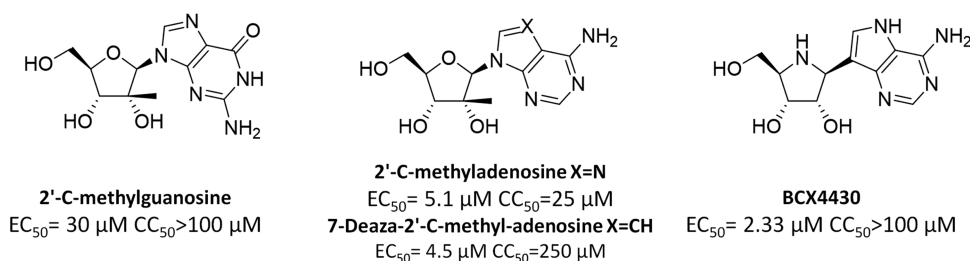
symptomatic.⁵ In this context, a drug repurposing strategy provided new drug candidates to fight emerging and re-emerging viruses⁶ but often the antiviral compounds are poorly active or are directed on viral enzymes and are thus generally characterized by a low genetic barrier to resistance (Figure 1).

In the last few years, the human adenosinetriphosphatase (ATPase)/RNA helicase X-linked DEAD-box polypeptide 3 (DDX3X) protein has been identified as a component of critical host-cell pathways, hijacked by several pathogenic human viruses.⁷ DDX3X, an adenosine 5'-triphosphate (ATP)-dependent RNA helicase, is involved in many aspects of RNA metabolism, such as transcription, translation, and RNA decay. It localizes to P-bodies, cytoplasmic foci related to mRNA turnover that are disrupted in response to the infection of viruses such as WNV or dengue virus (DENV).⁸ Furthermore, after WNV infection, DDX3X was released from P-bodies and colocalized at a perinuclear region with viral NS3.⁹ It was found,

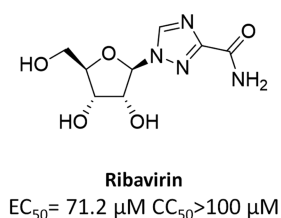
Received: September 10, 2018

Published: February 5, 2019

RNA-DEPENDENT RNA POLYMERASE (RdRP) INHIBITORS



MULTIPLE TARGETS



FLAVIVIRAL METHYLTRANSFERASE INHIBITOR

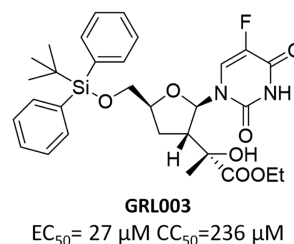


Figure 1. Two-dimensional (2D) chemical structures of the known WNV inhibitors and their potential inhibitory target.

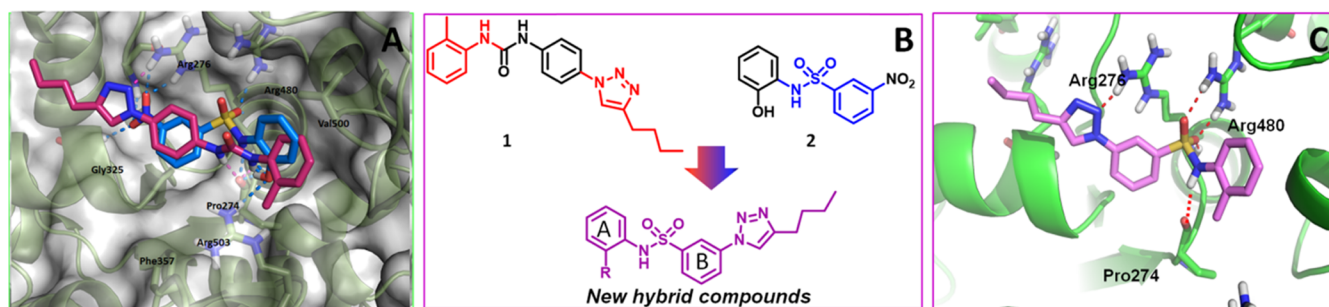


Figure 2. (A) Overlapped binding mode of compound 1 (pink) and 2 (blue marine) in DDX3X helicase pocket. Main interactions of both compounds with key residues of the active site are highlighted. Remarkably, Arg276, Arg480, and Gly302 make important contacts also with RNA phosphate backbone, whereas Gly325, Pro274, and Arg503 interact directly with the nucleobases. (B) Two-dimensional (2D) structure representation of the schematic idea behind the merged series design. (C) Proposed binding mode for merged derivative 13.

moreover, that DDX3X knockdown strongly decreased WNV replication, suggesting an important implication not yet completely understood.⁹ Although its role in the life cycle of different viruses was extensively studied,^{10–15} only few DDX3X inhibitors have been published as antiviral agents^{16–20} and the mechanism of action is clearly described only for HIV-1.²¹ In a recent work,¹⁸ we identified the first inhibitor of the helicase binding site of DDX3X also active against WNV. Such a compound belonged to a family of DDX3X RNA-competitive molecules characterized by high selectivity and no cytotoxic effects in both *in vitro* and *in vivo* models. Among them, compound 16d (compound 1 of the manuscript), belonging to the urea series, was the first DDX3X inhibitor endowed with a broad spectrum of antiviral activity against HIV-1 (both wild-type and drug-resistant strains), HCV, and new emerging viruses (WNV and DENV).¹⁸ Despite 1 representing the proof of concept that DDX3X inhibitors could be used as novel antiviral drugs, its poor aqueous (aq) solubility limited its bioavailability in preclinical models, causing its accumulation in fat tissues ($\text{Log } S = -7.05$).

With the attempt to enlarge our library of DDX3X inhibitors, we performed a homology model-based virtual screening¹⁹ that

led us to identify another small-molecule inhibitor of DDX3X helicase activity (compound 2 of the present paper) characterized by a sulfonamide moiety. Despite its low passive permeability, compound 2 was characterized by a very good aqueous solubility and at the same time by a promising antienzymatic activity value of $0.36 \mu\text{M}$.¹⁹ Pursuing our research of novel druglike DDX3X inhibitors, we performed a docking analysis of the two hit compounds 1 and 2. On the basis of the three-dimensional (3D) overlap of the two molecules within the binding site, we designed a new series of hybrid compounds by merging the key structural moieties of 1 and 2 able to interact with the main residues involved in the binding of both of them (Arg276, Pro274, and Arg480). Novel compounds (8–20 and 31–36) were then synthesized and validated against DDX3X enzyme and evaluated for their ability to inhibit WNV replication, leading to a small library of derivatives endowed with antiviral activities comparable or higher than the broad spectrum antiviral compound 1- β -D-ribofuranosyl-1,2,4-triazole-3-carboxamide (ribavirin). Moreover, the time of addition experiments highlighted that compounds likely act in the first phases of WNV replication. Finally, absorption, distribution, metabolism, and excretion (ADME) analysis of the most potent

derivatives revealed 100 times improved aqueous solubility with respect to the hit **1**, thus allowing to overcome an important limitation of our compound.

RESULTS AND DISCUSSION

Molecular Modeling. With the purpose of identifying novel small-molecule inhibitors of the DDX3X helicase binding site, we analyzed the docking poses of our hit compounds **1** and **2** within the DDX3X RNA binding pocket. The 3D structure of DDX3X in its RNA-bound closed conformation previously generated by homology modeling¹⁹ was used to perform our studies. As shown in Figure 2A, the docking analysis of compound **2** highlighted favorable hydrogen bond interactions between the nitrobenzene oxygen atom and Arg276 and Gly325, as well as between the sulfonamide group and Pro274 and Arg480 whereas the hydroxyl substituent is engaged in profitable H-bond interactions with the residues Pro274 and Arg503. Furthermore, hydrophobic interactions were found with Phe357, Val500, and Arg503. The predicted binding mode of compound **1** (Figure 2A) confirmed some key interactions, as seen for compound **2**; more in detail, the triazole ring interacted with the guanidine group of Arg276, whereas the urea NH groups and carbonyl moiety were involved in hydrogen bonds with Pro274 and Arg480, respectively. Moreover, the butyl terminus established beneficial interactions with Arg326 and Gly302. Finally, the tolyl ring established hydrophobic contacts with Arg503 and Pro274 side chains and the phenyl ring made hydrophobic interactions with Phe357.

It is worthy to note that two compounds were both able to interact with Arg276 and Arg480 and also make profitable contacts with Gly325, Pro274, and Arg503, which our computational model¹⁹ suggested to be important in RNA strand interactions into the helicase binding site (Figure 3).

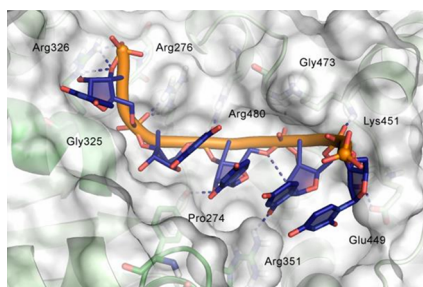


Figure 3. Surface and cartoon representation of RNA's main interactions within the helicase binding site of our homology model.

Starting from this analysis, we merged the key structural units of **1**¹⁸ and **2**¹⁹ to provide a new series of compounds able to interact at the same time with most of the residues involved in the binding of both of them, with particular attention to Arg276, Pro274, and Arg480, according to their suggested role in RNA strand binding. To this aim, as shown in Figure 2B, the *n*-alkyl substituted triazole group was selected from **1** structure whereas the phenyl-substituted sulfonamide moiety was chosen from the structure of compound **2**; the “hybrid” structure was finally composed by using the common aromatic ring (B) as a linker, and a small library of compounds were designed around this starting structure to explore the chemical space in relation to the activity against DDX3X.

Chemistry. The synthesis of compounds was accomplished following the synthetic route reported in Scheme 1. Amino-

thiophenol **3** was first converted into azide **4** by diazotization; a subsequent click reaction with the opportune terminal alkynes **5a–c** provides triazoles **6a–c**. Oxidative chlorination of thiols **6a–c** led to the corresponding sulfonyl chloride intermediates that were immediately converted into final compounds **8–20** by nucleophilic reaction with the opportune aromatic amines.

Terminal alkynes **5a** and **5b** were, respectively, synthesized from propargyl alcohol and but-3-yn-1-ol by Haworth alkylation and purified by distillation (Scheme 2). As shown in Scheme 3, aniline **25** was synthesized by nucleophilic displacement of 1-fluoro-3-nitrobenzene **23** with morpholine in the presence of K₂CO₃ and subsequent reduction catalyzed by Pd on charcoal.

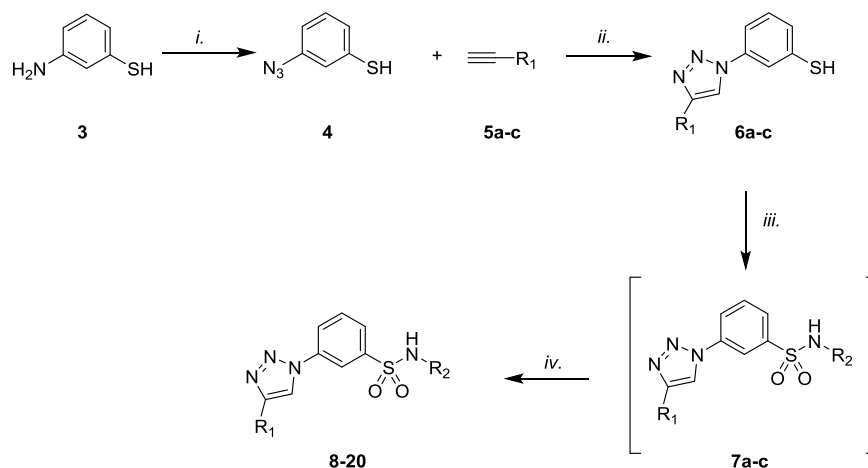
As shown in Scheme 4, the synthetic route to the final compounds **31–34** first entailed the preparation of the common azide intermediate **30**, using synthetic procedures described in Scheme 1. Derivatives **31–34** were then obtained by click reaction with the opportune terminal alkyne. Para-substituted compounds **35** and **36** were synthesized analogously.

Biological Evaluation. Derivatives **8–20** and **31–36** were first evaluated for their ability to inhibit the helicase activity of DDX3X; results are reported in Table 1. Seven compounds showed promising inhibitory values higher than of 80% (compounds **8–10**, **14**, **15**, **19**, and **31**). The meta substitution of triazole on ring B was more a favorite with respect to the para position, **36** being about 26% less active than the corresponding meta derivative **8**. This is also confirmed by the docking studies, due to the higher shape complementarity of the binding site and **8** with respect to **36**. Three-dimensional conformations of the latter results into being much more constrained within the pocket, and this is likely responsible for the lower activity.

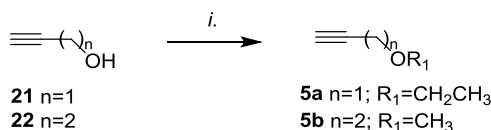
Replacement of triazole butyl chain with isopentyl was well tolerated (compound **31**); when the length was reduced to two carbons, the activity decreased to about 25% in compound **33**, in line with a lower occupancy of the binding site and poorer complementarity between ligand and protein cavity, as also shown by the docking model. Yet, according to this observation, the introduction of bulkier substituents, such as cyclohexyl and phenyl, was detrimental for the activity, which decreased to 41 and 52% for compounds **34** and **32**, respectively.

Alkyl chain of the triazole ring was also explored by checking the effect of introducing a polar atom. As a result, methyl-ethyl ether derivatives **10** and **15** retained their activities; in contrast, ethyl-methyl ether **11** was found 31% less active than the corresponding isomer **10**. According to our docking studies, the ether oxygen atom can establish a hydrogen bond interaction with Arg326. In fact, in the ethyl-methyl ether derivatives, the distance between the ether oxygen atom and its counterpart is less favorable to the hydrogen bond interaction. On the whole, pocket-hosting the substituted triazole moiety requires a precise spatial disposition (meta substitution preferred over the para one) while preferring more flexible, less constrained triazole substituents (butyl and isopentyl preferred over phenyl and cyclohexyl rings) occupying as much space as possible (lower activity in the presence of ethyl substituent). Polar atoms are tolerated, and a proper distance to efficiently interact with Arg326 appears to favor compound activity.

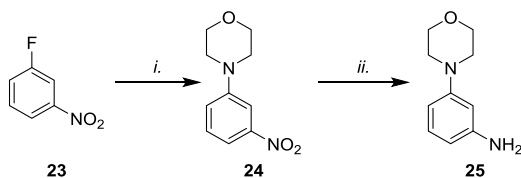
Analogously, the pocket that houses the other terminal side of our compound series, i.e., ring A, also presents distinctive hallmarks. In particular, a proper combination of both polar and hydrophobic interactions appears to be beneficial to compounds' activity. Noteworthy, the presence of a hydrogen bond acceptor on ring A leads to a high percentage of DDX3X inhibition across this chemical series, hydrogen bond

Scheme 1. Synthesis of Sulfonamides 8–20^a

^aReagents and conditions: (i) (a) *t*-BuONO, acetonitrile (ACN), 20 min, 0 °C; (b) TMSN₃, ACN, 2 h, room temperature (r.t.); (ii) CuSO₄·5 H₂O, sodium ascorbate, H₂O/*t*-BuOH (1:1), microwave (MW), 10 min, 120 °C; (iii) H₂O₂, SOCl₂, ACN, from 0 °C to r.t., 15 min; (iv) opportune amine, pyridine (dry), 5 h, r.t.

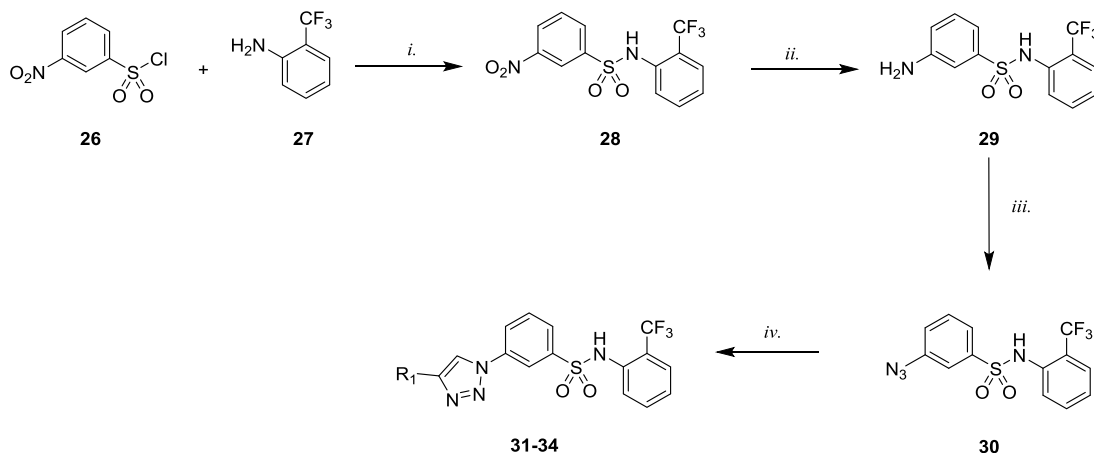
Scheme 2. Synthesis of Ethers 5a and 5b^a

^aReagents and conditions: (i) (a) NaOH(aq) (6 M), 20 min, r.t.; (b) dimethylsulfate or diethylsulfate, 60 min, 50–55 °C.

Scheme 3. Synthesis of Aniline 25^a

^aReagents and conditions: (i) (a) morpholine, K₂CO₃, dimethyl sulfoxide (DMSO) (dry), 3 h, 200 °C, (ii) H₂, Pd/C, MeOH, 1 h.

interactions being feasible with Pro274 and Arg503 of the binding pocket, as revealed by our docking studies. On confirmation of that, the introduction of an isoquinolyl-ring (compounds 14 and 15) on ring A was well tolerated as well as the –OH and the –OCH₃ ortho substitution (compounds 8 and 19), all bearing hydrogen-bonding moieties. Also, compounds 9 and 10, bearing the –CF₃ moiety at the ortho position of ring A, satisfy such requirements, being the trifluoromethyl group reported to have both hydrophobic and polar (hydrogen-bonding) properties.²² Substitution of the trifluoromethyl or hydroxyl groups of compounds 8–10 with a methyl group (compound 13), which shows only hydrophobic properties, leads to a lower DDX3X % of inhibition in the sulfonamide series. Activity further decreases in the presence of fluorine or hydrogen substituents (compounds 12 and 20), which have similar percent of inhibition values. Lower activity of compound 12 is likely due to the lower occupancy combined with a less effective hydrogen-bonding interaction, both exerted by the fluorine atom; the unsubstituted derivative 20 likewise showed a reduced activity value of 31%. The abolishment of the

Scheme 4. Synthesis of Sulfonamides 31–34^a

^aReagents and conditions: (i) Pyr, 5 h, r.t. (ii) H₂, Pd/C, MeOH; (iii) (a) *t*-BuONO, CH₃CN, 20 min, 0 °C; (b) TMSN₃, CH₃CN, 2 h, r.t.; (iv) opportune terminal alkyne, CuSO₄·5H₂O, sodium ascorbate, H₂O/*t*-BuOH (1:1), MW, 10 min, 120 °C.

Table 1. DDX3X Antienzymatic Activity^a

Cmpd.ID	Structure	Inhibition ^b (%)	Cmpd.ID	Structure	Inhibition ^b (%)
1		98±1	17		nd
2		98±2	18		80±1
8		83±3	19		98±0.5
9		98±1	20		31±2
10		98±0.5	31		96±1
11		67±2	32		52±2
12		24±2	33		71±2
13		59±2	34		41±2.1
14		99±0.5	35		nd
15		98±1	36		57±0.5
16		na ^c			

^aData represent mean two values of the least two experiments. ^b% inhibition at a fixed concentration of 20 μ M. ^cna: not active. nd: not determined, compound precipitated from medium.

activity for compound 16, where a morpholine moiety was introduced on ring A, is explained by docking studies to be due to the spatial constraints of the region of the binding site, being able to accommodate the planar isoquinoline system but unfavorable in hosting the morpholine ring.

Also, the ortho position of the substituents on ring A results in being preferred although the para-methoxy substitution of derivative 18 is tolerated with a slight loss of activity. Unfortunately, the low solubility of 17 and 35 limited their enzymatic evaluation.

The docking studies suggested that compounds could act as competitive inhibitors in the helicase binding site. To prove our hypothesis, we generated dose–response curves, titrating compound **8** in DDX3X helicase assays, in the presence of increasing fixed concentrations of the RNA substrate. As shown in Figure 4, the inhibitory potency (ID_{50}) of the compound

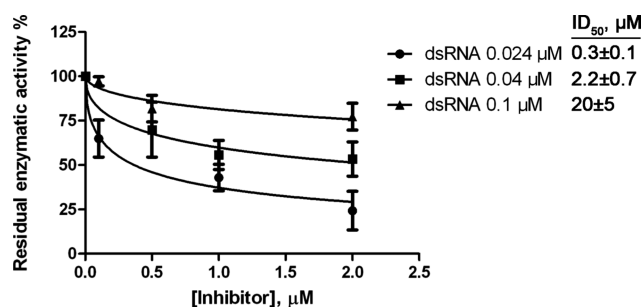


Figure 4. Increasing concentrations of the inhibitor **8** were titrated in helicase assays, in the presence of 30 pmol of DDX3X and increasing fixed concentrations of the dsRNA substrate. Values are the mean of three independent measurements \pm standard deviation (S.D.). The residual enzymatic activity values were plotted as a function of the inhibitor concentrations, and the corresponding ID_{50} values calculated for each dsRNA concentration are indicated on the right side of the panel.

decreased (higher absolute values) as the RNA concentrations increased. This is consistent with the hypothesized competitive mechanism of inhibition, with respect to the RNA substrate.

The compounds described here have been rationally designed to specifically target the helicase activity of DDX3X. To confirm the selectivity of our compounds, we tested the ability of **1**, **2**, **9**, and **14** to inhibit the ATPase activity of DDX3X and the helicase activity of the related human DEAD-box helicase DDX1. As shown in Table 2, no inhibition was found with any compound concentration.

Table 2. Enzymatic Data on Selected Compounds

cpd ID	ATPase DDX3, IC_{50} (μM)	DDX1, IC_{50} (μM)
1	>200 ^a	>200 ^a
2	>200 ^a	>200 ^a
9	>200 ^a	>200 ^a
14	>200 ^a	>200 ^a

^aThe value >200 indicates that less than 20% of inhibition was observed at 200 μM , the highest concentration tested.

Then, we quantified the cellular concentrations of the protein DDX3X, to confirm the presence of our target before carrying out anti-WNV and cytotoxicity assays. As reported in Table 3, African green monkey kidney epithelial (VERO) cells are

Table 3. DDX3X Cellular Expression in Huh7, A549, and VERO^a

	Huh7 ^b	VERO ^c	A549 ^d
DDX3X (nM)	755 \pm 170	421 \pm 140	103 \pm 20

^aValues represent mean \pm S.D. of three independent experiments. For details, see Methods. ^bEvaluated in Huh7: hepatocellular carcinoma cells. ^cEvaluated in VERO: African green monkey kidney cells. ^dEvaluated in A549: adenocarcinomic human alveolar basal epithelial cells.

endowed by a DDX3X concentration of 421 nM, higher than adenocarcinomic human alveolar basal epithelial cells (A549) but lower than human hepatocellular carcinoma cell line Huh7 (respectively valued 103 and 755 nM).

The three cell lines were infected with WNV at a multiplicity of infection (MOI) of 0.1, and the antiviral activity of compound **9** was assayed. As reported in Table 4, its activities seemed proportional to the DDX3X concentrations. Probably due to the DDX3X implications in pulmonary cancer,²³ **9** showed a cytotoxic activity of 21.3 μM . For these reasons, to avoid interferences due to anticancer-related cytotoxic effects, the human Huh7 cells characterized by a higher DDX3X concentration of 755 nM were chosen to perform our studies.

Subsequently, Huh7 cells were infected with WNV and compounds endowed with the best IC_{50} s against DDX3X were assayed for their antiviral properties. As reported in Table 5, compounds showed interesting antiviral activities, ranging from 2.3 to 65.9 μM , comparable or even higher than those of the broad spectrum antiviral ribavirin, which was used as a reference compound. Compound **8** showed the highest antiviral activity value of 2.3 μM , followed by **15**, **9**, **13**, **14**, and **10**. All of these compounds had comparable antienzymatic profiles; the overall trend of their cellular activities could be ascribed to their different physicochemical parameters, which may influence the cellular penetration and consequently antiviral effects. Compound **15** resulted to be particularly promising, since it showed good antiviral activity together with favorable aqueous solubility, 100 times higher than that of hit compound **1**. Compound **2** showed the lowest activity, probably due to the limited cellular permeability (see ADME Assay and Table 6). The mild antiviral activity of compound **13** is in line with its % inhibition of about 60% against DDX3X and was considered not worthy of further investigation. Finally, compound **12** endowed with the worst DDX3X inhibitory activity was found to be inactive in the cell-based assay.

To better evaluate the antiviral activities of our compounds, we selected **9** as a representative of the series, to investigate the mechanism of action (Figure 5). Time of addition studies, performed at compound inhibitory concentration near and under the IC_{50} values, clearly demonstrated that **9** acted in the first 2 h of the WNV life cycle, since the addition of **9** after 3 h post infection did not affect viral replication (Figure 5A). In particular, although an antiviral effect was visible when added before viral infection and cell entry occurred, the substantial activity of compound **9** after 2 h of infection also could indicate that its main target activity was in subsequent steps of the viral replication. Consequently, we evaluated the effect of **9** in the production of both genomic and complementary viral RNA. Importantly, our inhibitor was able to interfere with the concentration of genomic RNA at an early time of the infection (from 2 to 12 h post infection) only when added 1 h post infection and caused no significant changes when added 3 h post infection. Moreover, although the complementary RNA was not revealed up to 12 h post infection, 24 h post infection the quantity of complementary RNA was slightly lower after the addition of compound **9** 1 h post infection. Moreover, our inhibitor was able to interfere marginally with the concentration of genomic RNA, without significant changes in the quantity of the complementary noninfective RNA. Finally, we evaluated its effect on the production of WNV nucleocapsid (NC) protein. As highlighted in Figure 5C, the addition of **9** 1 h post infection significantly reduced the concentration of NC whereas according to the results shown in panel C, its addition after 3

Table 4. Comparison of Antiviral Activities of 9 in Different Cell Lines Infected with WNV^a

cpd ID	Huh7 ^d		VERO ^e		A549 ^f	
	EC ₅₀ ^b (μM)	CC ₅₀ ^c (μM)	EC ₅₀ ^b (μM)	CC ₅₀ ^c (μM)	EC ₅₀ ^b (μM)	CC ₅₀ ^c (μM)
9	23.1 ± 0.4	>200	12 ± 1.1	>200	3.4 ± 0.8	21.3 ± 1.1
ribavirin	90 ± 2.5	>200	95 ± 5.1	nt	46 ± 2.3	nt

^aData represent the mean of two values of the least two experiments. ^bEC₅₀: half-maximal effective concentration or the needed concentration to inhibit 50% viral-induced cell death. ^cCC₅₀: cytotoxic concentration 50 or the needed concentration to induce 50% death of noninfected cells. ^dEvaluated in Huh7: hepatocellular carcinoma cells. ^eEvaluated in VERO: African green monkey kidney cells. ^fEvaluated in A549: adenocarcinomic human alveolar basal epithelial cells. Ribavirin was used as a reference compound. nt = not tested.

Table 5. Antiviral Activities and Cytotoxicity of Selected Compounds against WNV-Infected Huh7 Cells^a

cpd ID	WNV ^d		Huh7
	EC ₅₀ ^b (μM)	CC ₅₀ ^c (μM)	
1	8.8 ± 0.2	>200	
2	120 ± 5.2	175 ± 11	
8	2.3 ± 0.5	>200	
9	23.1 ± 0.4	>200	
10	65.9 ± 2.3	>200	
12	>200	>200	
13	39.9 ± 1.1	>200	
14	55 ± 1.1	>200	
15	13 ± 0.8	>200	
ribavirin	95.5 ± 3.2	>200	

^aData represent mean ± standard deviation of three experiments. ^bEC₅₀: half-maximal effective concentration or needed concentration to inhibit 50% viral-induced cell death. ^cCC₅₀: cytotoxic concentration 50 or needed concentration to induce 50% death of noninfected cells. ^devaluated in Huh7 cells. nt = not tested. Ribavirin was used as a reference compound.

Table 6. In Vitro ADME Analysis of Selected Compounds

cpd ID	P _{app} ^a	Log S ^b	HLM stability ^c
1	2.86 × 10 ⁻⁶	-7.05	99.0 ± 0.6
2	<0.1 × 10 ⁻⁶	-4.36	98.3 ± 1.1
8	0.1 × 10 ⁻⁶	-7.5	95.6 ± 0.8
9	0.21 × 10 ⁻⁶	-7.5	99.0 ± 1.2
10	0.71 × 10 ⁻⁶	-4.6	97.1 ± 0.6
14	0.68 × 10 ⁻⁶	-5.4	98.0 ± 0.9
15	0.44 × 10 ⁻⁶	-4.7	96.0 ± 0.4

^aApparent permeability reported in cm s⁻¹. ^bAqueous solubility expressed as Log of molar concentration. ^cHuman liver microsomal (HLM) metabolic stability.

h did not change NC concentration, which was comparable to the control. Overall, these results suggested a possible implication of 9 in the first phases of viral replication, probably during protein translation, after the entry process.

In Vitro ADME Analysis. Compounds 2, 8, 9, 10, 14, and 15 were in vitro profiled for aqueous solubility, liver microsomal stability, and membrane permeability. As reported in Table 6, compounds were characterized by improved aqueous solubility values, in particular, compounds 14, 15, and 10, even if less active against WNV than compound 1 and about 100 times more soluble than hit compound 1 with Log S comparable to that of 2. Furthermore, passive membrane permeability assay (PAMPA) indicated nonlimiting values with the exception of hit compound 2, that showed a minor value of 0.1 × 10⁻⁶ cm s⁻¹ that is probably the cause of its inactivity in antiviral assay. Finally, stability tests in human liver microsomes (HLM)

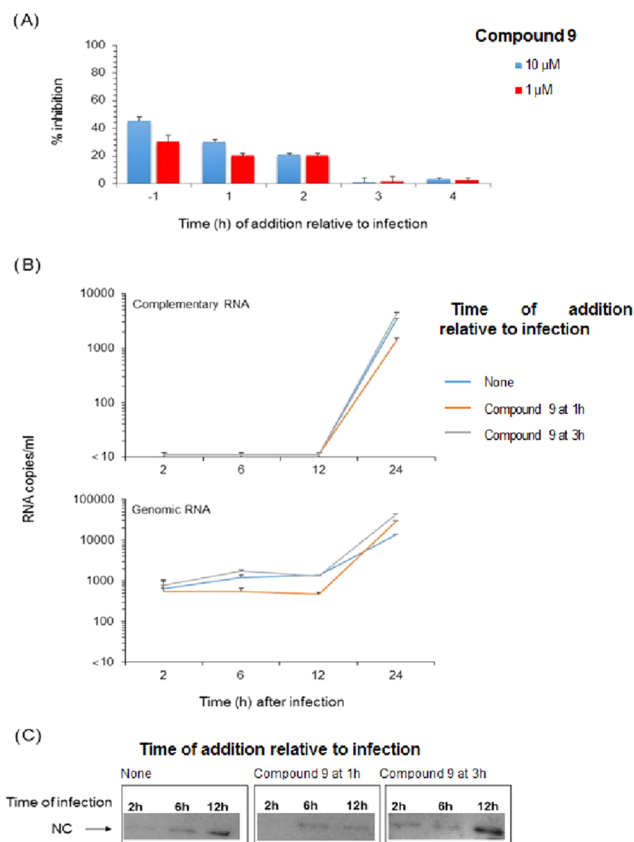


Figure 5. Effect of varying anti-DDX3X compound 9 at the time of administration on WNV replication. (A) WNV infection of Huh7 cells at MOI of 0.1 in presence of compound 9 at 1 and 10 μM added at the indicated time (h) relative to the infection and assayed with the viral plaque reduction assay. Data represent mean ± standard deviation. (B) WNV genomic and complementary viral RNA in Huh7 cells assayed after infection in absence or in presence of compound 9 at 1 μM added at 1 and 3 h of the infection. Data represent mean ± standard deviation. (C) WNV capsid protein electrophoretic mobility obtained from Huh7 cells after infection in absence or in presence of compound 9 at 1 μM added at 1 and 3 h of the infection. No compound 9 addition performed.

disclosed that all selected compounds showed a high metabolic stability major of 95.6%.

CONCLUSIONS

We identified a completely new family of selective inhibitors of the helicase activity of DDX3X. The compounds described here have been rationally designed to specifically target the helicase activity of DDX3X. Accordingly, they were inactive in the ATPase assay and in the helicase assay against the related human DEAD-box helicase DDX1. Future plans for improving the assessment of selectivity of our compounds include their

evaluation on a broader panel of DDX-family helicases, as well as the exploitation of Huh7 cells with inducible silencing of DDX3X expression. Both approaches are currently under development in our laboratory and will be the subject of future communications. Among the 21 compounds reported, six of them (namely, compounds 8, 9, 10, 13, 14, and 15) are characterized by promising antiviral activities against WNV, lower than those of the broad spectrum antiviral ribavirin, and more importantly without signs of cellular toxicities. It is worth pointing out that the antiviral activities are DDX3X-dependant, since compound 12, endowed with the worst inhibitory activity, did not show any antiviral effect up to 200 μM . Furthermore, merged derivatives 10, 14, and 15, even if less active against WNV than compound 1, are endowed with very good aqueous solubility, with values 100 times higher than those of the hit 1, thus overcoming an important limitation of the previously published compounds. Furthermore, the time of addition experiments is consistent with literature studies previously published on DDX3X recruitment on WNV replication site,²¹ highlighting an involvement of our compounds in the first phases of WNV replication and suggesting their possible role in the step of protein translation, after the entry process. Noteworthy, although tolerability and bioavailability need to be proved in vivo, the effectiveness of the compounds also when added before viral cell infection suggests their possible use as prophylactic antiviral drugs. Even if we are aware that deep investigations are needed to elucidate the mechanism of action of our compounds, to date, the exact implications of our own target on the WNV life cycle remain poorly understood.

In the absence of any available antiviral compound for the treatment of WNV infection,²⁴ the present study confirms our previous findings, suggesting that DDX3X helicase inhibitors can represent the Achilles' hell of viruses and that human proteins can be manipulated to fight novel emerging viral threats.

METHODS

Docking Studies. All compounds studied herein were docked within the RNA binding site of the modeled human DDX3X closed conformation previously published¹⁹ using the software package GOLD 4.1.^{25,26} The pocket under investigation was inserted into a grid box centered on residue Phe357 and enclosing residues lying within 10 Å from such amino acid. The genetic algorithm parameter settings were employed using the search efficiency set at 100%, and 100 runs were carried out for each ligand. Chemscore was chosen as the fitness function. Finally, results differing by less than 1.5 Å in ligand-all atom root-mean-square deviation were clustered together. For each inhibitor, the first ranked solution was selected for further analysis. Pictures of the modeled ligand–enzyme complexes together with graphic manipulations were rendered using PyMOL molecular graphic system.²⁷

Chemistry. Reagents were obtained from commercial suppliers (for example, Sigma-Aldrich, Alfa Aesar). All commercially available chemicals were used as purchased without further purification. CH_2Cl_2 and MeOH were dried prior to use by distilling from calcium hydride or magnesium methoxide. Anhydrous reactions were run under positive pressure of dry N_2 or argon. Thin-layer chromatography (TLC) was carried out using Merck TLC plate silica gel 60 F254. Chromatographic purifications were performed on columns packed with Merck 60 silica gel, 23–400 mesh, for the flash technique.

All NMR spectra were recorded on a Bruker Avance DPX400 spectrometer at 400 MHz for ^1H NMR or 100 MHz for ^{13}C NMR. Chemical shifts are reported relative to tetramethylsilane at 0.00 ppm. ^1H patterns are described using the following abbreviations: s = singlet,

d = doublet, t = triplet, q = quartet, quint = quintet, sx = sextet, sept = septet, m = multiplet, br = broad signal, and br s = broad singlet.

Mass spectra (MS) data were obtained using an Agilent 1100 LC/mass spectra detection (MSD) VL system (G1946C) with a 0.4 mL min^{-1} flow rate using a binary solvent system 25 of 95:5 methyl alcohol/water ratio. UV detection was monitored at 254 nm. Mass spectra were acquired in positive and negative mode scanning over the mass range.

Microwave Irradiation Experiments. These were conducted using CEM Discover Synthesis Unit (CEM Corp., Matthews, NC). The machine consists of a continuous focused microwave power delivery system with operator selectable power output from 0 to 300 W. The temperature of the content vessels was monitored using a calibrated infrared temperature control mounted under the reaction vessel. All experiments were performed using a stirring option whereby the contents of the vessels are stirred by means of a rotating magnetic plate located below the floor of the microwave cavity and a Teflon-coated magnetic stir bar in the vessel.

UV/Layer Chromatography (LC)-MS Method. For the quantitative analysis, a UV/LC-MS system was used. LC analysis was performed by Agilent 1100 LC/MSD VL system (G1946C) (Agilent Technologies, Palo Alto, CA) constituted by a vacuum solvent degassing unit, a binary high-pressure gradient pump, and a 1100 series UV detector, and a 1100 MSD model VL benchtop mass spectrometer was used. The Agilent 1100 series mass spectra detection (MSD) single-quadrupole instrument was equipped with the orthogonal spray atmospheric pressure ionization electrospray (API-ES, Agilent Technologies, Palo Alto, CA). Nitrogen was used as nebulizing and drying gas. The pressure of the nebulizing gas, the flow of the drying gas, the capillary voltage, the fragmentor voltage, and the vaporization temperature were set at 40 psi, 9 L min^{-1} , 3000 V, 70 V, and 350 °C, respectively. UV detection was monitored at 280 nm. The LC-electrospray ionization (ESI)-MS determination was performed by operating the MSD in the positive-ion mode. Spectra were acquired over the scan range m/z 50–1500 using a step size of 0.1 u. Chromatographic analysis was performed using a Varian Polaris 5 C18-A column (150 \times 4.6 mm², 5 μm particle size) at room temperature. Analysis was carried out using gradient elution of a binary solution; eluent A was ACN, whereas eluent B consisted of water. The analysis started at 0% A for 3 min, then rapidly increased up to 98% in 12 min, finally remaining at 98% A until 18 min. The analysis was performed at a flow rate of 0.8 mL min^{-1} , and the injection volume was 20 μL . LC retention times, molecular ion (m/z), and LC purity (by UV) were based on the method below. Purity of compounds (as measured by the peak area ratio) was >97%.

3-Azidobenzenethiol (4). 3-Aminothiols (2.0 g, 15.97 mmol) was dissolved in CH_3CN and cooled to 0 °C in an ice-salt bath. To this stirred solution was added *t*-BuONO (2.84 mL, 23.9 mmol), and the mixture was stirred for 10 min; after this time, TMSN_3 (2.53 mL, 19.17 mmol) was added dropwise, during 10 min, and the resulting brown solution was stirred at r.t. One hour later the solvent was removed at reduced pressure and the residue was purified by flash chromatography on silica gel. Purification eluent: EP/EA 8:2, yield 80%. Pale white solid. ^1H NMR (400 MHz, CDCl_3): δ 7.3–7.2 (m, 2H), 7.1 (s, 1H), 6.9 (d, J = 6.4 Hz, 1H) ppm.

General Procedure for the Preparation of Compounds 5a and 5b. To a stirring solution of 200 g of NaOH in 300 mL of water (0.3 mol, 16.8 g) was added the opportune alcohol (2.5 mL, 33.02 mmol). To this was slowly added the corresponding sulfate (15 mmol, 2082 mg) in 2 h dropwise, and the mixture was heated at 50 °C. The final product was distilled off; the distillation was stopped at 95 °C; then, the content of the receiver was washed with cold NH_4Cl (aq) solution and separated.

3-Ethoxyprop-1-yne (5a). Yield 68% colorless oil. ^1H NMR (400 MHz, CDCl_3 -d): δ 4.13–4.13 (d, J = 2.4 Hz, 2H), 3.60–3.55 (q, J = 6.9 Hz, 2H), 2.41–2.40 (t, J = 4.8 Hz, 1H), 1.24–1.22 (t, J = 6.9 Hz, 3H) ppm.

4-Methoxybut-1-yne (5b). Yield 52% colorless oil. ^1H NMR (400 MHz, CDCl_3 -d): δ 3.52–3.49 (m, 2H), 3.33 (s, 3H), 2.47–2.43 (m, 2H), 1.99–1.97 (m, 1H) ppm.

General Procedure for the Preparation of Triazoles (6a–c).

The appropriate alkyne (6.08 mmol) and the opportune azide (5.07 mmol) were suspended in a 1:1 mixture of water and *t*-BuOH (1.5 mL each) in a 10 mL glass vial equipped with a small magnetic stirring bar. To this was added sodium ascorbate (2.5 mmol) and copper(II) sulfate pentahydrate (2.50 mmol). The mixture was then heated for 10 min at 80 °C under microwave irradiation, using an irradiation power of 300 W. Thereafter, the solvent was removed at reduced pressure, water was added, and the mixture was extracted with EtOAc (3 × 20 mL). The organic layers were collected, washed with brine, and dried over Na₂SO₄. The crude was purified by flash chromatography on silica gel using the opportune eluent to give the desired triazole compounds.

3-(4-(Ethoxymethyl)-1H-1,2,3-triazol-1-yl)benzenethiol (6a). Purification eluent: EP/EA 7:3, white solid, yield 62%. ¹H NMR (400 MHz, MeOD): δ 7.97 (s, 1H), 7.94 (s, 1H), 7.60–7.57 (m, 2H), 7.49 (t, *J* = 8.0 Hz, 1H), 4.70 (s, 2H), 3.66 (q, *J* = 6.8 Hz, 2H), 0.89 (t, *J* = 6.8 Hz, 3H) ppm.

3-(4-(2-Methoxyethyl)-1H-1,2,3-triazol-1-yl)benzenethiol (6b). Purification eluent: EP/EA 7:3, white solid, yield 50%. ¹H NMR (400 MHz, MeOD): δ 8.02 (s, 1H), 7.45–7.29 (m, 2H), 7.28 (d, *J* = 7.4 Hz, 1H), 7.18 (t, *J* = 7.5, 1H), 3.75 (t, *J* = 6.6 Hz, 2H), 3.38 (s, 3H), 2.97 (t, *J* = 6.6 Hz, 2H).

3-(4-Butyl-1H-1,2,3-triazol-1-yl)benzenethiol (6c). Purification eluent: EP/EA 8:2, pale white solid, yield 78%. ¹H NMR (400 MHz, CDCl₃): δ 7.95 (s, 1H), 7.72 (s, 1H), 7.6–7.53 (m, 2H), 7.47 (t, *J* = 8.0 Hz, 1H), 2.81 (t, *J* = 7.6 Hz, 2H), 1.75–1.67 (m, 2H), 1.47–1.39 (m, 2H), 0.97 (t, *J* = 7.6 Hz, 3H) ppm.

General Procedure for the Synthesis of Sulfonamides 8–20.

The opportune benzenethiol (6a–c) (0.43 mmol) was dissolved in 2 mL of acetonitrile; to this, 30% H₂O₂ (1.2 mmol, 133 μL) and SOCl₂ (0.43 mmol, 31 μL) were added and the corresponding solution was stirred at room temperature for 30 min. After this time, the reaction mixture was extracted with EtOAc (3 × 25 mL), washed with brine, and dried over Na₂SO₄. The solvent was removed at reduced pressure, and the resulting residue was dissolved in 5 mL of dichloromethane (DCM). To this, a solution of the opportune aromatic amine in 1 mL of pyridine was added drop by drop. The resulting mixture was stirred at r.t. for 4 h. Thereafter, water was added and the mixture was extracted with DCM (6 × 30 mL), washed with brine, and dried over anhydrous Na₂SO₄. The corresponding residue was purified on silica with the opportune eluent.

3-(4-Butyl-1H-1,2,3-triazol-1-yl)-N-(2-hydroxyphenyl)benzenesulfonamide (8). Purification eluent: hexane/AcOEt 3:1, yield 80%. ¹H NMR (400 MHz, acetone): δ 8.79–8.35 (m, 2H), 8.34–8.31 (m, 2H), 8.11–8.09 (d, *J* = 8.0 Hz, 1H), 7.81–7.79 (d, *J* = 8.0 Hz, 1H), 7.71–7.67 (t, *J* = 8.0 Hz, 1H), 7.37–7.35 (d, *J* = 8.0 Hz, 1H), 6.99–6.95 (t, *J* = 8.0 Hz, 1H), 6.81–6.77 (m, 2H), 2.84 (t, *J* = 7.6 Hz, 2H), 1.77–1.69 (m, 2H), 1.46–1.38 (m, 2H), 0.99 (t, *J* = 7.6 Hz, 3H). ¹³C NMR (100 MHz, acetone): δ 149.88, 142.46, 131.77, 137.68, 130.44, 126.66, 126.50, 124.40, 124.19, 123.58, 119.90, 119.47, 118.32, 115.59, 31.30, 24.94, 21.95, 13.19. High-resolution mass spectrometry (HRMS) (ESI) *m/z* calcd for C₁₈H₁₉N₄O₃S [M – H][–] 371.1178, found 371.1180.

3-(4-Butyl-1H-1,2,3-triazol-1-yl)-N-(2-(trifluoromethyl)phenyl)benzenesulfonamide (9). Purification eluent: hexane/AcOEt 3:1, yield 90%. ¹H NMR (acetone): δ 8.78 (s, 1H), 8.41–8.37 (m, 2H), 8.18–8.16 (d, *J* = 8.2 Hz, 1H), 7.89–7.87 (d, *J* = 7.6 Hz, 1H), 7.82–7.78 (t, *J* = 7.8 Hz, 1H), 7.69–7.61 (m, 2H), 7.54–7.52 (d, *J* = 8 Hz, 1H), 7.45–7.44 (t, *J* = 7.4 Hz, 1H), 2.77–2.73 (t, *J* = 7.4 Hz, 2H), 1.71–1.67 (m, 2H), 1.45–1.35 (m, 2H), 0.94–0.89 (t, *J* = 8.0 Hz, 3H) ppm. ¹³C NMR (acetone): 149.1, 142.66, 137.89, 134.15, 133.28, 130.93 (2C), 127.40 (q, *J*_(C–F) = 5 Hz), 126.90, 126.28, 124.80, 123.85, 122.29 (q, *J*_(C–F) = 273 Hz), 119.54, 118.03, 31.22, 24.95, 21.95, 13.18 ppm. HRMS (ESI) *m/z* calcd for C₁₉H₁₈F₃N₄O₂S [M – H][–] 423.1103, found 423.1107.

3-(4-(Ethoxymethyl)-1H-1,2,3-triazol-1-yl)-N-(2-(trifluoromethyl)phenyl)benzenesulfonamide (10). Purification eluent: PE/EtOAc 7:2, yield 85%, white solid ¹H NMR (400 MHz, CDCl₃-*d*): δ 8.09 (1H, s), 7.99–7.97 (m, 2H), 7.79–7.75 (m, 2H), 7.60–7.47 (m, 3H), 7.26–7.22 (t, *J* = 7.2 Hz, 1H), 7.14 (s, 1H), 4.66 (s, 2H), 3.63–3.58 (q, *J* = 6.8 Hz, 2H), 1.24–1.20 (t, *J* = 6.8 Hz, 3H) ppm. ¹³C NMR (100 MHz,

CDCl₃-*d*): 146.95, 144.13, 140.78, 137.44, 133.39, 130.80, 126.99, 126.07 (2C), 125.84, 124.87, 124.69, 122.09, 120.58 (q, *J*_(C–F) = 280 Hz), 118.71, 66.39, 63.99, 15.07 ppm. HRMS (ESI) *m/z* calcd for C₁₈H₁₆F₃N₄O₃S [M – H][–] 425.0895, found 425.0890.

3-(4-(2-Methoxyethyl)-1H-1,2,3-triazol-1-yl)-N-(2-(trifluoromethyl)phenyl)benzenesulfonamide (11). Purification eluent: PE/EtOAc 7:2, yield 63%, white solid. ¹H NMR (400 MHz, CDCl₃-*d*): δ 8.07 (1H, s), 8.02–8.00 (d, *J* = 8.0 Hz, 1H), 7.86–7.84 (d, *J* = 7.9 Hz, 2H), 7.77–7.75 (d, *J* = 7.6 Hz, 1H), 7.61–7.50 (m, 3H), 7.28–7.24 (m, 2H), 3.72 (m, 2H), 3.394 (s, 3H), 3.08–3.07 (m, 2H) ppm. ¹³C NMR (CDCl₃): δ 145.32, 139.71, 133.11, 132.91, 132.43, 129.12, 128.81, 127.36, 126.04 (2C), 124.09, 119.21 (q, *J*_(C–F) = 268 Hz), 119.1, 116.66, 115.51, 77.81, 59.44, 30.91 ppm. HRMS (ESI) *m/z* calcd for C₁₈H₁₆F₃N₄O₃S [M – H][–] 425.0895, found 425.0893.

3-(4-Butyl-1H-1,2,3-triazol-1-yl)-N-(2-fluorophenyl)benzenesulfonamide (12). Purification eluent: PE/EtOAc 7:2, yield 71%, white solid. ¹H NMR (400 MHz, CDCl₃-*d*): 8.07 (s, 1H), 8.02–8.01 (d, *J* = 8.0 Hz, 1H), 7.77–7.76 (d, *J* = 8.0 Hz, 1H), 7.68 (s, 1H), 7.62–7.57 (m, 2H), 7.15–7.09 (m, 2H), 6.99–6.94 (m, 2H), 2.80–2.77 (t, *J* = 7.6 Hz, 2H), 1.74–1.66 (m, 2H), 1.46–1.37 (m, 2H), 0.97–0.93 (t, *J* = 7.6 Hz, 3H) ppm. ¹³C NMR (100 MHz, CDCl₃): 157.9 (d, *J*_(C–F) = 238 Hz), 149.77, 140.75, 137.65, 130.69, 127.13, 126.59, 124.96, 124.70, 124.59, 124.38, 118.44 (d, *J*_(C–F) = 20 Hz), 115.79, 115.58 (d, *J*_(C–F) = 9 Hz), 31.32, 25.23, 22.26, 13.78 ppm. HRMS (ESI) *m/z* calcd for C₁₈H₁₈FN₄O₂S [M – H][–] 373.1134, found 373.1129.

3-(4-Butyl-1H-1,2,3-triazol-1-yl)-N-(*o*-tolyl)benzenesulfonamide (13). Purification eluent: hexane/AcOEt 3:1, yield 90%. ¹H NMR (400 MHz, acetone): δ 8.56 (s, 1H), 8.35–8.33 (d, *J* = 8.0 Hz, 1H), 8.25–8.23 (d, *J* = 8.0 Hz, 1H), 8.14–8.11 (t, *J* = 7.2 Hz, 1H), 7.74–7.72 (m, 2H), 7.17–7.10 (m, 4H), 2.77–2.73 (t, *J* = 7.4 Hz, 2H), 2.72 (s, 3H), 1.73–1.65 (m, 2H), 1.43–1.37 (m, 2H), 0.95–0.91 (t, *J* = 7.8 Hz, 3H) ppm. ¹³C NMR (100 MHz, acetone): 149.06, 142.56, 137.76, 134.78, 134.16, 130.91, 130.72, 126.78, 126.51, 126.37, 126.28, 123.51, 119.46, 118.11 31.22, 24.95, 21.95, 17.18, 13.18 ppm. HRMS (ESI) *m/z* calcd for C₁₉H₂₁N₄O₂S [M – H][–] 369.1385, found 369.1387.

3-(4-Butyl-1H-1,2,3-triazol-1-yl)-N-(isoquinolin-6-yl)benzenesulfonamide (14). Purification eluent: hexane/AcOEt 3:1, yield 77%. ¹H NMR (400 MHz, CDCl₃-*d*): δ 9.23 (s, 1H), 8.42 (s, 1H), 8.26 (s, 1H), 7.89–7.83 (m, 4H), 7.66–7.62 (m, 3H), 7.55–7.46 (m, 2H), 2.74–2.71 (t, *J* = 7.8 Hz, 2H), 1.66–1.59 (m, 2H), 1.39–1.25 (m, 2H), 0.90–0.86 (t, *J* = 8.0 Hz, 3H) ppm. ¹³C NMR (100 MHz, CDCl₃-*d*): 152.43, 149.84, 142.93, 141.34, 137.68, 132.70, 131.10, 130.51, 129.38, 129.01, 128.51, 127.62, 127.38, 126.85, 124.13, 118.81, 115.75, 31.36, 25.25, 22.26, 13.62 ppm. HRMS (ESI) *m/z* calcd for C₂₁H₂₂N₅O₂S [M + H]⁺ 408.1494, found 408.1489.

3-(4-(Ethoxymethyl)-1H-1,2,3-triazol-1-yl)-N-(isoquinolin-5-yl)benzenesulfonamide (15). Purification eluent: CHCl₃/acetone 98:2, white solid, yield 73%. ¹H NMR (400 MHz, CD₃OD): δ 9.50 (s, 1H), 8.51 (s, 1H), 8.45–8.43 (m, 2H), 8.23–8.18 (m, 3H), 8.07–8.05 (d, *J* = 8.0 Hz, 1H), 7.80–7.66 (m, 4H), 4.63 (s, 2H), 3.61–3.56 (q, *J* = 7.2 Hz, 2H), 1.32 (t, *J* = 7.2, 3H) ppm. ¹³C NMR (100 MHz, CDCl₃-*d*) δ 192.82, 174.69, 149.87, 146.32, 141.42, 137.79, 136.51, 134.59, 132.21, 131.44, 130.80, 129.22, 126.87, 124.19, 123.06, 121.88, 118.89, 65.82, 62.91, 14.31 ppm. HRMS (ESI) *m/z* calcd for C₂₀H₂₀N₅O₃S [M + H]⁺ 410.1287, found 410.1282.

3-(4-(Ethoxymethyl)-1H-1,2,3-triazol-1-yl)-N-(3-morpholinophenyl)benzenesulfonamide (16). Purification eluent: CHCl₃/acetone 98:2, white solid, yield 64%. ¹H NMR (400 MHz, CDCl₃): δ 8.17 (s, 1H), 7.99 (s, 1H), 7.92 (d, *J* = 7.4 Hz, 1H), 7.79 (d, *J* = 7.6 Hz, 1H), 7.72 (s, 1H), 7.59 (t, *J* = 8.0 Hz, 1H), 7.12 (t, *J* = 8.4 Hz, 1H), 6.78 (s, 1H), 6.68 (d, *J* = 8.4 Hz, 1H), 6.61 (d, *J* = 7.6 Hz, 1H), 4.71 (s, 2H), 3.81 (t, *J* = 4.4 Hz, 4H), 3.64 (q, *J* = 6.8 Hz, 2H), 3.1 (t, *J* = 4.4 Hz, 4H), 1.27 (t, *J* = 6.8 Hz, 3H) ppm. ¹³C NMR (100 MHz, CDCl₃-*d*) δ 152.8, 147.23, 141.24, 137.34, 137.13, 130.56, 129.88, 127.23, 124.35, 120.75, 119.00, 113.20, 112.88, 109.30, 66.56, 63.92 (2C), 48.91 (2C), 29.70, 15.15 ppm. HRMS (ESI) *m/z* calcd for C₂₁H₂₆N₅O₄S [M + H]⁺ 444.1706, found 444.1701.

3-(4-(Ethoxymethyl)-1H-1,2,3-triazol-1-yl)-N-(4-isopropylphenyl)benzenesulfonamide (17). Purification eluent: PE/EA 7:3, white solid, yield 71%. ¹H NMR (400 MHz, CDCl₃): δ 8.07 (s,

1H), 7.98 (t, *J* = 8.4 Hz, 1H), 7.79 (d, *J* = 8.0 Hz, 1H), 7.61, (t, *J* = 8.0 Hz, 1H), 7.55 (s, 1H) 7.12 (d, *J* = 8.0 Hz, 2H), 7.25 (s, 1H), 7.05 (d, *J* = 8.4 Hz, 2H), 4.69 (s, 2H), 3.66–3.60 (m, 2H), 2.87–2.78 (m, 1H), 1.27 (t, *J* = 7.2 Hz, 3H), 1.19 (d, *J* = 6.8 Hz, 6H) ppm. ¹³C NMR (100 MHz, CDCl₃-d) δ 147.08, 141.22, 138.37, 137.35, 134.97, 133.40, 130.61, 129.60, 127.44, 127.14, 124.49, 122.99, 120.61, 118.86, 66.44, 64.06, 33.31, 24.10 (2C), 15.28 ppm. HRMS (ESI) *m/z* calcd for C₂₀H₂₃N₄O₃S [M – H][–] 399.1491, found 399.1488.

3-(4-Butyl-1H-1,2,3-triazol-1-yl)-N-(4-methoxyphenyl)benzenesulfonamide (18). Purification eluent: hexane/AcOEt 3:1, yield 79%. ¹H NMR (400 MHz, CDCl₃-d): δ 8.10 (s, 1H), 7.95–7.93 (d, *J* = 7.6 Hz, 1H), 7.71 (s, 1H), 7.68–7.66 (d, *J* = 7.7 Hz, 1H), 7.61 (s, 1H), 7.56–7.52 (t, *J* = 7.9 Hz, 1H), 7.07–7.04 (d, *J* = 8.2 Hz, 2H), 6.77–6.75 (d, *J* = 8.2 Hz, 2H), 3.73 (s, 3H), 2.78–2.75 (t, *J* = 7.7 Hz, 2H), 1.71–1.64 (m, 2H), 1.43–1.36 (m, 2H), 0.95–0.91 (t, *J* = 7.6 Hz, 3H) ppm. ¹³C NMR (100 MHz, MeOD-*d*₄): δ 158.45, 149.70, 141.20, 137.55, 130.75, 127.59, 125.89 (2C), 124.43, 119.27, 118.89, 118.68, 114.46 (2C), 55.90, 31.84, 25.52, 21.87, 13.85 ppm. HRMS (ESI) *m/z* calcd for C₁₉H₂₁N₄O₃S [M – H][–] 385.1334, found 385.1338.

3-(4-Butyl-1H-1,2,3-triazol-1-yl)-N-(2-methoxyphenyl)benzenesulfonamide (19). Purification eluent: hexane/AcOEt 4:1, yield 64%. ¹H NMR (400 MHz, CDCl₃) δ 8.28 (s, 1H), 8.08 (s, 1H), 7.97 (s, 1H), 7.62–7.60 (d, *J* = 8.0 Hz, 2H), 7.28–7.25 (t, *J* = 8.0 Hz, 1H), 6.68–6.65 (m, 4H), 3.80 (s, 3H), 2.78–2.73 (t, *J* = 8.0 Hz, 2H), 1.68–1.64 (m, 2H), 1.44–1.39 (m, 2H), 1.02–0.97 (m, 3H). ¹³C NMR (100 MHz, CDCl₃) δ 149.27, 149.11, 139.90, 139.74, 128.46, 127.64, 126.49, 124.93, 123.87, 123.11, 119.85, 119.72, 119.16, 114.93, 74.56, 31.00, 24.41, 21.46, 12.91 ppm. HRMS (ESI) *m/z* calcd for C₁₉H₂₁N₄O₃S [M – H][–] 385.1334, found 385.1329.

3-(4-Butyl-1H-1,2,3-triazol-1-yl)-N-phenylbenzenesulfonamide (20). Purification eluent: hexane/AcOEt 3:1, yield 89%. ¹H NMR (400 MHz, acetone): δ 8.51 (s, 1H), 8.08 (s, 1H), 7.88–7.74 (m, 2H), 7.69 (m, 1H), 7.45 (t, *J* = 7.9 Hz, 1H), 7.11 (t, *J* = 7.9 Hz, 2H), 6.90–6.79 (m, 1H), 6.60 (d, *J* = 7.5 Hz, 2H), 2.76 (t, *J* = 7.8 Hz, 2H), 1.70 (t, *J* = 7.9 Hz, 2H), 1.53–1.37 (m, 2H), 0.98 (t, *J* = 6.6 Hz, 3H) ppm. ¹³C NMR (100 MHz, acetone): 153.56, 141.73, 137.53, 137.00, 129.89, 129.42 (2C), 128.59, 126.40, 125.09, 123.98, 121.69 (2C), 119.95, 29.99, 27.98, 22.18, 14.05 ppm. HRMS (ESI) *m/z* calcd for C₁₈H₁₉N₄O₃S [M – H][–] 355.1229, found 355.1224.

4-(3-Nitrophenyl)morpholine (23). To a solution of 1-fluoro-3-nitrobenzene (1.0 g, 7.1 mmol) in DMSO, K₂CO₃ (2.930 g, 21.24 mmol) and morpholine (741 mg, 8.5 mmol) were added. The solution was stirred at 60 °C for 3 h. Thereafter, 5% LiCl(aq) was added and the reaction mixture was extracted with EtOAc (3 × 25 mL) and dried over Na₂SO₄. The solvent was removed at reduced pressure and the residue purified by flash chromatography on silica gel. Purification eluent: PE/EA 8:2, yield 80%. ¹H NMR (400 MHz, CDCl₃) δ 7.72 (d, *J* = 8.0 Hz, 1H), 7.43 (t, *J* = 8.0 Hz, 1H), 7.26 (s, 1H), 7.22 (d, *J* = 6.4 Hz, 1H) 3.90 (t, *J* = 4.8 Hz, 4H) 3.27 (t, *J* = 5.2 Hz, 4H) ppm.

3-Morpholinoaniline (24). **23** (500 mg, 2.5 mmol) was solubilized in 30 mL of anhydrous MeOH; to this, palladium on charcoal (50 mg) was added. The reaction mixture was stirred under hydrogen atmosphere for 1 h; then, the mixture was filtered off on a celite pad, the solvent evaporated at reduced pressure, and the residue purified by flash chromatography on silica gel.

Purification eluent: PE/EA = 8:2, yield 99%. ¹H NMR (400 MHz, CDCl₃): δ 7.05 (t, *J* = 7.2 Hz, 1H), 6.37 (d, *J* = 8.0 Hz, 1H), 6.25–6.20 (m, 2H), 4.24 (s, 2H), 3.19 (m, 4H), 2.6 (t, *J* = 4.4 Hz, 4H) ppm.

N-(2-Trifluoromethyl)-3-nitro-phenylbenzenesulfonamide (28). To a stirred solution of 2-(trifluoromethyl)aniline (1.09 g, 6.76 mmol) in 5 mL of anhydrous pyridine was added the corresponding 3-nitrobenzene sulfonyl chloride (1.5 g, 6.76 mmol) at 0 °C. The corresponding solution was stirred at r.t. under nitrogen atmosphere, for 5 h. After completion of the reaction, the mixture was acidified with 20 mL of 2 N HCl, the aqueous phase was extracted several times, and the combined organic phases were dried (Na₂SO₄) and concentrated. The residue was purified by flash chromatography on silica gel (hexane/AcOEt 3:1). Yield 84%. ¹H NMR (400 MHz, CDCl₃-d): δ 8.56 (s, 1H), 8.40–8.38 (d, *J* = 8.4 Hz, 1H), 8.06–8.04 (d, *J* = 8 Hz, 1H), 7.86–7.84 (d, *J* = 8 Hz, 1H), 7.69–7.64 (t, *J* = 8 Hz, 1H), 7.61–7.57 (t, *J* = 7.8 Hz,

1H), 7.52–7.50 (d, *J* = 8.0 Hz, 1H), 7.31–7.27 (t, *J* = 8.1 Hz, 1H), 6.86 (s, 1H). MS (ESI): *m/z* 346.8 [M + H]⁺.

3-Amino-N-(2-(trifluoromethyl)phenyl)benzenesulfonamide (29). Sulfonamide **28** (400 mg, 1.35 mmol) was solubilized in 20 mL of anhydrous EtOH, and palladium on charcoal (60 mg) was added. The reaction mixture was stirred under hydrogen atmosphere for 1 h. Then, the mixture was filtered off on a celite pad and concentrated in vacuo and the crude product was purified by flash chromatography on silica gel (purification eluent: hexane/AcOEt 3:1). Yield 84%. ¹H NMR (acetone): δ 7.63–7.61 (d, *J* = 8 Hz, 1H), 7.51–7.58 (m, 2H), 7.24–7.20 (t, *J* = 8 Hz, 1H), 7.19–7.17 (m, 3H), 7.07–7.05 (d, *J* = 8 Hz, 1H), 6.90–6.88 (d, *J* = 8 Hz, 1H), 4.91 (s, 2H). MS (ESI): *m/z* 338.8 [M + Na]⁺.

3-Azido-N-(2-(trifluoromethyl)phenyl)benzenesulfonamide (30). **29** (100 mg, 0.41 mmol) was dissolved in CH₃CN and cooled to 0 °C in an ice–salt bath. To this stirred solution, *t*-BuONO (225 μL, 1.89 mmol) was added and the mixture was stirred for 10 min; thereafter, TMSN₃ (200 μL, 1.52 mmol) was added dropwise, for 10 min, and the resulting brown solution was stirred at r.t. One hour later the solvent was removed at reduced pressure and the residue was purified by flash chromatography on silica gel with the appropriate eluent. Purification eluent: hexane/AcOEt 4:1. ¹H NMR (400 MHz, CDCl₃-d): δ 7.84–7.81 (d, *J* = 8.4 Hz, 1H), 7.56–7.50 (m, 3H), 7.43–7.37 (m, 2H), 7.27–7.23 (t, *J* = 7.6 Hz, 1H), 7.18–7.16 (d, *J* = 8 Hz, 1H), 6.87 (s, 1H) ppm. MS (ESI): *m/z* 364.8 [M + Na]⁺.

General Procedure for the Preparation of Compounds 31–34. The appropriate alkyne (6.08 mmol) and the opportune azide (5.07 mmol) were suspended in a 1:1 mixture of water and *t*-BuOH (1.5 mL each) in a 10 mL glass vial equipped with a small magnetic stirring bar. To this, sodium ascorbate (2.5 mmol) and copper(II) sulfate pentahydrate (2.50 mmol) were added. The mixture was then heated for 10 min at 125 °C under microwave irradiation, using an irradiation power of 300 W. Thereafter, the solvent was removed at reduced pressure, water was added, and the mixture was extracted with EtOAc (3 × 20 mL). The organic layers were collected, washed with brine, and dried over Na₂SO₄. The crude was purified by flash chromatography on silica gel using the opportune eluent: to give the desired triazole compounds 31–34.

3-(4-Isopentyl-1H-1,2,3-triazol-1-yl)-N-(2-(trifluoromethyl)phenyl)benzenesulfonamide (31). Purification eluent: PE/EtOAc 7:2, yield 69%, yellow solid. ¹H NMR (CDCl₃): δ 8.06 (s, 1H), 8.01–8.00 (d, *J* = 7.6 Hz, 1H), 7.84–7.82 (d, *J* = 8.0 Hz, 1H), 7.76–7.74 (d, *J* = 7.6 Hz, 1H), 7.69 (1H, s), 7.60–7.56 (t, *J* = 8.4 Hz, 1H), 7.53–7.49 (m, 2H), 7.27–7.25 (d, *J* = 8.0 Hz, 1H), 6.98 (s, 1H), 2.80–2.78 (m, 2H), 1.62 (m, 3H), 0.99–0.94 (m, 6H) ppm. ¹³C NMR (CDCl₃): δ 149.95, 143.95, 137.71, 136.51, 133.39, 130.71, 130.14, 128.54, 126.68, 126.01, 125.29, 124.91, 124.15, 121.56 (q, *J*_(C–F) = 270 Hz), 118.51, 38.27, 27.62, 23.51, 22.36 (2C) ppm. HRMS (ESI) *m/z* calcd for C₂₀H₂₀F₃N₄O₂S [M – H][–] 437.1259, found 437.1255.

3-(4-Cyclohexyl-1H-1,2,3-triazol-1-yl)-N-(2-(trifluoromethyl)phenyl)benzenesulfonamide (32). Purification eluent: PE/EtOAc 7:3, yield 71%, pale white solid. ¹H NMR (CDCl₃): δ 8.39 (s, 1H), 8.35 (s, 1H), 8.18–8.16 (d, *J* = 7.8 Hz, 1H), 7.87–7.85 (d, *J* = 7.8 Hz, 1H), 7.80–7.76 (t, *J* = 7.8 Hz, 1H), 7.68–7.66 (d, *J* = 7.8 Hz, 1H), 7.63–8.60 (m, 2H), 7.52–7.50 (d, *J* = 7.8 Hz, 1H), 7.44–7.40 (t, *J* = 8.0 Hz, 1H), 3.47–3.41 (m, 1H), 2.51–2.37 (m, 4H), 1.80–1.63 (m, 6H). ¹³C NMR (CDCl₃): δ 149.31, 141.73, 138.07 (q, *J*_(C–F) = 32 Hz), 137.00, 134.84, 123.37, 128.55, 128.22, 127.57, 127.48, 127.07, 126.24, 123.95, 123.67 (q, *J*_(C–F) = 270 Hz), 119.92, 37.20, 32.15 (2C), 25.92, 25.15 (2C) ppm. HRMS (ESI) *m/z* calcd for C₂₁H₂₀F₃N₄O₂S [M – H][–] 449.1259, found 449.1262.

3-(4-Ethyl-1H-1,2,3-triazol-1-yl)-N-(2-(trifluoromethyl)phenyl)benzenesulfonamide (33). Purification eluent: PE/EtOAc 7:2, yield 78%, white solid. ¹H NMR (CDCl₃): δ 8.77 (s, 1H), 8.40 (s, 1H), 8.35 (s, 1H), 8.17–8.15 (d, *J* = 7.6 Hz, 1H), 7.88–7.86 (d, *J* = 7.6 Hz, 1H), 7.81–7.77 (t, *J* = 8.0 Hz, 1H), 7.69–7.67 (t, *J* = 8.0 Hz, 1H), 7.64–7.60 (t, *J* = 8.0 Hz, 1H), 7.52–7.50 (d, *J* = 8.0 Hz, 1H), 7.45–7.41 (t, *J* = 8.0 Hz, 1H), 2.76–2.78 (q, *J* = 7.6 Hz, 2H), 1.30–1.26 (t, *J* = 7.6 Hz, 3H) ppm. ¹³C NMR (CDCl₃): δ 149.1, 142.76, 137.94, 134.22, 133.37, 130.97, 127.47, 126.97, 126.37, 125.31, 124.80, 123.87, 121.89 (q,

$J_{(C-F)} = 270$ Hz), 119.26 (m), 118.29 (m), 18.75, 12.92 ppm. HRMS (ESI) m/z calcd for $C_{17}H_{14}F_3N_4O_2S$ $[M - H]^-$ 395.0790, found 395.0787.

3-(4-Phenyl-1H-1,2,3-triazol-1-yl)-N-(2-(trifluoromethyl)phenyl)benzenesulfonamide (34). Purification eluent: PE/EtOAc 7:2, yield 78%, yellow solid. 1H NMR ($CDCl_3$): δ 9.09 (s, 1H), 8.82 (s, 1H), 8.44 (s, 1H), 8.28–8.26 (d, $J = 7.6$ Hz, 1H), 7.99–7.97 (d, $J = 8.0$ Hz, 2H), 7.94–7.92 (d, $J = 7.6$ Hz, 1H), 7.86–7.82 (t, $J = 7.6$ Hz, 1H), 7.70–7.68 (d, $J = 8.1$ Hz, 1H), 7.65–7.61 (t, $J = 7.6$ Hz, 1H), 7.55–7.53 (t, $J = 8.0$ Hz, 1H), 7.48–7.42 (m, 3H), 7.36–7.34 (t, $J = 8.0$ Hz, 1H) ppm. ^{13}C NMR ($CDCl_3$): δ 148.29, 142.80, 137.76, 134.10, 133.37, 131.09, 130.54, 129.00 (2C), 128.82, 128.45, 127.63, 127.40, 126.96, 126.74, 125.66 (2C), 124.94, 124.14 (m), 121.90, 118.84 (q, $J_{(C-F)} = 30.3$ Hz), ppm. HRMS (ESI) m/z calcd for $C_{21}H_{14}F_3N_4O_2S$ $[M - H]^-$ 443.0790, found 443.0793.

4-(4-Butyl-1H-1,2,3-triazol-1-yl)-N-(2-(trifluoromethyl)phenyl)benzenesulfonamide (35). Purification eluent: hexane/AcOEt 3:1, yield 93%. 1H NMR (400 MHz, $CDCl_3$ -d): δ 8.89–7.81 (m, 5H) 7.75 (s, 1H), 7.57–7.53 (t, $J = 8.0$ Hz, 1H), 7.51–7.49 (d, $J = 8.0$ Hz, 1H), 7.26–7.22 (m, 1H), 6.94 (s, 1H), 2.79–2.75 (t, $J = 7.4$ Hz, 2H), 1.73–1.65 (m, 2H), 1.43–1.36 (m, 2H), 0.95–0.91 (t, $J = 8.0$ Hz, 3H) ppm. ^{13}C NMR (100 MHz, $CDCl_3$ -d): 149.9, 140.8, 137.99, 133.88, 133.81, 133.56, 129.53 (2C), 126.71 (q, $J_{(C-F)} = 4.4$ Hz), 125.70, 123.89, 122.27 (q, $J_{(C-F)} = 27.4$ Hz), 120.88 (2C), 118.45, 31.32, 25.24, 22.24, 13.76 ppm. HRMS (ESI) m/z calcd for $C_{19}H_{18}F_3N_4O_2S$ $[M - H]^-$ 423.1103, found 423.1107.

4-Nitro-N-(2-(trifluoromethyl)phenyl)benzenesulfonamide. The residue was purified by flash chromatography on silica gel (hexane/AcOEt 3:1), yield 84%. 1H NMR (400 MHz, acetone- d_6): δ 8.82 (s, 1H), 8.27–8.25 (d, $J = 8.0$ Hz, 2H), 7.91–7.89 (d, $J = 8.0$ Hz, 1H), 7.87–7.85 (d, $J = 8.0$ Hz, 2H), 7.61–7.57 (t, $J = 8.0$ Hz, 1H), 7.53–7.51 (d, $J = 8.0$ Hz, 1H), 7.32–7.25 (t, $J = 8$ Hz, 1H) ppm. MS: m/z 345.8 $[M - H]^-$.

4-Amino-N-(2-(trifluoromethyl)phenyl)benzenesulfonamide. Purification eluent: hexane/AcOEt 2:1, yield 97%. 1H NMR (acetone- d_6): δ 7.89 (s, 1H), 7.53–7.51 (d, $J = 8.0$ Hz, 2H), 7.49–7.47 (d, $J = 8.0$ Hz, 1H), 7.45–7.43 (d, $J = 8$ Hz, 2H), 7.30–7.28 (t, $J = 8$ Hz, 1H), 6.62–6.60 (t, $J = 7.8$ Hz, 1H), 6.50 (d, $J = 8.0$ Hz, 1H), 4.62 (s, 2H). MS (ESI): m/z 338.8 $[M + Na]^+$.

4-Azido-N-(2-(trifluoromethyl)phenyl)benzenesulfonamide. Purification eluent: hexane/AcOEt 4:1. 1H NMR (400 MHz, $CDCl_3$ -d): δ 7.81–7.79 (m, 2H), 7.74–7.71 (d, $J = 7.4$ Hz, 1H), 7.52–7.46 (m, 2H), 7.22–7.18 (t, $J = 8$ Hz, 1H), 7.02–6.98 (m, 3H) ppm. m/z 364.7 $[M + Na]^+$.

N-(2-Hydroxyphenyl)-4-nitrobenzenesulfonamide. 1H NMR (acetone- d_6): δ 8.25–8.22 (d, $J = 8.4$ Hz, 2H), δ 7.93–7.91 (m, 3H), 7.33–7.31 (m, 2H), 6.97–6.94 (t, $J = 7.6$ Hz, 1H), 6.76–6.73 (t, $J = 7.6$ Hz, 1H), 6.66–6.64 (d, $J = 8$ Hz, 1H) ppm. MS: m/z 292.8 $[M - H]^-$.

4-Amino-N-(2-hydroxyphenyl)benzenesulfonamide. 1H NMR (acetone- d_6): δ 7.55–7.53 (d, $J = 8.0$ Hz, 2H), 7.42–7.40 (d, $J = 8.0$ Hz, 2H), 7.22–7.18 (m, 1H), 6.90–6.84 (m, 2H), 6.70–6.66 (m, 2H), 6.55–6.53 (d, $J = 8.8$ Hz, 1H) ppm. MS: m/z 265.0 $[M + H]^+$.

4-Azido-N-(2-hydroxyphenyl)benzenesulfonamide. Purification eluent: hexane/AcOEt 3:1. 1H NMR (MeOD- d_4): δ 7.73–7.72 (d, $J = 8.0$ Hz, 2H), 7.36–7.35 (d, $J = 6.4$ Hz, 1H), 7.09–7.07 (d, $J = 8.0$ Hz, 2H), 6.94–6.90 (m, 2H), 6.73–6.66 (m, 2H) ppm. MS: m/z 312.8 $[M + Na]^+$.

4-(4-Butyl-1H-1,2,3-triazol-1-yl)-N-(2-hydroxyphenyl)benzenesulfonamide (36). Purification eluent: hexane/AcOEt 4:1, yield 80%. 1H NMR (400 MHz, MeOD- d_4): δ 8.34 (s, 1H), 7.93–7.87 (m, 4H), 7.33–7.31 (d, $J = 6.8$ Hz, 1H), 6.96–6.92 (m, 1H), 6.76–7.73 (t, $J = 7.6$ Hz, 1H), 6.67–6.65 (d, $J = 8.0$ Hz, 1H), 2.78–2.74 (t, $J = 7.6$ Hz, 2H), 1.74–1.66 (m, 2H), 1.45–1.36 (m, 2H), 1.27–1.22 (t, $J = 7.2$ Hz, 3H) ppm. ^{13}C NMR (100 MHz, MeOD- d_4): δ 150.25, 149.21, 139.89, 139.78, 128.89 (2C), 126.49, 124.93, 123.87, 119.85, 119.55 (2C), 119.16, 114.93, 30.99, 24.39, 21.44, 12.89 ppm. HRMS (ESI) m/z calcd for $C_{18}H_{19}N_4O_3S$ $[M - H]^-$ 371.1178, found 371.1173.

■ ASSAYS

Enzymatic Assays. Protein Expression and Purification.

Recombinant his-tagged human full length DDX3X was cloned in the *Escherichia coli* expression vector pET-30a(+). ShuffleT7 *E. coli* cells were transformed with the plasmid and grown at 37 °C up to $OD_{600} = 0.7$. DDX3X expression was induced with 0.5 mM isopropyl β -D-1-thiogalactopyranoside at 15 °C O/N. Cells were harvested by centrifugation and lysed and the crude extract centrifuged at 100,000xg for 60 min at 4 °C in a Beckman centrifuge before being loaded onto a FPLC Ni-NTA column (GE Healthcare). The column was equilibrated in buffer A (50 mM Tris-HCl pH 8.0, 250 mM NaCl, 25 mM imidazole and 20% glycerol). After extensive washing in buffer A, the column was eluted with a linear gradient in buffer A from 25 to 250 mM imidazole. Proteins in the eluted fractions were visualized on a sodium dodecyl sulfate (SDS)-polyacrylamide gel electrophoresis (PAGE) and tested for the presence of DDX3X by Western blot with anti-DDX3X A300-A450 (BETHYL) at 1:2000 dilution in 5% milk. Fractions containing the purest DDX3X protein were pooled and stored at –80 °C.

Helicase Assay Based on Fluorescence Resonance Energy Transfer. The dsRNA substrate for the helicase assay was prepared by hybridizing two ssRNA oligonucleotides with the following sequences:

Fluo-FAM 5' UUUUUUUUUUUUUUAGUACCGC-CACCCUCAGAACC 3'

Qu-BHQ1 5' GGUUCUGAGGGUGGCGGUACUA 3'
DNA capture 5' TAGTACCGCCACCCTCAGAACC 3'

The sequence in Fluo-FAM complementary to Qu-BHQ1 is underlined. Fluo-FAM carries a 6-carboxyfluorescein fluorophore at its 3' end, whereas Qu-BHQ1 carries a Black Hole Quencher group at its 5' end. The DNA capture oligonucleotide is complementary to the Qu-BHQ1 oligonucleotide but bears no modifications.

Helicase assay using the dsRNA substrate was performed in 20 mM Tris-HCl (pH 8), 70 mM KCl, 2 mM $MgCl_2$, 2 mM dithiothreitol, 12 units RNasin, 2 mM ATP, 50 nM dsRNA, and 100 nM capture strand in 20 μ L of reaction volume. The unwinding reaction was started by adding 60 pmol of DDX3X recombinant protein and carried out at 37 °C for 40 min using a LightCycler 480 (Roche). The fluorescence intensity was recorded every 30 s. Data of fluorescence signal were analyzed by linear interpolation, and the corresponding slope values were used to determine the apparent unwinding rate.

Kinetic Analysis. The IC_{50} values have been calculated from dose–response curves. Data (in triplicate) were plotted and analyzed by least-squares nonlinear regression, according to the method of Marquardt–Levenberg, with the computer program GraphPad Prism 6.0. Data were fitted to the following equation

$$E_{obs} = E_{max} / (1 + (IC_{50}/[I])^n) \quad (1)$$

where $E_{(obs)}$ is the observed enzymatic activity in the presence of each inhibitor dose $[I]$, $E_{(max)}$ is the maximal enzymatic activity in the absence of the inhibitor, and n is an exponential term to take into account sigmoidal dose–response curves.

Cell Extracts (CEs) and DDX3X Quantification. Ten million cells were ruptured with a Dounce homogenizer in lysis buffer (50 mM Tris-HCl pH 8.0, 0.1% SDS, 350 mM NaCl, 0.25% Triton X-100, protease inhibitor cocktail (Sigma-Aldrich)). The lysate was incubated for 30 min on ice, sonicated for 5 min (at 30 s intervals), and centrifuged at 15,000xg for 10 min at 4 °C. The protein concentration in the supernatant (crude extract) was

quantified with Bradford. For DDX3X quantification, increasing concentrations of crude extract (5, 10, 20, and 40 μg) were loaded on a SDS-PAGE alongside known concentrations (50, 100, 150, and 200 ng) of recombinant purified DDX3X. Separated proteins were subjected to Western blot analysis with anti-DDX3X A300-A450 (BETHYL) at 1:2000 dilution in 5% milk. The blot was next incubated with a horseradish peroxidase-conjugated secondary antibody, and the bands corresponding to DDX3X were visualized with enhanced chemiluminescent substrate (Westar Nova 2.0, Cyanagen) using a ChemiDoc XRS (Bio-Rad) apparatus. The intensity of the bands was measured by densitometry, and the values obtained for the purified DDX3X were plotted as a function of the protein concentration and analyzed by linear interpolation to derive a reference curve, whose slope corresponded to the estimated intensity (I) \times ng^{-1} (DDX3X) value. This parameter was used to calculate the $I \times \text{ng}^{-1}$ values for the DDX3X in the cell extract, from the intensities of the DDX3X bands in the corresponding cell extract (CE) samples. The mean $I \times \text{ng}^{-1}$ (CE) value was used to calculate the ng of DDX3X \times μL^{-1} of extract and then the total ng of DDX3X present in the extract. This value was divided for the total number of cells used (10^7), to derive the ng DDX3X/cell. On the basis of the known molecular weight of DDX3X, the Avogadro number, and assuming a mean cellular volume of 6.55×10^{-11} L, the final molar concentration of DDX3X per cell was calculated. Each experiment was repeated three times, with each blot carrying a reference curve alongside the extract samples, to account for variations in loading/transfer efficiency. The reference $I \times \text{ng}^{-1}$ (DDX3X) value obtained was anyway comparable across the different experiments ($\pm 20\%$ variation).

ATPase Assay. The ATPase assay was carried out by using the commercial kit Promega ADP-Glo Kinase Assay. The reaction was performed in 30 mM Tris-HCl, 9 mM MgCl_2 , 0.05 mg mL^{-1} bovine serum albumin, 50 μM ATP, and 4 μM DDX3. The reaction was performed following the ADP-Glo Kinase Assay Protocol, and luminescence was measured with MicroBeta TriLux PerkinElmer.

The anti-DDX1 activity was evaluated as previously reported.²⁸

Antiviral Assay. WNV Inhibitory Viral Plaque Reduction Assay. Huh7 cells, derived from human hepatoma (kindly provided from Istituto Toscano Tumori, Core Research Laboratory, Siena, Italy) was used for the inhibitory viral plaque reduction assay. The cell propagation medium was Dulbecco's modified Eagle's medium (DMEM; Sigma, Milano, Italy) supplemented with 10% fetal bovine serum (Sigma) and 1% penicillin/streptomycin (Sigma). WNV (strain of lineage 2) viral stock, consisting of cell-free supernatants of acutely infected Huh7 cells, was aliquoted and stored at -80°C until used. Titration of the viral stocks as a plaque forming unit (PFU) was carried out in Huh7 cells. WNV was used to infect Huh7 cell line in duplicate, and viral plaques were visualized 4 days following infection. Briefly, six-well plates were seeded with 2.5×10^5 cells in 3 mL of growth medium and kept overnight at 37°C with 5% CO_2 . On the day of infection, after removal of the growth medium, cell monolayers at 80–90% confluence were infected with WNV viral stock with a multiplicity of infection (MOI) of 0.1 in a final volume of 0.3 mL and incubated for 1 h at 37°C with 5% CO_2 . Then, cells were washed with phosphate-buffered saline (PBS) 1 \times and 30 μL of dimethyl sulfoxide (DMSO) alone (viral positive control) or with 10-fold serial dilutions of DDX3X inhibitory compounds immediately added in duplicates together

with 300 μL of fresh DMEM complete medium (compound final concentrations of 100, 10, 1, 0.1, and 0.01 μM). 1- β -D-Ribofuranosyl-1,2,4-triazole-3-carboxamide (ribavirin; Sigma) diluted in DMSO was used as inhibitory reference control. Then, the overlay medium composed by 0.5% SeaPlaque Agarose (Lonza, Basel, Switzerland) diluted in propagation medium was added to each well. After 4 days (Huh7) of incubation at 37°C , the monolayers were fixed with methanol (Carlo Erba Chemicals, Milan, Italy) and stained with 0.1% crystal violet (Carlo Erba Chemicals) and the viral titers were calculated by plaque forming unit (PFU) counting. The percent of plaque reduction activity was calculated by dividing the average PFU of treated samples by the average of DMSO-treated samples (viral positive control). Fifty percent inhibitory concentrations (IC_{50}) were calculated using the predicted exponential growth function in Microsoft Excel, which uses existing x - y data to estimate the corresponding anti-DDX3X compound concentration (x) from a known value (y), which in this case was 50% PFU. Mean $\text{IC}_{50} \pm$ standard deviations (S.D.) were calculated using all replicates. All experiments were repeated at least twice. All experimental procedures were conducted under biosafety level 3 containment.

Cytotoxicity Assay. Monolayers of 2.5×10^4 Huh7 cells per well were kept in flat-bottom 96-well culture plates and allowed to adhere overnight. Then, when the cell layers were confluent, the medium was removed, the wells were washed twice with PBS, treated with 100 μL of DMEM, with 10 μL of DMSO alone (cell positive control), or with various concentrations of DDX3X inhibitory compounds under study (compound final concentrations of 100, 10, 1, 0.1, and 0.01 μM) and incubated for 3 days at 37°C in a CO_2 atmosphere. After treatment, an 3-(4,5-dimethylthiazol-2-yl)-2,5-diphenyltetrazolium bromide kit (Roche, Milan, Italy) was used according to the supplier's instructions and the absorbance of each well was determined using a microplate spectrophotometer at a wavelength of 570 nm. Cytotoxicity was calculated by dividing the average optical density of treated samples by the average of DMSO-treated samples (cell positive control).

Virus RNA Quantification and Capsid Protein Detection Assay. Total RNA was extracted and purified from infected and control cells using an RNAeasy mini Kit (Qiagen). Two hundred nanograms of total RNA of each sample in a 20 μL reaction mixture were reverse-transcribed by using the indicated primers (primer PROCf 5' C C T g T g T g A g C T g A C A A A C T T A g T 3' for the transcription of WNV complementary RNA and primer PROCr 5' g C g T T T T A g C A T A T T g A C A g C C 3' for the transcription of WNV genomic RNA) and amplified by real-time PCR in a Rotor-gene 3000 real-time thermal cycler (Corbett Research, Australia) with the following WNV specific primer and probe (primer PROCf 5' C C T g T g T g A g C T g A C A A A C T T A g T 3' and primer PROCr 5' g C g T T T T A g C A T A T T g A C A g C C 3'), and probe PROC-TMD VIC-5' CCTGGTTTCTTAGACATCGAGATCTTCGTGC 3').²⁴ Plasmid calibration standards were used for quantification of the template concentration. The sensibility of the assay was 10 copies.

The specific WNV capsid protein was investigated with Western blot analysis of Huh7-infected cells electrophoresed on 10% SDS-PAGE and then probed with anticapsid protein polyclonal antibody followed by peroxidase-conjugated anti-rabbit IgG polyclonal antibody.

ADME Assay. Chemicals. All solvents and reagents were from Sigma-Aldrich Srl (Milan, Italy), brain polar lipid extract

(porcine) was from Avanti Polar Lipids, INC. (Alabama). Dodecane was purchased from Fluka (Milan, Italy). Pooled male donors 20 mg mL⁻¹ HLM were from BD Gentest-Biosciences (San Jose, California). Milli-Q quality water (Millipore, Milford, MA) was used. Hydrophobic filter plates (MultiScreen-IP, Clear Plates, 0.45 μm diameter pore size), 96-well microplates, and 96-well UV-transparent microplates were obtained from Millipore (Bedford, MA).

Parallel Artificial Membrane Permeability Assay (PAMPA and PAMPA–Blood–Brain Barrier (BBB)). Donor solution (0.5 mM) was prepared by diluting 1 mM dimethyl sulfoxide (DMSO) compound stock solution using phosphate buffer (pH 7.4, 0.025 M). Filters were coated with 5 μL of a 1% (w/v) dodecane solution of phosphatidylcholine or 4 μL of brain polar lipid solution (20 mg mL⁻¹ 16% CHCl₃, 84% dodecane) prepared from CHCl₃ solution 10% w/v, for intestinal permeability and BBB permeability, respectively. Donor solution (150 μL) was added to each well of the filter plate. To each well of the acceptor plate was added 300 μL of solution (50% DMSO in phosphate buffer). All compounds were tested in three different plates on different days. The sandwich was incubated for 5 h at room temperature under gentle shaking. After the incubation time, the plates were separated and samples were taken from both receiver and donor sides and analyzed using LC with UV detection at 280 nm. LC analysis was performed with a PerkinElmer (series 200) instrument equipped with an UV detector (PerkinElmer 785A, UV/vis detector). Chromatographic separation was conducted using a Polaris C18 column (150 × 4.6 mm², 5 μm particle size) at a flow rate of 0.8 mL min⁻¹ with a mobile phase composed of 60% ACN/40% H₂O–formic acid 0.1% for all compounds. Permeability (P_{app}) was calculated according to the following equation with some modification to obtain permeability values in cm s⁻¹

$$P_{app} = \frac{V_D V_A}{(V_D + V_A)At} - \ln(1 - r)$$

where V_A is the volume in the acceptor well, V_D is the volume in the donor well (cm³), A is the “effective area” of the membrane (cm²), t is the incubation time (s), and r is the ratio between drug concentration in the acceptor and equilibrium concentration of the drug in the total volume ($V_D + V_A$). Drug concentration is estimated by using the peak area integration. Membrane retentions (%) were calculated according to the following equation

$$\%MR = \frac{[r - (D + A)]100}{Eq}$$

where r is the ratio between drug concentration in the acceptor and equilibrium concentration and D , A , and Eq represented drug concentration in the donor, acceptor and equilibrium solution, respectively.

Water Solubility Assay. Compound 1 (1 mg) was added to 1 mL of water. The sample was shaken in a shaker bath at room temperature for 24–36 h. The suspensions were filtered through a 0.45 μm nylon filter (Acrodisc) and the solubilized compound determined by LC-MS-MS assay. The determination was performed in triplicate. For the quantification was used an LC-MS system consisting of a Varian apparatus (Varian Inc.), including a vacuum solvent degassing unit, two pumps (212-LC), a Triple Quadrupole MSD (mod. 320-LC) mass spectrometer with ES interface and Varian MS Workstation System Control vers. 6.9 software. Chromatographic separation

was obtained using a Pursuit C18 column (50 × 2.0 mm²) (Varian) with 3 μm particle size and gradient elution: eluent A being ACN and eluent B consisting of an aqueous solution of formic acid (0.1%). The analysis started with 0% of eluent A, which was linearly increased up to 70% in 10 min, then slowly increased up to 98% up to 15 min. The flow rate was 0.3 mL min⁻¹, and the injection volume was 5 μL. The instrument operated in positive mode and parameters were: detector 1850 V, drying gas pressure 25.0 psi, desolvation temperature 300.0 °C, nebulizing gas 45.0 psi, needle 5000 V, and shield 600 V. Nitrogen was used as nebulizer gas and drying gas. Collision-induced dissociation was performed using argon as the collision gas at a pressure of 1.8 mTorr in the collision cell. Quantification of the single compound was made by comparison with apposite calibration curves realized with standard solutions in methanol.

Microsomal Stability Assay. Each compound in DMSO solution was incubated at 37 °C for 60 min in 125 mM phosphate buffer (pH 7.4) and 5 μL of human liver microsomal protein (0.2 mg mL⁻¹), in the presence of a NADPH-generating system at a final volume of 0.5 mL (compounds' final concentration, 50 μM); DMSO did not exceed 2% (final solution). The reaction was stopped by cooling in ice and adding 1.0 mL of acetonitrile. The reaction mixtures were then centrifuged, and the parent drug and metabolites were subsequently determined by LC-UV-MS. Chromatographic analysis was performed with an Agilent 1100 LC/MSD VL system (G1946C) (Agilent Technologies, Palo Alto, CA) constituted by a vacuum solvent degassing unit, a binary high-pressure gradient pump, an 1100 series UV detector, and an 1100 MSD model VL benchtop mass spectrometer. Chromatographic separation was obtained using a Varian Polaris C18-A column (150 × 4.6 mm², 5 μm particle size) and gradient elution: eluent A being ACN and eluent B consisting of an aqueous solution of formic acid (0.1%). The analysis started with 2% of eluent A, which was rapidly increased up to 70% in 12 min, then slowly increased up to 98% in 20 min. The flow rate was 0.8 mL min⁻¹, and the injection volume was 20 μL. The Agilent 1100 series mass spectra detection (MSD) single-quadrupole instrument was equipped with the orthogonal spray API-ES (Agilent Technologies, Palo Alto, CA). Nitrogen was used as nebulizing and drying gas. The pressure of the nebulizing gas, the flow of the drying gas, the capillary voltage, the fragmentor voltage, and the vaporization temperature were set at 40 psi, 9 L min⁻¹, 3000 V, 70 V, and 350 °C, respectively. UV detection was monitored at 280 nm. The LC-ESI-MS determination was performed by operating the MSD in the positive-ion mode. Spectra were acquired over the scan range m/z 100–1500 using a step size of 0.1 u. The percentage of a nonmetabolized compound was calculated by comparison with reference solutions.

■ ASSOCIATED CONTENT

☛ Supporting Information

The Supporting Information is available free of charge on the ACS Publications website at DOI: 10.1021/acs.jmedchem.8b01403.

Western blot experiments for the quantification of DDX3X in cell extracts, representative IC₅₀ curves, anti-WNV dose–response and cytotoxicity curves (PDF)

Molecular formula strings (CSV)

AUTHOR INFORMATION

Corresponding Author

*E-mail: botta.maurizio@gmail.com.

ORCID

Annalaura Brai: 0000-0001-6395-9348

Giovanni Maga: 0000-0001-8092-1552

Maurizio Botta: 0000-0003-0456-6995

Author Contributions

The manuscript was written through contributions of all authors. All authors have given approval to the final version of the manuscript.

Notes

The authors declare no competing financial interest.

ACKNOWLEDGMENTS

This work was supported by First Health Pharmaceuticals B.V. (Amsterdam) for M.B. Financial support has been also provided by Tuscany Region Grant FAS Salute 2014 (DD 4042/2014) to M.B. and S.G.

DEDICATION

This paper is dedicated to the memory of Pier Giovanni Baraldi, Emeritus Professor at the University of Ferrara and beloved chemist.

ABBREVIATIONS

WNV, West Nile virus; *t*-BuONO, *tert*-butyl nitrite; ADME, absorption, distribution, metabolism, and excretion

REFERENCES

- (1) Chancey, C.; Grinev, A.; Volkova, E.; Rios, M. The global ecology and epidemiology of West Nile Virus. *BioMed Res. Int.* **2015**, *2015*, No. 376230.
- (2) European Centre for Disease Prevention and Control. Epidemiological update: West Nile virus transmission season in Europe, 2017 [online], 2018. Available at: <https://ecdc.europa.eu/en/news-events/epidemiological-update-west-nile-virus-transmission-season-europe-2017> (Accessed 22 Aug, 2018).
- (3) Cdc.gov. Preliminary maps & data for 2017 | West Nile Virus | CDC [online], 2018. Available at: <https://www.cdc.gov/westnile/statsmaps/preliminarymapsdata2017/index.html> (Accessed 22 Aug, 2018).
- (4) European centre for disease prevention and control. Weekly Updates: 2018 West Nile Fever Transmission Season [online], 2018. Available at: <https://ecdc.europa.eu/en/west-nile-fever/surveillance-and-disease-data/disease-data-ecdc> (Accessed 31 Aug, 2018).
- (5) Wilder-Smith, A.; Gubler, D. J.; Weaver, S. C.; Monath, T. P.; Heymann, D. L.; Scott, T. W. Epidemic arboviral diseases: priorities for research and public health. *Lancet Infect. Dis.* **2017**, *17*, e101–e106.
- (6) Mercorelli, B.; Palù, G.; Loregian, A. Drug repurposing for viral infectious diseases: how far are we? *Trends Microbiol.* **2018**, *26*, 865–876.
- (7) Valiente-Echeverría, F.; Hermoso, M. A.; Soto-Rifo, R. RNA helicase DDX3: at the crossroad of viral replication and antiviral immunity. *Rev. Med. Virol.* **2015**, *25*, 286–299.
- (8) Chen, S.; Chahar, H. S.; Abraham, S.; Wu, H.; Pierson, T. C.; Wang, X. A.; Manjunath, N. Ago-2-mediated slicer activity is essential for anti-flaviviral efficacy of RNAi. *PLoS One* **2011**, *6*, No. e27551.
- (9) Chahar, H. S.; Chen, S.; Manjunath, N. P-body components LSM1, GW182, DDX3, DDX6 and XRN1 are recruited to WNV replication sites and positively regulate viral replication. *Virology* **2013**, *436*, 1–7.
- (10) Owsianka, A. M.; Patel, A. H. Hepatitis C virus core protein interacts with a human DEAD box protein DDX3. *Virology* **1999**, *257*, 330–340.

(11) Mamiya, N.; Worman, H. J. Hepatitis C virus core protein binds to a DEAD box RNA helicase. *J. Biol. Chem.* **1999**, *274*, 15751–15756.

(12) Ariumi, Y.; Kuroki, M.; Abe, K.-i.; Dansako, H.; Ikeda, M.; Wakita, T.; Kato, N. DDX3 DEAD-box RNA helicase is required for hepatitis C virus RNA replication. *J. Virol.* **2007**, *81*, 13922–13926.

(13) Li, C.; Ge, L. L.; Li, P. P.; Wang, Y.; Dai, J. J.; Sun, M. X.; Huang, L.; Shen, Z. Q.; Hu, X. C.; Ishag, H.; Mao, Z. Cellular DDX3 regulates Japanese encephalitis virus replication by interacting with viral untranslated regions. *Virology* **2014**, *449*, 70–81.

(14) Noble, C. G.; Chen, Y. L.; Dong, H.; Gu, F.; Lim, S. P.; Schul, W.; Wang, Q. Y.; Shi, P. Y. Strategies for development of Dengue virus inhibitors. *Antiviral Res.* **2010**, *85*, 450–462.

(15) Benfield, C. T.; Ren, H.; Lucas, S. J.; Bahsoun, B.; Smith, G. L. Vaccinia virus protein K7 is a virulence factor that alters the acute immune response to infection. *J. Gen. Virol.* **2013**, *94*, 1647–1657.

(16) Tintori, C.; Brai, A.; Fallacara, A. L.; Fazi, R.; Schenone, S.; Botta, M. Protein-protein interactions and human cellular cofactors as new targets for HIV therapy. *Curr. Opin. Pharmacol.* **2014**, *18*, 1–8.

(17) Radi, M.; Falchi, F.; Garbelli, A.; Samuele, A.; Bernardo, V.; Paolucci, S.; Baldanti, F.; Schenone, S.; Manetti, F.; Maga, G.; Botta, M. Discovery of the first small molecule inhibitor of human DDX3 specifically designed to target the RNA binding site: towards the next generation HIV-1 inhibitors. *Bioorg. Med. Chem. Lett.* **2012**, *22*, 2094–2098.

(18) Brai, A.; Fazi, R.; Tintori, C.; Zamperini, C.; Bugli, F.; Sanguinetti, M.; Stigliano, E.; Esté, J.; Badia, R.; Franco, S.; Martinez, M. A.; Martinez, J. P.; Meyerhans, A.; Saladini, F.; Zazzi, M.; Garbelli, A.; Maga, G.; Botta, M. Human DDX3 protein is a valuable target to develop broad spectrum antiviral agents. *Proc. Natl. Acad. Sci. U.S.A.* **2016**, *113*, 5388–5393.

(19) Fazi, R.; Tintori, C.; Brai, A.; Selvaraj, M. K.; Bavagnoli, L.; Garbelli, A.; Maga, G.; Botta, M. Homology model-based virtual screening for the identification of helicase human DDX3X inhibitors. *J. Chem. Inf. Model.* **2015**, *55*, 2443–2454.

(20) Yedavalli, V. S.; Zhang, N.; Cai, H.; Zhang, P.; Starost, M. F.; Hosmane, R. S.; Jeang, K. T. Ring expanded nucleoside analogues inhibit RNA helicase and intracellular human immunodeficiency virus type 1 replication. *J. Med. Chem.* **2008**, *51*, 5043–5051.

(21) Yedavalli, V. S.; Neuveut, C.; Chi, Y. H.; Kleiman, L.; Jeang, K. T. Requirement of DDX3X DEAD box RNA helicase for HIV-1 Rev-RRE export function. *Cell* **2004**, *119*, 381–392.

(22) Chaudhari, S. R.; Mogurampelly, S.; Suryaprakash, N. Engagement of CF₃ group in N-H...F-C hydrogen bond in the solution state: NMR spectroscopy and MD simulation studies. *J. Phys. Chem. B* **2013**, *117*, 1123–1129.

(23) Bol, G. M.; Vesuna, F.; Xie, M.; Zeng, J.; Aziz, K.; Gandhi, N.; Levine, A.; Irving, A.; Korz, D.; Tantravedi, S.; Heerma van Voss, M. R.; Gabrielson, K.; Bordt, E. A.; Polster, B. M.; Cope, L.; van der Groep, P.; Kondaskar, A.; Rudek, M. A.; Hosmane, R. S.; van der Wall, E.; van Diest, P. J.; Tran, P. T.; Raman, V. Targeting DDX3 with a small molecule inhibitor for lung cancer therapy. *EMBO Mol. Med.* **2015**, *7*, 648–669.

(24) Linke, S.; Ellerbrok, H.; Niedrig, M.; Nitsche, A.; Pauli, G. Detection of West Nile virus lineages 1 and 2 by real-time PCR. *J. Virol. Methods* **2007**, *146*, 355–358.

(25) Verdonk, M. L.; Cole, J. C.; Hartshorn, M. J.; Murray, C. W.; Taylor, R. D. Improved protein-ligand docking using GOLD. *Proteins* **2003**, *52*, 609–623.

(26) Cole, J. C.; Nissink, J. W. M.; Taylor, R. Protein–Ligand Docking and Virtual Screening with GOLD. In *Virtual Screening in Drug Discovery*; Shoichet, B., Alvarez, J., Eds.; Taylor & Francis CRC Press: Boca Raton, Florida, 2005.

(27) PyMOL Molecular Graphics System, version 0.99; Schrödinger, LLC: New York, NY, 2011.

(28) Maga, G.; Falchi, F.; Radi, M.; Botta, L.; Casaluze, G.; Bernardini, M.; Irannejad, H.; et al. Toward the discovery of novel anti-HIV drugs. Second-generation inhibitors of the cellular ATPase DDX3 with improved anti-HIV activity: synthesis, structure-activity relationship

analysis, cytotoxicity studies, and target validation. *ChemMedChem* 2011, 6, 1371–1389.

Article

Synthesis and Antiviral Activity of Novel 1,3,4-Thiadiazole Inhibitors of DDX3X

Annalaura Brai ^{1,†} , Stefania Ronzini ^{1,†} , Valentina Riva ^{2,†}, Lorenzo Botta ¹, Claudio Zamperini ¹ , Matteo Borgini ¹ , Claudia Immacolata Trivisani ¹, Anna Garbelli ², Carla Pennisi ², Adele Boccuto ³, Francesco Saladini ³, Maurizio Zazzi ³ , Giovanni Maga ^{2,*} and Maurizio Botta ^{1,4,*}

¹ Dipartimento Biotecnologie, Chimica e Farmacia, Università degli Studi di Siena, Via A. Moro 2, I-53100 Siena, Italy; annalaura.brai@gmail.com (A.B.); ronzinis@gmail.com (S.R.); lor.botta83@gmail.com (L.B.); claudiozamperini@yahoo.it (C.Z.); borgini.m4@gmail.com (M.B.); c.trivisani@gmail.com (C.I.T.)

² Istituto di Genetica Molecolare, IGM-CNR “Luigi Luca Cavalli-Sforza”, Via Abbiategrasso 207, I-27100 Pavia, Italy; valentina.riva01@universitadipavia.it (V.R.); agarbelli@gmail.com (A.G.); carlapennisi@outlook.it (C.P.)

³ Dipartimento di Biotecnologie Mediche, Università degli Studi di Siena, 53100 Siena, Italy; adele.boccuto@gmail.com (A.B.); france.saladini@gmail.com (F.S.); maurizio.zazzi@gmail.com (M.Z.)

⁴ Biotechnology College of Science and Technology, Temple University, BioLife Science Building, Suite 333, 1900 North 12th Street, Philadelphia, PA 19122, USA

* Correspondence: giovanni.maga@igm.cnr.it (G.M.); botta.maurizio@gmail.com (M.B.)

† These authors contributed equally to this work.

Received: 2 September 2019; Accepted: 4 October 2019; Published: 4 November 2019



Abstract: The human ATPase/RNA helicase X-linked DEAD-box polypeptide 3 (DDX3X) emerged as a novel therapeutic target in the fight against both infectious diseases and cancer. Herein, a new family of DDX3X inhibitors was designed, synthesized, and tested for its inhibitory action on the ATPase activity of the enzyme. The potential use of the most promising derivatives it has been investigated by evaluating their anti-HIV-1 effects, revealing inhibitory activities in the low micromolar range. A preliminary ADME analysis demonstrated high metabolic stability and good aqueous solubility. The promising biological profile, together with the suitable in vitro pharmacokinetic properties, make these novel compounds a very good starting point for further development.

Keywords: DDX3X; HIV-1; host proteins; antivirals

1. Introduction

Human ATPase/RNA helicase X-linked DEAD-box polypeptide 3 (DDX3X) belongs to the DEAD-box proteins, a large family of ATP-dependent RNA helicases that are involved in many aspects of RNA metabolism [1]. In 2004, Yedavalli et al. highlighted its fundamental role in HIV-1 life cycle as a shuttle protein that is able to export the viral RNA from the nucleus to the cytoplasm [2], subsequently Ishaq and coworkers [3] demonstrated that DDX3X knockdown suppressed HIV replication without inducing apoptosis. Besides HIV, DDX3X is known to be an essential host factor for other major human viral pathogens, such as Hepatitis B and C viruses [4–6], as well as for emerging viruses, such as Dengue virus (DENV), West-Nile virus (WNV), and Japanese Encephalitis Virus (JEV) [7,8].

DDX3X has multiple enzymatic activities (ATPase and RNA helicase) and functional domains that might be targeted by potential inhibitors [9,10]. Drug discovery activity in this area has been mostly oriented towards ATPase inhibitors, while only few efforts have been devoted to affect the helicase activity of DDX3X by targeting the RNA binding pocket with small molecules [11–14]. Figure 1 shows the structures of known DDX3X ATPase inhibitors. The first ATPase DDX3X inhibitors were discovered

in 2008 [15]. Among them, we identified **FE15** through a virtual screening approach. This compound, characterized by a rhodanine scaffold, showed low micromolar potency of inhibition against the DDX3X ATPase activity and it was able to inhibit the HIV-1 replication in MT4 cells with an EC_{50} of 86.7 μ M, without showing cytotoxicity. Similarly, the ring expanded nucleosides (RENs) were found able to inhibit the ATP dependent activity of DDX3X and suppress HIV-1 replication in T cells and monocyte-derived macrophages [16]. In 2011, through a hit optimization protocol, we identified the second generation of rhodanine DDX3X inhibitors endowed with an improved activity profile (as an example **FE109** showed a K_i of 0.2 μ M) [17]. In parallel, some REN derivatives were synthesized, among them compound **NZ51** has been reported to inhibit the ATP dependent helicase activity of DDX3X, as well as the proliferation of cancer cells expressing high levels of DDX3X [18]. Raman and coworkers have recently reported compound **RK-33** containing the diimidazo[4,5-d;4',5'-f] [1,3]diazepine ring. **RK-33** has been extensively studied as an anticancer compound, and its spectrum of activity includes different tumor cell lines derived from lung (A-549 and H-460), prostate (PC-3), breast (MCF-7 and MDA-MB-231), and ovarian (OVCAR-3) cancers [19–21]. At the same time, **ketorolac** salt has been identified as a novel DDX3X inhibitor able to affect the ATPase activity and endowed with anticancer activity against oral squamous cell carcinoma (OSCC) cell lines [22].

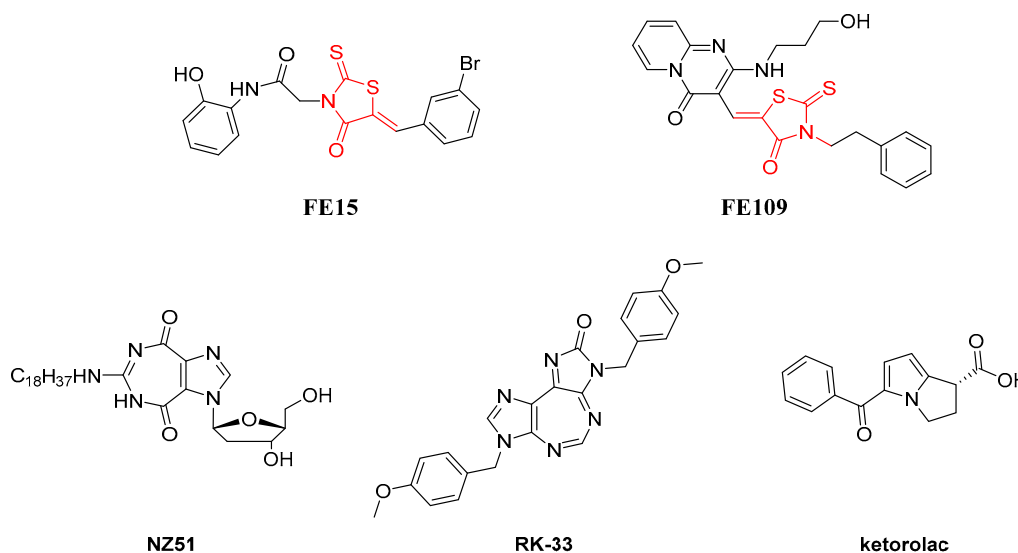


Figure 1. Two-dimensional (2D) Structures of previously identified DDX3X ATPase inhibitors.

Herein, docking studies were employed to guide the design of new DDX3X inhibitors endowed with a thiadiazole nucleus. Being the rhodanines promiscuous binders with poor selectivity and also considered to be Pan Assay Interference Compounds (PAINS) [23], we pursued the idea of replacing the rhodanine moiety with a different ring maintaining profitable interactions within the ATP binding pocket of DDX3X. As a result, a new series of inhibitors of the ATPase activity of DDX3X was identified that showed good anti-HIV activity. Taken together, our results led to the identification of a new family of DDX3X inhibitors that can be used as a starting point to identify novel preclinical candidates to treat viral diseases that are caused by DDX3X dependent pathogens.

2. Results

2.1. Molecular Modeling

Docking simulations were performed on the known ATPase DDX3X inhibitors **RK33** and **ketorolac** in order to study the key molecular interactions on the basis of their inhibitory activity and the predicted binding modes were compared to those previously published for the active rhodanine derivative **FE15**

as well as with that of the crystallized ligand AMP (Figure 2). Calculations were performed according to the already published protocol [15].

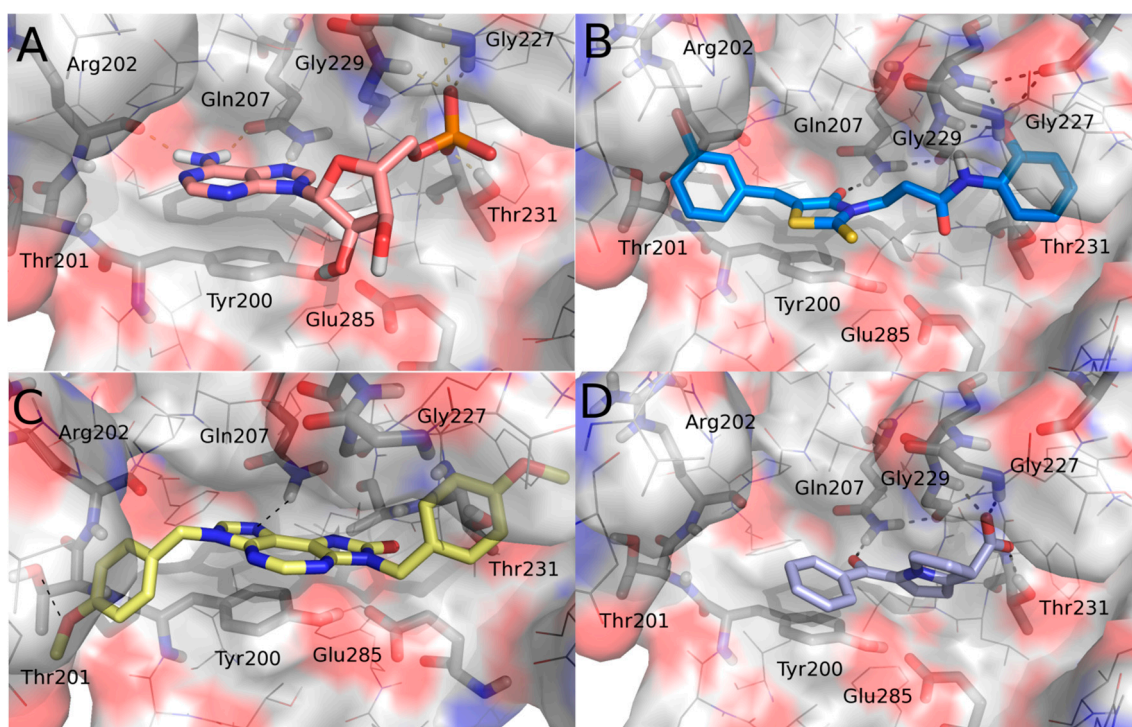


Figure 2. Binding poses of (A) AMP (salmon), (B) FE15 (blue), (C) RK-33 (yellow), and (D) ketorolac (periwinkle) into the ATP pocket of human DDX3. For the sake of clarity, only a few key residues are labeled, hydrogen atoms are omitted, and hydrogen-bonding interactions are represented by black dashed lines. Compounds and key amino acids are in stick representation.

An analysis of the interactions established by the studied DDX3X inhibitors within the ATP binding pocket was performed. Common interactions emerged from such investigation. In detail, the studied inhibitors established a hydrogen bond with Gln207 and a π - π interaction with Tyr200 that resulted in being crucial for their inhibitory activity. Furthermore, FE15 and ketorolac made polar contacts with Gly227 and Gly229, mimicking the phosphate group of AMP. Ketorolac, being endowed with an acidic group, better reproduced the phosphate interactions and indeed additionally interacted with Thr231. FE15 and RK-33 both also occupied a region delineated by the amino acids Thr201 and Arg202. Taking into consideration all of the interactions made by the known active ligands, a new series of compounds was designed that contains all of the features identified as being crucial for the activity against DDX3X. The rhodanine group included in our previous hit compound, FE15, was discarded. Indeed, rhodanine derivatives are promiscuous binders that have been associated with multiple biological activities. Furthermore, rhodanines have been described as PAINS and highly problematic frequent hitters [23,24]. Viceversa, the thiadiazole ring, is an important framework in medicinal chemistry. Thiadiazole is a bioisostere of pyrimidine and oxadiazole and given the prevalence of pyrimidine in nature it is unsurprising that thiadiazoles exhibit significant therapeutic potential. Accordingly, a number of thiadiazole-containing drugs are currently on the market [25]. For the above reasons, we decided to replace the rhodanine nucleus of the hit compound FE15 with a 1,3,4-thiadiazole ring.

Docking studies predicted good poses for the novel series of compounds within the ATP binding pocket of DDX3X. The binding mode of compound 23 (as representative of the novel series) revealed its ability to establish (Figure 3), similarly to the active inhibitors RK33, ketorolac, and FE15, hydrogen bond interactions with the crucial residues Gln207, Gly227, Gly229, Thr231, Thr201, and Arg202.

Furthermore, its binding mode is stabilized by a π - π contact between the thiadiazole heterocycle and the side-chain of Tyr200. Starting from this result, a small library of 1,3,4-thiadiazole derivatives has been rationally designed and synthesized.

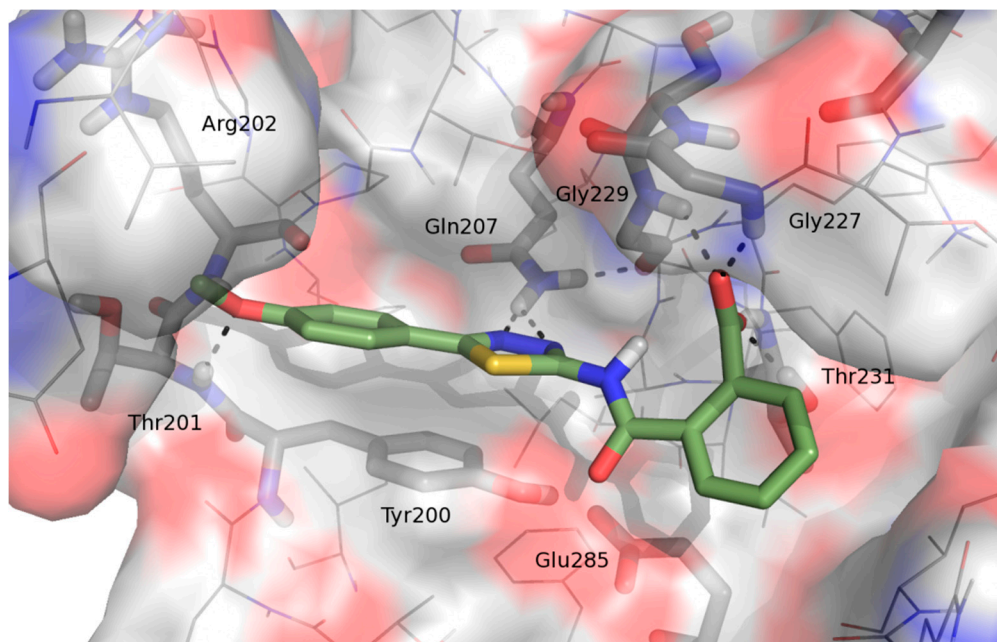
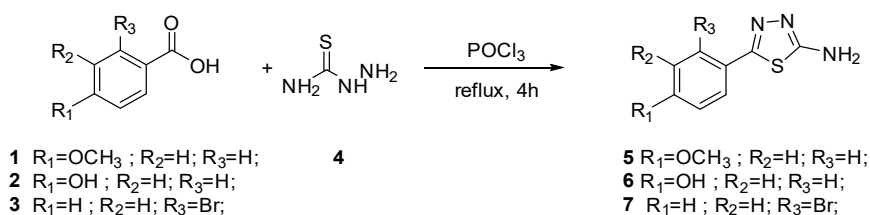


Figure 3. Binding mode of **1** within the ATP binding pocket of human DDX3.

2.2. Chemistry

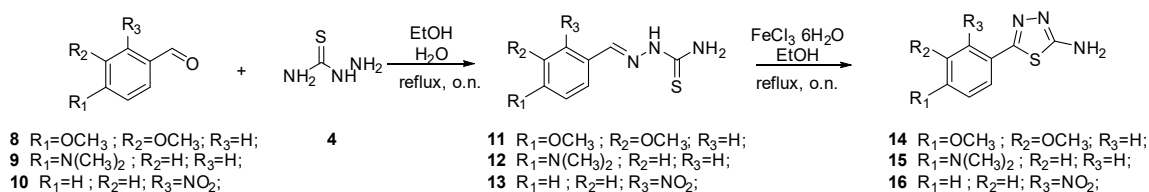
The synthesis of final compounds **23–28** and **29–32** first entailed the synthesis of the key intermediates **5–7** and **14–16**.

According to Scheme 1, **5**, **6**, and **7** were obtained by condensation of the thiosemicarbazide **4** with the opportune benzoic acid **1–3**.



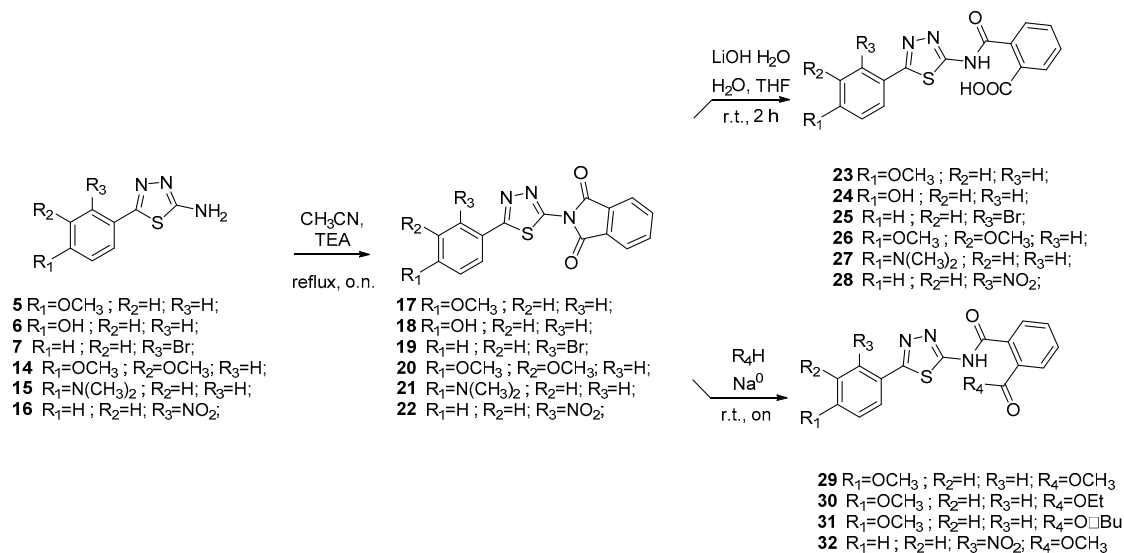
Scheme 1. Synthesis of intermediates **5–7**.

The synthesis of intermediates **14**, **15**, and **16** is depicted in Scheme 2. Aromatic aldehydes **8–10** reacted with thiosemicarbazide **4** to furnish thiosemicarbazones **11–13**. Subsequent cyclization in the presence of FeCl_3 provides intermediates **14–16**.

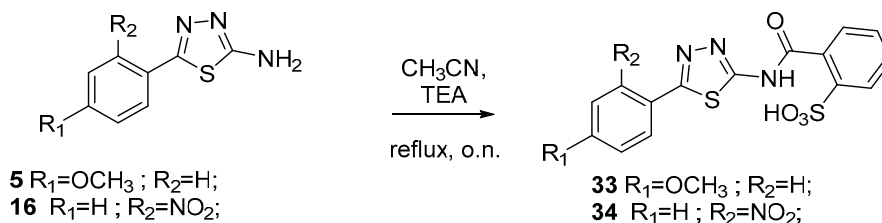


Scheme 2. Synthesis of intermediates **14–16**.

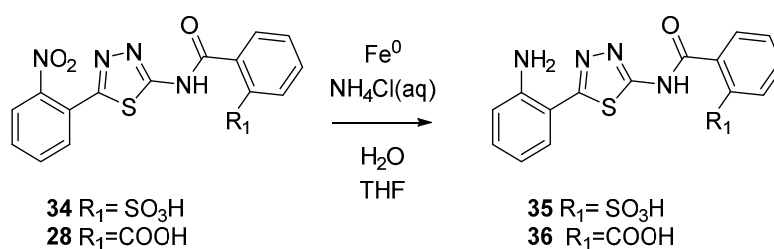
Intermediates 5–7 and 14–16 were reacted with phthalimide to furnish compounds 17–22. Subsequent hydrolysis in presence of LiOH provides final acids 23–28. Esters 29–32 were synthesized by the reaction of acids 23–28 with the opportune alcohols (Scheme 3). As depicted in Scheme 4 sulfonic acids 33 and 34 were produced by reacting between aminothiazoles 5 and 16 and 2-Sulfobenzoyl cyclic anhydride. Finally, reduction of compounds 34 and 28 led to anilines 35 and 36 (Scheme 5).



Scheme 3. Synthesis of final compounds 23–32.



Scheme 4. Synthesis of final compounds 33–34.



Scheme 5. Synthesis of final compounds 35 and 36.

2.3. Biological Evaluation

Derivatives 23–36 were next evaluated for their ability to inhibit the ATPase activity of DDX3X.

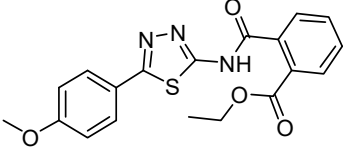
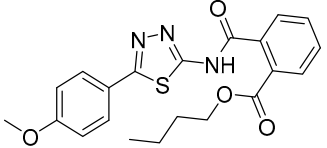
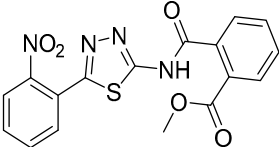
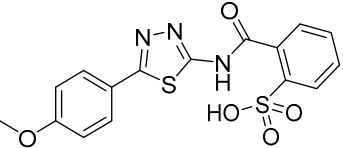
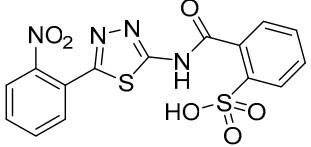
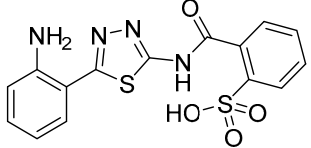
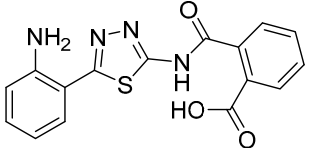
As reported in Table 1, compounds were characterized by K_i values in the low micromolar range against the ATPase binding site, confirming the validity of the reported approach. The phthalimido compound 17 was found to be completely inactive, probably due to its chemical instability. The para-methoxy derivative 23 and its corresponding phenol derivative 24 are endowed with the best affinity values (K_i) of 1.5 μM and 1.9 μM , respectively. The substitution of acidic function with ester slightly reduced the activities, being derivatives 29, 30 and 31 respectively 12.5, 16.8 and 18.8 times less active than compound 23. The introduction of electron withdrawing groups, such as bromine and nitro in ortho position, abolished (compound 25) or reduced the activity (compound 28), despite even in this

case the substitution of the carboxylic acid with a methyl ester (compound **32**) annulled enzymatic inhibition. The introduction of dimethylamino group in para position slightly decreased the activity in compound **27** ($K_i = 11.9$), while the introduction of amino group induced the total loss of inhibitory capability of compound **36**. Finally, the replacement of the carboxylic group with sulfonic acid was detrimental for the activity of compounds **33**, **34**, and **35**.

Table 1. Biological evaluation of selected compounds against DDX3X ATPase and HIV-1 infected cells [a].

Cpd. ID	Structure	DDX3X ATPase	HIV-1 (NL4-3)	
		K_i [b] (μM)	IC_{50} [b] (μM)	CC_{50} [c,d] (μM)
17		>50	NT	NT
23		1.3 ± 0.2	>50	>200
24		1.9 ± 0.4	2.8 ± 1.5	125
25		NA	NT	NT
26		NA	NT	NT
27		11.9 ± 1.9	>50	130
28		18.3 ± 1.8	42.3 ± 5.2	74
29		15.6	10	45

Table 1. Cont.

Cpd. ID	Structure	DDX3X ATPase	HIV-1 (NL4-3)	
		K _i ^[b] (μM)	IC ₅₀ ^[b] (μM)	CC ₅₀ ^[c,d] (μM)
30		20.1 ± 2.1	>50	>200
31		23.5 ± 2.5	16.0 ± 10	100
32		NA	NT	NT
33		NA	NT	NT
34		35.4 ± 3.5	>50	110
35		20.1 ± 2.1	>50	130
36		NA	NT	NT

^[a] Data represent mean ± standard deviation of three experiments. ^[b] K_i, apparent dissociation constant for inhibitor binding; IC₅₀: half maximal inhibitory concentration or needed concentration to inhibit 50% viral replication. ^[c] CC₅₀ Cytotoxic concentration 50 or needed concentration to induce 50% death of non-infected cells. ^[d] Evaluated on H9 cells. NA: not active; NT: not tested.

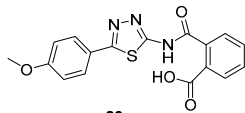
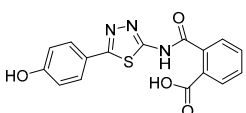
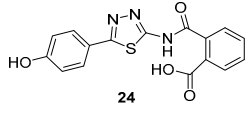
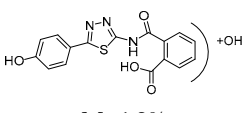
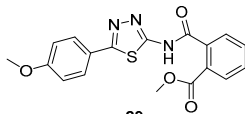
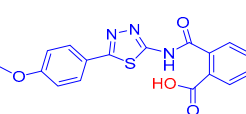
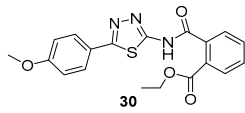
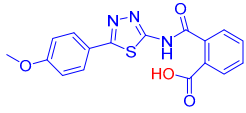
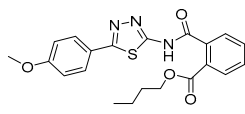
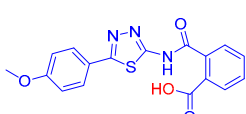
Compounds that were endowed of the best anti-enzymatic activity values were then essayed against HIV-1 in H9 cells. As reported in Table 1, esters derivatives **29** and **31** had promising antiviral activity values of 36 μM and 16 μM. However, compound **28** had some antiviral activity that can be attributable to its cytotoxic effect (SI = 1.7). The best result is represented by compound **24**, characterized by a promising antiviral activity of 3.9 μM without signs of cytotoxicity (CC₅₀ = 125 μM, SI = 45). Strikingly, its p-methoxy derivative **23** was found to be inactive. The reasons are unknown and under investigation.

2.4. ADME Assays

Selected compounds were then analyzed *in vitro* for liver microsomal stability, membrane passive permeability, and aqueous solubility at pH 7.4.

Microsomal metabolic stability was evaluated by incubating each compound at 37 °C for 60 min. in phosphate buffer in presence of human liver microsomes. The reaction mixtures were then centrifuged, and the parent drug and metabolites were subsequently determined by LC-UV-MS. As reported in Table 2, compounds **23** and **24** had good metabolic stability, and only little percentage of the parent compound was metabolized into the dealkylated and into the oxidized derivatives. Contrarily, esters **29–31** revealed low stability, and they were rapidly converted into their corresponding carboxylic acids. In particular, compound **29** was rapidly converted into methoxy derivative **23** and phenol derivative **24**.

Table 2. *In vitro* ADME studies of selected compounds.

CPD ID	Metabolism ^a	AppP ^b	AqS ^c
 23 P 98.1%	 M ₁ 1.9%	<0.1 (0%)	3.3 (−5.03)
 24 P 98.8%	 M ₁ 1.2%	<0.1 (0%)	27.8 (−4.08)
 29 P 25.3%	 M ₁ 61.7%	0.7 (36%)	0.5 (−5.87)
 30 P 75.7%	 M ₁ 22.3	2.1 (4.6%)	<0.1 (>−6)
 31 P 53.8%	 M ₁ 42.8%	6.1 (25.9%)	<0.1 (>−6)

^a Human Liver Microsomal Metabolic Stability expressed as percentage of unmodified parent drug, metabolites M₁ and M₂ are reported. ^b Apparent permeability reported in cm·s^{−1}. ^c Aqueous solubility expressed as μg/mL and as Log of molar concentration.

Kinetic solubility was calculated adding 1 mg of compound into 1 mL of water. After 24 h of stirring at 27 °C, the mixture was filtered and the quantity of solubilized compound determined by LC-MS-MS. As reported in Table 1, compounds **23**, **24**, and **29** showed very promising solubility values. By contrast, esters **30** and **31** due to their lipophilicity have values outside the recommended range (−2 < LogS < −6).

Finally, we evaluated passive membrane permeability (AppP) while using Parallel Artificial Membrane Permeability Assay (PAMPA). The quantity of compound able to diffuse through a semipermeable artificial membrane was calculated by LC-MS-MS. As reported in Table 1, acids **23** and

24 showed low AppP, in contrast esters derivatives **29–31** possessing very good permeability values, directly proportional to the length of their sidechains.

3. Experimental Section

3.1. General Procedures

The reagents were from Sigma-Aldrich (Milan, Italy), Alfa Aesar (Kandel, Germany) and Merck. Commercially available CH_2Cl_2 and MeOH were dried to remove calcium hydride or magnesium methoxide contaminants.

Anhydrous reactions were performed at positive pressure in dry N_2 or argon atmosphere. TLC was carried out on Merck silica gel 60 F254 TLC plates. Flash chromatography was performed on Merck 60 silica gel, 23–400 mesh, columns.

For NMR spectra, a Bruker Avance DPX400 spectrometer (Bruker, Billerica, MA, USA) at 400 MHz for ^1H -NMR or 100 MHz for ^{13}C -NMR was used. Reported chemical shifts are relative to tetramethylsilane at 0.00 ppm. The abbreviations used for 1H patterns were: s = singlet, d = doublet, t = triplet, q = quartet, quint = quintet, sx = sextet, sept = septet, m = multiplet, br = broad signal, and br s = broad singlet.

For mass spectra (MS), an Agilent 1100 LC/MSD VL system (G1946C, Agilent Technologies, Palo Alto, CA, USA) with a 0.4 mL/min. flow rate was used in a binary solvent system 25 of 95:5 methyl alcohol/water. UV were monitored at 254 nm. Positive and negative mode scanning for mass spectra acquisition over the mass range was used.

3.1.1. General Procedure for the Synthesis of Amino Thiazoles **5–7**

A mixture of the opportune substituted benzoic acid (6.57 mmol), thiosemicarbazide (9.85 mmol) and phosphorus oxychloride (5 mL) was stirred at 75 °C for 4 h under N_2 atmosphere. After cooling to room temperature, water was added and the reaction mixture was further refluxed for 4 h. The mixture was cooled and basified to pH 8 by the addition of 1N $\text{NaOH}_{(\text{aq})}$ solution. The resulting mixture was then extracted three times with EtOAc and then washed with water. Organic layer was dried over Na_2SO_4 and evaporated under reduced pressure. The crude mass was recrystallized from EtOH. The compounds were obtained as light-yellow solids in a yield of 75–80%.

5-(4-Methoxyphenyl)-1,3,4-thiadiazol-2-amine (5): crystallization in EtOH. Yellow solid, yield 75%. ^1H -NMR (400 MHz, Acetone): δ 7.73–7.71 (d, J = 8.0 Hz, 2H), 7.01–6.99 (d, J = 8.0 Hz, 2H), 6.56 (bs, 2H), 3.84 (s, 3H) ppm. LC-MS (ES): m/z 230 $[\text{M} + \text{Na}]^+$.

4-(5-Amino-1,3,4-thiadiazol-2-yl)phenol (6): crystallization in EtOH. Yellow solid, yield 30%. ^1H -NMR (400 MHz, Acetone): δ 8.88 (bs, 1H), 7.65–7.64 (d, J = 5.2 Hz, 2H), 6.92–6.91 (d, J = 5.2 Hz, 2H), 6.57 (bs, 2H) ppm.

5-(2-Bromophenyl)-1,3,4-thiadiazol-2-amine (7): Purification eluent DCM/MeOH 98:2, yield 50%, yellow solid. ^1H -NMR (400 MHz, CDCl_3): δ 7.95–7.93 (d, J = 8.0 Hz, 1H), 7.68–7.66 (d, J = 8.0 Hz, 1H), 7.42–7.38 (t, J = 8.0 Hz, 1H), 7.32–7.30 (t, J = 8.0 Hz, 1H), 7.26 (bs, 2H) ppm.

3.1.2. General Procedure for the Synthesis of Thiosemicarbazones **11–13**

The opportune aromatic aldehyde **8–10** (40 mmol) was dissolved in warm EtOH was added to an aqueous solution of thiosemicarbazide (40 mmol) with continuous stirring. After 1 h, the white solid that formed was filtered off as pure **11–13**.

(2-(3,4-Dimethoxybenzylidene)hydrazine-1-carbothioamide (11): crystallization in EtOH. Yellow solid, yield 60%. ^1H -NMR (400 MHz, $\text{DMSO}-d_6$): δ 11.20 (bs, 1H), 8.07 (s, 1H), 7.88 (s, 1H), 7.43 (bs, 2H), 7.06–7.04 (d, J = 8.0 Hz, 1H), 6.88–6.86 (d, J = 8.0 Hz, 1H), 3.73 (s, 3H), 3.70 (s, 3H) ppm.

2-(4-(Dimethylamino)benzylidene)hydrazine-1-carbothioamide (**12**): crystallization in EtOH, yellow solid, yield 50%, ¹H-NMR (400 MHz, DMSO-*d*₆): δ 12.3 (bs, 1H), 8.41 (s, 1H), 7.75 (bs, 2H), 7.48–7.46 (d, *J* = 8.0 Hz, 2H), 6.81–6.679 (d, *J* = 8.0 Hz, 1H), 3.02 (s, 6H) ppm.

3.1.3. General Procedure for the Synthesis of Thiadiazoles 14–16

Te opportune thiosemicarbazone (5 mmol) was suspended in EtOH, to this FeCl₃·6H₂O (20 mmol) was added and the reaction mixture was stirred under reflux for further 12 h. The reaction mixture was quenched with aqueous Na₂S₂O₃, cooled to room temperature, poured into 30 mL water under stirring, and then extracted with CH₂Cl₂ (three times). The organic layer was dried over anhydrous Na₂SO₄. The organic solvent evaporated and the corresponding residue was purified by recrystallization from EtOH to afford the corresponding thiadiazoles 14–16.

5-(3,4-Dimethoxyphenyl)-1,3,4-thiadiazol-2-amine (**14**): crystallization in EtOH. Yellow solid, yield 44%. ¹H-NMR (400 MHz, DMSO-*d*₆): δ 7.28 (s, 1H), 7.22 (bs, 2H), 7.13–7.12 (d, *J* = 2.8 Hz, 1H), 6.65–6.64 (d, *J* = 2.8 Hz, 1H), 3.75 (s, 3H), 3.72 (s, 3H) ppm.

5-(4-(Dimethylamino)phenyl)-1,3,4-thiadiazol-2-amine (**15**): crystallization in EtOH. yellow solid, yield 50%, ¹H-NMR (400 MHz, DMSO-*d*₆): δ 7.72–7.70 (d, *J* = 8.0 Hz, 2H), 7.57 (bs, 2H), 6.90–6.88 (d, *J* = 8.0 Hz, 2H), 3.14 (s, 6H) ppm.

5-(2-Nitrophenyl)-1,3,4-thiadiazol-2-amine (**16**). To a suspension of **2** (100 mg, 0.44 mmol) in EtOH (10 mL), FeCl₃·6H₂O (482.1 mg, 1.78 mmol) in EtOH (10 mL) was added and the resulting mixture was heated at reflux for 12 h. The reaction mixture was diluted with water, alkalized by 10% NaOH solution, and then extracted with DCM. The organic layer was evaporated and the residue was recrystallized from Ethanol (60% yield). ¹H NMR (DMSO-*d*₆): δ 7.93 (d, *J* = 7.4 Hz, 1H), 7.74–7.64 (m, 3H), 7.53 (s, 2H) ppm. ¹³C-NMR (DMSO-*d*₆): δ 170.4, 150.9, 148.7, 133.2, 131.7, 131.2, 124.7, 124.0. LC-MS(ES) *m/z* = 222.7 [M + H]⁺, *m/z* = 244.8 [M + Na]⁺.

3.1.4. General Procedure for the Synthesis of Isoindoline-1,3-Diones 17–22

To a solution of substituted-1,3,4-thiadiazol-2-amine (0.48 mmol) in CH₃CN, phthalic anhydride (1.4 mmol) and triethylamine (1.05 mmol) were added, and the corresponding mixture was stirred at reflux overnight under N₂ atmosphere. The product was filtered and washed with EtOAc to give a light yellow solid.

2-(5-(4-Methoxyphenyl)-1,3,4-thiadiazol-2-yl)isoindoline-1,3-dione (**17**): Yellow solid, yield 78%. ¹H-NMR (400 MHz, DMSO-*d*₆): δ 8.06–8.04 (m, 2H), 7.98–7.96 (m, 4H), 7.12–7.10 (d, *J* = 8.0 Hz, 2H), 3.84 (s, 3H). ¹³C-NMR (DMSO-*d*₆): δ 167.05, 164.74, 162.25, 152.88, 136.03, 131.59, 129.67, 124.74, 122.41, 115.95, 115.43, 114.87 ppm.

2-(5-(4-Hydroxyphenyl)-1,3,4-thiadiazol-2-yl)isoindoline-1,3-dione (**18**): filtration, yellow solid, yield 80%. ¹H-NMR (400 MHz, DMSO-*d*₆): δ 10.23 (bs, 1H), 8.05–8.02 (m, 2H), 7.97–7.94 (m, 2H), 7.86–7.84 (d, *J* = 8.0 Hz, 2H), 6.93–6.91 (d, *J* = 8.0 Hz, 2H).

2-(5-(2-Bromophenyl)-1,3,4-thiadiazol-2-yl)isoindoline-1,3-dione (**19**): filtration, yellow solid, yield 45%. ¹H-NMR (400 MHz, CDCl₃): δ 8.21–8.19 (d, *J* = 8.0 Hz, 1H), 8.08–8.04 (m, 2H), 7.91–7.88 (m, 2H), 7.75–7.73 (d, *J* = 8.0 Hz, 1H), 7.49–7.46 (t, *J* = 7.2 Hz, 1H), 7.38–7.34 (t, *J* = 8.0 Hz, 1H), 7.26 (s, 1H).

2-(5-(3,4-Dimethoxyphenyl)-1,3,4-thiadiazol-2-yl)isoindoline-1,3-dione (**20**): filtration, Yellow solid, yield 63%. ¹H-NMR (400 MHz, DMSO-*d*₆): δ 8.08 (s, 1H), 8.00–7.98 (d, *J* = 8 Hz, 1H), 7.91–7.89 (d, *J* = 8.0 Hz, 1H), 7.50 (s, 1H), 7.42–7.40 (d, *J* = 8.0 Hz, 1H), 7.07–7.05 (d, *J* = 8.0 Hz 1H), 3.81 (s, 3H), 3.78 (s, 3H).

2-(5-(4-(Dimethylamino)phenyl)-1,3,4-thiadiazol-2-yl)isoindoline-1,3-dione (**21**): filtration, Yellow solid, yield 45%. ¹H-NMR (400 MHz, CDCl₃): δ 8.06–8.08 (d, *J* = 8.0 Hz, 2H), 7.92–7.88 (m, 4H), 7.26–7.25 (d, *J* = 3.2 Hz, 1H), 6.92–6.91 (d, *J* = 3.2 Hz, 1H).

2-(5-(2-Nitrophenyl)-1,3,4-thiadiazol-2-yl)isoindoline-1,3-dione (**22**). Crystallization MeCN (81% yield, brown solid). $^1\text{H NMR}$ (DMSO- d_6): δ 8.14 (d, $J = 7.3$ Hz, 1H), 8.08–8.06 (m, 2H), 7.97–7.94 (m, 3H), 7.90–7.82 (m, 2H). LC-MS(ES) $m/z = 352.9$ [M + H] $^+$, $m/z = 375.0$ [M + Na] $^+$.

3.1.5. General Procedure for the Synthesis of Acids 23–28

Lithium hydroxide monohydrate (0.18 mmol) was added to a suspension of substituted-(1,3,4-thiadiazol-2-yl)isoindoline-1,3-dione (0.15 mmol) in a (1:1) mixture of H₂O:THF. The reaction mixture was stirred at room temperature for 2 h, and was then acidified with HCl 1N and extracted three times with EtOAc. The organic layer was dried over anhydrous Na₂SO₄ and the solvent was removed at reduced pressure to provide the final product as white solid, which was used in the next step without further purification.

2-((5-(4-Methoxyphenyl)-1,3,4-thiadiazol-2-yl)carbamoyl)benzoic acid (**23**): crystallization MeCN, yield 67% $^1\text{H NMR}$ (DMSO): δ 12.98 (s, 1H), 7.90–7.86 (m, 2H), 7.65–7.56 (m, 2H), 7.06–7.04 (m, 2H), 3.79 (s, 3H) ppm $^{13}\text{C-NMR}$ (DMSO): δ 167.55, 167.01, 161.76, 161.09, 158.06, 135.97, 131.87, 130.38, 130.30, 129.76, 128.56, 128.52, 128.48, 128.17, 122.17, 114.78, 55.42 ppm LC-MS(ES) $m/z = 352.9$ [M + H] $^+$, $m/z = 354.0$ [M – H] $^-$.

2-((5-(4-Hydroxyphenyl)-1,3,4-thiadiazol-2-yl)carbamoyl)benzoic acid (**24**): crystallization in EtOH. white solid, yield 75%, $^1\text{H-NMR}$ (400 MHz, DMSO- d_6): δ 13.16 (bs, 1H), 10.04 (s, 1H), 7.93–7.91 (d, $J = 8.0$ Hz, 1H), 7.79–7.77 (d, $J = 8.0$ Hz, 2H), 7.69–7.60 (m, 3H), 6.90–6.88 (d, $J = 8.0$ Hz, 2H). $^{13}\text{C-NMR}$ (100 MHz, DMSO- d_6): δ 167.96, 167.49, 162.60, 160.17, 158.21, 136.50, 132.32, 130.82, 130.22, 129.10, 128.64, 121.70, 116.56 ppm.

2-((5-(2-Bromophenyl)-1,3,4-thiadiazol-2-yl)carbamoyl)benzoic acid (**25**): Purification eluent DCM/MeOH 96:4, yield 50%, white solid. $^1\text{H-NMR}$ (400 MHz, DMSO- d_6): δ 13.40 (bs, 1H), 7.97–7.93 (t, $J = 8.0$ Hz, 2H), 7.85–7.83 (d, $J = 8.0$ Hz, 1H), 7.68–7.61 (m, 3H), 7.58–7.54 (t, $J = 8.0$ Hz, 1H), 7.49–7.45 (t, $J = 8.0$ Hz, 1H). $^{13}\text{C-NMR}$ (100 MHz, DMSO- d_6): δ 168.18, 167.56, 160.70, 159.82, 136.20, 134.32, 132.44, 132.30, 132.21, 131.60, 130.96, 130.35, 128.79, 128.75, 121.89 ppm.

2-((5-(3,4-Dimethoxyphenyl)-1,3,4-thiadiazol-2-yl)carbamoyl)benzoic acid (**26**): crystallization in EtOH. White solid, yield 60%. $^1\text{H-NMR}$ (400 MHz, DMSO- d_6): δ 7.87–7.85 (d, $J = 8$ Hz, 1H), 7.64–7.54 (m, 3H), 7.45–7.41 (m, 2H), 7.04–7.02 (d, $J = 8$ Hz, 1H), 3.8 (s, 3H), 3.76 (s, 3H). $^{13}\text{C-NMR}$ (100 MHz, CDCl₃): δ 168.06, 167.43, 162.44, 158.58, 151.36, 149.65, 136.54, 132.41, 130.85, 130.61, 130.18, 128.60, 123.31, 120.86, 112.57 ppm.

2-((5-(4-(Dimethylamino)phenyl)-1,3,4-thiadiazol-2-yl)carbamoyl)benzoic acid (**27**): crystallization in EtOH. white solid, yield 98%, $^1\text{H-NMR}$ (400 MHz, DMSO- d_6): δ 13.13 (bs, 1H), 7.92–7.90 (d, $J = 8.0$ Hz, 1H), 7.76–7.74 (d, $J = 8.0$ Hz, 2H), 7.96–7.59 (m, 3H), 6.80–6.68 (d, $J = 8.0$ Hz, 2H). $^{13}\text{C-NMR}$ (100 MHz, DMSO- d_6): δ 167.86, 167.50, 163.07, 152.15, 136.62, 132.32, 130.77, 130.18, 128.62, 128.49, 117.90, 112.52 ppm.

2-((5-(2-Nitrophenyl)-1,3,4-thiadiazol-2-yl)carbamoyl)benzoic acid (**28**): Crystallization MeCN (73% yield, pale yellow solid). $^1\text{H NMR}$ (DMSO- d_6): δ 8.06–8.00 (m, 3H), 7.90–7.74 (m, 3H), 7.59–7.51 (m, 2H). $^{13}\text{C-NMR}$ (DMSO- d_6): δ 170.5, 167.7, 156.6, 149.0, 138.0, 133.5, 133.2, 132.2, 131.7, 131.3, 130.5, 130.0, 124.9, 124.5. LC-MS(ES) $m/z = 370.9$ [M + H] $^+$, $m/z = 393.0$ [M + Na] $^+$, $m/z = 368.9$ [M – H] $^-$.

3.1.6. General Procedure for the Synthesis of Esters 29–32

A mixture of substituted-(1,3,4-thiadiazol-2-yl)isoindoline-1,3-dione (0.29 mmol) and the opportune alcohol (0.29 mmol) was stirred at room temperature for 16 h under N₂ atmosphere. Mixture was diluted with diluted CH₃COOH, the residue was filtered and the solvent was evaporated at a reduced pressure. The product was purified via flash chromatography on silica gel (eluent CHCl₃/EtOH, 98/2) to furnish a white solid product.

Methyl 2-((5-(4-methoxyphenyl)-1,3,4-thiadiazol-2-yl)carbamoyl)benzoate (29): Crystallization MeCN (53% yield, white solid). $^1\text{H-NMR}$ ($\text{DMSO-}d_6$): δ 8.04–8.02 (m, 2H), 7.96–7.92 (m, 2H), 7.10–7.07 (m, 2H), 3.81 (s, 3H) ppm. $^{13}\text{C-NMR}$ ($\text{DMSO-}d_6$): δ 167.05, 164.74, 162.25, 152.88, 136.03, 131.59, 129.67, 124.74, 122.41, 115.95, 115.43, 114.87 ppm. LC-MS(ES) $m/z = 370.1$ $[\text{M} + \text{H}]^+$.

Ethyl 2-((5-(4-methoxyphenyl)-1,3,4-thiadiazol-2-yl)carbamoyl)benzoate (30): Purification eluent $\text{CHCl}_3/\text{EtOH}$ 98:2, yield 10%, white solid. $^1\text{H-NMR}$ (400 MHz, CDCl_3): δ 8.00–7.98 (d, $J = 8.0$ Hz, 1H), 7.84–7.82 (d, $J = 8.0$ Hz, 2H), 7.63–7.54 (m, 3H), 6.97–6.95 (d, $J = 8.0$ Hz, 2H), 4.29–4.23 (q, $J = 7.2$ Hz, 2H), 3.83 (s, 3H), 1.22–1.20 (t, $J = 8.0$ Hz, 3H). $^{13}\text{C-NMR}$ (100 MHz, CDCl_3): δ 167.48, 165.99, 164.74, 132.24, 130.68, 130.38, 129.43, 128.82, 127.85, 114.61, 61.82, 55.44, 13.87 ppm. LC-MS(ES) $m/z = 384.2$ $[\text{M} + \text{H}]^+$.

Butyl 2-((5-(4-methoxyphenyl)-1,3,4-thiadiazol-2-yl)carbamoyl)benzoate (31): Purification eluent $\text{CHCl}_3/\text{EtOH}$ 98:2, crystallization in EtOH, yield 23%, white solid. $^1\text{H-NMR}$ (400 MHz, CDCl_3): δ 8.07–8.05 (d, $J = 8$ Hz, 1H), 7.77–7.75 (d, $J = 8.0$ Hz, 3H), 7.70–7.62 (m, 2H), 6.99–6.97 (d, $J = 8$ Hz, 2H), 4.23–4.19 (t, $J = 6.8$ Hz, 2H), 3.88 (s, 3H), 1.58–1.54 (q, $J = 6.8$ Hz, 2H), 1.33–1.28 (q, $J = 7.6$ Hz, 2H), 0.82–0.79 (t, $J = 7.2$ Hz, 3H). $^{13}\text{C-NMR}$ (100 MHz, CDCl_3): δ 167.44, 166.16, 162.39, 161.56, 159.59, 135.58, 132.19, 130.55, 130.39, 129.96, 128.60, 128.51, 123.11, 114.49, 65.57, 55.47, 53.43, 30.47, 19.15, 13.64 ppm. LC-MS(ES) $m/z = 412.1$ $[\text{M} + \text{H}]^+$.

Methyl 2-((5-(2-nitrophenyl)-1,3,4-thiadiazol-2-yl)carbamoyl)benzoate (32): The crude was purified by flash chromatography using 99:1 DCM:MeOH (35% yield, white solid). $^1\text{H-NMR}$ ($\text{Acetone-}d_6$): δ 8.07–7.67 (m, 8H), 3.82 (s, 3H). $^{13}\text{C-NMR}$ ($\text{Acetone-}d_6$): δ 167.3, 166.0, 160.0, 157.7, 149.2, 136.2, 132.9, 132.3, 132.0, 131.4, 130.7, 129.9, 129.5, 128.3, 52.0 ppm. LC-MS(ES) $m/z = 385.0$ $[\text{M} + \text{H}]^+$, $m/z = 406.9$ $[\text{M} + \text{Na}]^+$.

3.1.7. General Procedure for the Synthesis of Sulfonic Acids 33 and 34

2-Sulfobenzoic acid cyclic anhydride (0.99 mmol) and TEA (0.54 mmol) were added to a stirred solution of the opportune aminothiazole (0.25 mmol) in MeCN (5 mL). The reaction mixture was heated at reflux for 90 min. Then, water was added to the mixture and acidified to pH 2 with 1N HCl. The resulting mixture was extracted with AcOEt, the organic layer was washed with brine, dried over Na_2SO_4 , filtered, and evaporated in vacuo. The crude was purified by flash chromatography while using the opportune eluent.

2-((5-(4-Methoxyphenyl)-1,3,4-thiadiazol-2-yl)carbamoyl)benzenesulfonic acid (33): The crude was purified by flash chromatography on silica gel (from 4:6 PE:AcOEt to 100% AcOEt). (68% yield, white solid). $^1\text{H-NMR}$ ($\text{DMSO-}d_6$): δ 8.05 (d, $J = 7.9$ Hz, 1H), 7.88 (d, $J = 7.9$ Hz, 2H), 7.74 (t, $J = 8.0$ Hz, 1H), 7.64–7.61 (m, 2H), 7.06 (d, $J = 7.9$ Hz, 2H), 3.87 (s, 3H) ppm. $^{13}\text{C-NMR}$ (MeOD): δ 166.88, 163.42, 161.89, 158.65, 143.12, 131.83, 130.88, 130.20, 129.95, 128.52, 127.30, 122.90, 114.50, 54.77 ppm. LC-MS(ES) $m/z = 390.1$ $[\text{M} - \text{H}]^-$.

2-((5-(2-Nitrophenyl)-1,3,4-thiadiazol-2-yl)carbamoyl)benzenesulfonic acid (34): The crude was purified by flash chromatography using from 4:6 PE:AcOEt to 100% AcOEt. (54% yield, yellow solid). $^1\text{H-NMR}$ ($\text{DMSO-}d_6$): δ 13.85 (s, 1H), 8.10 (d, $J = 7.9$ Hz, 1H), 7.93 (d, $J = 7.9$ Hz, 2H), 7.89–7.78 (m, 3H), 7.65–7.55 (m, 2H). $^{13}\text{C-NMR}$ ($\text{DMSO-}d_6$): δ 166.6, 160.2, 157.6, 149.0, 154.3, 133.6, 132.5, 132.0, 131.9, 131.4, 130.2, 127.4, 125.1, 124.0. LC-MS(ES) $m/z = 404.9$ $[\text{M} - \text{H}]^-$.

3.1.8. General Procedure for the Synthesis of Compounds 35 and 36

Iron dust (0.61 mmol) and NH_4Cl (0.061 mmol) were added to a solution of the opportune nitrocompound (0.12 mmol) in a 3:1 mixture of EtOH/ H_2O (13 mL). The reaction mixture was stirred at reflux for 30 min. After that, the mixture was filtered through a Celite pad, concentrated in vacuo, and then purified by flash chromatography on silica gel while using the opportune eluent.

2-((5-(2-Aminophenyl)-1,3,4-thiadiazol-2-yl)carbamoyl)benzenesulfonic acid (**35**): From EtOAc to 98:2 AcOEt:MeOH (76% yield, yellow solid). ^1H NMR (DMSO- d_6): δ 7.91 (d, J = 8.2 Hz, 1H), 7.80 (d, J = 8.4 Hz, 1H), 7.60–7.49 (m, 3H), 7.91 (d, J = 8.2 Hz, 1H), 7.15 (t, J = 7.6 Hz, 1H), 6.87–6.83 (m, 3H), 6.62 (t, J = 7.4 Hz, 1H). ^1H NMR (DMSO- d_6 + D_2O): δ 7.91 (d, J = 8.2 Hz, 1H), 7.80 (d, J = 8.4 Hz, 1H), 7.60–7.49 (m, 3H), 7.91 (d, J = 8.2 Hz, 1H), 7.15 (t, J = 7.6 Hz, 1H), 6.83 (d, J = 8.3 Hz, 1H), 6.62 (t, J = 7.4 Hz, 1H). ^{13}C -NMR (DMSO- d_6): δ 166.5, 164.7, 157.0, 147.1, 144.8, 131.8, 131.4, 131.2, 130.5, 130.3, 127.4, 116.7, 116.5, 111.6. LC-MS(ES) m/z = 376.9 $[\text{M} + \text{H}]^+$, m/z = 374.9 $[\text{M} - \text{H}]^-$.

2-((5-(2-Aminophenyl)-1,3,4-thiadiazol-2-yl)carbamoyl)benzoic acid (**36**). The residue was purified by flash chromatography from 100% AcOEt to 95:5 AcOEt:MeOH (31% yield, yellow solid). ^1H NMR (DMSO- d_6): δ 7.86 (d, J = 7.4 Hz, 1H), 7.79 (d, J = 7.6 Hz, 1H), 7.56–7.44 (m, 3H), 7.14 (t, J = 7.6 Hz, 1H), 6.90–6.84 (m, 3H), 6.63 (t, J = 7.6 Hz, 1H). ^1H NMR (DMSO- d_6 + D_2O): δ 7.86 (d, J = 7.4 Hz, 1H), 7.79 (d, J = 7.6 Hz, 1H), 7.56–7.44 (m, 3H), 7.14 (t, J = 7.6 Hz, 1H), 6.82 (d, J = 9.2 Hz, 1H), 6.63 (t, J = 7.6 Hz, 1H). ^{13}C -NMR (DMSO- d_6): δ 169.3, 167.4, 164.3, 158.2, 147.4, 134.2, 131.4, 131.2, 131.0, 130.8, 130.5, 129.8, 116.6, 116.2, 111.9. LC-MS(ES) m/z = 339.0 $[\text{M} - \text{H}]^-$.

3.2. Enzymatic Assays

3.2.1. Protein Expression and Purification

Recombinant his-tagged human full length DDX3X was cloned into the *E. coli* expression vector pET-30a(+). Shuffle T7 *E. coli* cells were transformed with the plasmid and grown at 37 °C up to OD_{600} = 0.7. DDX3X expression was induced with 0.5 mM IPTG at 15 °C O/N. The cells were harvested by centrifugation, lysed, and the crude extract centrifuged at 100,000xg for 60 min. at 4 °C in a Beckman centrifuge before being loaded onto a FPLC Ni-NTA column (GE Healthcare). Column was equilibrated in Buffer A (50 mM Tris-HCl pH 8.0, 250 mM NaCl, 25 mM Imidazole, and 20% glycerol). After extensive washing in Buffer A, the column was eluted with a linear gradient in Buffer A from 25 mM to 250 mM Imidazole. Proteins in the eluted fractions were visualized on SDS-PAGE and then tested for the presence of DDX3X by Western blot with anti-DDX3X A300-475A (BETHYL) at 1:2000 dilution in 5% milk. Fractions containing the purest DDX3X protein were pooled and stored at –80 °C.

3.2.2. ATPase Assay

The ATPase assay was carried out by using the commercial kit Promega (Milan, Italy), ADP-Glo™ Kinase Assay. Reaction was performed in 30 mM TrisHCl pH 8, 9 mM MgCl_2 , 0.05 mg/mL BSA, 50 μM ATP, and 4 μM of recombinant DDX3X. Reaction was performed following the ADP-Glo™ Kinase Assay Protocol and luminescence was measured with MicroBeta TriLux (Perkin Elmer, Milan, Italy).

3.3. Antiviral Assay

The antiviral activity was evaluated by measuring the half maximal inhibitory concentration (IC_{50}) values against the HIV-1 wild-type reference strain NL4-3 in a TZM-bl cell line based phenotypic assay, named BiCycle Assay [26]. The method includes a first round of infection of human T cell lymphoma derived clone H9 at multiplicity of infection of 0.03 in the presence of serial dilution of compounds in a 96-well plate. After 72 h, 50 microliters of supernatants from each well were used to infect the TZM-bl cell line, which allow the quantitative analysis of HIV infection by measuring the expression of the luciferase gene integrated in the genome of the cells under the control of HIV-1 LTR promoter. The contribution of DDX3X expression in TZM-bl cells does not contribute in a relevant way to the determination of viral activity, as the reporter TZM-bl cells are minimally exposed to investigational compounds.

After 48 h, dose-response curves were generated by measuring reporter gene expression in each well by using the Bright-Glo Luciferase Assay (Promega) through the GloMax Discovery reader (Promega). Relative luminescence units measured in each well were elaborated with the GraphPad

Software v.6.0 to calculate IC₅₀ values. All the viruses and cell lines were obtained through the NIH AIDS Reagent Program (www.aidsreagent.org).

3.4. Cytotoxicity Assay

Cytotoxicity in H9 cells was determined by using the CellTiter-Glo 2.0 assay (Promega). H9 cells were seeded at 40,000 cells/well in duplicate in the presence of serial two-fold dilutions of compounds (range 200–1.56 µM) and incubated for 72 h. Cell viability was calculated by measuring cellular ATP as a marker of metabolically active cells through a luciferase based chemical reaction and expressed as the concentration that reduce cell viability by 50%.

3.5. ADME Assay

Chemicals. All solvents and reagents were from Sigma-Aldrich Srl (Milan, Italy). Dodecane was purchased from Fluka (Milan, Italy). Pooled Male Donors 20 mg/mL HLM were from BD Gentest-Biosciences (San Jose, California). Milli-Q quality water (Millipore, Milford, MA, USA) was used. Hydrophobic filter plates (MultiScreen-IP, Clear Plates, 0.45 µm diameter pore size), 96-well microplates, and 96-well UV-transparent microplates were obtained from Millipore (Bedford, MA, USA).

3.5.1. Parallel Artificial Membrane Permeability Assay (PAMPA)

Donor solution (0.5 mM) was prepared by diluting 1 mM dimethylsulfoxide (DMSO) compound stock solution while using phosphate buffer (pH 7.4, 0.025 M). Filters were coated with 5 µL of a 1% (w/v) dodecane solution of phosphatidylcholine for intestinal permeability. Donor solution (150 µL) was added to each well of the filter plate. To each well of the acceptor plate was added 300 µL of solution (50% DMSO in phosphate buffer). All of the compounds were tested in three different plates on different days. The sandwich was incubated for 5 h at room temperature under gentle shaking. After the incubation time, the plates were separated, and samples were taken from both receiver and donor sides and analyzed while using LC with UV detection at 280 nm. LC analysis was performed with a PerkinElmer (series 200) instrument that was equipped with an UV detector (PerkinElmer 785A, UV/vis Detector). Chromatographic separation was conducted using a Polaris C18 column (150–4.6 mm, 5 µm particle size) at a flow rate of 0.8 mL min⁻¹ with a mobile phase composed of 60% ACN/40% H₂O-formic acid 0.1% for all compounds. Permeability (P_{app}) was calculated according to the following equation with some modification to obtain permeability values in cm/s,

$$P_{app} = \frac{VDVA}{(VD + VA)At} - \ln(1 - r) \quad (1)$$

where V_A is the volume in the acceptor well, V_D is the volume in the donor well (cm³), A is the “effective area” of the membrane (cm²), t is the incubation time (s), and r the ratio between drug concentration in the acceptor and equilibrium concentration of the drug in the total volume ($V_D + V_A$).

Drug concentration is estimated by using the peak area integration. Membrane retentions (%) were calculated according to the following equation:

$$\%MR = \frac{[r - (D + A)]100}{Eq} \quad (2)$$

where r is the ratio between drug concentration in the acceptor and equilibrium concentration, D , A , and Eq represented drug concentration in the donor, acceptor, and equilibrium solution, respectively.

3.5.2. Water Solubility Assay

The appropriate (1 mg) was added to 1 mL of water. The sample was shaken in a shaker bath at room temperature for 24–36 h. The suspensions were filtered through a 0.45 µm nylon filter (Acrodisc,

Sigma Aldrich, Milan, Italy) and the solubilized compound determined by LC-MS-MS assay. The determination was performed in triplicate. For the quantification, an LC-MS system consisting of a Varian apparatus (Varian Inc., Palo Alto, CA, USA), including a vacuum solvent degassing unit, two pumps (212-LC), a Triple Quadrupole MSD (Mod. 320-LC) mass spectrometer with ES interface, and Varian MS Workstation System Control Vers. 6.9 software, was used. Chromatographic separation was obtained while using a 3 μm particle size Pursuit C18 column (50 \times 2.0 mm) (Varian). Column was equilibrated in Buffer B (aqueous solution of 0.1% formic acid) and eluted with a linear increase from 0% to 70% gradient of Buffer A (ACN) for 10 min. and subsequent increase up to 98% for additional 5 min. The instrument operated in positive mode and the following parameters were used: injection volume 5 μL , flow rate 0.3 mL/min, detector 1850 V, drying gas pressure 25.0 psi, desolvation temperature 300.0 $^{\circ}\text{C}$, nebulizing gas 45.0 psi, needle 5000 V, and shield 600 V. Nebulizer gas and drying gas was Nitrogen. Argon was the collision gas at a pressure of 1.8 mTorr in the collision cell. Single compound quantification was performed in comparison with standard calibration curves in methanol.

3.5.3. Microsomal Stability Assay

Each compound was incubated at a final concentration of 50 μM in a final volume of 0.5 mL in 2% (final solution) DMSO for 60 min. at 37 $^{\circ}\text{C}$ under the following conditions: 125 mM phosphate buffer (pH 7.4), 5 μL of human liver microsomal protein (0.2 mg/mL) and NADPH-generating system. The reactions were stopped by adding 1.0 mL of acetonitrile and cooled in ice. Parent drug and metabolites in the reaction mixtures were determined after centrifugation of the samples by LC-UV-MS.

An Agilent 1100 LC/MSD VL system (G1946C) (Agilent Technologies, Palo Alto, CA, USA) was used for chromatographic analysis. A vacuum solvent degassing unit constituted the instrument, a binary high-pressure gradient pump, an 1100 series UV detector, and an 1100 MSD model VL benchtop mass spectrometer. A Varian Polaris C18-A column (150–4.6 mm, 5 μm particle size) was used under the following conditions: eluent A: ACN; eluent B: aqueous solution of formic acid (0.1%); linear gradient 2–70% of eluent A for 12 min, then increased to 98% up to 20 min.; flow rate 0.8 mL min.⁻¹; injection volume 20 μL . The LC-ESI-MS determination was performed with Agilent 1100 series mass spectra detection (MSD) single-quadrupole instrument in the positive ion mode and an orthogonal spray API-ES (Agilent Technologies, Palo Alto, CA, USA). Nebulizing and drying gas was Nitrogen. Pressure of the nebulizing gas 40 psi, flow of the drying gas 9 L/min, capillary voltage 3000 V, fragmentor voltage 70 V, and vaporization temperature 350 $^{\circ}\text{C}$. UV were monitored at 280 nm. Scan range for spectra acquisition was m/z 100–1500 while using a step size of 0.1 u. The percentage of compound not metabolized was determined by comparison with reference solutions.

4. Discussion

In the present paper, 15 novel inhibitors of the ATPase activity of the human helicase DDX3X were designed, synthesized, and biologically characterized. The compounds were designed starting from hits previously published, by replacing their rohdanine moiety, already reported in the list of PAINS, with the 1,3,4-thiadiazole ring. As a result, nine compounds showed promising anti-enzymatic activities varying from 1.5 μM to 35 μM . Compounds that were endowed of the most interesting activities against the enzyme were then evaluated on HIV-1 infected H9 cells to discover potential antiviral drugs. The antiviral screening led to the identification of seven antiviral compounds endowed of activities ranging from 2.8 μM to 42 μM . Among them, compound **24** was characterized by the best anti-HIV-1 activity of 2.8 μM and by a promising selectivity index (CC_{50} = 125 μM , SI = 45). The ADME assays were finally performed to preliminary evaluate the pharmacokinetic parameters of compounds and to rationalize results. Acid derivatives showed very good metabolic stability, in contrast to their corresponding esters, which were rapidly metabolized into the acid precursors. The aqueous solubility was found very promising; in fact, the values of the most active compounds were below 6, as recommended for drug candidates. Finally, compounds were characterized by low but not limiting passive permeability. Taking into account ADME results, the antiviral activities of the esters

29 and **31** is probably due to their enhanced membrane permeability, followed by a cellular conversion into compound **24**. Caco-2 experiments will be performed in the due time to evaluate the involvement of active transport mechanisms.

In conclusion, in the present work, we have successfully replaced the rhodanine moiety of compound **FE15** with 1,3,4-thiadiazole ring. This approach is useful in reducing the interferences in assays that are generally associated with PAINS. The most promising derivative, compound **24**, is characterized by good inhibition of the ATPase activity of DDX3X protein and by promising anti-HIV-1 activity in a reference virus-cell system without signs of in vitro cytotoxicity. These data, together with suitable in vitro PK properties, make inhibitor **24** a good starting point for further optimization.

Author Contributions: Conceptualization, G.M. and M.B.; Data curation, A.B. (Annalaura Brai), S.R., V.R., L.B., C.Z., M.B. (Matteo Borgini), C.I.T., A.G., A.B. (Adele Boccuto) and F.S.; Formal analysis, A.B. (Annalaura Brai), S.R., V.R., L.B., C.Z., M.B. (Matteo Borgini), C.I.T., A.G., A.B. (Adele Boccuto) and F.S.; Funding acquisition, G.M. and M.B. (Maurizio Botta); Investigation, A.B. (Annalaura Brai), S.R., V.R., L.B., C.Z., M.B. (Matteo Borgini), C.I.T., A.G., C.P., A.B. (Adele Boccuto) and F.S.; Methodology, A.B. (Annalaura Brai), V.R. and M.Z.; Project administration, G.M. and M.B. (Maurizio Botta); Supervision, M.Z., G.M. and M.B. (Maurizio Botta); Validation, A.B. (Annalaura Brai), S.R., V.R., and M.Z.; Writing—original draft, A.B. (Annalaura Brai); Writing—review & editing, M.Z., G.M.

Notes: Dedicated to the memory of Maurizio Botta, full professor at the University of Siena, excellent chemist, beloved master and friend.

Funding: This research was funded by First Health Pharmaceutical B.V; G.M. and V.R. were partially supported by the CNR Project “Identification of novel molecules with therapeutic potential against Zika virus and other emerging viruses”.

Acknowledgments: The pNL4-3 plasmid, the H9 and the TZM-bl cell lines were obtained through the AIDS Reagent Program.

Conflicts of Interest: The authors declare no conflict of interest.

References

1. Soto-Rifo, R.; Ohlmann, T. The role of the DEAD-box RNA helicase DDX3 in mRNA metabolism. *Wiley Interdiscip. Rev. RNA* **2013**, *4*, 369–385. [[CrossRef](#)] [[PubMed](#)]
2. Yedavalli, V.S.R.K.; Neuveut, C.; Chi, Y.-H.; Kleiman, L.; Jeang, K.-T. Requirement of DDX3 DEAD box RNA helicase for HIV-1 Rev-RRE export function. *Cell* **2004**, *119*, 381–392. [[CrossRef](#)] [[PubMed](#)]
3. Ishaq, M.; Hu, J.; Wu, X.; Fu, Q.; Yang, Y.; Liu, Q.; Guo, D. Knockdown of cellular RNA helicase DDX3 by short hairpin RNAs suppresses HIV-1 viral replication without inducing apoptosis. *Mol. Biotechnol.* **2008**, *39*, 231–238. [[CrossRef](#)] [[PubMed](#)]
4. Owsianka, A.M.; Patel, A.H. Hepatitis C virus core protein interacts with a human DEAD box protein DDX3. *Virology* **1999**, *257*, 330–340. [[CrossRef](#)]
5. Ariumi, Y.; Kuroki, M.; Abe, K.I.; Dansako, H.; Ikeda, M.; Wakita, T.; Kato, N. DDX3 DEAD-Box RNA Helicase Is Required for Hepatitis C Virus RNA Replication. *J. Virol.* **2007**, *81*, 13922–13926. [[CrossRef](#)]
6. Upadya, M.H.; Aweya, J.J.; Tan, Y.J. Understanding the interaction of hepatitis C virus with host DEAD-box RNA helicases. *World J. Gastroenterol.* **2014**, *20*, 2913–2926. [[CrossRef](#)]
7. Chahar, H.S.; Chen, S.; Manjunath, N. P-body components LSM1, GW182, DDX3, DDX6 and XRN1 are recruited to WNV replication sites and positively regulate viral replication. *Virology* **2013**, *436*, 1–7. [[CrossRef](#)]
8. Li, C.; Ge, L.; Li, P.; Wang, Y.; Dai, J.; Sun, M.; Huang, L.; Shen, Z.; Hu, X.; Ishag, H.; et al. Cellular DDX3 regulates Japanese encephalitis virus replication by interacting with viral un-translated regions. *Virology* **2014**, *449*, 70–81. [[CrossRef](#)]
9. Park, S.H.; Lee, S.G.; Kim, Y.; Song, K. Assignment of a human putative RNA helicase gene, DDX3, to human X chromosome bands p11.3→p11.23. *Cytogenet. Cell Genet.* **1998**, *81*, 178–179. [[CrossRef](#)]
10. Högbom, M.; Collins, R.; van den Berg, S.; Jenvert, R.-M.; Karlberg, T.; Kotenyova, T.; Flores, A.; Hedestam, G.B.K.; Schiavone, L.H. Crystal Structure of Conserved Domains 1 and 2 of the Human DEAD-box Helicase DDX3X in Complex with the Mononucleotide AMP. *J. Mol. Biol.* **2007**, *372*, 150–159. [[CrossRef](#)]

11. Radi, M.; Falchi, F.; Garbelli, A.; Samuele, A.; Bernardo, V.; Paolucci, S.; Baldanti, F.; Schenone, S.; Manetti, F.; Maga, G.; et al. Discovery of the first small molecule inhibitor of human DDX3 specifically designed to target the RNA binding site: Towards the next generation HIV-1 inhibitors. *Bioorg. Med. Chem. Lett.* **2012**, *22*, 2094–2098. [[CrossRef](#)] [[PubMed](#)]
12. Fazi, R.; Tintori, C.; Brai, A.; Botta, L.; Selvaraj, M.; Garbelli, A.; Maga, G.; Botta, M. Homology Model-Based Virtual Screening for the Identification of Human Helicase DDX3 Inhibitors. *J. Chem. Inf. Model.* **2015**, *55*, 2443–2454. [[CrossRef](#)] [[PubMed](#)]
13. Brai, A.; Fazi, R.; Tintori, C.; Zamperini, C.; Bugli, F.; Sanguinetti, M.; Stigliano, E.; Esté, J.; Badia, R.; Franco, S.; et al. Human DDX3 protein is a valuable target to develop broad spectrum antiviral agents. *Proc. Natl. Acad. Sci. USA* **2016**, *113*, 5388–5393. [[CrossRef](#)] [[PubMed](#)]
14. Brai, A.; Martelli, F.; Riva, V.; Garbelli, A.; Fazi, R.; Zamperini, C.; Pollutri, A.; Falsitta, L.; Ronzini, S.; Maccari, L.; et al. DDX3X Helicase Inhibitors as a New Strategy To Fight the West Nile Virus Infection. *J. Med. Chem.* **2019**, *62*, 2333–2347. [[CrossRef](#)]
15. Maga, G.; Falchi, F.; Garbelli, A.; Belfiore, A.; Witvrouw, M.; Manetti, F.; Botta, M. Pharmacophore modeling and molecular docking led to the discovery of inhibitors of human immunodeficiency Virus-1 replication targeting the human cellular aspartic acid–glutamic acid–alanine–aspartic acid box polypeptide 3. *J. Med. Chem.* **2008**, *51*, 6635–6638. [[CrossRef](#)]
16. Yedavalli, V.S.R.K.; Zhang, N.; Cai, H.; Zhang, P.; Starost, M.F.; Hosmane, R.S.; Jeang, K.-T. Ring expanded nucleoside analogues inhibit RNA helicase and intracellular human immunodeficiency virus type 1 replication. *J. Med. Chem.* **2008**, *51*, 5043–5051. [[CrossRef](#)]
17. Maga, G.; Falchi, F.; Radi, M.; Botta, L.; Casaluce, G.; Bernardini, M.; Irannejad, H.; Manetti, F.; Garbelli, A.; Samuele, A.; et al. Toward the discovery of novel Anti-HIV Drugs. Second-Generation inhibitors of the cellular ATPase DDX3 with improved Anti-HIV activity: Synthesis, structure-activity relationship analysis, cytotoxicity studies, and target validation. *Chem. Med. Chem.* **2011**, *6*, 1371–1389. [[CrossRef](#)]
18. Xie, M.; Vesuna, F.; Botlagunta, M.; Bol, G.M.; Irving, A.; Bergman, Y.; Hosmane, R.S.; Kato, Y.; Winnard, P.T.; Raman, V. NZ51, a ring-expanded nucleoside analog, inhibits motility and viability of breast cancer cells by targeting the RNA helicase DDX3. *Oncotarget* **2015**, *6*, 29901–29913. [[CrossRef](#)]
19. Bol, G.M.; Vesuna, F.; Xie, M.; Zeng, J.; Aziz, K.; Gandhi, N.; Levine, A.; Irving, A.; Korz, D.; Tantravedi, S.; et al. Targeting DDX3 with a small molecule inhibitor for lung cancer therapy. *EMBO Mol. Med.* **2015**, *7*, 648–669. [[CrossRef](#)]
20. Xie, M.; Vesuna, F.; Tantravedi, S.; Bol, G.M.; Heerma van Voss, M.R.; Nugent, K.; Malek, R.; Gabrielson, K.; van Diest, P.J.; Tran, P.T.; et al. RK-33 Radiosensitizes prostate cancer cells by blocking the RNA helicase DDX3. *Cancer Res.* **2016**, *76*, 6340–6350. [[CrossRef](#)]
21. Kondaskar, A.; Kondaskar, S.; Kumar, R.; Fishbein, J.C.; Muvarak, N.; Lapidus, R.G.; Sadowska, M.; Edelman, M.J.; Bol, G.M.; Vesuna, F.; et al. Novel, Broad spectrum anticancer agents containing the tricyclic 5:7:5-fused diimidazodiazepine ring system. *ACS Med. Chem. Lett.* **2011**, *2*, 252–256. [[CrossRef](#)] [[PubMed](#)]
22. Samal, S.K.; Routray, S.; Veeramachaneni, G.K.; Dash, R.; Botlagunta, M. Ketorolac salt is a newly discovered DDX3 inhibitor to treat oral cancer. *Sci. Rep.* **2015**, *5*, 9982. [[CrossRef](#)] [[PubMed](#)]
23. Baell, J.B.; Holloway, G.A. New substructure filters for removal of pan assay interference compounds (PAINS) from screening libraries and for their exclusion in bioassays. *J. Med. Chem.* **2010**, *53*, 2719–2740. [[CrossRef](#)] [[PubMed](#)]
24. Tomašić, T.; Peterlin Mašič, L. Rhodanine as a scaffold in drug discovery: A critical review of its biological activities and mechanisms of target modulation. *Expert Opin. Drug Discov.* **2012**, *7*, 549–560. [[CrossRef](#)] [[PubMed](#)]
25. Li, Y.; Geng, J.; Liu, Y.; Yu, S.; Zhao, G. Thiadiazole-a promising structure in medicinal chemistry. *Chem. Med. Chem.* **2013**, *8*, 27–41. [[CrossRef](#)]

26. Saladini, F.; Giannini, A.; Boccuto, A.; Vicenti, I.; Zazzi, M. Agreement between an in-house replication competent and a reference replication defective recombinant virus assay for measuring phenotypic resistance to HIV-1 protease, reverse transcriptase, and integrase inhibitors. *J. Clin. Lab. Anal.* **2018**, *32*, e22206. [[CrossRef](#)]

Sample Availability: Samples of the compounds **23**, **24** and **29** are available from the authors.



© 2019 by the authors. Licensee MDPI, Basel, Switzerland. This article is an open access article distributed under the terms and conditions of the Creative Commons Attribution (CC BY) license (<http://creativecommons.org/licenses/by/4.0/>).